LC/MS Methods for Targeted Lipid Analyses

by

SI MI

A thesis submitted in partial fulfillment of the requirements for the degree of

Doctor of Philosophy

in

FOOD SCIENCE AND TECHNOLOGY

Department of Agricultural, Food and Nutritional Science
University of Alberta

Abstract

Lipidomics is a research field that attempts to achieve the comprehensive analysis of the entire lipidome in a biological system. The emergence and rapid expansion of lipidomic studies is driven by the great advances in chromatographic separation and mass spectrometry. For this dissertation, I have focused on the development of analytical strategies for targeted and quantitative lipidomics. The targeted lipid and lipid-related compounds include bile acids (including free and conjugated forms), sphingolipids, trimethylamine (TMA) and trimethylamine *N*-oxide (TMAO) as well as conjugated linolenic acids (CLnA). Quantitative methods were established based on liquid chromatography/ tandem mass spectrometry (LC/MS/MS) techniques.

Parenteral nutrition-associated liver disease (PNALD) is a cholestatic liver disease partially caused by developmental immaturity with regards to hepatic bile acids metabolism and transport. Glucagon-like peptide-2 (GLP-2) has been reported to be associated with improved bile flow, and serum and histologic markers of cholestasis. A universal method comprised of C18-based solid-phase extraction (SPE) procedure and LC/MS/MS was developed and validated to monitor the alterations in the bile acids compositions in piglet bile samples in a control group compared to a GLP-2 treated group. As a result, up to 12 different bile acids species were identified in bile sample extracts. Bile acid quantification showed that GLP-2 therapy did improve the clinical phenotype of PNALD by altering bile acids synthesis and transport.

Chronic Lymphocytic Leukemia (CLL) is the most common leukemia in North American and European adults. Sphingolipid metabolism is altered in numerous cancers, but strong evidence is still lacking to support this finding in CLL In order to investigate the distributions of sphingolipids in both cancerous and healthy B cells, an LC/MS/MS method along with a single-phase extraction

was established. 17 sphingolipid species were successfully detected in the lipid extracts of B cells collected from CLL patients (n=5) and healthy donors (n=4). Quantitative data shows that there was an altered sphingolipid composition (increased levels) observed in the B cells from the CLL patients compared to those from healthy donors.

Trimethylamine (TMA) and trimethylamine *N*-oxide (TMAO) are metabolites of choline-related compounds. Abnormal TMA and TMAO concentration levels in biological materials could lead to the occurrence of diseases, such as atherosclerosis and trimethylaminuria. A new HILIC LC/MS/MS method with prior derivatization procedure to TMA enables the simultaneous identification and quantification of TMA and TMAO in mouse plasma samples in a single LC run within 5 min.

Conjugated linolenic acid (CLnA) isomers are present in high levels in pomegranate seed oils (PSO) and tung seed oils (TSO). These isomers are considered as health-enhancing compounds and the conjugated unsaturation facilitates the manufacture of organic coatings and polymers. Silver ion liquid chromatography coupled to in-line ozonolysis/mass spectrometry (Ag^+-LC/O_3-MS) has been proposed for unambiguous identification of CLnA isomers in PSO and TSO samples. Using this novel method, we have achieved the most comprehensive CLnA profiles in PSO and TSO samples reported to date.

Overall, the LC/MS-based lipidomic strategies developed in these studies provide us with an informative platform for comprehensive analysis of lipids and lipid-related compounds in various biological samples. The quantitative data collected in lipidomics experiments could be further applied in different areas, such as medical research, pharmaceutical and nutritional studies.

Preface

Chapter 2 of this thesis has been published as S. Mi, D.W. Lim, J.M. Turner, P.W. Wales and J.M. Curtis, "Determination of Bile Acids in Piglet Bile by Solid Phase Extraction and Liquid Chromatography-Electrospray Tandem Mass Spectrometry", *Lipids*, 51 (2016) 359-372. I was responsible for the experimental design, performance of experiments, data collection and analysis, as well as the manuscript composition. D.W. Lim, J.M. Turner and P.W. Wales assisted with sample preparation and contributed to manuscript edits. J.M. Curtis was the supervisory author and was involved with experimental design and manuscript composition.

Chapter 3 of this thesis has been published as S. Mi, Y-Y Zhao, R.F. Dielschneider, S.B. Gibson and J.M. Curtis, "An LC/MS/MS Method for the Simultaneous Determination of Individual Sphingolipid Species in B Cells", *Journal of Chromatography B*, 1031 (2016) 50-60. I contributed to the experimental design, performance of experiments, data collection and analysis, as well as the manuscript composition. Y-Y Zhao, R.F. Dielschneider and S.B. Gibson assisted with cell isolation, sample preparation and contributed to manuscript edits. J.M. Curtis was the supervisory author and was involved with experimental design and manuscript composition.

Appendix 1 of this thesis has been published as J.M. Curtis, S. Mi, "Hydrophilic Interaction Liquid Chromatography for Determination of Betaine" (Chapter 10) in: Victor R. Preedy (Ed.), *Betaine: Chemistry, Analysis, Function and Effects*, RSC publishing, London, 2015, pp. 139-158. I contributed to the literature review. J.M. Curtis and I wrote and revised the manuscript.

Appendix 2 of this thesis has been published as D.W. Lim, P.W. Wales, S. Mi, J.Y. Yap, J.M. Curtis, D.R. Mager, V.C. Mazurak, P.R. Wizzard, D.L. Sigalet, J.M. Turner, "Glucagon-Like Peptide-2 Alters Bile Acid Metabolism in Parenteral Nutrition-Associated Liver Disease", *Journal*

of Parenteral and Enteral Nutrition, 40 (2016) 22-35. J.M. Curtis and I contributed to conception and design of the tandem spectrometry work, and the acquisition, analysis of the tandem spectrometry data, interpretation of the bile acid composition in bile samples as well as the revision of the manuscript. D.W. Lim, P.W. Wales, J.Y.K. Yap, D.R. Mager, V.C. Mazurak, and J.M. Turner contributed to the conception and design of the research. D.W. Lim and P.R. Wizzard contributed to the acquisition of the data. D.W. Lim, P.W. Wales, J.Y.K. Yap, D.R. Mager, V. C. Mazurak, D.L. Sigalet, and J.M. Turner contributed to the analysis and interpretation of the data. D.W. Lim, P.W. Wales, and J.M. Turner drafted the manuscript.

Appendix 3 of this thesis has been published as R.F. Dielschneider, H. Eisenstat, S. Mi, J.M. Curtis, W. Xiao, J.B. Johnston, S.B. Gibson, "Lysosomotropic Agents Selectively Target Chronic Lymphocytic Leukemia Cells Due to Altered Sphingolipid Metabolism", *Leukemia*, 30 (2016) 1290-1300. J.M. Curtis and I performed the HPLC analysis of sphingolipids, collected and analyzed the data, as well as interpretation of the sphingolipid composition in the cell samples. Dielschneider and Eisenstat performed experiments and analyzed results. Work by R.F. Dielschneider and W. Xiao contributed to the funding for this project. J.B. Johnston and S.B. Gibson provided invaluable experimental design and editorial advice. R.F. Dielschneider and S.B. Gibson wrote paper.

Dedication

This work is dedicated to my parents, Shuying Wang and Yanjun Mi, for their endless support, guidance and love.

Acknowledgements

First and foremost I want to express my sincere appreciation and thanks to my supervisor Dr. Jonathan M. Curtis, for all his contributions of time, ideas and guidance during my 4-year PhD study and research. Dr. Curtis has supported me both academically and emotionally through the rough road to finish this dissertation. His patience and knowledge make my PhD experience amazing and stimulating.

I am grateful to the generous support from the China Scholarship Council (CSC) for the award and sponsorship throughout my PhD program.

I would also like to thank Dr. Richard Lehner and Dr. Rene Jacobs for serving as my committee members and for their insight and practical advice on the research projects and dissertation.

The members of the Lipid Chemistry Group have contributed immensely to my personal and professional life at University of Alberta. The group has been a constant source of friendship, collaboration and concern. A very special thanks goes out to Dr. Yuan-Yuan Zhao and Dr. Xiaohua Kong for continuous support, advice and encouragement. Mr. Ereddad Kharraz and Dr. Tolibjon Omonov, I am grateful to them for the great help in the lab and for creating good coffee breaks. I am also thankful to the following past and present labmates for their support and care during the course of my graduate studies--Dr. Brenna Ayre Black, Dr. Tuan Nurul Sabiquah Tuan Anuar, Dr. Chenxing Sun, Dr. Justice Asomaning, Metz, Yiran, Nuanyi, Siewmeng, Magdalena and Hossein.

The bile acid studies discussed in this dissertation would not have been possible without the help and advice from Dr. Justine Turner and David Lim of the Dept. of Pediatrics, University of Alberta. They collected piglet bile samples for this study and helped me improve my knowledge in the biomedical and clinical areas. Appreciation also goes out to Dr. Khosrow Adeli and Sarah

Farr at University of Toronto for supplying mouse intestinal samples to extend the application of the established method.

In regards to the sphingolipid analysis, I thank Dr. David Brindley and Raie Bekele from Dept. of Biochemistry, University of Alberta for providing me with ceramide standard solutions. Thanks also goes out to Dr. Spencer Gibson and Rebecca (DeLong) Dielschneider at University of Manitoba for their collaboration and provision of the B cell pellets.

Dr. Rene Jacobs and Yumna Zia from University of Alberta have provided me with mouse plasma samples for TMA and TMAO study. Many thanks to them.

I would also like to acknowledge Dr. Randall Weselake and his group from University of Alberta for providing us with tung oil and pomegranate oil samples for the in-line ozonolysis experiments.

Lastly, but absolutely not least, I would like to express my heart-felt gratitude to my family: my parents and my younger brother Siyuan Mi, for their endless encouragement, love and strength through my entire life.

Si Mi

University of Alberta

June 2016

Table of Contents

Abstract ii

Preface iv

Dedication vi

Acknowledgements vii

List of Tables xv

List of Figures xvii

List of Abbreviation xxi

Chapter 1 1

Introduction 1

1.1. Lipid Fundamentals 1

1.1.1. Definition 1

1.1.2. Lipid classification 1

1.2. Lipidomics 7

1.2.1. The emergence of lipidomics 7

1.2.2. The significance of analytical lipidomics 10

1.3. Sample Preparation Techniques for Lipid Analysis 11

1.4. Methods for Lipidomic Analysis 13

1.4.1. Chromatography-based methods 14

1.4.2. Spectroscopy-based methods 18

1.4.3. Mass spectrometry-based lipidomics 19

1.4.4. Capillary electrophoresis methods 23

1.5. Concluding Remarks 24

1.6. Hypothesis and Objectives 25

1.7. References 26

Chapter 2 36

A Method for the Determination of Bile Acids in Piglet Bile Using Solid Phase Extraction and Liquid Chromatography-Electrospray Tandem Mass Spectrometry 36

2.1. Introduction 36

2.2. Materials and Methods 40

2.2.1. Materials and reagents 40

2.2.2. Preparation of stock, work and quality control (QC) standard solutions 41

2.2.3. Sample preparation 42

2.2.4. Optimization of SPE conditions 42

2.2.5. LC/MS/MS conditions 43

2.2.6. Method validation 45

2.3. Results and Discussion 45

2.3.1. Optimization of SPE conditions 45

2.3.2. Optimization of chromatographic separation and mass spectrometric parameters 47

2.3.3. Method validation 52

2.3.4. Application to piglet bile samples 56

2.4. Conclusions 59

2.5. References 60

Chapter 3 63

An LC/MS/MS Method for the Simultaneous Determination of Individual Sphingolipid Species in B Cells 63

3.1. Introduction 63

3.2. Materials and Methods 68

3.2.1. Chemicals and reagents 68

3.2.2. Preparation of stock, work and quality control standard solutions 68

3.2.3. Sample preparation 69

3.2.4.LC/MS/MS conditions 70

3.2.5.Method validation 72

3.3. Results and Discussion 74

3.3.1. LC/MS/MS method development 74

3.3.2. Method validation 81

3.3.3. Stability 84

3.3.4.Application to cell samples 85

3.4. Conclusions 88

3.5. References 89

Chapter 4 92

Simultaneous Determination of Trimethylamine and Trimethylamine *N*-Oxide by HILIC LC/MS/MS: Quantification of Phospholipid Metabolites in Mouse Plasmas 92

4.1. Introduction 92

4.2. Materials and Methods 95

4.2.1. Materials 95

4.2.2. Preparation of stock, working and quality control standard solutions 95

4.2.3. Sample extraction 95

4.2.4. Optimization of parameters for derivatization 96

4.2.5. HPLC/MS/MS analysis 97

4.2.6. Method validation 98

4.3. Results and Discussion 100

4.3.1. Development of the derivatization procedure in standard solutions 100

4.3.2. Mass detection and chromatographic separation of TMA and TMAO 104

4.3.3. Method validation 108

4.3.4. Application to mouse plasma samples 111

4.4. Conclusions 114

4.5. References 115

Chapter 5 118

A Method for the Identification of Conjugated Linolenic Acid isomers in Pomegranate and Tung Seed Oils by Silver Ion-LC/MS with In-Line Ozonolysis (Ag^+-LC/O_3-MS) 118

5.1. Introduction 118

5.2. Materials and Methods 121

5.2.1. Materials 121

5.2.2. Preparation of CLnA methyl esters 122

5.2.3. Ag+-LC/O3-MS analysis of CLnA methyl esters 123

5.3. Results and Discussion 124

5.3.1. Preparation of CLnA methyl esters 124

5.3.2. Method development by Ag+-LC/O3-MS 125

5.3.3. Ag+-LC/O3-MS analysis of FAME mixtures from TSO samples 132

5.3.4. Ag+-LC/O3-MS analysis of FAME mixtures from PSO samples 136

5.4. Conclusions 139

5.5. References 140

Chapter 6 143

General Conclusions and Future Work 143

6.1. References 148

Bibliography 149

Appendix 1 168

Hydrophilic Interaction Liquid Chromatography for Determination of Betaine 168

A1.1. Introduction 168

A1.1.1. Basics of HILIC 168

A1.1.2. Summary and comparison to other analytical techniques used for analysis of betaine 173

A1.2. The Use of HILIC in the Determination of Betaine Concentrations 174

A1.2.1. Betaine in standard mixtures 174
A1.2.2. Betaine in samples of plant origin 175
A1.2.3. Betaine in samples of animal origin 178
A1.2.4. Betaine in food samples 181
A1.3. Conclusions and Future Perspectives 187
A1.4. References 187
Appendix 2 192
Glucagon-Like Peptide-2 Alters Bile Acid Metabolism in Parenteral Nutrition-Associated Liver Disease 192
A2.1. Introduction 192
A2.2. Materials and Methods 194
A2.2.1. Animals and surgical procedures 194
A2.2.2. Postsurgical animal care 194
A2.2.3. Parenteral nutrition 195
A2.2.4. Study design 196
A2.2.5. Data collection 197
A2.2.6. Data analysis and statistics 199
A2.3. Results 199
A2.3.1. Bile acid synthesis 199
A2.3.2. Bile acid transport 201
A2.3.3. Regulators of bile acid synthesis 203
A2.3.4. TGR5 messenger RNA (mRNA) expression 205
A2.3.5. Bile acid composition in bile 206
A2.3.6. Individual bile acid species in bile 209
A2.3.7. Rates of biliary output of bile acid species 210
A2.3.8. Liver bile acid concentration and content 211
A2.4. Discussion 213

A2.5. Conclusions 222

A2.6. References 223

Appendix 3 227

Lysosomotropic Agents Selectively Target Chronic Lymphocytic Leukemia Cells due to Altered Sphingolipid Metabolism 227

A3.1. Introduction 227

A3.2. Materials and Methods 229

A3.2.1. Cell culture 229

A3.2.2. Drugs and stimuli 230

A3.2.3. Western blotting 230

A3.2.4. Flow cytometry 231

A3.2.5. Confocal microscopy 231

A3.2.6. Lipid analysis 232

A3.2.7. Statistical analysis 233

A3.3. Results 233

A3.3.1. CLL cells are sensitive to lysosome disruption 233

A3.3.2. Siramesine-induced LMP causes mitochondrial dysfunction and subsequent cell death 238

A3.3.3. Siramesine-induced cell death requires lipid peroxidation 240

A3.3.4. Altered sphingolipid metabolism in CLL cells primes the lysosomes for disruption 243

A3.4. Discussion 247

A3.5. References 250

List of Tables

Table 1-1. Online resources with information on lipid molecular structures, classification and functions 10

Table 2-1. MRM transitions and optimized parameters for each compound 44

Table 2-2. Recoveries of tested bile acids under different SPE conditions 47

Table 2-3. Calibration curves, LODs, LOQs and linear dynamic ranges in the quantitative analysis 53

Table 2-4. Accuracy and precision for triplicate measurements of QC 54

Table 2-5. Extraction recovery of bile acids in a piglet sample 55

Table 2-6. Contents of bile acids determined in piglet bile sample extract (quantification with GCA-d_4 as IS). 59

Table 3-1. MRM transitions and optimized parameters for each compound. 71

Table 3-2. Calibration curves, LODs, LOQs and linear dynamic ranges in the quantitative analysis. 81

Table 3-3. Accuracy and precision for triplicate measurements of QC. 83

Table 3-4. Extraction recovery of sphingolipid metabolites in cellular extracts. 84

Table 4-1. Parameters assessed in the optimization of the derivatization reaction between TMA and ethyl bromoacetate. 97

Table 4-2. MRM transitions and optimized parameters for each compound. 98

Table 4-3. Calibration curves, LODs, LOQs and linear dynamic ranges. 109

Table 4-4. Extraction recoveries of TMA and TMAO in mouse plasma samples 110

Table 4-5. (A) Intraday accuracy and precision for triplicate measurements of QC; (B) Accuracy and precision for measurements of QC over 3 days 110

Table 5-1. Nominal *m/z* for in-line O_3/APCI(+)-MS diagnostic ions for CLnA positional isomer identification 129

Table A1-1. The determination of betaine from HILIC-based methods. A summary of published HILIC-based methods used for betaine analysis in a variety of samples 185

Table A2-1. Bile acid identification and quantification in pig bile..... 207

Table A2-2. Estimated rates of biliary output for bile acid species 210

List of Figures

Figure 1-1. Representative structures for each lipid category. 7

Figure 1-2. Analytical workflows in lipidomics. 9

Figure 2-1. A typical structure and classification of bile acid molecules. R5 can be replaced either by a free carboxylic acid group (classified as free bile acids) or by a glycine group or taurine group via an amide linkage (classified as conjugated bile acids). 40

Figure 2-2. ESI-MS/MS product ion spectra of (A) free bile acids (LCA as an example), (B) taurine-conjugated bile acids (TCA as an example), (C) glycine-conjugated bile acids (GDCA as an example), and (D) IS: GCA-d_4. 51

Figure 2-3. A representative chromatogram of bile acids in standard mixture solution at a concentration of 500 ng mL^{-1} using an Ascentis Express C18 column with established gradient elution. (1) TαMCA; (2) TβMCA; (3) THCA; (4) TCA; (5) GUDCA; (6) ωMCA; (7) αMCA; (8) βMCA; (9) TDCA; (10) HCA; (11) UDCA; (12) CA; (13) HDCA; (14) TLCA; (15) GDCA; (16) CDCA; (17) GLCA; (18) DCA; (19) LCA. 51

Figure 2-4. A representative chromatogram of bile acids in piglet bile sample extract under the established conditions. (A) THCA; (B) 1-THDCA, 2-TCDCA; (C) 1-GHDCA, 2-GCDCA; (D) IS: GCA-d_4; (E) HCA; (F) HDCA; (G) TLCA; (H) GLCA; (I) LCA. 58

Figure 3-1. Structures of the compounds under investigation 67

Figure 3-2. Metabolic pathway of sphingolipids (only including the target analytes in this study) (1), glucosylceramidase; (2), glucosylceramide synthase; (3), sphingomyelinase; (4), sphingomyelin synthase; (5), ceramidase; (6), ceramide synthase; (7), sphingosine kinase; (8), sphingosine phosphatase; (9), (10), dihydroceramide synthase; (11) (12) (13), Δ4-desaturase 67

Figure 3-3. ESI-MS/MS product ion spectra of (A) ceramide standard (C16:0-Cer as an example), (B) dihydroceramide standard (C16:0-dHCer as an example), (C) glucosylceramide standard (C16:0-GlcCer as an example), (D) d18:1-sphingosine and (E) d18:0-sphinganine-1-phosphate. 78

Figure 3-4. A representative chromatogram of sphingosine, sphinganine, sphingosine-1-phosphate, sphinganine-1-phosphate, ceramides, dihydroceramides and glucosylceramides in standard mixture solution at a concentration of 0.1 μM using an Ascentis Express C18 column with the established gradient elution. (1) d17:1-So; (2) d17:0-Sa; (3) d18:1-So; (4) d18:0-Sa; (5) d17:1-So1P; (6) d17:0-Sa1P; (7) d18:1-So1P; (8) d18:0-Sa1P; (9) C2:0-Cer; (10) C16h:0-GlcCer; (11) C16:0-GlcCer; (12) C18:1-GlcCer; (13) C17:0-GlcCer; (14) C16:0-Cer; (15) C18:0-GlcCer; (16) C16:0-dHCer; (17) C17:0-Cer; (18) C18:0-Cer; (19) C24:1-GlcCer; (20) C22:0-GlcCer; (21) C24:1-Cer; (22) C22:0-Cer; (23) C24:0-GlcCer; (24) C24:0-Cer; (25) C24:0-dHCer. 80

Figure 3-5. A representative LC chromatogram of sphingolipid metabolites detected in the B cell extracts under the established conditions. (1) d17:1-So; (2) d17:0-Sa; (3) d18:1-So; (4) d17:1-So1P; (5) d17:0-Sa1P; (6) C16:0-GlcCer; (7) C18:1-GlcCer; (8) C17:0-GlcCer (9) C16:0-Cer; (10) C18:1-Cer; (11) C18:0-GlcCer; (12) C17:0-Cer; (13) C18:0-Cer; (14) C20:0-GlcCer; (15) C22:1-GlcCer; (16) C22:1-Cer; (17) C20:0-Cer; (18) C24:1-GlcCer; (19) C22:0-GlcCer; (20) C24:1-Cer; (21) C22:0-Cer; (22) C24:0-GlcCer; (23) C24:0-Cer. 87

Figure 3-6. Contents of individual SPL species determined in B cells..... 88

Figure 4-1. Effects of experimental variables on the peak area of derivatized TMA: (A) amount of ethyl bromoacetate (4 mg mL^{-1} in acetonitrile), (B) amount of concentrated ammonium hydroxide and (C) reaction time. 103

Figure 4-2. ESI-MS/MS spectra of (A) TMAO, (B) TMAO-d_9, (C) Derivatized TMA and (D) Derivatized TMA-d_9. 107

Figure 4-3. An MRM chromatogram of an authentic standard mixture at a level of 50 ng mL^{-1}.. 107

Figure 4-4. A representative MRM chromatogram of (A) Derivatized TMA-d_9, (B) Derivatized TMA, (C) TMAO-d_9 and (D) TMAO in fasting male mouse plasma samples under the established conditions. 113

Figure 4-5. TMA and TMAO concentrations in fasting plasma samples taken from male mice.. 114

Figure 5-1. (A) the Ag^+-HPLC chromatogram of the conjugated linolenic acid methyl ester (CLnAMe) mixture (methylated using 8% (*v/v*) sulfuric acid at 40 ºC for 10 min): peaks at tR of 13.6, 16.4 and 19.8 min were identified as isomer 1 (8*t*, 10*t,* 12*t*-18:3), isomers 2 and 3 (9*c*, 11*t*, 13*t*-18:3 and 8*t*, 10*t*, 12*c*-18:3) and isomer 4 (9*c*, 11*t*, 13*c*-18:3), respectively; (B) the APCI(+)/MS spectrum of 9*c*, 11*t*, 13*t*-CLnAMe (example). 127

Figure 5-2. In-line O_3-APCI (+)-MS spectrum of (A) *9c*, 11*t*, 13*c*-CLnA methyl ester and (B) 8*t*, 10*t*, 12*t*-CLnA methyl ester 130

Figure 5-3. (A) Ag^+-LC/O_3-MS chromatogram of the conjugated linolenic acid methyl ester (CLnAMe) mixture (methylated using 8% (*v/v*) sulfuric acid at 40 ºC for 10 min): peaks at tR of 13.6, 16.6 and 20.1 min were identified as isomer 1 (8*t*, 10*t*, 12*t*-18:3), isomers 2 and 3 (9*c*, 11*t*, 13*t*-18:3 and 8*t*, 10*t*, 12*c*-18:3) and isomer 4 (9*c*, 11*t*, 13*c*-18:3), respectively; (B) the mass spectrum of peak at 16.6 min (2 isomers overlapped). 131

Figure 5-4. Extracted ion chromatograms of C18:3 FAME at *m/z* 293 (methylated using 0.8% (*v/v*) sulfuric acid at 40 ºC for 10 min) derived from TSO samples. 134

Figure 5-5. The Ag^+-LC/O_3-APCI(+)-MS analysis of CLnA components in TSO samples (methylated using 8% (*v/v*) sulfuric acid at 40 ºC for 10 min) (A) XIC of *m/z* 293; (B) mass spectrum averaged at 12.1 min and (C) mass spectrum averaged at 14.7 min. 135

Figure 5-6. Extracted ion chromatogram of C18:3 FAME at *m/z* 293 (methylated using 8% (*v/v*) sulfuric acid at 40 ºC for 10 min) derived from PSO samples. 137

Figure A1-1. The HILIC chromatography apparatus.. 169

Figure A2-1. (A) Schematic representation of the genes involved in bile acid homeostasis that were analyzed. (B) CYP7A1 expression is controlled by a complex regulatory mechanism. ... 200

Figure A2-2. Relative expression of genes involved in bile acid synthesis and regulation. 201

Figure A2-3. Relative expression of genes involved in hepatic bile acid export. 203

Figure A2-4. Relative expression of genes involved in the regulation of CYP7A1. 205

Figure A2-5. Relative expression of GPBAR1 mRNA. 206

Figure A2-6. Bile acid composition in bile. 208

Figure A2-7. (A) Mean liver total bile acid concentration; (B) Mean liver total bile acid content. 212

Figure A3-1. CLL cells are sensitive to lysosome disruptors. 237

Figure A3-2. Lysosome permeabilization is accompanied by TFEB translocation. 236

Figure A3-3. Siramesine-induced cell death involves lipid peroxidation and loss of mitochondrial membrane potential. 239

Figure A3-4. Siramesine-induced cell death requires lipid ROS, but not soluble ROS. 241

Figure A3-5. Early lipid peroxidation is required to affect mitochondria. 242

Figure A3-6. CLL cells are more sensitive to siramesine and have more lysosomes, SPP1, and sphingosine than normal B cells. 245

Figure A3-7. Excess sphingosine causes lysosome disruption. 246

List of Abbreviation

Ag^+-LC/O_3-MS	Silver Ion-Liquid Chromatography/in-line Ozonolysis/Mass Spectrometry
APCI	Atmospheric Pressure Chemical Ionization
APPI	Atmospheric Pressure Photoionization
BA	Bile Acid
CA	Cholic Acid
CE	Capillary Electrophoresis
Cer	Ceramide
CDCA	Chenodeoxycholic Acid
CID	Collision-Induced Dissociation
CLA	Conjugated Linoleic Acid
CLL	Chronic Lymphocytic Leukemia
CLnA	Conjugated Linolenic Acid
DAG	Diacylglycerol
DCA	Deoxycholic Acid
dHCer	Dihydroceramide
ESI	Electrospray Ionization
FA	Fatty Acid
FAME	Fatty Acid Methyl Esters
FT	Fourier Transform
GC	Gas Chromatography
GCA-d_4	Glycocholic Acid-2, 2, 4, 4-d_4

GCDCA	Glycochenodeoxycholic Acid
GDCA	Glycodeoxycholic Acid
GHDCA	Glycohyodeoxycholic Acid
GL	Glycerolipids
GLC	Gas Liquid Chromatography
GLCA	Glycolithocholic Acid
GlcCer	Glucosylceramides
GLP-2	Glucagon-Like Peptide-2
GP	Glycerolphospholipids
GSL	Glycosphingolipids
GUDCA	Glycoursodeoxycholic Acid
HCA	Hyocholic Acid
HDCA	Hyodeoxycholic Acid
HILIC	Hydrophilic Interaction Chromatography
HR/AM	High-Resolution/Accurate-Mass
IS	Internal Standard
LA	Linoleic Acid
LC/MS/MS	Liquid Chromatography-Tandem Mass Spectrometry
LCA	Lithocholic Acid
LLE	Liquid-Liquid Extraction
LN	α-Linolenic Acid
LOD	Limit of Detection
LOQ	Limit of Quantification

MAG	Monoacylglycerols
MALDI	Matrix-Assisted Laser Desorption Ionization
MCA	Muricholic Acid
MRM	Multiple Reaction Monitoring
MUFA	Mono-Unsaturated Fatty Acids
m/z	Mass-to-Charge Ratio
NL	Neutral Loss
NMR	Nuclear Magnetic Resonance
NP	Normal Phase
PA	Phosphatidic Acid
PC	Phosphatidylcholine
PE	Phosphatidylethanolamine
PG	Phosphatidylglycerol
PI	Phosphatidylinositol
PK	Polyketides
PL	Phospholipids
PNALD	Parenteral Nutrition-Associated Liver Disease
PR	Prenol Lipids
PS	Phosphatidylserine
PSO	Pomegranate Seed Oils
PUFA	Poly-Unsaturated Fatty Acids
QC	Quality Control
RP	Reverse Phase

Sa	Sphinganine
Sa1P	Sphinganine-1-Phosphate
SFC	Supercritical Fluid Chromatography
SFE	Supercritical Fluid Extraction
SIMS	Secondary Ion Mass Spectrometry
SIR	Selected Ion Recording
SL	Saccharolipids
SM	Sphingomyelin
sn	Stereospecific Number
So	Sphingosine
So1P	Sphingosine-1-Phosphate
SP	Sphingolipids
SPE	Solid Phase Extraction
SRM	Selected Reaction Monitoring
ST	Sterol Lipids
TAG	Triacylglycerol
TCA	Taurocholic Acid
TCDCA	Taurochenodeoxycholic Acid
TDCA	Taurodeoxycholic Acid
THCA	Taurohyocholic Acid
THDCA	Taurohyodeoxycholic Acid
TIMS	Tissue Imaging Mass Spectrometry
TLC	Thin-Layer Chromatography
TLCA	Taurolithocholic Acid

TMA	Trimethylamine
TMAO	Trimethylamine *N*-Oxide
TMCA	Tauromuricholic Acid
TOF	Time-of-Flight
RT	Retention Time
TSO	Tung Seed Oils
UDCA	Ursodeoxycholic Acid
UPLC	Ultra Performance Liquid Chromatography

Chapter 1

Introduction

1.1. Lipid Fundamentals

1.1.1. Definition

There is no precise definition of what is meant by a “lipid”. Lipids are chemically regarded as a group of compounds that are insoluble in water, but soluble in organic solvents, such as hexane, ether or acetone [1]. They are derived from living organisms and involved in many biological activities [2]. For example, lipids (such as triacylglycerols) are important storage sources of energy, especially for the long-term storage [3]. Lipids are also known as structural components of biological membranes [4]. An example of this is demonstrated by phospholipids and sphingolipids which can form membrane bilayers owing to the amphiphilic properties and maintain fluidity and flexibility of the membrane [5]. Meanwhile, many lipids play vital roles in intracellular signal transmission [2, 3]. Sphingolipids, such as ceramides and sphingosine-1-phosphate, can act as second messengers during signal transduction; diacylglycerols (DG) and acyl-CoA can be used as signaling molecules; fatty acids (FA), FA-CoA and bile acids (BA) can work as ligands for nuclear receptor.

1.1.2. Lipid classification

Lipids consist of a vast number of molecular species that are distinct both structurally and functionally. The estimated number of lipid molecular species is at the order of hundreds of thousands [3, 6]. They are divided into eight categories by the International Lipid Classification and Nomenclature Committee, including fatty acyls (FA), glycerolipids (GL), glycerolphospholipids (GP), sphingolipids (SP), sterol lipids (ST), prenol lipids (PR),

saccharolipids (SL), and polyketides (PK) [7, 8]. Examples of chemical structures for the eight lipid categories are shown in **Figure 1-1**. As for SL and PK, there is no single general structure for the whole lipid class. Thus, a representative structure for each class was selected and displayed in **Figure 1-1**. Four categories of lipids and their metabolites including ST (Chapter 2), SP (Chapter 3), GP (Chapter 4) and FA (Chapter 5), were studied in this thesis.

Fatty acids (FA) are widely distributed in natural fats, dietary oils and living organisms [9, 10]. They are a group of molecules with a relatively simple structure, existing in free forms or as building blocks of more complex lipid classes, such as phospholipids (PL) and SP [11]. A typical FA molecule consists of a carboxylic acid attached to an aliphatic hydrocarbon chain [9]. FA molecules vary in chain length (number of carbon atoms), the degree of unsaturation (number of double bonds) and in the configuration of their double bonds. Therefore, various classifications of FA can be proposed. Taking the degree of unsaturation as an example, FA can be categorized into saturated (no double bonds), monounsaturated (one double bond) and polyunsaturated (more than two double bonds) types. If the configuration of double bonds is taken into consideration, monounsaturated FA (MUFA) can be described as *cis* or *trans*, with the latter one receiving more attention because of their possible negative health effects [11, 12]. For each single polyunsaturated FA (PUFA) molecular species, there are numerous possible FA isomers that are combinations of *trans/cis* isomers and double bond positional isomers. Other major lipid species within this category are the fatty esters, fatty amides, fatty aldehydes, fatty nitriles, branched- and oxidized-FA (such as eicosanoids, docosanoids and FA containing hydroxylated and epoxylated groups) [13, 14, 15].

Glycerolipids (GL) refer to a class of lipid compounds which contain the structural features of a glycerol backbone usually esterified to a FA chain. On the basis of the number of esterified FA,

it can be categorized as triacylglycerols (TAG), diacylglycerols (DAG) and monoacylglycerols (MAG). TAG are the main constitutes of vegetable oils and animal fats [16]. MAG and DAG are widely used as emulsifiers in the food industry [17], which can be produced by the hydrolysis of TAG.

Glycerolphospholipids (GP) contain a vast number of compounds which have similar structural composition of a glycerol moiety, one or two esterified fatty acids and a distinct phosphoryl head group. The phosphoryl head group is usually attached at the *sn*-3 position of the glycerol moiety. Different substitutions on the phosphate group lead to the sub-classification of GP into phosphatidic acid (PA), phosphatidylcholine (PC), phosphatidylethanolamine (PE), phosphatidylinositol (PI), and phosphatidylserine (PS) [18]. Within each GP class, individual molecular species vary in the characteristics of esterified FA chains with respect to the chain length and degree of unsaturation. Amongst phospholipid (PL) molecules, sphingomyelin (SM) is an exception because of its distinct molecular structure derived from sphingosine rather than glycerol. Hence, it is classified as a sphingolipid molecule (SP) rather than as a GP.

Sphingolipids (SP) mainly include free sphingoid bases, ceramides (Cer), neutral glycosphingolipids (GSL), sphingomyelins (SM), sulfatides and gangliosides. The sphingoid base (or long-chain base) is the common structure of all SP molecules [19]. Cer is derived from the sphingoid base by linking a fatty acid chain (varying in length and degree of unsaturation) via an amide bond [20, 21]. Addition of sugar moieties or PC to the 1-hydroxyl group of Cer leads to the formation of more complex SP, GSL and SM [20]. Gangliosides are structured by a modified GSL molecule with one or more sialic acids linked on the sugar moiety [22]; similarly, sulfatides are also formed via esterified linkage of a sulfate group to the sugar group on GSL molecules [19]. Considering all these structural characteristics of SP, a tremendous number of individual molecular

species are possible due to variations in their polar head groups, FA chains and the long-chain sphingoid bases [21].

Sterol lipids (ST) represent a vital class of bioactive compounds derived from hydroxylated polycyclic isopentenoids having a 1, 2-cycopentanophenthrene structure [23]. In general, ST can be divided into two subclasses depending on their different origins, that is, phytosterols from plants and zoosterols from animals. There is a great deal of interest in the analysis of phytosterols (both free and conjugated forms) from different sources due to their important biological and nutritional roles [24, 25]. The major sources of phytosterols are vegetable oils and margarines, followed by vegetables, seeds and pods [25]. In addition to ST, compounds studied under this topic also contain cholesterol (metabolites of ST), steryl esters, bile acids and other related steroids. Cholesterol is an important part of the biological membrane and widely distributed in various animal tissues in high abundance [15, 23]. It serves as a precursor of bile acids which contain a group of compounds characterized by a common steroid skeleton.

Prenol lipids (PR) are synthesized via the polymerization of the five-carbon precursors dimethylallyl pyrophosphate and isopentenyl pyrophosphate [26]. Within this class, lipid compounds can be subdivided into isoprenoids, quinones and hydroquinones, polyprenols and hopanoids according to their structural features [26]. The isoprenoids are formed by the successive addition of C5 isoprene units and when there are >8 isoprene units (more than 40 carbons) present in the molecular structures, they are defined as polyterpenes. Note that vitamin A and carotenoids are also considered as simple isoprenoids. As for quinones and hydroquinones, their molecular structures are characterized by a quinonoid core of non-isoprenoid origin and an attached isoprenoid tail. Examples of this type of lipids include the fat-soluble vitamins E and K, as well as the ubiquinones (also known as Coenzyme Q10) [26, 27]. Polyprenols has been found to be present

in bacteria, animal and plants. The hopanoids are five-ring pentacyclic compounds and have been relocated to the PR category from the SL category [28].

Saccharolipids (SL) consist of compounds which contain a sugar backbone and the ester-bonded FA. It includes a considerable number of molecules due to the combination of different carbohydrates and lipids. According to the LIPID MAPS Lipid Classification System, SL are further classified as acylaminosugars, acylaminosugar glycans, acyltrehaloses and acyltrehalose glycans [26]. A well-known example of SL is the acylated glucosamine precursors of the lipid A component of the lipopolysaccharides (LPS) that are present in the outer membranes of most Gram-negative bacteria [8, 26].

Polyketides (PK) account for a class of natural compounds with diverse biological activities and pharmacological properties. They are produced by certain living organisms including bacteria, fungi, plants, and invertebrates at the presence of classic enzymes as well as iterative and multimodular enzymes [26, 28]. They have been classified as lipids because most of them are relatively soluble in organic solvents. Based on the structural features, PK are divided into three subclasses: type I (macrolides polyketides produced by multimodular megasynthases), type II (aromatic polyketides produced by the iterative action of dissociated enzymes), and type III (small aromatic polyketides produced by fungal species). Polyketide antibiotics, antifungals, cytostatics, anticholesteremic, antiparasitics, coccidiostats, animal growth promoters and natural insecticides are commercially available [26].

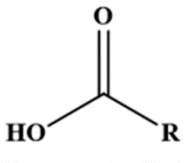

Fatty acids (FA)

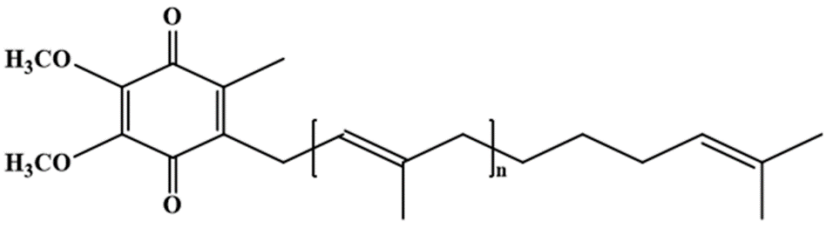

Prenol lipids (PR)

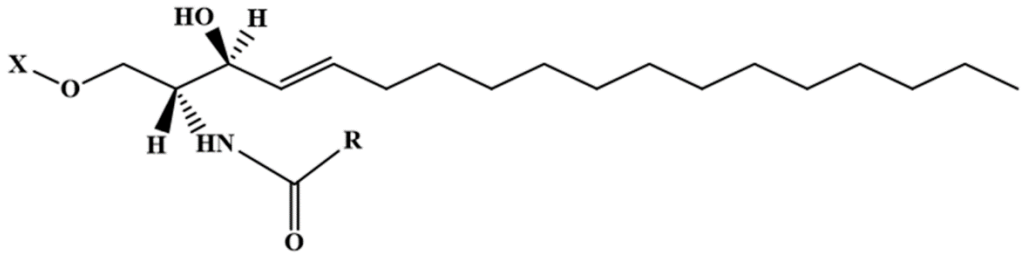

Sphingolipids (SP)

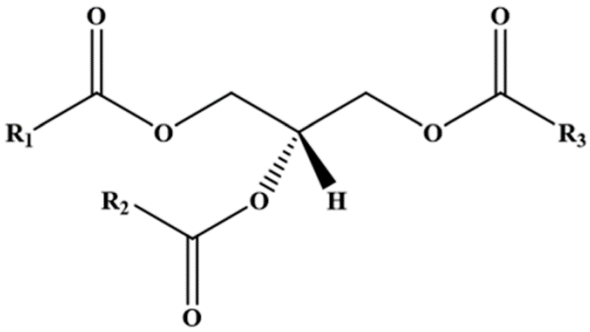

Glycerolipids (GL)

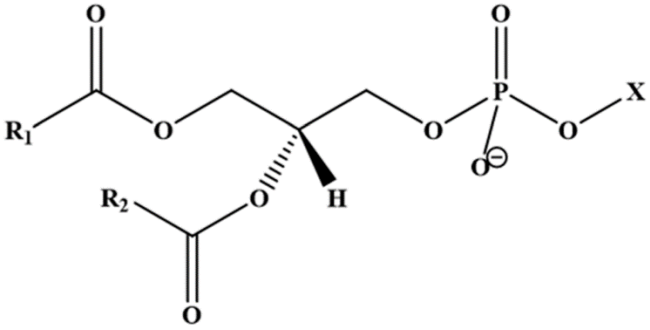

Glycerophospholipids (GP)

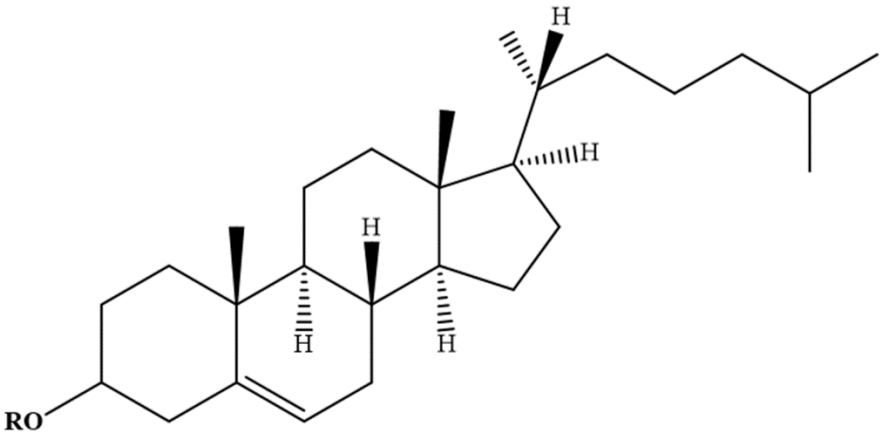

Sterol lipids (ST)

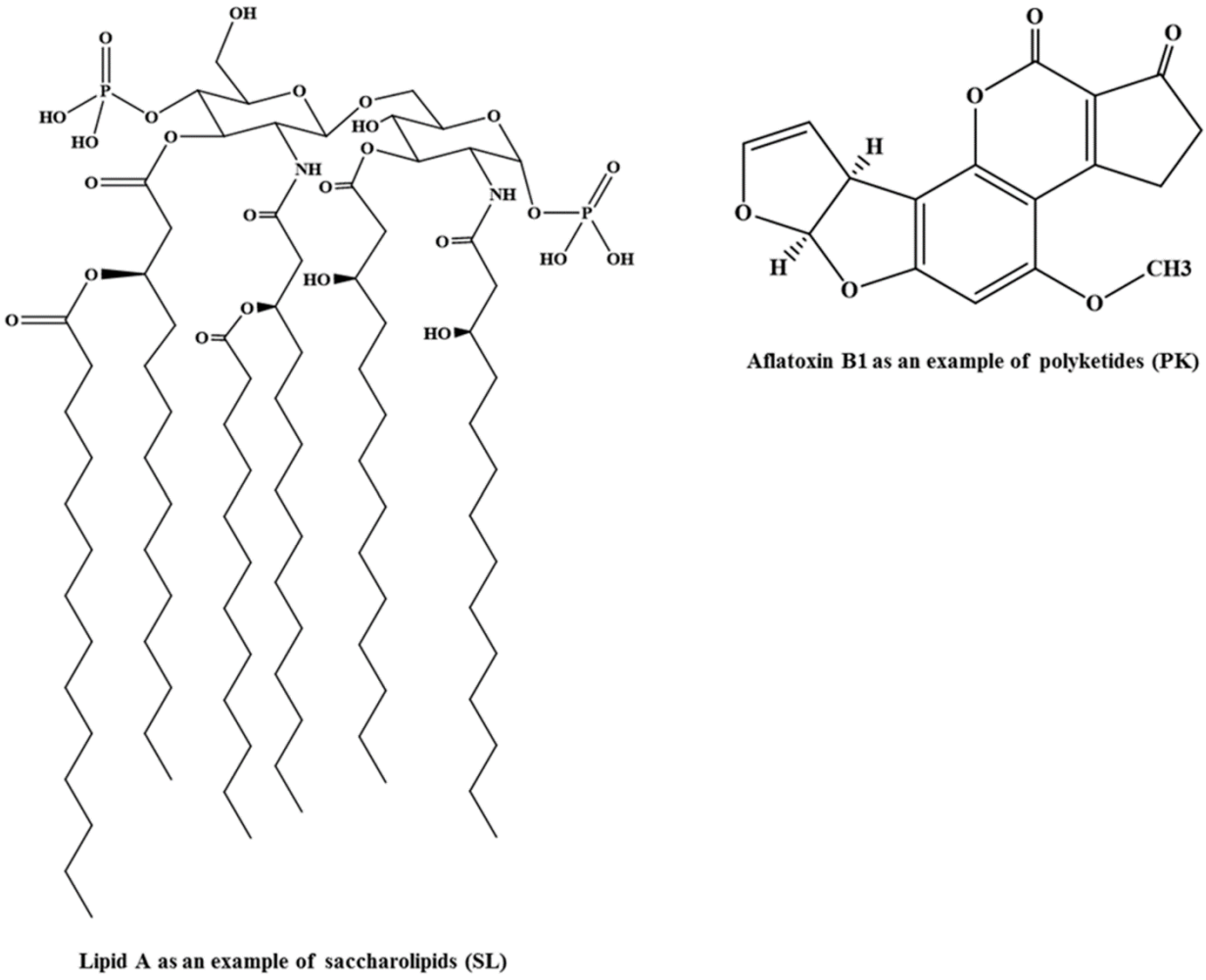

Figure 1-1. Representative structures for each lipid category.

1.2. Lipidomics

1.2.1. The emergence of lipidomics

In recognition of their roles in biology, lipids were intensively studied during the period from 1960s to 1980s [3, 5]. Later, research attention moved towards the "omics" science in biology, where comprehensive system level bioanalysis is performed, such as in genomics and proteomics. More recently, this approach has been extended into studies of the diversity of lipid structures and

functions as well as their interaction with other biomolecules such as proteins. Hence, lipidomics has been included into the ongoing "omics" revolution [5]. The advancements in analytical techniques such as mass spectrometry (MS) and chromatography, combined with sophisticated computational tools (including data acquisition, bioinformatics, etc.) have largely driven the emergence and expansion of lipidomics [3, 15, 29].

Lipidomics is a research discipline aiming at the comprehensive analyses of the entire lipid components of a system. Based on the range of investigated analytes, the emerging field of lipidomics can be categorized into targeted lipidomics and non-targeted lipidomics (also known as global lipidomics) [3, 8]. For targeted lipid analysis, the focus is mainly on a few lipids or a defined class of lipid metabolites which are expected to be crucial in a given context. The targeted lipidomic approach is usually more specific, highly sensitive and confers relative ease in terms of data processing, but with inevitable loss of information pertaining to other lipid species [7]. In non-targeted lipid profiling, the aim is to reliably analyze as a wide range of lipids as possible in a single run [7, 29, 30]. This strategy is excellent for discovery of novel lipids or unexpected lipid species, but that it makes huge assumptions based on response factors, ion suppression, standardized separations and extractions to allow comprehensive analyses without detailed knowledge of the lipids that are actually present. It is important to note that different analytical aims require different analytical techniques. By way of example, LC/MS-based platforms are most widely performed for the targeted lipid profiling in biological samples (cell, tissues and biofluids), while MS in full scan mode (profiles) without chromatographic separation is more feasible for a global (non-targeted) lipidomic analysis. When the research objectives are taken into account, lipidomics studies can be classified as qualitative lipidomics and quantitative lipidomics. Qualitative lipidomics aims to address the question of which lipids are present in the samples,

while quantitative lipidomics can be further divided into two categories: absolute *vs*. relative quantifications [100]. Absolute quantification can measure the actual smount of a lipid species, subclass or total lipids in the target samples. Absolute quantification gives a reliable meaure of the magnitude of an analyte which should be reproducible between laboratories and over time, as well as having intrinsic significance to the system being studied. In contrast, relative quantification is widely used show to show the changes in the abundances of lipid molecular species, subclasses or total lipid amounts when comparing between treatment groups, over time or with controls. This approach is extremely valuable as a tool to find better treatments or therapeutic strategies [100, 101]. However, relative quantification only applies to the biological system tested and hence only general comparisons with experiments in other laboraties can be made. The focus of this thesis is on the absolute and accurate quantifications of individual lipid molecular species in the biological systems, which was mainly achieved using the constructed internal calibration curves. Analytical workflows in lipidomics are illustrated in **Figure 1-2**.

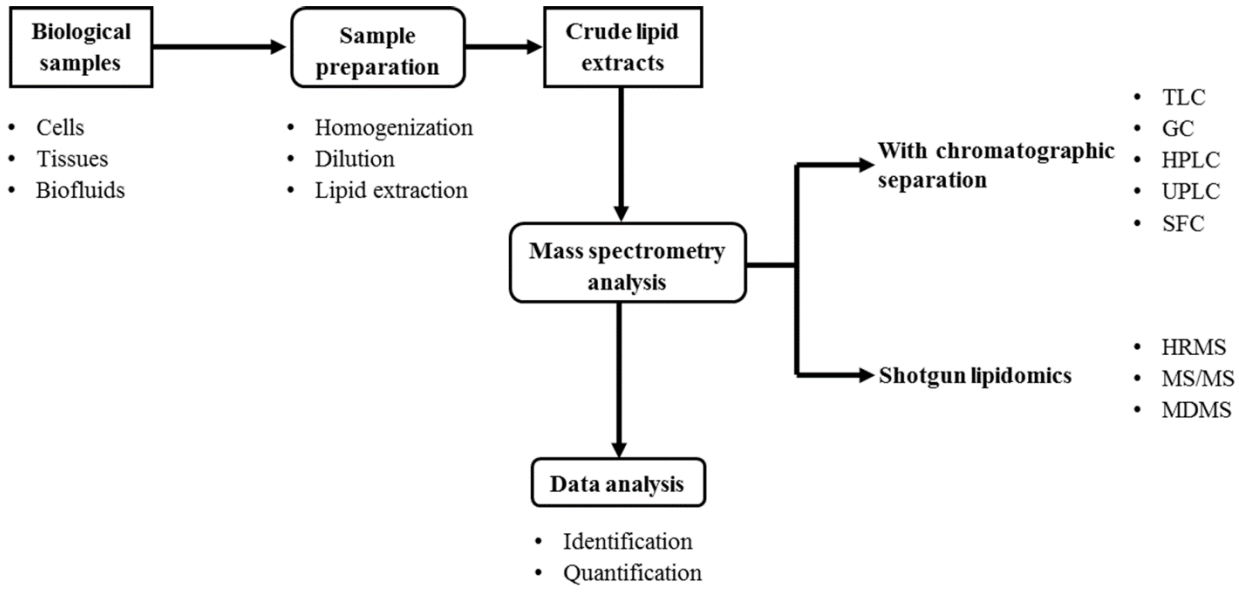

Figure 1-2. Analytical workflows in lipidomics.

1.2.2. The significance of analytical lipidomics

There is an increasing awareness across many disciplines of the biological importance of lipid metabolites [32]. Lipid homeostasis plays an integral role in health maintenance [7] and imbalances in lipid metabolism can cause many diseases, such as insulin-resistant diabetes [29, 32], Alzheimer's disease and cancer [3]. Accordingly, lipidomics can be used as a powerful tool for the investigation of biochemical and biological mechanisms underlying lipid-related diseases and their comorbidities through monitoring alterations in lipid signaling, metabolism, trafficking, and homeostasis [30, 33, 34]. In addition, by employing targeted and quantitative approaches, lipidomics can be performed for disease biomarker and drug target discovery that facilitates diagnosis of disease states and development of potential therapeutic strategies [29, 33]. Furthermore, the data obtained from lipidomic investigations is complementary to that from other investigations on tissues, cells and biological fluids using genomics, proteomics, and metabolomics. There are many useful online resources providing a wealth of information on lipid molecular structures, classification and functions. They are summarized in **Table 1-1**.

Table 1-1. Online resources with information on lipid molecular structures, classification and functions.

Resources	URL[a]	Description
LIPID MAPS	http://www.lipidmaps.org	LIPID MAPS is sponsored by a grant from the Wellcome Trust.
LIPID BANK	http://lipidbank.jp	LIPID BANK is official database of the Japanese Conference on the Biochemistry of Lipids (JCBL).
AOCS Lipid Library	http://lipidlibrary.aocs.org	This resource is owned and managed by American Oil Chemists' Society and mainly provides information on lipid science and technology.
Lipidomics Expertise Platform	http://www.lipidomics-expertise.de	This platform is supported by the European Lipidomics Initiative,

		European Commission. It gathers information on lipidomics expertise, lipid standards and methods.
LIPIDAT	http://www.lipidat.chemistry.ohio-state.edu	It is supported by the National Science Foundation, LIPIDAT Group, Department of Chemistry, The Ohio State University. This database provides thermo data and association information on lipid mesomorphic and polymorphic transitions.
Cyberlipid Center	http://www.cyberlipid.org	This is an online, non-profit scientific website aiming to collect, study and diffuse information on all aspects of lipidology.

[a] These are open access website.

1.3. Sample Preparation Techniques for Lipid Analysis

In most analytical methodologies, sample preparation is the first and an unavoidable step. The major aims of these procedures are to quantitatively recover the analytes from the matrix, reduce interferences from other substances and concentrate the target analytes so as to achieve optimal measurement accuracy and precision [35, 36].

With respect to the techniques applied for lipid extraction, many advances have taken place going from conventional solvent extraction, to solid-phase extraction (SPE) and finally to some more recent innovations such as supercritical fluid extraction (SFE) [36, 37]. The “classic” lipid extraction protocols were proposed by Folch and co-workers in 1957 using a solvent composition of $CHCl_3$: CH_3OH (2:1, *v/v*) in brain tissues [37, 38]. Solvent extraction is achieved based on the relative solubility of target analytes in the selected extraction solvents. There is a very large polarity range for lipid compounds, for example, TAG compounds are very hydrophobic whereas gangliosides are much more polar [8]. Hence, there is no single ideal organic solvent suitable for

comprehensive lipid extraction. Thus, various solvent and reagent compositions were exploited to fulfill different analytical objectives. Amongst these, a combination of $CHCl_3$, CH_3OH and H_2O (1:2:0.8, *v/v/v*) is the most famous, called the Bligh-Dyer method originally used for the extraction and purification of lipids from frozen fish [39, 40]. In classical organic solvent extraction, the volume and toxicity of the extraction solvent used need to be taken into consideration, especially for food lipid extraction. With the development of column techniques, a more modern technique known as SPE was introduced for lipid extraction from foods and biological tissues in the late 1970s [41]. This technique allows minimizing the toxic solvent consumption [42] and is characterized by the usage of cartridges which could possibly be packed with polar (normal phase), non-polar (reverse phase), ionic or polymeric materials [35]. Availability of these sorbents with different properties makes this technique very reproducible and applicable for various lipid types ranging from polar to neutral. More recently, another extraction technique, SFE, has gained an increasing interest in its application for isolation of lipids from sample matrices. This is, to a large extent, due to the advent of supercritical CO_2 as the extraction medium which is nontoxic, cost-effective and non-explosive. These properties greatly ease the worries about health and safety-related issues along with the use of organic solvents in the solvent extraction [43] and make this as a green extraction technique which is the focus of Green Analytical Chemistry (GAC) [44]. Also, no extra procedures, such as evaporation, are needed for solvent removal after extraction. However, there are also some drawbacks brought by the properties of supercritical CO_2. It is an extraction medium with low polarity; its application is therefore limited to the extraction of lipids with similar polarity. To address this problem, a modifier, such as methanol, ethanol or even water [1], is added to the supercritical CO_2, hence extending the adoption of SFE to a larger scale. The examples of its application include dehydrated foods, meats and fried foods [1].

Apart from the sample treatment strategies discussed above, several other methods based on novel technologies have been proposed for lipid extraction. Although they may not be employed in such a wide range as the previous three ones, the advent of them is still important and provides a clear improvement of the extraction processes based on a dramatic reduction in time and temperature and solvent requirements [44]. These new methods contain microwave-assisted extraction (MAE), ultrasound-assisted extraction and dispersive liquid-liquid micro-extraction (DLLME) [37]. Examples of their introduction and application for lipid extraction can be found in the published papers [11, 45, 46, 47].

The selection of an appropriate extraction procedure depends largely on the chemical and physical properties of target analytes, the matrix (gas, liquid or solid) and on the final measurement mode [44]. There is no one standard extraction protocol which is optimal for all of these types of samples. For lipids which exhibit a large diversity in structure and polarity, combined extraction strategies (two or more) would be carried out to accomplish the desired analytical goal [48].

1.4. Methods for Lipidomic Analysis

The molecular diversity and complexity of lipid species result in a wide range of physiochemical properties such as solubility and polarity. This poses a significant challenge for researchers when attempting the global analyses of the lipidome in biological samples, such as in tissues, cells and biofluids. Hence, the development of more comprehensive analytical/biochemical technologies for the identification and quantification of the various lipid species in the lipidome is required [7]. The system-wide lipid analysis (lipidomics) may involve the determination of total lipid contents, separation into specific lipid class according to their structural properties as well as identification and eventually quantitative determination of a

specific class, subclass or individual lipid molecular species (also including the metabolites) [49]. There have been numerous analytical strategies created over the years for the characterization of lipids in many different sample origins. These include, but are not limited to, enzymatic methods, immunochemical methods and sophisticated instrumental methods [1].

The present chapter introduces the instrumental techniques used in this thesis, including chromatography-based methods and mass spectrometry (MS)-based approaches. In addition, spectroscopy-based methods and capillary electrophoresis (CE) which are also important in lipidomics (but were not used in this thesis research) are introduced.

1.4.1. Chromatography-based methods

Chromatographic techniques have a large number of applications in the area of lipidomics. They mainly consist of thin layer chromatography (TLC), gas chromatography (GC) or gas-liquid chromatography (GLC), liquid chromatography (LC), supercritical fluid chromatography (SFC) and silver-ion chromatography.

In the 1980s, crude lipid extracts were mostly analyzed by TLC using precoated glass or plastic plates to determine which lipid classes (such as non-polar lipids, GSL and PL) were present, but not the individual lipid species [5, 50, 51]. There are three major types in usage, including normal-phase TLC (NP-TLC), reversed-phase TLC (RP-TLC) and silver ion TLC (Ag^+-TLC) [51]. TLC is a relatively easy and cost-effective technique, but its widespread application in lipidomics has been limited by the low resolution and sensitivity [27, 51].

Nowadays, GC-based methods still enjoy popularity in lipid research, especially for those volatile and thermally-stable lipid compounds such as isovaleric acid and α-methylbutyric acid [11]. For compounds without these properties, derivatization steps, such as methylation or

silylation prior to analysis, are always required in order to attain the volatility and improve the peak configuration and the sensitivity [11].

LC has been utilized in lipidomics to aid in the identification, quantification and structure elucidation of lipid classes and molecular species in complex biological system. Two widely used separation modes are NPLC and RPLC. NPLC separation is obtained according to the surface adsorption of involving hydrogen bonding, electrostatic forces and dipole-dipole interactions between the analytes and the stationary phase. For RPLC version, separation is achieved based on the partition of analytes between relatively non-polar stationary phases and polar mobile phases which consist of aqueous phase and organic phase, mostly acetonitrile, methanol and isopropanol based mixtures [51]. According to the separation mechanisms, NPLC is especially suitable for the lipid class separation, whereas RPLC is capable of the separation of individual molecular species within the same class.

Apart from the above-described NPLC and RPLC, hydrophilic interaction chromatography (HILIC) is another LC-based method introduced by Andrew Alpert in 1990 to separate extremely polar and hydrophilic compounds such as PL and PL-related metabolites [52, 53, 54]. The HILIC LC technique is comprised of a hydrophilic stationary phase and a binary mobile phase system of water and acetonitrile [54]. This technique is readily compatible with ESI-MS, resulting in high sensitivity and improved peak shapes [55, 56]. In comparison with the more conventional RPLC techniques, HILIC has the advantage of providing high retention of highly hydrophilic and polar molecules but with less requirement for ion-pair reagents. The typical elution order is similar to that found in NPLC with the less polar compounds eluting ahead of the more polar ones [54].

Another important LC-based technology for lipid analysis comes along with the advent of

high-resolution "Ultra Performance" liquid chromatography (UPLC) which builds on the same principles of HPLC but employs alkyl-bonded porous particles with a particle size less than 2 μm in diameter performed at elevated pressures (15, 000 psi) [4, 57]. UPLC allows high peak capacity and fast separation without loss of chromatographic performance [57]. One recent review article exists focused on the summary of UPLC/MS techniques in lipidomic applications [37].

SFC was originally proposed as an alternative to LC and GC. In this separation technique, a supercritical fluid is used as the mobile phase. Supercritical carbon dioxide (SC-CO_2) is most commonly used for this purpose owing to its physiochemical properties, such as low critical pressure (73 bar), temperature (31 ˚C) and chemical inertness [27, 58]. Also, the low viscosity and high molecular diffusiveness of SC-CO_2 will lead to higher column efficiencies and increased flow rates, allowing for rapid analysis with lower backpressure [27, 58]. Considering the nonpolar character of neat CO_2, separation of polar compounds such as SP and PL could be achieved by addition of small amounts of a polar organic modifier or additive such as methanol [27, 58, 59]. Like the SFE technique used for sample preparation, SFC represents a trend in separation techniques towards green analytical chemistry (GAC) by using non-toxic and non-explosive SC-CO_2 as the mobile phase.

Silver ion chromatography (SIC) was developed relying on the property that silver ions (Ag^+) form weak reversible charge-transfer complexes with π-electrons of unsaturated centres in organic molecules, thus allowing for separation based on the total number, configuration and position of the double bonds [51]. It has been has been adopted in TLC (Ag^+-TLC), HPLC (Ag^+-HPLC), SFC (Ag^+-SFC) and SPE (Ag^+-SPE) [60]. Sun *et al*. [61] proposed a new method in which silver ion liquid chromatography was coupled to in-line ozonolysis/MS (Ag^+-HPLC/O_3-MS) to identify conjugated linoleic acid (CLA) isomers. Results demonstrated that the newly created method could

be applied for identification of CLA positional isomers and most of the geometric isomers in complex samples such as milk fat; moreover, in-line ozonolysis used here was another advance in the identification of CLA isomers. A limitation of silver ion column is the short lifetime which is caused by the release of silver ions from the stationary phase. Another drawback of this technique is the frequent formation of corrosive silver nitrate precipitates which may damage the tubing and detection system [51].

There are several analytical challenges that cannot be addressed satisfactorily with a singly-used analytical technique even with high resolution chromatographic techniques [30]. To overcome these limitations, hyphenated and orthogonal technologies have been extensively developed [62]. These include two-dimensional (2D) TLC [50], 2D-LC [63], 2D-GC [64, 65], 2D-SFC [66] and on-line LC-GC [67, 68, 69]. The use of two chromatographic techniques with different separation mechanisms in combination greatly contributes to the improvement of separation power, thus allowing comprehensive lipid analysis. Sun *et al*. [70] developed a 2D-LC method system for the separation and identification of PC isobaric species in the lipid extract samples. In this method system, HILIC was used as the first dimension for lipid class separation, while RPLC separation with a C18 column was performed as the second dimension to obtain the structural information of individual molecular species. The advent of these techniques has greatly improved the separation efficiency and potentially reduced the amount of work sample preparation needed.

At the moment, probably the most universal couplings is the combination of a chromatographic separation and mass spectrometry or tandem mass spectrometry, such as LC/MS or LC/MS/MS [62]. These can be used in conjunction with different types of ionization techniques and scan modes. Electrospray ionization (ESI) is the most commonly used ion source for the “omic”

sciences, although other ionization techniques such as Atmospheric Pressure Chemical Ionization (APCI) and Atmospheric Pressure Photoionization (APPI) are also involved [57]. Several scan modes exist, such as full scan, precursor ion (Pre) scan, product ion (Pro) scan, neutral loss (NL) scan, selected reaction monitoring (SRM) scan and multiple reaction monitoring (MRM) scan. The development of these integrated tools promises to greatly advance our understanding of the diverse biological roles of lipids.

1.4.2. Spectroscopy-based methods

The major spectroscopic techniques used in lipidomics are Fourier transform infrared (FT-IR) spectroscopy and nuclear magnetic resonance (NMR) spectroscopy.

FT-IR is a non-destructive and non-invasive spectroscopic method, offering inherent advantages of short analysis time and simplicity in the sample preparation protocols [9]. Chemical information is obtained according to the infrared spectrum of absorption or emission over a broad range of wavelengths at a time. This methodology has been reported to be used for analysis of PUFA composition in various marine oils [71], TAGs in microalgal consortia [72], phospholipids [73], ceramides [74, 75] and steryl ferulates [76].

NMR spectroscopy, also a non-destructive strategy, is capable of providing structural information of the lipid molecules based on the chemical shifts of different functional groups. This technique mainly includes two types: ^{13}C-NMR and ^{1}H-NMR. Both one-dimensional (1D) and two-dimensional (2D) NMR (^{1}H- and ^{13}C-) have been utilized by Rozema *et al.* [77] for structural characterization of glucocerebrosides (GlcCer) and the active metabolite 4, 8-sphingadienine from *Arisaema amurense* and *Pinellia ternata*. Besides, ^{31}P NMR is another type that has been specifically developed for phospholipids quantification, but it cannot differentiate FA chains

within each subclass such as PG [33]. 2D ^{31}P, ^{1}H NMR spectroscopy was considered as a valuable platform for the assignment and verification of known and uncommon phospholipids in the samples [78]. It is interesting to mention that NMR can be either used as a stand-alone technique [22] or as a component of a hyphenated technique [79]. A related paper published in 2007 introduced the identification and quantification of α- and γ-linolenic acid in lipid extract by means of LC-NMR without the need of any derivatization [79]. In this hyphenated method system, LC separation was conducted by utilizing two columns of C8 and C18 in series and ^{1}H NMR spectroscopy was used for quantification. NMR-based lipidomics approaches have not been widely used in lipidomics, mainly because it is often challenging to obtain the identities of each individual molecular species in the extremely complex mixtures. The similarity of the spectra of lipids with respect to the limited structural carbon chain information is another challenge in lipid analysis with NMR [15].

In addition to the commonly-used FT-IR and NMR techniques, Raman spectroscopy expands the list of available spectroscopic tools to researchers in the newly-emerged field of lipidomics for multiple applications [80]. It is a label-free, non-destructive and real-time manner for direct and quantitative analysis of lipids at the single-cell level without requiring any exogenous modification of samples [80]. To determine the ability of Raman spectroscopy, Sosińska *et al.* [81] implemented Raman spectroscopy for structural characterization of dimeric oxidation products of phytosterols. Also, in vivo lipid profiling of oil-producing microalgae was achieved by applying a method based on single-cell laser-trapping Raman spectroscopy [80].

1.4.3. Mass spectrometry-based lipidomics

MS has gained great popularity since its first introduction into the field of lipidomics. This can

be attributed to its high level of sensitivity, molecular specificity, speed and most importantly, its capacity to generate structural information of the analyzed lipid molecules [22, 82]. MS-based technologies for lipid analysis in complex biological matrices (such as tissues, blood and cellular extracts) are mainly fallen into three categories: shotgun lipidomics, LC/MS-based platforms and tissue-imaging MS (particularly in mapping lipid distributions in tissues or cells) [8, 32, 33].

Shotgun lipidomics is a powerful tool widely performed in lipidomics. It refers to direct infusion (without prior fractionation) of crude lipid extracts to MS instrument for identification and quantification. Shotgun lipidomics can be accomplished by utilizing high-resolution mass spectrometry (HRMS), tandem mass spectrometry (MS/MS or MS^2) or multiple-dimensional mass spectrometry (MDMS or MS^n).

HRMS-based lipidomics strategies are capable of resolving the extensive compositional and structural diversity of lipids in biological systems, further allowing for global non-targeted screening. Classic HRMS instruments, such as sector and Fourier-transform ion cyclotron resonance (FT-ICR), were slow, complex to handle, and probably expensive to buy and to maintain. Modern time-of-flight (TOF) MS and Orbitrap MS have undergone tremendous technological advances which are demonstrated by the high mass-resolving power and mass accuracy as well as a sufficient dynamic range enabling to rapidly characterize lipidomes. Hence, HRMS is considered as a promising and powerful technology that can be used in routine environments [62]. In a work conducted by Porcari *et al.* [83], three fast and direct MS approaches including MALDI(+)-TOF-MS, ESI(+)-FT-ICR-MS and thermal imprinting easy ambient sonic-ionization mass spectrometry (TI-EASI(+)-MS) with a single quadrupole mass spectrometer were simultaneously carried out and compared for global profiling of lipid molecular species in S and P caviars. Conclusively, TI-EASI (+)-MS was selected as a more comprehensive and easier-operated approach for that specific

analytical purpose.

MS/MS is an important and widespread technique for both qualitative and quantitative performance. Triple quadrupole (QqQ) is the most commonly employed instrument for MS/MS approach [84]. Along with MRM scan where specific molecular ion-fragment ion pairs are monitored, this mass spectrometer is a good option for quantitative analyses of well-defined groups of lipid compounds in complex samples [8, 85]. Compared to HRMS, QqQ is now a mature technology, where the rate of innovation has slowed down considerably [62]. Quadrupole-based MS/MS is approximately two orders of magnitude more sensitive than it was 10 or 20 years ago. However, the selectivity provided by these unit-resolving instruments has remained virtually unchanged [62]. In addition to QqQ mass spectrometer, hybrid quadrupole time-of-flight (QqTOF) mass spectrometer [86] and LTQ Orbitrap mass spectrometer [87] has been also employed as MS/MS platforms for high throughput molecular lipidomics.

MDMS-based shotgun lipidomics is a well-recognized platform to analyze individual lipid molecular species directly from lipid extracts of biological matrices [84, 88]. The general protocol for analysis usually consists of intrasource separation (introduced by Han and Gross in the mid 1990's) and MS^n experiments, followed by computer-assisted array analysis [57, 89]. Multidimensional MS refers to construction of additional dimension of mass spectrum based on a 2D mass spectrum by varying experimental conditions such as infused solution conditions, ionization conditions and fragmentation conditions [89, 90]. As for the 2D mass spectrum, it is built by using the molecular ions (x-axis) in *m/z* values as the first dimension and the mass corresponding to the neutrally lost fragments in mass values or the monitored fragment ions in *m/z* values (y-axis) as the second dimension [90]. MDMS-based approach has been successfully performed for monitoring lipid changes (including plasmalogen PE, sulfatides and ceramides) in

Alzheimer's disease [90]. This technique enables us to obtain the detailed structural information necessary for characterization of novel lipids and the selectivity required for the determination of individual lipid species present in complex mixtures [91].

Moreover, Byrdwell [92] introduced a 'quadruple parallel mass spectrometry' technique for analysis of TAGs in a dietary supplement. This involves the use of four mass spectrometers in parallel with three different API interfaces including atmospheric pressure chemical ionization (APCI), atmospheric pressure photoionization (APPI) and electrospray ionization (ESI). The simultaneous employment of multiple ionization techniques is beneficial from the reasons that some classes of compounds responds better to some specific ionization technique and different ionization methods provide different types of mass spectra [92].

MS is often used in combination with LC or GC (LC/MS or GC/MS). LC/MS-based methodologies has been discussed in Section **1.4.1.** LC/MS or LC/MS/MS is generally sufficient for performing high quality lipidomics analysis. Shotgun lipidomics is a straightforward and rapid analytical strategy and faster than LC/MS-based methodologies. However, this approach is limited by its poor abilities in resolving isobaric compounds and also by a possible risk of ion suppression, which may lead to decreased sensitivity in the analysis of very low abundance lipids [29]. Coupling LC separation prior to MS detection can effectively resolve these problems by decreasing the number of competing analytes entering the MS ion source to reduce the risk of ion suppression and by setting up suitable gradient conditions to separate and identify the isobaric and isomeric lipid species [29].

Tissue-imaging MS methods generate ions directly from the surface of materials, which can be accomplished by three separate desorption/ionization approaches, namely, desorption

electrospray ionization (DESI), secondary ion mass spectrometry (SIMS) and matrix-assisted laser desorption ionization (MALDI) [8, 93]. DESI is the latest lipid-imaging techniques and is also the most gentle of the three desorption/ionization protocols. DESI can generate lipid ions directly from a tissue section (typically, 10 to 100 mm in diameter) under ambient conditions using an electrically-charged solvent, avoiding the use of matrix and its associated weaknesses such as interference of matrix peaks in the low-mass region [8, 93, 94]. In SIMS, ions are produced by bombarding the sample surface (nanometers to sub-micrometers in diameter) with a focused primary ion beam [8]. Both DESI and SIMS can be used to produce molecular images of samples. Like ESI, MALDI is also a soft ion technique, in which ions are generated from a solid or solvent matrix by irradiation with a laser beam [93]. It can be used in couple with TOF mass spectrometer (traditionally) and also relatively new instrumentations such as triple quadrupole linear ion trap (QqQ/LIT) [91]. In recent times, MALDI-MS of lipids has received increased popularity for lipid analysis, due to its high speed, simplicity for sample preparation, stability and largely its ability to measure the ions of interest as a function of position in tissues [91, 93]. MALDI-MS has been extensively applied to the lipidomics analysis of brain tissue [91]. In the future, more efforts are needed to determine whether the spectacular images produced by imaging MS can be confidently interpreted as lipid distributions [93].

1.4.4. Capillary electrophoresis methods

Capillary electrophoresis (CE) is an attractive analytical methodology with respect to its relatively high efficiency, high resolution, various versatilities and more importantly, the ability to separate the compounds in a wide range of polarity by changing the electrolyte composition [95, 96]. Similar to the chromatographic techniques, it is commonly used in combination with the other detectors such as MS. Micellar electrokinetic chromatography (MEKC) and non-aqueous CE

(NACE) are two most useful modes for CE techniques. Montealegre *et al.* [95, 97] introduced the application of CE operated in different modes for the determination of phospholipids in several food and biological samples. Capillary electro-chromatography (CEC) is a hyphenated separation technique combining the selectivity of HPLC and the high efficiency of CE [98]. The utility of this technique for TAGs analysis in vegetable oils from different botanical origins was assessed by Lerma-García *et al.* [98] using octadecyl acrylate (ODA) ester-based monolithic column.

In comparison with other analytical techniques discussed above, publications about the application of CE for lipidomics are relatively scarce [95]. Nevertheless, it is still a powerful separation technique with analytes separated according to their ionic mobility in an electric field [35].

1.5. Concluding Remarks

The technological improvements in instrumentations and bioinformatics tools have driven the emergence and rapid expansion of lipidomics especially in the past two decades. This chapter provides a review on methodologies currently available for extraction and analysis of lipid compounds from various sample resources. Considering the enormous diversity and complexity in lipid structures and functions, it is not surprising that up to now, there is no approach technically applicable for a lipidomic analysis to encompass the full lipidome [8]. In order to build up a more complete picture of lipids including metabolic pathways, metabolic flux and systems integration [99, 84], new solutions and strategies for comprehensive determination of all lipid molecules from a large range of samples, are clearly needed. In turn, the establishment of new strategies for lipid research needs to rely on the new technologies, such as more sophisticated mass spectrometers. In the near future, advances in MS and chromatography instrumentations will allow the screening of

more lipids with greater accuracy and higher resolution than ever before and also allow more detailed studies of individual lipid molecular species and their crosstalk with other biomolecules such as proteins [99]. Along with the goal for global lipidomics, much work remains to be done to process and interpret the resulted large amounts of data. Manual data analysis is not enough and thereby novel bioinformatic tools for automated data processing is required to ensure that data acquired across different platforms can be integrated and compared and that any new structural information can be incorporated and utilized [91, 93]. This will offer new insights into interdisciplinary programs which focus on integration of lipidomics with chemical biology, proteomics, and genomics to span the entire flow of information encoded in biological systems [32]. All of these advances will finally provide us with a powerful tool for elucidating the biochemical mechanisms underlying lipid-mediated diseases, and at the same time could probably contribute to discover critical components (candidate biomarkers) of lipid homeostasis in health and disease [32, 89].

Although lipidomics was initially developed in specialized research groups, it has now evolved into a method which can be applied in general analytical laboratories or in cooperative approach between analytical and biological labs as long as following the typical lipidomics workflows. It is common for labs working on different areas to carry out lipidomics research together and share lipidomics data [5].

1.6. Hypothesis and Objectives

The overall goal of this thesis is to develop and validate methods based on LC/MS or LC/MS/MS technologies to address specific analytical problems in lipidomics. The novel analytical methods need to be sufficiently accurate, rapid, sensitive and reproducible so as to be

suitable for biological and clinical studies.

It is hypothesized that LC/MS-based technologies (employing different mass spectrometric and chromatographic techniques) can be used for the structural studies and quantitative measurements of individual lipid molecular species in biomedical, clinical and nutritional research areas.

In order to test this hypothesis, experiments were conducted to meet the following objectives:

(1) To optimize the solid-phase extraction (SPE) procedures for bile acids in piglet bile samples and to establish an improved approach for rapid qualification and quantification of bile acids and their conjugates in the piglet bile extracts (Chapter 2);

(2) To develop and validate a method for simultaneous identification and quantification of individual sphingolipid molecular species in cellular extracts (Chapter 3);

(3) To optimize the derivatization conditions for phospholipid metabolites of trimethylamine (TMA) and to develop and validate a method for simultaneous separation and measurement of TMA and trimethylamine-*N*-oxide (TMAO) in plasma samples (Chapter 4);

(4) To extend the liquid chromatography/in-line ozonolysis/mass spectrometry (LC/O_3-MS) method for the *de novo* identification of conjugated linolenic acid (CLnA) isomers in natural matrices including pomegranate and tung seed oils (Chapter 5).

1.7. References

[1] C.C. Akoh, D.B. Min, (2008). *Food lipids: chemistry, nutrition, and biotechnology*. New York: CRC press.

[2] J.L. Bernal, M.T. Martín, L. Toribio, Supercritical fluid chromatography in food analysis, J Chromatogr A. 1313 (2013) 24-36.

[3] M. Orešič, V.A. Hänninen, A. Vidal-Puig, Lipidomics: a new window to biomedical frontiers, Trends Biotechnol. 26 (2008) 647-652.

[4] P.D. Rainville, C.L. Stumpf, J.P. Shockcor, R.S. Plumb, J.K. Nicholson, Novel application of reversed-phase UPLC-oaTOF-MS for lipid analysis in complex biological mixtures: A new tool for lipidomics, J Proteome Res. 6 (2007) 552-558.

[5] A. Shevchenko, K. Simons, Lipidomics: coming to grips with lipid diversity, Nat Rev Mol Cell Biol. 11 (2010) 593-598.

[6] M. Orešič, Informatics and computational strategies for the study of lipids, Biochim Biophys Acta. 1811 (2011) 991-999.

[7] S.M. Lam, G. Shui, Lipidomics as a principal tool for advancing biomedical research, J Genet Genomics. 40 (2013) 375-390.

[8] B.M. Kenwood, A.H. Merrill Jr. Lipidomics, Encyclopedia of Cell Biology. 1 (2016) 147-159.

[9] M.A.L. de Oliveira, B.L.S. Porto, I.D.L. Faria, P.L. de Oliveira, P.M. de Castro Barra, R.D.J.C. Castro, R.T. Sato, 20 years of fatty acid analysis by capillary electrophoresis, Molecules. 19 (2014) 14094-14113.

[10] S.H. Chen, Y.J. Chuang, Analysis of fatty acids by column liquid chromatography, Anal Chim Acta. 465 (2002) 145-155.

[11] I. Brondz, Development of fatty acid analysis by high-performance liquid chromatography, gas chromatography, and related techniques, Anal Chim Acta. 465 (2002) 1-37.

[12] S.A. Mjøs, B.O. Haugsgjerd, Trans fatty acid analyses in samples of marine origin: the risk of false positives, J Agric Food Chem. 59 (2011) 3520-3531.

[13] C. Wolf, P.J. Quinn, Lipidomics: Practical aspects and applications, Prog Lipid Res. 47 (2008) 15-36.

[14] M. Wang, R.H. Han, X. Han, Fatty acidomics: global analysis of lipid species containing a carboxyl group with a charge-remote fragmentation-assisted approach. Anal Chem. 85 (2013) 9312-9320.

[15] T. Hyötyläinen, I. Bondia-Pons, M. Orešič, Lipidomics in nutrition and food research, Mol

Nutr Food Res. 57 (2013) 1306-1318.

[16] S. Qu, Z. Du, Y. Zhang, Direct detection of free fatty acids in edible oils using supercritical fluid chromatography coupled with mass spectrometry, Food Chem. 170 (2015) 463-469.

[17] S. Ng, Quantitative analysis of partial acylglycerols and free fatty acids in palm oil by 13C nuclear magnetic resonance spectroscopy, J Am Oil Chem Soc. 77 (2000) 749-755.

[18] J. Bian, Y. Xue, K. Yao, X. Gu, C. Yan, Y. Wang, Solid-phase extraction approach for phospholipids profiling by titania-coated silica microspheres prior to reversed-phase liquid chromatography-evaporative light scattering detection and tandem mass spectrometry analysis, Talanta. 123 (2014) 233-240.

[19] A. Uphoff, M. Hermansson, P. Haimi, P. Somerharju, (2007). Analysis of complex lipidomes. *Medical Applications of Mass Spectrometry*, pp. 217-243. Amsterdam: Elsevier.

[20] H. Farwanah, T. Kolter, K. Sandhoff, Mass spectrometric analysis of neutral sphingolipids:

methods, applications, and limitations, Biochim Biophys Acta. 1811 (2011) 854-860.

[21] H. Vesper, E.M. Schmelz, M.N. Nikolova-Karakashian, D.L. Dillehay, D.V. Lynch, A.H. Merrill, Sphingolipids in food and the emerging importance of sphingolipids to nutrition, J Nutr. 129 (1999) 1239-1250.

[22] J. Bernal, A. Mendiola, E. Ibáñez, A. Cifuentes, Advanced analysis of nutraceuticals, J Pharm Biomed Anal. 55 (2011) 758-774.

[23] S.L. Abidi, Chromatographic analysis of plant sterols in foods and vegetable oils, J Chromatogr A. 935 (2001)173-201.

[24] M.J. Lagarda, G. García-Llatas, R. Farré, Analysis of phytosterols in foods, J Pharm Biomed Anal. 41 (2006) 1486-1496.

[25] Š. Horník, M. Sajfrtová, J. Karban, J. Sýkora, A. Březinová, Z. Wimmer, LC-NMR technique in the analysis of phytosterols in natural extracts, J Anal Methods Chem. 2013 (2013) 1-7.

[26] E. Fahy, S. Subramaniam, H.A.C. Brown, K. Glass, A.H. Merrill, R.C. Murphy, C.R.H. Raetz, D.W. Russell, Y. Seyama, W. Shaw, T. Shimizu, F. Spener, G. van Meer, M.S. VanNieuwenhze, S.H. White, J.L. Witztum, E.A. Dennis, A comprehensive classification system for lipids, J Lipid

Res. 46 (2005) 839-862.

[27] M.R. Wenk, The emerging field of lipidomics, Nat Rev Drug Discov. 4 (2005) 594-610.

[28] E. Fahy, S. Subramaniam, R.C. Murphy, M. Nishijima, C.R.H. Raetz, T. Shimizu, F. Spener, G. van Meer, M.J. Wakelam, E.A. Dennis, Update of the LIPID MAPS comprehensive classification system for lipids, J Lipid Res. 50 (2009) S9-S14.

[29] C. Hu, R. van der Heijden, M. Wang, J. van der Greef, T. Hankemeier, G. Xu, Analytical strategies in lipidomics and applications in disease biomarker discovery, J Chromatogr B. 877 (2009) 2836-2846.

[30] T. Hyötyläinen, M. Orešič, Analytical lipidomics in metabolic and clinical research, Trends Endocrinol Metab. 26 (2015) 671-673.

[31] G. van Meer, Cellular lipidomics, EMBO J. 24 (2005) 3159-3165.

[32] M.R. Wenk, Lipidomics: new tools and applications, Cell. 143 (2010) 888-895.

[33] M. Wang, C. Wang, R.H. Han, X. Han, Novel advances in shotgun lipidomics for biology and medicine, Prog Lipid Res. 61 (2016) 83-108.

[34] K. Schmelzer, E. Fahy, S. Subramaniam, E.A. Dennis, The lipid maps initiative in lipidomics, Methods Enzymol. 432 (2007) 171-183.

[35] M. Herrero, M. Castro-Puyana, E. Ibanez, A. Cifuentes, (2013). Compositional analysis of foods. *Liquid Chromatography: Applications*, pp. 295-317. Amsterdam: Elsevier.

[36] D.S. Nichols, (2003). Principles of lipid analysis. *Chemical and Functional Properties of Food Lipids*, pp. 167-188. New York: CRC Press.

[37] Y.Y. Zhao, S.P. S. Wu, Liu, Y. Zhang, R.C. Lin, Ultra-performance liquid chromatography-mass spectrometry as a sensitive and powerful technology in lipidomic applications, Chem Biol Interact. 220 (2014) 181-192.

[38] J. Folch, M. Lees, G.H. Sloane-Stanley, A simple method for the isolation and purification of total lipids from animal tissues, J Biol Chem. 226 (1957) 497-509.

[39] R.A. Moreau, J.K. Winkler-Moser, (2012). Extraction and analysis of food lipids. *Methods of Analysis of Food Components and Additives,* pp. 115-134. New York: CRC Press.

[40] E.G. Bligh, W.J. Dyer, A rapid method of total lipid extraction and purification, Can J Biochem Physiol. 37 (1959) 911-917.

[41] J.D. EbeIer, SPE methodologies for the separation of lipids, Lipids. 8 (1996) 1094-1103.

[42] E. Bravi, P. Benedetti, O. Marconi, G. Perretti, Determination of free fatty acids in beer wort, Food Chem. 151 (2014) 374-378.

[43] F.J. Eller, J.W. King, Determination of fat content in foods by analytical SFE, Seminars in food analysis. 1 (1996) 145-165.

[44] S. Armenta, S. Garrigues, M. de la Guardia, The role of green extraction techniques in Green Analytical Chemistry, Trends Anal Chem. 71 (2015) 2-8.

[45] A. Zgoła-Grześkowiak, T. Grześkowiak, Dispersive liquid-liquid microextraction, Trends Anal Chem. 30 (2011) 1382-1399.

[46] H. Zhang, C. Wolf-Hall, C. Hall, Modified microwave-assisted extraction of ergosterol for measuring fungal biomass in grain cultures, J Agric Food Chem. 56 (2008) 11077-11080.

[47] A.H. Metherel, A.Y. Taha, H. Izadi, K.D. Stark, The application of ultrasound energy to increase lipid extraction throughput of solid matrix samples (flaxseed), Prostaglandins Leukot Essent Fatty Acids. 81 (2009) 417-423.

[48] C. Dejoye, M.A. Vian, G. Lumia, C. Bouscarle, F. Charton, F. Chemat, Combined extraction processes of lipid from Chlorella vulgaris microalgae: microwave prior to supercritical carbon dioxide extraction, Int J Mol Sci. 12 (2011) 9332-9341.

[49] J.G. McDonald, P.T. Ivanova, H.A. Brown, (2015). Approaches to lipid analysis. *Biochemistry of Lipids, Lipoproteins and Membranes*, pp. 41-71. Amsterdam: Elsevier.

[50] J.J. Myher, A. Kuksis, General strategies in chromatographic analysis of lipids, J Chromatogr B. 671 (1995) 3-33.

[51] M. Buchgraber, F. Ulberth, H. Emons, E. Anklam, Triacylglycerol profiling by using chromatographic techniques, Eur J Lipid Sci Technol. 106 (2004) 621-648.

[52] A.J. Alpert, Hydrophilic-interaction chromatography for the separation of peptides, nucleic acids and other polar compounds, J Chromatogr A. 499 (1990) 177-196.

[53] Y. Guo, S. Gaiki, Retention and selectivity of stationary phases for hydrophilic interaction chromatography, J Chromatogr A. 35 (2011) 5920-5938.

[54] J.M. Curtis, S. Mi, (2015). Hydrophilic interaction liquid chromatography for determination of betaine. *Betaine: Chemistry, Analysis, Function and Effects*, pp. 139-158. Royal Society of Chemistry (Great Britain).

[55] Y.Y. Zhao, Y. Xiong, J.M. Curtis, Measurement of phospholipids by hydrophilic interaction liquid chromatography coupled to tandem mass spectrometry: The determination of choline containing compounds in foods, J Chromatogr A. 1218 (2011) 5470-5479.

[56] V. Verardo, A.M. Gómez-Caravaca, C. Montealegre, A. Segura-Carretero, M.F. Caboni, A. Fernández-Gutiérrez, A. Bendini, Optimization of a solid phase extraction method and hydrophilic interaction liquid chromatography coupled to mass spectrometry for the determination of phospholipids in virgin olive oil, Food Res Int. 54 (2013) 2083-2090.

[57] W.J. Griffiths, Y. Wang, Mass spectrometry: from proteomics to metabolomics and lipidomics, Chem Soc Rev. 38 (2009) 1882-1896.

[58] F.J. Senorans, E. Ibanez, Analysis of fatty acids in foods by supercritical fluid chromatography, Anal Chim Acta. 465 (2002) 131-144.

[59] C. Turner, J.W. King, L. Mathiasson, Supercritical fluid extraction and chromatography for fat-soluble vitamin analysis, J Chromatogr A. 936 (2001) 215-237.

[60] S.M. Momchilova, B.M. Nikolova-Damyanova, Advances in silver ion chromatography for the analysis of fatty acids and triacylglycerols-2001 to 2011, Anal Sci. 28 (2012) 837-844.

[61] C. Sun, B.A. Black, Y.Y. Zhao, M.G. Gänzle, J.M. Curtis, Identification of conjugated linoleic acid (CLA) isomers by silver ion-liquid chromatography/in-line ozonolysis/mass spectrometry (Ag^+-LC/O_3-MS), Anal Chem. 85 (2013) 7345-7352.

[62] A. Kaufmann, Combining UHPLC and high-resolution MS: A viable approach for the analysis of complex samples, Trends Anal. Chem. 63 (2014) 113-128.

[63] M. Lísa, K. Netušilová, L. Franěk, H. Dvořáková, V. Vrkoslav, M. Holčapek, Characterization of fatty acid and triacylglycerol composition in animal fats using silver-ion and non-aqueous reversed-phase high-performance liquid chromatography/mass spectrometry and gas

chromatography/flame ionization detection, J Chromatogr A. 1218 (2011) 7499-7510.

[64] B. Tang, K.H. Row, Development of gas chromatography analysis of fatty acids in marine organisms, J Chromatogr Sci. 51 (2013) 599-607.

[65] Q. Gu, F. David, F. Lynen, P. Vanormelingen, W. Vyverman, K. Rumpel, G. Xu, P. Sandra, Evaluation of ionic liquid stationary phases for one dimensional gas chromatography–mass spectrometry and comprehensive two dimensional gas chromatographic analyses of fatty acids in marine biota, J Chromatogr A. 1218 (2011) 3056-3063.

[66] Y. Hirata, I. Sogabe, Separation of fatty acid methyl esters by comprehensive two-dimensional supercritical fluid chromatography with packed columns and programming of sampling duration, Anal Bioanal Chem. 378 (2004) 1999-2003.

[67] R. Esche, B. Scholz, K.H. Engel, Online LC–GC analysis of free sterols/stanols and intact steryl/stanyl esters in cereals, J Agric Food Chem. 61 (2013) 10932-10939.

[68] R.M. Toledano, J.M. Cortés, Á. Rubio-Moraga, J. Villén, A. Vázquez, Analysis of free and esterified sterols in edible oils by online reversed phase liquid chromatography-gas chromatography (RPLC-GC) using the through oven transfer adsorption desorption (TOTAD) interface, Food Chem. 135 (2012) 610-615.

[69] R.M. Toledano, J.M. Cortés, J.C. Andini, A. Vázquez, J. Villén, On-line derivatization with on-line coupled normal phase liquid chromatography-gas chromatography using the through oven transfer adsorption desorption interface: Application to the analysis of total sterols in edible oils, J Chromatogr A. 1256 (2012) 191-196.

[70] C. Sun, Y.Y. Zhao, J.M. Curtis, Elucidation of phosphatidylcholine isomers using two dimensional liquid chromatography coupled in-line with ozonolysis mass spectrometry, J Chromatogr A. 1351 (2014) 37-45.

[71] J. Vongsvivut, M.R. Miller, D. McNaughton, P. Heraud, C.J. Barrow, Rapid discrimination and determination of polyunsaturated fatty acid composition in marine oils by FTIR spectroscopy and multivariate data analysis, Food Bioprocess Tech. 7 (2014) 2410-2422.

[72] R. Miglio, S. Palmery, M. Salvalaggio, L. Carnelli, F. Capuano, R. Borrelli, Microalgae triacylglycerols content by FT-IR spectroscopy, J Appl Phycol. 25 (2013) 1621-1631.

[73] X. Meng, Q. Ye, Q. Pan, Y. Ding, M. Wei, Y. Liu, F.R. van de Voort, Total phospholipids in edible oils by in-vial solvent extraction coupled with FTIR analysis, J Agric Food Chem. 62 (2014) 3101-3107.

[74] M. Janssens, G.S. Gooris, J.A. Bouwstra, Infrared spectroscopy studies of mixtures prepared with synthetic ceramides varying in head group architecture: coexistence of liquid and crystalline phases, Biochim Biophys Acta. 1788 (2009) 732-742.

[75] T.M. Greve, K.B. Andersen, O.F. Nielsen, A. Engdahl, FTIR imaging and ATR-FT-Far-IR synchrotron spectroscopy of pig ear skin, J Spectrosc. 24 (2010) 105-111.

[76] E. Mandak, D. Zhu, T.A. Godany, L. Nyström, Fourier transform infrared spectroscopy and Raman spectroscopy as tools for identification of steryl ferulates, J Agric Food Chem. 61 (2013) 2446-2452.

[77] E. Rozema, R. Popescu, H. Sonderegger, C.W. Huck, J. Winkler, G. Krupitza, E. Urban, B.

Kopp, Characterization of glucocerebrosides and the active metabolite 4, 8-sphingadienine from arisaema amurense and pinellia ternata by NMR and CD spectroscopy and ESI-MS/CID-MS, J Agric Food Chem. 60 (2012) 7204-7210.

[78] S. Kaffarnik, I. Ehlers, G. Gröbner, J. Schleucher, W. Vetter, Two-dimensional 31P, 1H NMR spectroscopic profiling of phospholipids in cheese and fish, J Agric Food Chem. 61 (2013) 7061-7069.

[79] J. Sýkora, P. Bernášek, M. Zarevúcká, M. Kurfürst, H. Sovová, J. Schraml, High-performance liquid chromatography with nuclear magnetic resonance detection-A method for quantification of α-and γ-linolenic acids in their mixtures with free fatty acids, J Chromatogr A. 1139 (2007) 152-155.

[80] H. Wu, J.V. Volponi, A.E. Oliver, A.N. Parikh, B.A. Simmons, S. Singh, In vivo lipidomics using single-cell Raman spectroscopy, Proc Natl Acad Sci. 108 (2011) 3809-3814.

[81] E. Sosińska, R. Przybylski, F. Aladedunye, P. Hazendonk, Spectroscopic characterisation of dimeric oxidation products of phytosterols, Food Chem. 151 (2014) 404-414.

[82] B. Fong, L. Ma, C. Norris, Analysis of phospholipids in infant formulas using high performance liquid chromatography-tandem mass spectrometry, J Agric Food Chem. 61 (2013)

858-865.

[83] A.M. Porcari, G.D. Fernandes, K.R.A. Belaz, N.V. Schwab, V.G. Santos, R.M. Alberici, V.A. Gromova, M.N. Eberlin, A.T. Lebedev, A. Tata, High throughput MS techniques for caviar lipidomics, Anal Methods. 6 (2014) 2436-2443.

[84] X. Han, K. Yang, R.W. Gross, Multi-dimensional mass spectrometry-based shotgun lipidomics and novel strategies for lipidomic analyses, Mass Spectrom Rev. 31 (2012) 134-178.

[85] A. Carrasco-Pancorbo, N. Navas-Iglesias, L. Cuadros-Rodriguez, From lipid analysis towards lipidomics, a new challenge for the analytical chemistry of the 21st century. Part I: Modern lipid analysis, Trends Anal Chem. 28 (2009) 263-278.

[86] M. Ståhlman, C.S. Ejsing, K. Tarasov, J. Perman, J. Borén, K. Ekroos, High-throughput shotgun lipidomics by quadrupole time-of-flight mass spectrometry, J Chromatogr B. 877 (2009) 2664-2672.

[87] K. Schuhmann, R. Almeida, M. Baumert, R. Herzog, S.R. Bornstein, A. Shevchenko, Shotgun lipidomics on a LTQ Orbitrap mass spectrometer by successive switching between acquisition polarity modes, J Mass Spectrom. 47 (2012) 96-104.

[88] K. Yang, H. Cheng, R.W. Gross, X. Han, Automated lipid identification and quantification by multidimensional mass spectrometry-based shotgun lipidomics, Anal Chem. 81 (2009) 4356-4368.

[89] X. Han, R.W. Gross, Shotgun lipidomics: multidimensional MS analysis of cellular lipidomes, Expert Rev Proteomics. 2 (2005) 253-264.

[90] X. Han, Multi-dimensional mass spectrometry-based shotgun lipidomics and the altered lipids at the mild cognitive impairment stage of Alzheimer's disease, Biochim Biophys Acta. 1801 (2010) 774-783.

[91] N. Zehethofer, D.M. Pinto, Recent developments in tandem mass spectrometry for lipidomic analysis, Anal Chim Acta. 627 (2008) 62-70.

[92] W.C. Byrdwell, Quadruple parallel mass spectrometry for analysis of vitamin D and triacylglycerols in a dietary supplement, J Chromatogr A. 1320 (2013) 48-65.

[93] S.J. Blanksby, T.W. Mitchell, Advances in mass spectrometry for lipidomics, Annu Rev Anal Chem. 3 (2010) 433-465.

[94] R. Cozzolino, B. De Giulio, Application of ESI and MALDI-TOF MS for triacylglycerols analysis in edible oils, Eur J Lipid Sci Tech. 113 (2011) 160-167.

[95] C. Montealegre, V. Verardo, M. Luisa Marina, M.F. Caboni, Analysis of glycerophospho-and sphingolipids by CE, Electrophoresis. 35 (2014) 779-792.

[96] S. Flor, S. Lucangioli, M. Contin, V. Tripodi, Simultaneous determination of nine endogenous steroids in human urine by polymeric-mixed micelle capillary electrophoresis, Electrophoresis. 31 (2010) 3305-3313.

[97] C. Montealegre, L. Sanchez-Hernandez, A.L. Crego, M.L. Marina, Determination and characterization of glycerophospholipids in olive fruit and oil by nonaqueous capillary electrophoresis with electrospray-mass spectrometric detection, J Agric Food Chem. 61 (2013) 1823-1832.

[98] M.J. Lerma-García, M. Vergara-Barberán, J.M. Herrero-Martínez, E.F. Simó-Alfonso, Acrylate ester-based monolithic columns for capillary electro chromatography separation of triacylglycerols in vegetable oils, J Chromatogr A. 1218 (2011) 7528-7533.

[99] P.J. Crick, X.L. Guan, Lipid metabolism in mycobacteria-Insights using mass spectrometry-based lipidomics, Biochim Biophys Acta. 1861 (2016) 60-67.

[100] K. Yang, X. Han, Accurate quantification of lipid species by electrospray ionization mass spectrometry-meets a key challenge in lipidomics, Metabolites, 1 (2011) 21-40.

[101] M. Wang, C. Wang, X. Han, Selection of internal standards for accurate quantification of complex lipid species in biological extracts by electrospray ionization mass spectrometry-What, how and why?, Mass Spectrom. Rev. 9999 (2016) 1-22.

Chapter 2*

A Method for the Determination of Bile Acids in Piglet Bile Using Solid Phase Extraction and Liquid Chromatography-Electrospray Tandem Mass Spectrometry

2.1. Introduction

Bile acids (BA) are a group of compounds characterized by a common steroid skeleton which consists of three six-carbon rings and one five-carbon ring [1]. However, due to differences in their substitution pattern, side chain and whether or not they are free or bound, they span a considerable range of polarities.

Based on the functional group bound to the side chain of the molecular structure, BA can be classified as free BA or "non-bound" (with a free carboxylic acid group on the side-chain at R5, **Figure 2-1**) or conjugated BA (primarily either glycine-bound or taurine-bound with the glycine or taurine group at R5 connected via an amide linkage, **Figure 2-1**). Apart from these major forms, BA can also be present in conjugation with sulphuric acid, glucuronic acid, glucose or *N*-acetylglucosamine [2] which have been detected and characterized in urine [3]. In addition, BA molecules vary in the number and position of hydroxyl groups on the steroid nucleus (**Figure 2-1**). Consequently there are a large number of BA differing in polarity and stereochemistry.

From the perspective of metabolism, BA are considered as the oxidized products of cholesterol and are involved in the enterohepatic circulation. Consequently, they are widely distributed in

* This chapter has been published as S. Mi, D.W. Lim, J.M. Turner, P.W. Wales and J.M. Curtis, "Determination of Bile Acids in Piglet Bile by Solid Phase Extraction and Liquid Chromatography-Electrospray Tandem Mass Spectrometry", *Lipids*, 51 (2016) 359-372. I was responsible for the experimental design, performance of experiments, data collection and analysis, as well as the manuscript composition.

biological samples, including liver, bile, serum, urine [4], and fecal materials [5] with the highest concentration in bile. The most well-known biological roles of BA are in aiding digestion and absorption of fats via the formation of micelles [1]. Other important functions, like preventing the precipitation of cholesterol in the gallbladder and eliminating cholesterol from the body [6], have also been described. Due to these important biological roles, BA metabolism is closely associated with cholesterol homeostasis. It has been observed that abnormalities in BA metabolism can lead to the incidence of certain liver diseases. Taking parenteral nutrition-associated liver disease (PNALD) as an example, it is a cholestatic liver disease partially caused by developmental immaturity with regards to hepatic BA metabolism and transport and currently without established pharmacological treatments [7]. In summary, BA are of great importance for physiological well-being and any alterations in their profiles could be used as markers for possible therapies of related liver diseases. Hence, the quantitative analysis of BA and their conjugates is of great importance in medical and pharmaceutical research.

Over the past few decades, numerous methods have been devised for the qualitative and quantitative determination of individual BA molecular species in various samples. These include gas chromatography (GC) [8], high-performance liquid chromatography (HPLC) [9], mass spectrometry (MS) [5], ultra-performance liquid chromatography (UPLC) [4, 10], supercritical fluid chromatography (SFC) [11], and micellar electro-kinetic capillary electrophoresis (MEKCE) [12]. The application of GC to BA analysis is limited by the need for conversion of nonvolatile BA into more volatile derivatives. For example, Kumar *et al.* [8] compared derivatization reagents and finally selected *N*-methyl-*N*-(trimethylsilyl) trifluoroacetamide (MSTFA): ammonium iodide (NH_4I): dithioerythritol (DTE) (500:4:2, v/w/w) as the derivatization reagent to convert all BA to their TMS derivatives via their reaction at 60 °C for 30 min. The requirement for derivatization in

GC analysis is less favorable for the possible artifacts caused during reaction, which may increase the uncertainty in quantitative analysis. In contrast, LC methods not requiring derivatization have been more widely used for BA analyses, in conjunction with several types of detection systems such as flame ionization detector (FID), charged aerosol detector (CAD), refractive index (RI), evaporative light scattering detection (ELSD), ultraviolet (UV), and MS. Of these, LC/MS or LC/MS/MS is the most popular because of the high sensitivity and selectivity achieved by coupling with MS. Relatively newer separation approaches like UPLC and SFC have also been used in BA analyses. UPLC-ESI-MS/MS was performed by Want *et al.* [10] to profile BA in serum samples. The applicability of SFC as a rapid and efficient BA separation technique was demonstrated by the work of Taguchi *et al.* [11]. MEKCE was also tested in the determination of cholic acid (CA), hyodeoxycholic acid (HDCA), and chenodeoxycholic acid (CDCA) in artificial *Calculus bovis* [12]. However, this is far less complex than the BA composition analysis required in many biological matrices.

Despite these advances in analytical techniques, the prerequisite for successful analysis is the selection of an optimized sample preparation method giving high recovery and the removal of interfering substances. To this end, BA and their conjugates have been extracted by a variety of methods selected according to the sample types. For example, in the extraction of BA from plasma and liver samples, ice-cold acetonitrile or alkaline acetonitrile (5% NH_4OH), respectively, were used to allow the separation of BA from protein precipitates [4]. In the same paper, BA from mouse bile and urine samples were also extracted by solid phase extraction (SPE), prior to chromatographic analysis [4]. In other studies, primarily analysis of human or animal bile samples, a single dilution step with methanol [13] or distilled water [14] was the only sample preparation used prior to BA analysis. Although many different techniques have been used for BA enrichment,

SPE is still the most widely used one giving high selectivity. Various sorbent materials have been used with C18 being the predominant option [15, 16]. However, even considering one sorbent chemistry, many SPE protocols could be employed to extract bile acids due to the differences in sorbent particle sizes, pore diameter/volume and surface area. Perwaiz *et al.* [16] used a Bond-Elute C18 cartridge for extracting BA from human gallbladder bile samples. They loaded 20 μL of diluted sample onto the column and then washed it using 2 mL of water and *n*-hexane followed by 5 mL methanol for eluting BA. On the other hand, Siow *et al.* [15] reported the utilization of a Sep-Pak C18 cartridge for BA isolation from rat bile samples. In their work, 100 mL of sample was injected into the cartridge which was then washed with 10-20 mL of water and BA were finally recovered by pumping 5.0 mL of methanol through the cartridge. Thus, SPE parameters, like the volume of loading sample, appropriate solvents for washing and elution, and so forth, must be evaluated in order to maximize the extraction recovery yields.

To address PNALD, some co-authors of this paper have reported that intravenous administration of the ileum-derived trophic factor, glucagon-like peptide-2 (GLP-2), in a pre-clinical model of neonatal PNALD, was associated with improved bile flow, and serum and histologic markers of cholestasis [17]. The objective of the present study was to develop a universal method based on LC/MS/MS to monitor the alterations in the BA compositions in piglet bile samples in a control group compared to a GLP-2 treated group. Also, we optimized the SPE conditions for the extraction of BA from bile samples. Finally, the validation of the combined extraction method and single-stage LC/MS/MS analysis is described. The BA profiling data were used to illustrate the role of GLP-2 in PNALD therapy [7].

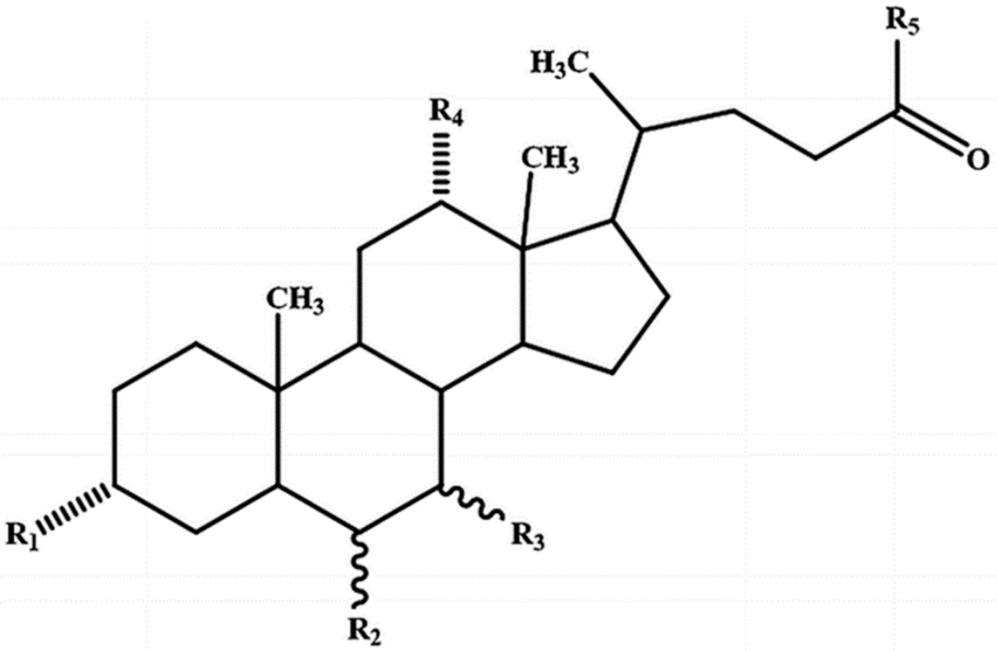

Group	Bile acids	R_1	R_2	R_3	R_4
Trihydroxy BA	Cholic acid	OH	H	α-OH	OH
	α-Muricholic acid	OH	β-OH	α-OH	H
	β-Muricholic acid	OH	β-OH	β-OH	H
	ω-Muricholic acid	OH	α-OH	β-OH	H
	Hyocholic acid	OH	α-OH	α-OH	H
Dihydroxy BA	Chenodeoxycholic acid	OH	H	α-OH	H
	Deoxycholic acid	OH	H	H	OH
	Ursodeoxycholic acid	OH	H	β-OH	H
	Hyodeoxycholic acid	OH	α-OH	H	H
Monohydroxy BA	Lithocholic acid	OH	H	H	H

Figure 2-1. A typical structure and classification of bile acid molecules. R5 can be replaced either by a free carboxylic acid group (classified as free bile acids) or by a glycine group or taurine group via an amide linkage (classified as conjugated bile acids).

2.2. Materials and Methods

2.2.1. Materials and reagents

Cholic acid, deoxycholic acid, ursodeoxycholic acid, taurocholic acid, taurodeoxycholic acid, taurolithocholic acid, glycodeoxycholic acid, hyodeoxycholic acid, hyocholic acid, *α*-muricholic acid, *β*-muricholic acid, *ω*-muricholic acid, tauro-*α*-muricholic acid, tauro-*β*-muricholic acid, taurohyocholic acid, glycolithocholic acid, and glycoursodeoxycholic acid were purchased from Steraloids, Inc. (Newport, RI). Lithocholic acid and chenodeoxycholic acid were obtained from Sigma-Aldrich Chemical Co. (St. Louis, MO). The deuterated internal standard glycocholic acid-2, 2, 4, 4-d_4 was ordered from C/D/N isotopes (Pointe-Claire, Quebec). HPLC-grade ammonium formate (≥99%) and ammonium acetate (≥98%) were supplied by Sigma-Aldrich Chemical Co. (St. Louis, MO). Formic acid and acetic acid of LC/MS grade were ordered from the Fisher Scientific Company (Ottawa, Ontario). Water and acetonitrile were of LC/MS grade from Fisher Scientific Company (Ottawa, Ontario). All the other solvents were of HPLC grade and were obtained from the Fisher Scientific Company (Ottawa, Ontario).

Bile samples were collected from neonatal male Landrace/Large White cross piglets provided by the Swine Research and Technology Center (University of Alberta, Edmonton, AB, Canada). All samples were stored in Eppendorf tubes and maintained at -20 °C for further use.

2.2.2. Preparation of stock, work and quality control (QC) standard solutions

All BA standards and the internal standard (IS: GCA-d_4) were accurately weighed and dissolved individually in LC-grade methanol to make stock solutions at 1 mg mL^{-1}. All stock solutions were stored in sealed vials at -20 °C until needed. Working standard solutions for calibration (2.5, 5, 10, 50, 100, 500, 2500, and 5, 000 ng mL^{-1}) were prepared by diluting stock solutions in methanol. Triplicate low-, medium-, and high-level quality control (QC) standards were separately prepared in methanol at 5 ng mL^{-1} (QC, L); 100 ng mL^{-1} (QC, M); 2500 ng mL^{-1}

(QC, H) for GUDCA, GDCA, GLCA, TDCA, and TLCA; 10 ng mL^{-1} (QC, L); 100 ng mL^{-1} (QC, M); 2500 ng mL^{-1} (QC, H) for TαMCA, TβMCA, THCA, TCA, ωMCA, αMCA, βMCA, HCA, CA, and DCA; 50 ng mL^{-1} (QC, L); 250 ng mL^{-1} (QC, M); 2500 ng mL^{-1} (QC, H) for UDCA, HDCA and CDCA; 100 ng mL^{-1} (QC, L); 250 ng mL^{-1} (QC, M); 2500 ng mL^{-1} (QC, H) for LCA.

2.2.3. Sample preparation

Piglet bile samples were obtained while simultaneously measuring bile flow as an outcome measure of liver disease. As previously described [17], following 17 days of study, the piglets were given general anesthesia and a laparotomy was performed. The gallbladder was emptied and the cystic duct was ligated to prevent back flow and ensure accurate measurements. An 8-cm long 7-French polyurethane catheter was inserted into the common bile duct and secured with 3-0 silk suture. After bile flow normalized for 5 min, bile was collected into pre-weighed micro-centrifuge tubes for 10 min, followed by a 5-min rest period to allow for normalization of bile flow. This process was repeated until there was less than a 10% difference between three successive 10-min collections or a total of six 10-min collections had been performed. Bile samples were then stored at -80 °C until further processing.

Bile samples were first thawed at room temperature and a 150-µL aliquot of each was transferred to a 1.5 mL glass vial. Each bile sample was then diluted tenfold with LC/MS grade water prior to the SPE process, due to their high content of inorganic salts. All bile samples were cleaned up in duplicate by SPE using conditions described in the “Results and Discussion”.

2.2.4. Optimization of SPE conditions

SPE was used to remove the hydrophilic salts present in the bile samples and to avoid the possibility of contaminating the mass spectrometer. Alltech C18 SPE cartridges (particle size: 50

μm; column phase: reversed; bed weight: 900 mg) (Grace Division Discovery Science, Deerfield, IL, USA) were used for this purpose. Extraction conditions were optimized in terms of the composition of loading buffer and the elution volume of methanol. The tested values of these two parameters are listed in **Table 2-2**. Optimization experiments were carried out on a standard solution with a concentration of 500 ng mL^{-1}. The performance of these conditions was evaluated by the recovery rate which was reported as the ratio of the peak area of each analyte in the extract after SPE compared to that in the original standard solution without extraction.

2.2.5. LC/MS/MS conditions

The HPLC system used a binary pump and autosampler (Agilent Technologies, Palo Alto, CA, USA) coupled to a 3200 QTRAP mass spectrometer (AB SCIEX, Concord, ON, Canada). The data was processed using Analyst 1.4.2. software.

2.2.5.1. LC separation

LC separation was performed in triplicate using an Ascentis Express C18 column (7.5 cm×2.1 mm i.d., 2.7 μm in particle size) (Sigma, St. Louis, MO). The mobile phase was composed of (A) water with 0.1% formic acid and 5 mM ammonium formate, and (B) methanol and acetonitrile (1:3, *v/v*) with 0.1% formic acid and 5 mM ammonium formate. The running time was 12 min (not including equilibration) with a constant flow rate of 300 μL min^{-1}. The detailed gradient elution process was: 0-3 min, 35-45% B; 3-10 min, 45-100% B; 10-12 min, 100% B. The column was then re-equilibrated under the initial conditions (35% B) for 5 min prior to the next analysis. The auto-sampler temperature was set to 15 °C and the injection volume was 5 μL. Since only a simple SPE sample clean-up procedure was used, automated column valve switching was used to divert the column eluent to waste before and after the data acquisition window of 1-12 min to prevent

the contamination of the mass spectrometer.

2.2.5.2. MS/MS conditions

A turbospray ion source (electrospray ionization) was used in the negative ion mode. A combination of selected ion recording (SIR) and multiple reaction monitoring (MRM) scan modes were developed for the quantification of the analytes of interest. Nitrogen was used as curtain gas, nebulizing gas, and drying gas. All other instrumental parameters used were as following: curtain gas, gas 1 and gas 2 at 25, 40, and 50 arbitrary units, respectively; ion spray voltage at -3.7 kV. Nitrogen nebulization and drying gas were 12 and 300 L h^{-1}, respectively and the ion source temperature was 400 °C.

The SIR and MRM transitions and optimized mass spectrometer parameters for each analyte and their reference internal standards are shown in **Table 2-1**. All eight transitions were monitored throughout the run with an overall cycle time of 100 ms.

Table 2-1. MRM transitions and optimized parameters for each compound.

Compounds	SIR or MRM transition (*m/z*)	DP[a] (V)	EP[a] (V)	CEP[a] (V)	CE[a] (V)	CXP[a] (V)
CA	407.3	-70	-10	-15	-15	-2
*α*MCA	407.3	-70	-10	-15	-15	-2
*β*MCA	407.3	-70	-10	-15	-15	-2
*ω*MCA	407.3	-70	-10	-15	-15	-2
HCA	407.3	-70	-10	-15	-15	-2
CDCA	391.3	-75	-10	-15	-15	-2
DCA	391.3	-75	-10	-15	-15	-2
UDCA	391.3	-75	-10	-15	-15	-2
HDCA	391.3	-75	-10	-15	-15	-2
LCA	375.3	-70	-10	-15	-15	-2
TCA	514.3→80.0	-80	-10	-15	-115	-1
T*α*MCA	514.3→80.0	-80	-10	-15	-115	-1

TβMCA	514.3→80.0	-80	-10	-15	-115	-1
THCA	514.3→80.0	-80	-10	-15	-115	-1
TDCA	498.3→80.0	-70	-8	-15	-105	-1
TLCA	482.3→80.0	-85	-10	-15	-110	-1
GUDCA	448.3→74.0	-65	-7	-15	-70	-1
GDCA	448.3→74.0	-65	-7	-15	-70	-1
GLCA	432.3→74.0	-65	-7	-15	-65	-1
IS: GCA-d_4	468.3→74.0	-70	-7	-15	-70	-1

[a] DP, EP, CEP, CE and CXP are declustering potential, entrance potential, collision cell entrance potential, collision energy and collision cell exit potential.

2.2.6. Method validation

To ensure the reliability and repeatability of the newly developed method, validation studies were carried out in terms of linearity, limits of detection (LOD) and quantification (LOQ), accuracy, precision and extraction recoveries. All these parameters were determined under optimized conditions.

2.3. Results and Discussion

2.3.1. Optimization of SPE conditions

In order to achieve retention of all 19 BA and conjugates onto the C18 SPE, it is necessary to include a weak acid in the solution loaded onto the cartridge. Initially, the optimal concentration of formic acid added to the solution containing all 19 compounds in methanol was evaluated. The SPE cartridge was conditioned with 5 mL methanol, followed by 5 mL water. Then solutions of BA standards (including the internal standard GCA-d_4) with or without added formic acid solutions or various concentrations were loaded onto the cartridge. The cartridge was then washed with 5 mL water and target BA molecules were eluted with 7 mL methanol. Finally, the collected eluents were dried under N_2 and reconstituted in 500 µL of methanol for subsequent HPLC analysis of

individual BA. As can be seen in **Table 2-2**, when the BA standard solution was directly loaded onto the cartridge without the addition of formic acid solution, the recovery rates for all of the target analytes were less than 80%. The lowest recovery rate was obtained with TαMCA which was only 7.3%. This is possibly due to the relatively weak interaction between the analytes and the stationary phase of the cartridge. To solve this problem, formic acid, as a buffer solution, was added to the standard solution. Three levels of concentration (0.1, 0.5, and 1%) were investigated. The results indicated that the recovery rates increased for most analytes with an increase in the concentration of the formic acid solution. When 1% formic acid was added to the tested standard solution, the recovery rates for most analytes were found to be all greater than 90% (**Table 2-2**). Therefore, 1% formic acid was selected as the optimal buffer solution to load onto the cartridge.

The volume of eluent was optimized to maximize the elution of the compounds of interest from the sorbent. Three different levels (5, 7, and 10 mL) were tested as indicated in **Table 2-2**. It was found that the highest recovery for the BA analytes was achieved by eluting with 7 mL methanol.

Ultimately, the optimized SPE procedure used an Alltech C18 SPE cartridge (Grace Division Discovery Science, Deerfield, IL, USA) conditioned with 5 mL methanol followed by 5 mL water. A solution containing a mixture of 125 µL sample solution, 125 µL IS (GCA-d_4) solution and 250 µL buffer solution (1% formic acid) was loaded onto the SPE cartridge, which was subsequently washed by 5 mL water. Target BA molecules were eluted by 7 mL methanol and the extracted BA fraction was dried under a stream of nitrogen. The dried sample was dissolved in 500 µL of methanol and injected into the HPLC system.

Table 2-2. Recoveries of tested bile acids under different SPE conditions.

Compounds	Recovery rate (%)						
	7 mL Methanol				1% formic acid		
	No buffer solution	0.1% formic acid	0.5% formic acid	1% formic acid	5 mL MeOH	7 mL MeOH	10 mL MeOH
CA	57.9	91.4	93.3	96.1	91.3	95.0	87.2
*α*MCA	49.3	90.5	92.9	93.5	88.7	92.4	84.8
*β*MCA	59.3	91.3	92.0	94.3	89.6	95.7	86.0
*ω*MCA	50.8	90.6	94.1	94.7	89.4	94.3	85.9
HCA	59.4	92.8	92.8	93.5	87.5	92.8	83.1
CDCA	66.9	90.4	92.8	94.2	89.9	95.2	83.8
DCA	62.9	87.8	89.0	90.3	83.7	89.1	77.8
UDCA	57.3	93.1	93.8	94.6	85.4	93.5	81.5
HDCA	65.6	98.9	97.8	97.5	94.0	99.9	87.3
LCA	78.8	92.7	99.6	98.7	96.3	99.8	89.8
TCA	8.9	94.8	98.6	99.0	95.0	100.2	95.4
T*α*MCA	7.3	89.4	91.9	91.8	87.4	94.7	88.4
T*β*MCA	7.6	90.9	92.7	92.1	88.9	95.7	89.3
THCA	8.5	94.2	97.3	98.4	94.1	98.0	96.9
TDCA	10.0	93.9	96.1	97.0	94.0	98.2	92.6
TLCA	12.0	89.4	91.9	92.3	85.9	91.1	82.7
GUDCA	54.1	91.5	93.5	94.7	92.1	97.2	87.6
GDCA	60.4	89.2	91.7	93.4	85.2	91.1	81.7
GLCA	75.7	87.6	89.5	91.9	84.3	90.5	78.4
IS: GCA-d_4	47.6	85.1	88.8	93.0	88.3	91.4	86.0

2.3.2. Optimization of chromatographic separation and mass spectrometric parameters

A solution of BA standards including the IS (GCA-d_4) was used for the optimization of the chromatographic conditions and the mass spectrometric parameters.

In order to achieve a good chromatographic separation of all 19 target BA analytes within a short analysis time and low backpressure, three analytical columns were compared, namely,

Ascentis C18 (15 cm×2.1 mm i.d., 3 μm in particle size), Ascentis Express C18 (7.5 cm×2.1 mm i.d., 2.7 μm in particle size), and Ascentis Express C18 (15 cm×2.1 mm i.d., 2.7 μm in particle size). As expected, the Ascentis Express column showed improved performance over the conventional porous C18 column since it contains solid-core particles with a porous outer layer resulting in a shorter diffusion path for analytes, lower resistance to mass transfer and ultimately higher resolution [18]. It was found that all analytes could be sufficiently resolved in the shortest time using the 7.5 cm column so this was selected for use in this work (data not shown).

The binary mobile phase composition and gradient were optimized on the three candidate columns. As a starting point, a mobile phase of (B): methanol/acetonitrile (3:1, *v/v*) and (A): 20 mM ammonium acetate (pH 4, adjusted by acetic acid) was tested. In this separation, both TαMCA and TβMCA isomers and αMCA and ωMCA isomers cannot be resolved despite changes to the gradient. Using a mobile phase of (B): acetonitrile with 0.1% formic acid and (A): water with 0.1% formic acid, it was found that UDCA and HDCA isomers overlapped. In summary, it should be noted that there are challenges in separating isomers of the sulfonated taurine bound BA, the less acidic glycine bound BA and the non-bound BA all in a single run. Finally, a solvent system of (B): methanol and acetonitrile (1:3, *v/v*) with 0.1% formic acid and 5 mM ammonium formate and (A): water with 0.1% formic acid and 5 mM ammonium formate was selected. The resulting chromatogram of the 19 BA standards showed that except for the partial co-elution of TαMCA and TβMCA isomers, all of the other 17 BA analytes including isomeric forms were well resolved (**Figure 2-3**). In spite of the incomplete separation of TαMCA and TβMCA isomers, their retention times were sufficiently different for their identification. Optimization of the mobile phase gradients included varying the initial percentage of the aqueous phase from 100 to 60%. A gradient starting at a 65% aqueous mobile phase was ultimately selected to achieve sufficient resolution and speed.

BA species are commonly detected using ESI in the negative-ion mode because of the presence of the carboxylate group in the molecular structure (**Figure 2-1**). Thus, deprotonated molecule $[M-H]^-$ is easily observed for all types of BA molecules (**Figure 2-2**). Due to the presence of different functional groups on the side chain, free, glycine- and taurine-conjugated BA have different fragmentation behaviors. When the collision energy was low (≤50 eV), only deprotonated molecular ions $[M-H]^-$ were detected for free and bound BA molecules, with no fragmentation (data not shown). When the collision energy was increased to 65-70 eV, fragment species were observed for glycine-conjugated BA. With a further increase in collision energy to >100 eV, product ions appeared for taurine-conjugated BA. In contrast to the conjugated BA molecules, no significant fragmentation was observed at any collision energy for the free BA so that only $[M-H]^-$ ions were observed. Examples of the product ion MS/MS spectra are shown in **Figure 2-2**.

An abundant product ion of each $[M-H]^-$ precursor was selected and optimized as the quantifier of conjugated BA for MRM. The proposed structures of these precursor and product ions were shown in **Figure 2-2**. The following abundant product ions were used for optimum sensitivity and selectivity for quantitative analysis: *m/z* 74.0 (a fragment ion of the glycine moiety) for glycine-conjugated BA (**Figure 2-2C**), *m/z* 80.0 (an SO_3-anion from the taurine moiety) for taurine-conjugated BA (**Figure 2-2B**), and *m/z* 74.0 (a fragment ion of the glycine moiety) for IS (GCA-d_4) (**Figure 2-2D**). Notably, owing to the lack of fragment species for free BA, the precursor ion itself was used as the quantifier for SIR (**Figure 2-2A**). The optimized collision energies for collision-induced dissociation (CID) were 15 V for free BA, 65-70 V for glycine-conjugated BA, 105-115 V for taurine-conjugated BA and 70 V for IS (GCA-d_4) (**Table 2-2**).

Using the the optimized conditions, the LC-ESI-MS/MS analysis of all 19 BA compounds including isomeric forms was complete in less than 12 min (not including equilibration) as

indicated in **Figure 2-3**. It can be seen from **Figure 2-3** that the reversed-phase elution order of the free BA standards is UDCA>C > HDCA>CDCA>DCA>LCA, and that taurine-conjugated BA elute ahead of glycine-conjugated BA which elute ahead of free BA species. This result is consistent with the results reported by Monte *et al.* [1].

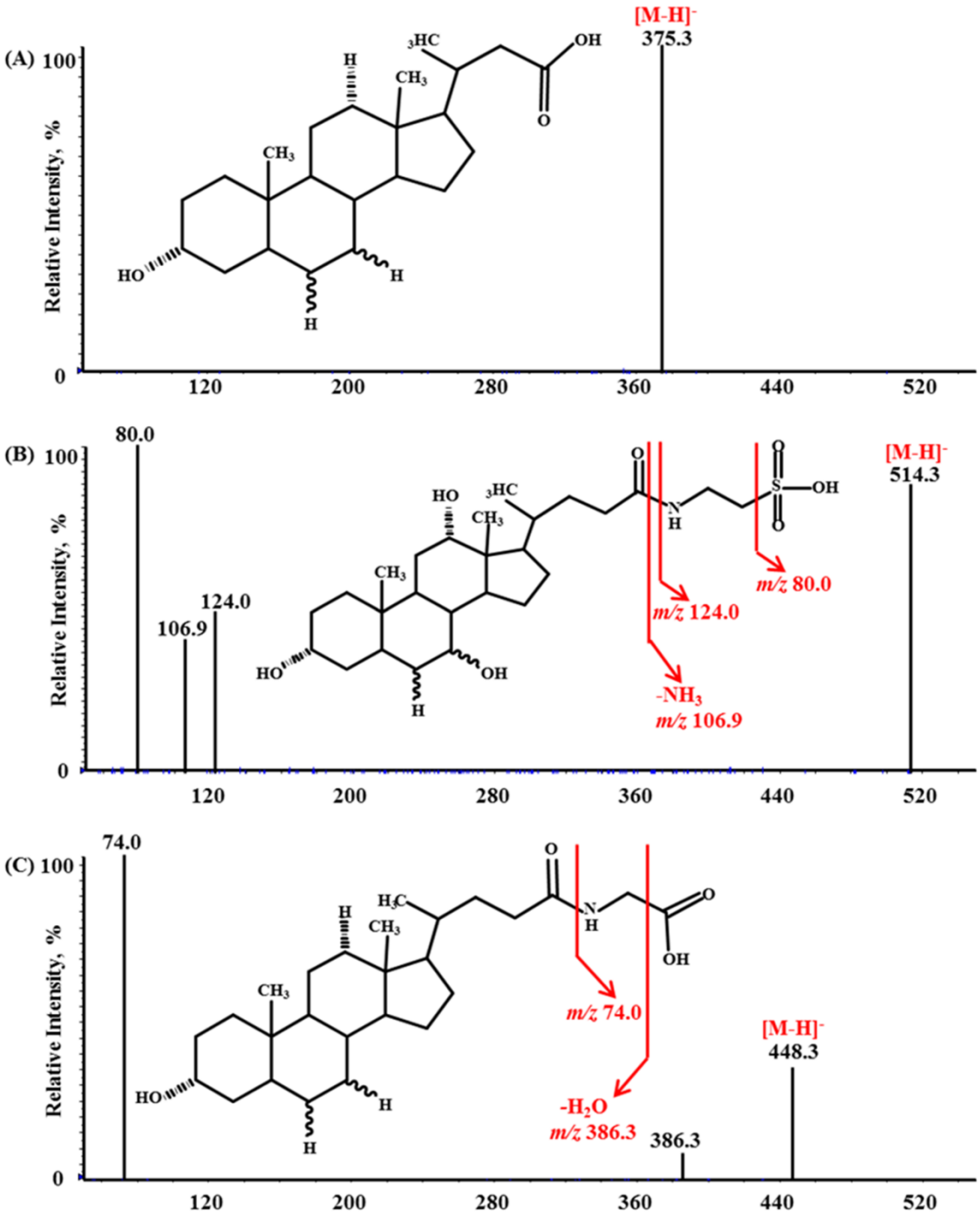

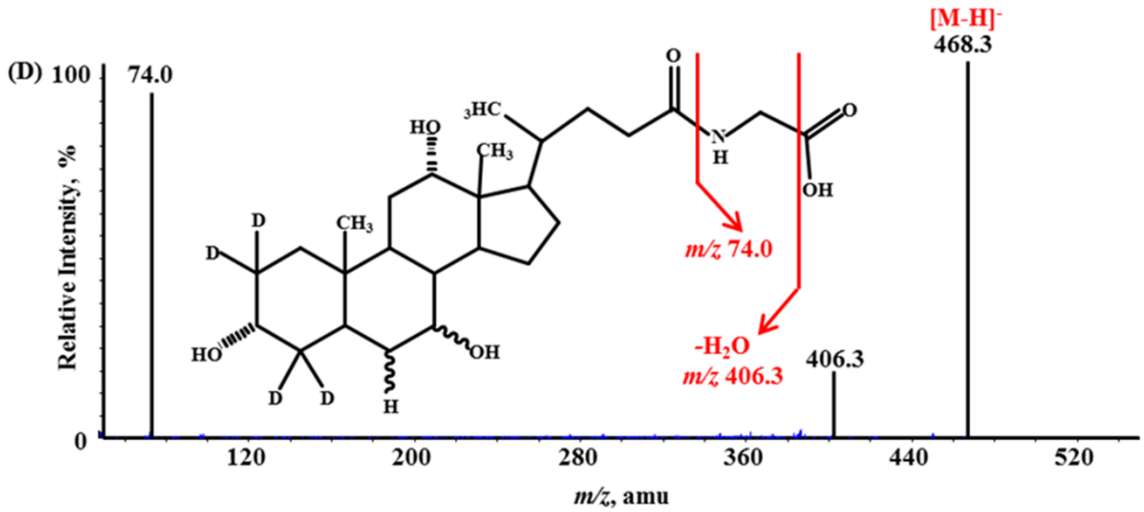

Figure 2-2. ESI-MS/MS product ion spectra of (A) free bile acids (LCA as an example), (B) taurine-conjugated bile acids (TCA as an example), (C) glycine-conjugated bile acids (GDCA as an example), and (D) IS: GCA-d_4. The chemical structures, molecular information, fragmentation patterns, as well as masses of parent and fragment ions for each compound are also shown.

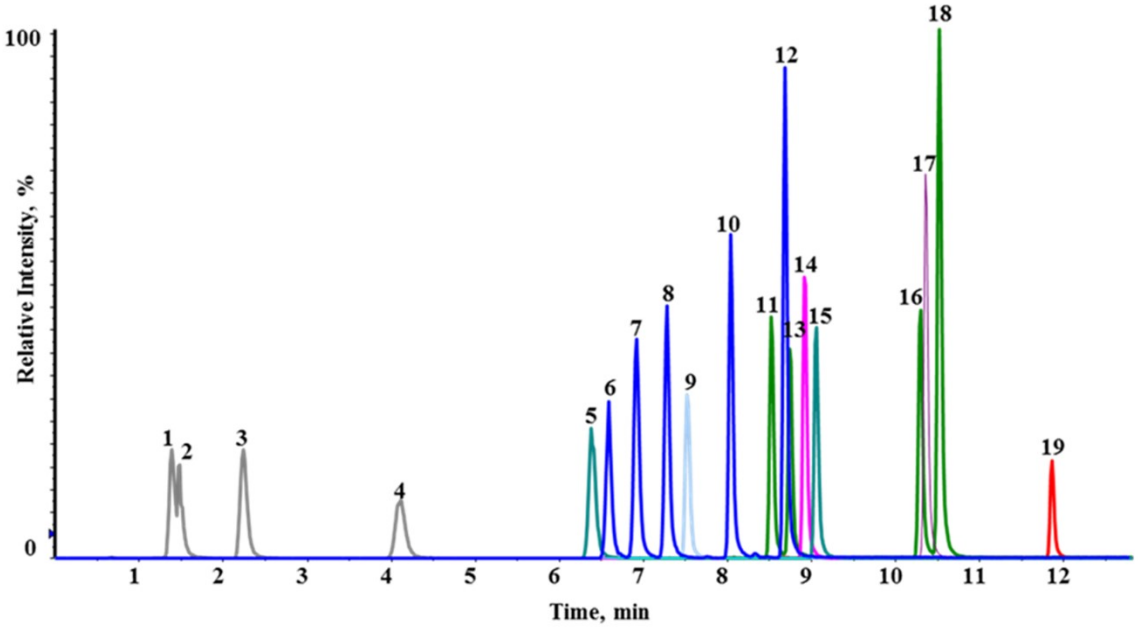

Figure 2-3. A representative chromatogram of bile acids in standard mixture solution at a concentration of 500 ng mL^{-1} using an Ascentis Express C18 column with established gradient elution. (1) TαMCA; (2) TβMCA; (3) THCA; (4) TCA; (5) GUDCA; (6) ωMCA; (7) αMCA; (8) βMCA; (9) TDCA; (10) HCA; (11) UDCA; (12) CA; (13) HDCA; (14) TLCA; (15) GDCA; (16) CDCA; (17) GLCA; (18) DCA; (19) LCA. Peaks with the same color are isomers.

2.3.3. Method validation

2.3.3.1. Calibration curves and linearity

Calibration curves were constructed with ranges of 2.5-5,000 ng mL^{-1} for GUDCA, GDCA, GLCA, TDCA, and TLCA; 5-5,000 ng mL^{-1} for TαMCA, TβMCA, THCA, TCA, ωMCA, αMCA, βMCA, HCA, CA, and DCA; 10-5,000 ng mL^{-1} for UDCA, HDCA, and CDCA; 50-5,000 ng mL^{-1} for LCA. GCA-d_4 at a constant concentration of 250 ng mL^{-1} was spiked as the internal standard for all BA analytes. Calibration curves were constructed by plotting the peak area ratios of analytes to their reference internal standards against the analyte concentrations. All BA standards displayed good linearity over the test ranges with R^2 values greater than 0.992 (**Table 2-3**). Subsequently, the calibration curves established in this manner were used for the quantification of BA in the piglet bile samples.

2.3.3.2. Limits of detection and quantification

In this work, limits of detection (LOD) and quantification (LOQ) were defined as the lowest concentration with a signal-to-noise ratio (S/N) greater than three and ten, respectively. LOD and LOQ values for this method were estimated independently for each BA analyte in a standard solution by serial dilution. The LOQ values of the analytes were also used as the lower ends of their corresponding calibration curves. The LOD and LOQ results in the low ng mL^{-1} range demonstrate that the method described here is of sufficiently high sensitivity for BA measurements.

The calibration curve equations, R^2 value, LOD, LOQ and linear dynamic range data for all BA standards used in this study are shown in **Table 2-3**.

Table 2-3. Calibration curves, LODs, LOQs and linear dynamic ranges in the quantitative analysis.

Compounds	Calibration curves	R^2 value	LOD (ng mL^{-1})	LOQ (ng mL^{-1})	Tested linear dynamic range (ng mL^{-1})
CA	y=2.69x+0.0235	0.9940	2.50	5.00	5-5,000
αMCA	y=1.53x+0.0092	0.9960	2.50	5.00	5-5,000
βMCA	y=1.44x+0.0032	0.9968	2.50	5.00	5-5,000
ωMCA	y=1.02x+0.0054	0.9974	2.50	5.00	5-5,000
HCA	y=1.59x+0.0062	0.9925	2.50	5.00	5-5,000
CDCA	y=1.52x+0.0084	0.9957	5.00	10.00	10-5,000
DCA	y=3.23x+0.0092	0.9948	2.50	5.00	5-5,000
UDCA	y=1.42x-0.0011	0.9969	5.00	10.00	10-5,000
HDCA	y=1.21x+0.0096	0.9968	5.00	10.00	10-5,000
LCA	y=0.429x-0.0024	0.9956	10.00	50.00	50-5,000
TCA	y=0.572x-0.0024	0.9975	2.50	5.00	5-5,000
TαMCA	y=0.732x-0.0003	0.9988	2.50	5.00	5-5,000
TβMCA	y=0.645x-0.0014	0.9981	2.50	5.00	5-5,000
THCA	y=0.569x-0.0014	0.9983	2.50	5.00	5-5,000
TDCA	y=1.04x+0.0004	0.9940	1.25	5.00	5-5,000
TLCA	y=1.76x-0.0001	0.9937	1.25	2.50	2.5-5,000
GUDCA	y=1.14x+0.0021	0.9987	1.25	2.50	2.5-5,000
GDCA	y=1.45x-0.0022	0.9952	1.25	2.50	2.5-5,000
GLCA	y=2.38x+0.0006	0.9954	1.25	2.50	2.5-5,000

2.3.3.3. Accuracy and precision

The precision and accuracy of the newly developed method were determined based on the analysis of triplicate preparation of three QC concentration points (high, medium, and low) distributed throughout the calibration range for all BA analytes (see Section **2.2.2.**). Each QC solution was analyzed by LC/MS in triplicate. The results obtained are summarized in **Table 2-4**. As can been seen from the table, the accuracy, defined as the percentage ratio of the measured concentration to the known concentration of the standard, ranged from 89.1 to 108.0% for QC low

(mean 98.9±5.1%), from 84.6 to 107.1% for QC medium (mean 99.3±7.1%), and from 87.9 to 107.4% for QC high (mean 97.1±6.4%). In contrast, the precision (for intraday triplicate measurements) of the method, presented as relative standard deviation (RSD), ranged from 0.5 to 9.3% for all QC samples. These data demonstrate that the proposed method is accurate and precise over the range studied in this work and can be used for the quantitative analysis of BA.

Table 2-4. Accuracy and precision for triplicate measurements of QC.

Compounds	QC-low		QC-medium		QC-high	
	Precision (RSD, %)	**Accuracy (%)**	**Precision (RSD, %)**	**Accuracy (%)**	**Precision (RSD, %)**	**Accuracy (%)**
CA	3.6	102.6	0.7	106.8	1.5	100.8
*α*MCA	4.5	92.8	4.2	100.6	2.9	104.8
*β*MCA	2.8	100.1	2.9	99.3	0.5	107.4
*ω*MCA	4.3	95.8	6.7	100.7	2.3	98.4
HCA	4.4	101.0	2.5	106.7	2.9	104.0
CDCA	4.9	100.4	1.8	92.0	2.1	91.0
DCA	5.4	98.9	2.3	107.1	2.1	103.3
UDCA	4.6	94.6	7.2	99.1	1.0	95.7
HDCA	1.0	100.5	3.4	94.7	2.1	99.2
LCA	5.3	93.5	1.1	84.6	1.5	87.9
TCA	5.5	92.7	1.6	86.7	3.1	89.8
T*α*MCA	1.5	99. 7	3.2	98.6	3.0	100.7
T*β*MCA	1.0	106.4	2.8	103.1	4.9	103.1
THCA	3.1	105.7	3.3	105.3	2.6	104.2
TDCA	9.3	97.6	3.2	101.2	2.7	91.5
TLCA	5.1	99.6	4.0	103.9	1.6	90.5
GUDCA	7.5	89.1	1.8	87.5	2.1	88.4
GDCA	7.7	100.6	2.8	102.6	3.0	94.1
GLCA	9.3	108.0	4.2	106.2	1.8	90.9

2.3.3.4. Extraction recovery

The optimized SPE method was validated by evaluating the recovery rates of the analytes. In the absence of a matrix blank, extraction recovery experiments were performed by spiking into piglet bile at two different levels, a solution containing known amounts of 19 authentic standards. All recovery trials were carried out in duplicate. The selected sample was firstly tenfold diluted with HPLC-grade water and then six aliquots of 125 μL were taken out from the diluted samples. Of these aliquots, four were spiked with the authentic standards at high and low levels (see **Table 2-5** for the detailed amounts), each in duplicate. The remaining two blank aliquots and the four spiked aliquots were extracted by the SPE procedure and each was analyzed in triplicate by the established LC-ESI-MS/MS method. The concentrations of the target analytes in all extracts were calculated determined based on their corresponding calibration curves (**Table 2-3**). Extraction recoveries were reported as a ratio of the measured spiked amount to the known spiked amount. **Table 2-5** displays the results of these recovery measurements. The average recovery rate of the low-level spiked concentration was 96.9±7.3% and the average recovery rate of the high-level spiked concentration was 98.3±6.8%. These values demonstrate that successful recovery of all tested BA analytes was obtained throughout the linear dynamic range of the analysis by the use of the optimized SPE procedures.

Table 2-5. Extraction recovery of bile acids in a piglet sample.

Compounds	Spiked concentration (ng mL^{-1})			Measured concentration (ng mL^{-1})		Extraction recovery (%)	
	Low	High	Non	Low	High	Low	High
CA	100	1000	ND	93.0±1.4	999.3±59.8	93.0	99.9
*α*MCA	100	1000	ND	105.8±0.8	1072.9±49.2	105.8	107.2
*β*MCA	100	1000	ND	104.4±2.3	1036.3±34.1	104.4	103.6
*ω*MCA	100	1000	ND	107.7±3.2	1060.5±57.1	107.7	106.1

HCA	100	1000	13.9±3.0	118.4±6.6	1095.9±104.0	104.2	108.1
CDCA	50	100	ND	47.0±2.1	96.7±4.1	94.0	96.7
DCA	100	1000	ND	92.0±1.9	950.4±37.8	92.0	95.0
UDCA	100	1000	ND	94.8±2.4	905.1±36.5	94.8	90.5
HDCA	50	100	1.6±0.9	54.9±1.9	105.5±6.7	106.4	103.9
LCA	50	100	16.9±2.4	67.1±3.7	113.5±4.1	100.3	97.1
TCA	500	5000	897.2±22.5	1279.0±53.8	4761.6±263.5	80.7	91.5
TαMCA	100	1000	ND	100.0±1.7	972.9±39.7	100.0	97.3
TβMCA	100	1000	ND	96.4±2.8	1008.7±58.3	96.4	100.9
THCA	500	5000	8339.8±35.2	8461.0±72.4	12172.0±679.3	95.7	91.2
TDCA	100	1000	ND	102.4±3.6	1086.3±20.1	102.4	108.6
TLCA	100	1000	2.6±0.7	90.3±2.1	908.9±43.1	88.1	90.7
GUDCA	100	1000	ND	95.1±2.8	979.8±40.0	95.1	97.9
GDCA	100	1000	ND	94.2±1.8	957.3±30.6	94.2	95.7
GLCA	100	1000	2.9±0.4	88.6±1.5	851.4±16.5	86.1	84.9

Data of bile acids were presented as mean±standard deviation (SD); ND not detected.

2.3.4. Application to piglet bile samples

To test the utility of the validated method, our experimental protocol was applied to the qualitative identification and quantitative determination of individual BA species in piglet bile samples from a clinical trial testing the efficacy of GLP-2 treatment in PNALD, as described in the Introduction. The piglet bile samples were first extracted using the optimized SPE procedure and then subjected to LC/MS/MS analysis. Up to 12 different BA species were identified in bile sample extracts from the control and GLP-2 treated groups, with the difference being that CDCA was not found in the GLP-2 treated group above the LOD.

Figure 2-4 shows a sample chromatogram of piglet bile extract. Note that in this figure, TCA and CDCA are not readily evident in the chromatograms because of their relatively low intensity compared to their isomers THCA and HDCA, respectively. Additionally, there are two unidentified peaks detected in the chromatogram of MRM transition *m/z* 498→80 at RT of 3.14

and 6.91 min, which are most likely isomers of TDCA (RT=7.61 min). From **Table 2-2**, it can be seen that possible isomers include TCDCA, TUDCA, and THDCA but standards of these taurine-conjugated BA are not available. Thus, assignment of the two observed isomers was performed by identifying the presence of the corresponding non-conjugated species: HDCA and CDCA were found in this case (**Table 2-6**). Further confirmation was derived from the relative elution order of the observed peaks by comparison to the observed elution order of non-conjugated standards (UDCA< HDCA<CDCA<DCA), as shown in **Figure 2-3**. Hence it was concluded that the two unknown peaks are in fact THDCA (RT=3.14 min) and TCDCA (RT=6.91 min).

There are also two unidentified peaks in the chromatogram of MRM transition *m/z* 448→74 at 6.53 and 8.58 min which are isomers of GUDCA (RT =6.28 min) and GDCA (RT =8.85 min) and therefore must be either GHDCA or GCDCA (**Table 2-2**). As above, comparison to the observed non-conjugated species and the elution order of non-conjugated standards indicates clearly that the unknown peak at 6.53 min is GHDCA and that at 8.58 min is GCDCA.

For quantification of the BA identified in the piglet bile test samples, there were eight of them for which authentic standards were available so could be accurately quantified based on the established calibration curves (**Table 2-3**). For the other four BA (THDCA, TCDCA, GHDCA, and GCDCA) for which authentic standards were not available, estimation of their concentrations was carried out based on the calibration curves for their corresponding isomers. Specifically, THDCA and TCDCA were estimated using to the calibration curve of TDCA, GHDCA was estimated using the calibration curve of GUDCA, and GCDCA was estimated based on the calibration curve of GDCA. The measured concentrations for the 12 identified BA are presented in **Table 2-6**. A detailed analysis of these results and the biological implications have been recently reported in a separate publication [7].

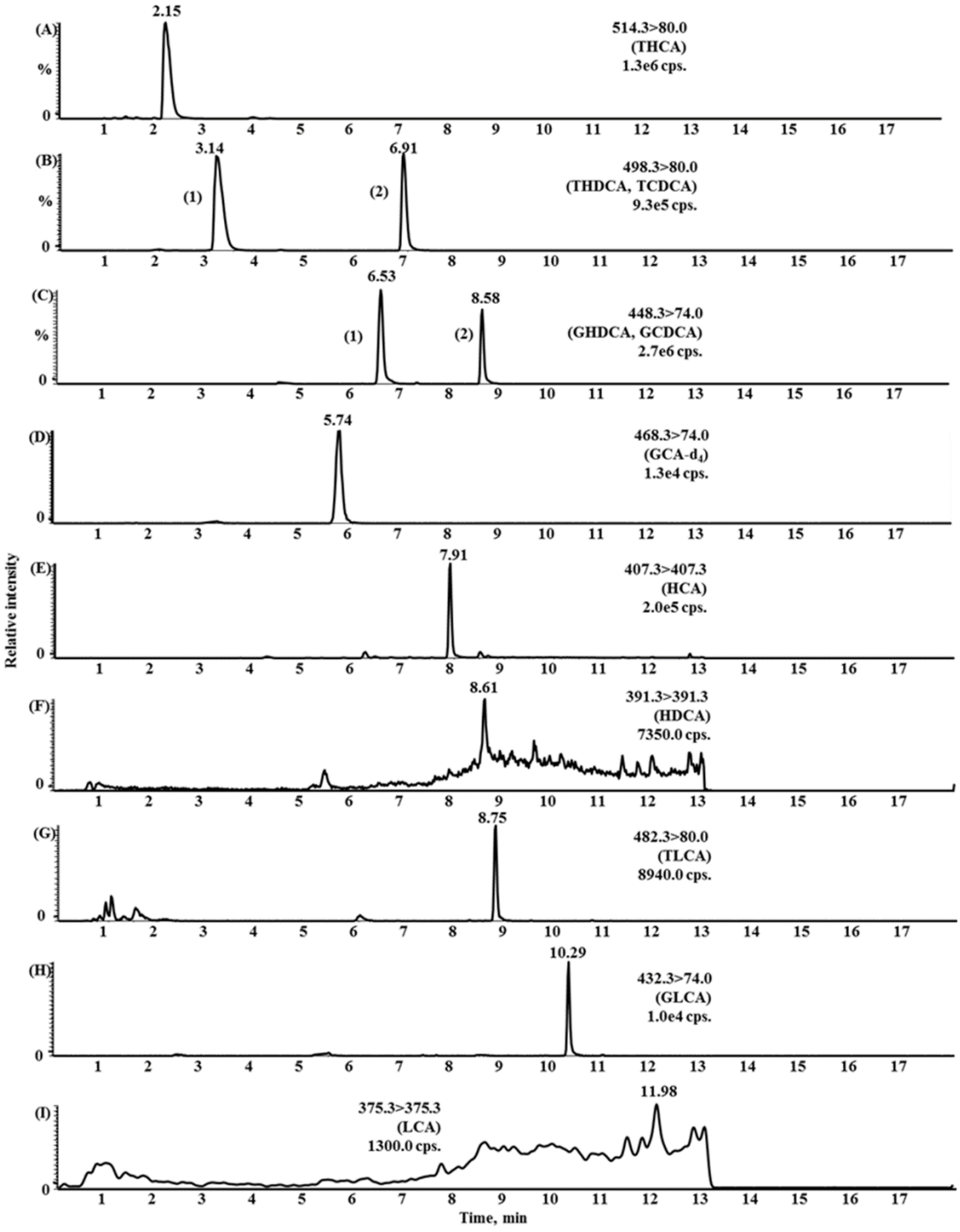

Figure 2-4. A representative chromatogram of bile acids in piglet bile sample extract under the established conditions. (A) THCA; (B) 1-THDCA, 2-TCDCA; (C) 1-GHDCA, 2-GCDCA; (D) **IS:** GCA-d_4; (E) HCA; (F) HDCA; (G) TLCA; (H) GLCA; (I) LCA.

Table 2-6. Contents of bile acids determined in piglet bile sample extract (quantification with GCA-d_4 as IS).

Compounds	Control group (n=8)	GLP-2 treated group (n=7)
	Mean (min-max)	Mean (min-max)
LCA	0.09 (0.07-0.12)	0.09 (0.03-0.13)
TLCA	1.62 (0.51-3.10)	0.14 (0.11-0.16)
GLCA	0.82 (0.37-1.07)	0.15 (0.12-0.18)
HCA	9.10 (5.24-14.31)	0.24 (0.11-0.72)
THCA	1353.18 (1004.83-2120.49)	157.61 (27.06-350.14)
TCA	46.82 (20.09-61.46)	23.97 (3.76-88.12)
HDCA	0.09 (0.06-0.13)	0.08 (0.05-0.13)
CDCA	0.11 (0.05-0.17)	---
THDCA	543.29 (240.95-813.66)	11.97 (1.36-29.15)
TCDCA	476.24 (335.26-685.22)	64.03 (8.45-148.26)
GHDCA	498.35 (157.48-827.69)	64.59 (23.73-173.29)
GCDCA	449.05 (209.17-638.87)	104.64 (14.34-401.63)

Values were expressed as μg bile acids/mL of tested piglet bile samples. Each value represented the average value of all samples from the same group. The quantified content range for each analyte was presented in the bracket after the mean value. All these values have been corrected according to the recovery rates.

2.4. Conclusions

In this study, we have established and validated a rapid and reliable method for the identification and determination of BA in piglet bile samples with an optimized SPE procedure for sample pretreatment. An efficient separation of 19 BA in a single chromatographic run was achieved with improvements in terms of the run time, the total number of analytes and the isomer separation compared to the literature [8, 18]. The LOD of the current method were similar to previously published results using comparable instrumentation [19], although achieving the lowest possible LOD was not an objective of this study due to the high levels of BA present in bile. However, lower LOD values may be desirable for studies of other extracts and there is scope to

achieve this via manipulation of sample concentrations and the use of more sensitive analytical equipment. The method described was specifically proposed as a tool to monitor the changes of BA contents, in this case for piglet bile samples treated with GLP-2 *vs* those in the control group. The quantification results showed that GLP-2 therapy did improve the clinical phenotype of PNALD by altering BA synthesis and transport. Based on all of these findings, conclusions could be drawn that BA can be used as biomarkers for the diagnosis of related liver diseases and the newly proposed analytical method can be used as a general means for BA analysis in various bio-samples, such as plasma, urine and feces for clinical and pharmaceutical purposes. For example, clinicians have been aware for some time that immaturities in the metabolism of BA contribute to a number of neonatal cholestatic diseases and to the increased risk of parenteral nutrition associated liver diseases for premature infants. Despite this, the molecular mechanisms of BA transport, metabolism and ultimately the associated composition of the BA pool have been inadequately studied and more often in rodent models that do not translate well to the developing human neonate. Furthermore, the differential diagnosis of neonatal cholestatic diseases requires prompt analysis of BA composition, which is not yet routinely clinically available [20]. The method described here could be readily adapted to apply to the noninvasive assessment of bile in urine for that purpose.

2.5. References

[1] M.J. Monte, J.J. Marin, A. Antelo, J. Vazquez-Tato, Bile acids: chemistry, physiology, and pathophysiology, World J Gastroenterol. 15 (2009) 804-816.

[2] J. Sjövall, Fifty years with bile acids and steroids in health and disease, Lipids. 39 (2004) 703-722.

[3] I. Bobeldijk, M. Hekman, J. de Vries-van der Weij, L. Coulier, R. Ramaker, R. Kleemann, T. Kooistra, C. Rubingh, A. Freidig, E. Verheij, Quantitative profiling of bile acids in biofluids and tissues based on accurate mass high resolution LC-FT-MS: compound class targeting in a

metabolomics workflow, J Chromatogr B. 871 (2008) 306-313.

[4] Y. Alnouti, I.L. Csanaky, C.D. Klaassen, Quantitative-profiling of bile acids and their conjugates in mouse liver, bile, plasma, and urine using LC-MS/MS, J Chromatogr B. 873 (2008) 209-217.

[5] P. Shahid, M. Diane, T. Beatriz, M.Y. Ibrahim, Rapid and improved method for the determination of bile acids in human feces using MS, Lipids. 37 (2002) 1093-1100.

[6] R.S. Kirti, Review on bile acid analysis, Int J Pharm Biomed Sci. 3 (2012) 28-34.

[7] D.W. Lim, P.W. Wales, S. Mi, J.Y. Yap, J.M. Curtis, D.R. Mager, V.C. Mazurak, P.R. Wizzard, D.L. Sigalet, J.M. Turner, Glucagon-like peptide-2 alters bile acid metabolism in parenteral nutrition-associated liver disease, J Parenter Enteral Nutr. 40 (2016) 22-35.

[8] B.S. Kumar, B.C. Chung, Y.J. Lee, H.J. Yi, B.H. Lee, B.H. Jung, Gas chromatography–mass spectrometry-based simultaneous quantitative analytical method for urinary oxysterols and bile acids in rats, Anal Biochem. 408 (2011) 242-252.

[9] X. Qiao, M. Ye, C. Xiang, T. Bo, W. Yang, C. Liu, W. Miao, D. Guo, Metabolic regulatory effects of licorice: a bile acid metabonomic study by liquid chromatography coupled with tandem mass spectrometry, Steroids. 77 (2012) 745-755.

[10] E.J. Want, M. Coen, P. Masson, H.C. Keun, J.T. Pearce, M.D. Reily, D.G. Robertson, C.M. Rohde, E. Holmes, J.C. Lindon, R.S. Plumb, J.K. Nicholson, Ultra performance liquid chromatography mass spectrometry profiling of bile acid metabolites in biofluids: application to experimental toxicology studies, Anal Chem. 82 (2010) 5282-5289.

[11] K. Taguchi, E. Fukusaki, T. Bamba, Simultaneous and rapid analysis of bile acids including conjugates by supercritical fluid chromatography coupled to tandem mass spectrometry, J Chromatogr A. 1299 (2013) 103-109.

[12] Z. Hu, L. He, J. Zhang, G. Luo, Determination of three bile acids in artificial Calculus bovis and its medicinal preparations by micellar electrokinetic capillary electrophoresis, J Chromatogr B. 837 (2006) 11-17.

[13] C.A. Bloch, J.B.Watkins, Determination of conjugated bile acids in human bile and duodenal fluid by reverse-phase high performance liquid chromatography, J Lipid Res. 19 (1978) 510-513.

[14] R.S. Plumb, P.D. Rainville, W.B. Potts, K.A. Johnson, E. Gika, I.D. Wilson, Application of ultra-performance liquid chromatography-mass spectrometry to profiling rat and dog bile, J Proteome Res. 8 (2009) 2495-2500.

[15] Y. Siow, A. Schurr, G.C. Vitale, Diabetes-induced bile acid composition changes in rat bile determined by high performance liquid chromatography, Life Sci. 49 (1991) 1301-1308.

[16] S. Perwaiz, B. Tuchweber, D. Mignault, T. Gilat, I.M. Yousef, Determination of bile acids in biological fluids by liquid chromatography-electrospray tandem mass spectrometry, J Lipid Res. 42 (2001) 114-119.

[17] D.W. Lim, P.W. Wales, J.K. Josephson, P.N. Nation, P.R. Wizzard, C.M. Sergi, C.J. Field, D.L. Sigalet, J.M. Turner, Glucagonlike peptide 2 improves cholestasis in parenteral nutrition-associated liver disease, J Parenter Enteral Nutr. 40 (2014) 14-21.

[18] E.R. Badman, R.L. Beardsley, Z. Liang, S. Bansal, Accelerating high quality bioanalytical LC/MS/MS assays using fused core columns, J Chromatogr B. 878 (2010) 2307-2313.

[19] M. Sergi, C. Montesano, S. Napoletano, D. Pizzoni, C. Manetti, F. Colistro, R. Curini, D. Compagnone, Analysis of bile acids profile in human serum by ultrafiltration clean-up and LC-MS/MS, Chromatographia. 75 (2012) 479-489.

[20] D. Haas, H. Gan-Schreier, C.D. Langhans, T. Rohrer, G. Engelmann, M. Heverin, D.W. Russell, P.T. Clayton, G.F. Hoffmann, J.G. Okun, Differential diagnosis in patients with suspected bile acid synthesis defects, World J Gastroenterol. 18 (2012) 1067-1076.

Chapter 3*

An LC/MS/MS Method for the Simultaneous Determination of Individual Sphingolipid Species in B Cells

3.1. Introduction

Sphingolipids include a wide range of bioactive compounds that can be found in eukaryotic organisms as well as some prokaryotes and viruses [1]. In mammalian bio-fluids and tissues, the sphingolipid family mainly includes the subclasses of ceramides (Cer), sphingomyelins (SM), cerebrosides, sulfatides and gangliosides. All of these lipid molecules are derived from a sphingoid base backbone which varies in chain length, degree of unsaturation and in the presence of a hydroxyl group [1, 2]. Specifically, Cer is produced from the sphingoid base by linking with a fatty acid (FA) chain (varying in length and degree of unsaturation) via an amide bond [1, 2]. Addition of sugar moieties or phosphatidylcholines (PC) to the 1-hydroxyl group of Cer leads to the formation of more complex glycosphingolipids (GSL) and SM [2]. Because of its structural composition, SM is often classified as a phospholipid (PL) and analyzed alongside other PL species [3]. Furthermore, gangliosides are characterized by a GSL molecule containing one or more sialic acids linked onto the sugar moiety [4]; similarly, sulfatides are formed via esterified linkage of a sulfate group to the sugar group on GSL molecules [5]. Considering the diversity and complexity of the structural characteristics of sphingolipid compounds, a tremendous number of individual molecular species can be present in biological samples. Following from their structural

* This chapter has been published as S. Mi, Y-Y Zhao, R.F. Dielschneider, S.B. Gibson and J.M. Curtis, "An LC/MS/MS Method for the Simultaneous Determination of Individual Sphingolipid Species in B Cells", *Journal of Chromatography B*, 1031 (2016) 50-60. I contributed to the experimental design, performance of experiments, data collection and analysis, as well as the manuscript composition.

diversity, sphingolipids are also well-known for their critical roles in many biological processes, such as cell apoptosis [6], cell mitogenesis and signal transduction [7]. Therefore, monitoring changes in sphingolipid profiles in biological materials has important implications for clinical and biological studies, such as discovery of new disease biomarkers [7], diagnosis of cognitive impairment in Parkinson's disease [8] and in the explanation of underlying related disease mechanisms [9]. The structural complexity of sphingolipids and their varied biological functions makes the characterization of this lipid class both a challenging and worthwhile task.

The analysis of sphingolipids is usually performed by combining LC separation techniques with different detection systems such as ultraviolet/visible (UV), fluorescence [10] and evaporating light scattering detector (ELSD) [11]. In addition, LC combined with mass spectrometry (MS) [6, 11, 12] has been widely used. Of these techniques, LC/ELSD has the advantage over LC/UV and LC/fluorescence that it avoids the need for derivatization [13]. Nonetheless, MS is still the most powerful tool due to its high sensitivity and ability to provide detailed structural information which is critical for the identification of individual sphingolipid molecules. Supercritical fluid chromatography (SFC) in conjunction with MS or ELSD is another choice for characterization of sphingolipids. An example of this was described by Lee *et al.* [14]. They reported the application of SFC/tandem mass spectrometry (SFC/MS/MS) for the analysis of seven subcategories of sphingolipids including SM, ceramide-1-phosphate (Cer1P), sphingosine-1-phosphate (So1P), sphinganine-1-phosphate (Sa1P), Cer, sphingosine (So) and sphinganine (Sa). This method has high throughput and high resolution, but requires a methylation procedure using trimethylsilyldiazomethane (TMSD) for the analysis of the more polar analytes which contain phosphate groups, such as phosphatidylserine, phosphatidic acid, lysophosphatidylserine, lysophosphatidylinositol and lysophosphatidic acid. Methylation was

shown to greatly improve chromatographic peak shapes and detection limits, further allowing for the quantification of low-abundance polar lipids.

Instead of simultaneously profiling multiple sphingolipid molecular species in a single run, many methods have been proposed that focus on only one [11] or two [7] specific analytes. However, since sphingolipid metabolism involves a dynamic network comprised of many different species, it is necessary to evaluate the comprehensive sphingolipid profile rather than a single metabolite in order to understand the function of these compounds [15]. Shaner *et al.* [12] described a reversed-phase LC-ESI-MS/MS approach to the quantitative analysis of a large set of sphingolipids, although fully validated assays were not included. The method proposed by Scherer *et al.* [15] applied hydrophilic interaction chromatography (HILIC) coupled to MS to quantify sphingolipid species from cultured cells. HILIC, as a separation technique, was used to separate the sphingolipids into classes based on their head group polarities, while species within the same class were eluted over a very narrow retention time (RT) window. Hence, most sphingolipid classes such as hexosyl-ceramide (HexCer) or SM can be resolved as an individual peak by HILIC chromatography. In this case [15], although some information about species with different FA substitutions within the same class is given based on MS data, these species coelute and are not readily quantified.

Here, we describe the development and validation of a more comprehensive method for the simultaneous qualitative and quantitative analysis of individual molecular species within each sphingolipid subclass. Specifically, we have investigated how sphingolipid metabolism is altered as a result of Chronic Lymphocytic Leukemia (CLL). CLL is the most common leukemia in North American and European adults [16]. Sphingolipid metabolism is altered in numerous cancers, but

strong evidence is still lacking to support this finding in CLL. To address this problem, an LC/MS/MS-based method was established in this study to investigate the distributions of sphingolipids in both cancerous and healthy B cells. In addition, we demonstrate the use of a simple method for the extraction of sphingolipid subgroups (covering a large polarity range) into a single phase. Finally, validation of the combined extraction procedure and the single stage of LC/MS/MS analysis, is described in detail. The analytical results obtained from cancerous and healthy B cells are compared to provide scientific evidence of altered sphingolipid metabolism in CLL cells. Such data will aid in the understanding of CLL biology and in the development of potential therapeutic strategies. For this specific purpose, seven subclasses of sphingolipids including So, Sa, So1P, Sa1P, Cer, dihydroceramide (dHCer) and glucosylceramide (GlcCer) (see **Figure 3-1**) were selected as the target analytes in this work. For reference, the metabolic pathways that interconvert these compounds are illustrated in **Figure 3-2** [1, 13, 17].

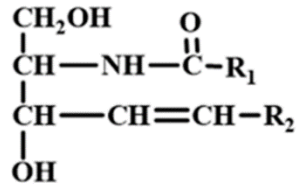

Ceramide (Cer)

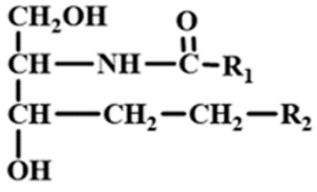

Dihydroceramide (dHCer)

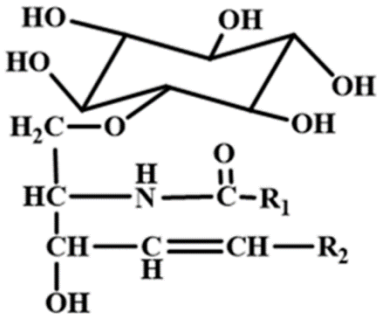

Glucosylceramide (GlcCer)

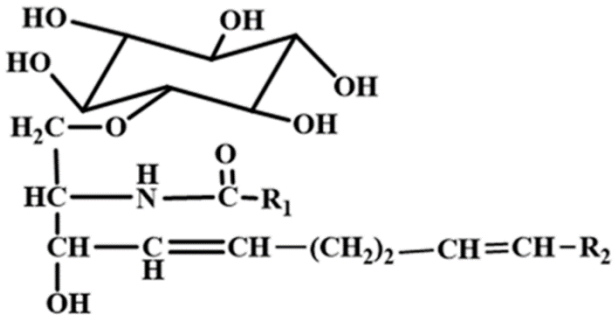

Glucosylceramide (GlcCer) from plant

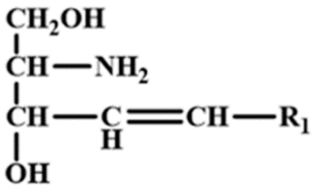

Sphingosine (So)

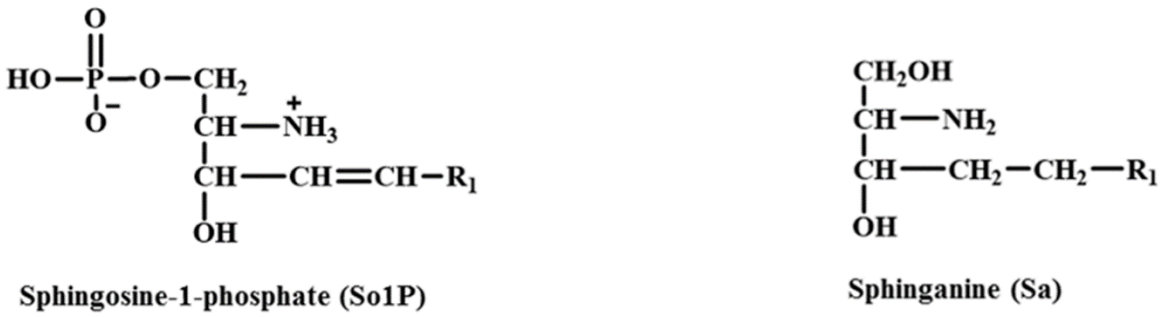

Figure 3-1. Structures of the compounds under investigation.

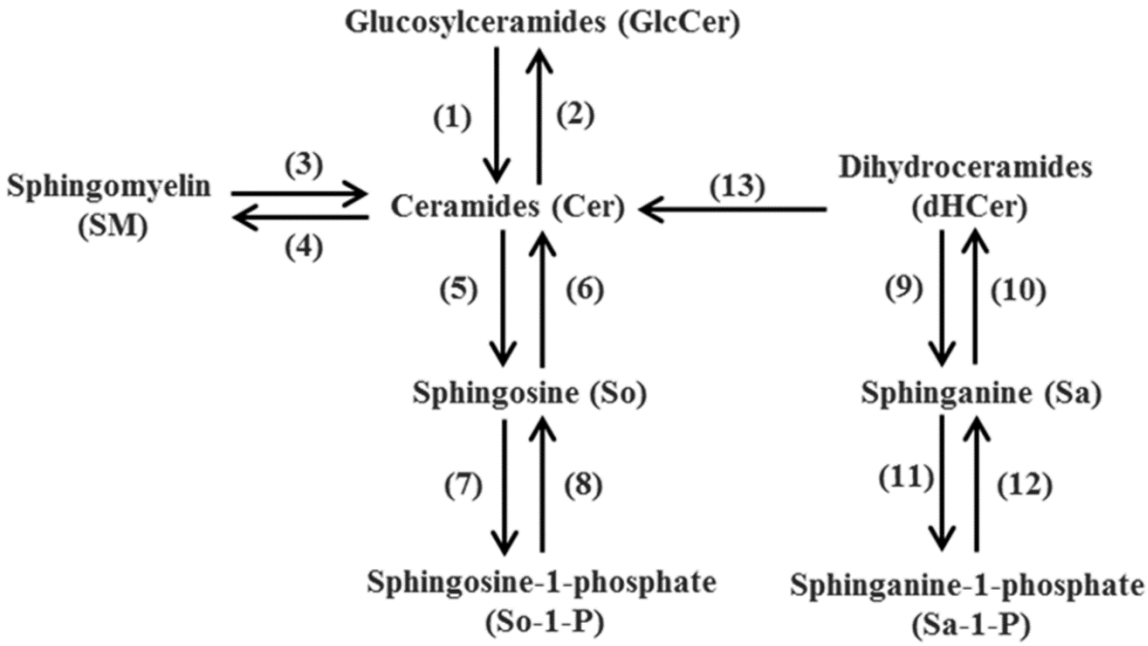

Figure 3-2. Metabolic pathway of sphingolipids (only including the target analytes in this study) (1), glucosylceramidase; (2), glucosylceramide synthase; (3), sphingomyelinase; (4), sphingomyelin synthase; (5), ceramidase; (6), ceramide synthase; (7), sphingosine kinase; (8), sphingosine phosphatase; (9), (10), dihydroceramide synthase; (11) (12) (13), Δ4-desaturase. Adapted from references [1, 13, 17].

3.2. Materials and Methods

3.2.1. Chemicals and reagents

Glucosylceramide (d18:1/16:0), glucosylceramide (d18:1/18:0), glucosylceramide (d18:1/18:1), glucosylceramide (d18:1/24:1), sphingosine (d18:1), sphinganine (d18:0), sphingosine-1-phosphate (d18:1), sphinganine-1-phosphate (d18:0) and the internal standards (ISs) of glucosylceramide (d18:1/17:0), sphingosine (d17:1) and sphingosine-1-phosphate (d17:1) were obtained from Avanti Polar Lipids Inc. (Alabaster, AL, USA). Glucocerebrosides from bovine buttermilk and glucocerebrosides from plant were ordered from ^{MJS}BioLynx Inc. (Brockville, ON, Canada). Ceramide (d18:1/2:0) and ceramide from bovine brain (a mixture of ceramide (d18:1/18:0) and ceramide (d18:1/24:1)) were purchased from Sigma-Aldrich (St. Louis, MO, USA). Individual standard solutions of ceramide (d18:1/16:0), ceramide (d18:1/22:0), ceramide (d18:1/24:1), ceramide (d18:1/24:0), ceramide (d18:0/16:0), ceramide (d18:0/24:0), the internal standards of Cer (d18:1/17:0), sphinganine (d17:0) and sphinganine-1-phosphate (d17:0) were prepared in chloroform/methanol (9:1, *v/v*) at 200 μM. Formic acid of Optima LC/MS grade was ordered from Fisher Scientific Company (Ottawa, ON, Canada). Water and acetonitrile were of Optima LC/MS grade from Fisher Scientific Company (Ottawa, ON, Canada). Except where noted, all the other solvents were of HPLC grade and were obtained from Fisher Scientific Company (Ottawa, ON, Canada).

3.2.2. Preparation of stock, work and quality control standard solutions

All the purchased standards were precisely weighted and dissolved individually in chloroform-methanol (2:1, *v/v*) to make stock solutions at 500 μM. All stock solutions were stored in sealed vials at -20 ˚C until needed.

Working standard solutions for calibration curves (2.5, 5, 10, 50, 100, 500, 1,000, 5,000 and 10,000 nM) were prepared by diluting stock solutions in methanol. Triplicate low, medium and high quality control (QC) standards were separately prepared in methanol at 10 nM (QC, L), 500 nM (QC, M), 5,000 nM (QC, H) for d18:1-So and d18:0-Sa; 50 nM (QC, L), 500 nM (QC, M), 5,000 nM (QC, H) for d18:1-So1P, d18:0-Sa1P, C16:0-dHCer and C24:0-dHCer; 5 nM (QC, L), 100 nM (QC, M), 5,000 nM (QC, H) for C16h:0-GlcCer, C16:0-GlcCer, C18:0-GlcCer, C18:1-GlcCer, C22:0-GlcCer, C24:1-GlcCer, C2:0-Cer, C16:0-Cer, C22:0-Cer, C24:1-Cer and C24:0-Cer.

3.2.3. Sample preparation

Peripheral blood samples were collected from Cancer Care Manitoba CLL patients or healthy age-matched donors after informed consent in accordance with the Research Ethics Board at the University of Manitoba. Samples were isolated as done previously [16]. Briefly, blood was centrifuged at 1500 rpm for 10 min and the buffy coat was isolated. To obtain B cells, the buffy coat was mixed with RosetteSep (Stem Cell Technologies, Vancouver, BC, Canada) and purified on a Ficoll-Paque gradient (GE Healthcare, Mississauga, ON, Canada) for 30 min at 1500 rpm. Residual red blood cells were lysed using RBClysis buffer (eBioscience, San Diego, CA, USA) for 10 min at room temperature. All blood samples were processed within 24 h after collection. Cell pellets were frozen in Eppendorf tubes and maintained at -20 °C until lipid extraction. CLL cell pellets contained 1×10^8 CLL cells and healthy B cell pellets contained 1×10^7 B cells.

For lipid extraction, the cell pellets were thawed at room temperature, re-suspended in LC/MS-grade water, vortexed for 15 s and sonicated for 20 min. Considering the large polarity range of the target analytes, the sample solution was subjected to extraction based on a modified Bligh and

Dyer method. In brief, an aliquot of 80 µL cell suspension solution was added into a 0.5 mL Eppendorf tube, spiked with recovery standards of d17:1-So, d17:0-Sa, d17:1-So1P, d17:0-Sa1P, C17:0-Cer and C17:0-GlcCer and mixed well with 300 µL of extraction solvent (chloroform/methanol, 1:2 by volume) to reach a final ratio of chloroform/methanol/water, 1:2:0.8 by volume. The mixture was then vortexed for 20 s and centrifuged at 2500 rpm for 15 min. The resultant supernatant was transferred into a separate glass vial. The extraction procedure was repeated once more and the supernatant extract was combined with the previous one. The final extract was dried under a nitrogen stream, re-dissolved into 500 µL of methanol and then filtered through a 0.22 µm PVDF membrane for subsequent LC/MS/MS analysis.

3.2.4. LC/MS/MS conditions

The HPLC system used a binary pump and autosampler (Agilent Technologies, Palo Alto, CA, USA) coupled to a 3200 QTRAP mass spectrometer (AB SCIEX, Concord, ON, Canada). The data was processed using Analyst 1.4.2.software.

LC separation was performed using an Ascentis Express C18 column (7.5 cm×2.1 mm i.d., 2.7 µm in particle size) (Sigma, St. Louis, MO). The mobile phase was composed of (A) water with 0.1% formic acid, and (B) methanol/acetonitrile/isopropanol (4:1:1, *v/v/v*) with 0.1% formic acid. The total run time was 25 min (including re-equilibration) with a constant flow rate of 300 µL min^{-1}. The gradient elution used was as follows: 0-4 min, 70 to 100% B; 4-20 min, 100% B and then brought back to 70% B at 20.1 min for column re-equilibrium over 5 min prior to the next injection. The auto-sampler temperature was set to 15 ˚C and the injection volume was 5 µL. An automated column valve switching was employed in this work to divert the column eluent to waste before and after the data acquisition window of 1 min to 20 min to prevent the contamination of the mass

spectrometer.

A Turbo Spray ion source (electrospray ionization) was used under positive ion mode. Multiple reaction-monitoring (MRM) scan mode was developed for the quantification of the analytes of interest. Nitrogen was used as curtain gas, nebulizing gas and drying gas. The instrument was operated using the following settings: curtain gas, gas 1and gas 2 at 25, 50 and 60 arbitrary units, respectively; ionspray voltage at 5.2 kV. Nitrogen nebulization and drying gas were held at 12 and 300 L h^{-1}, respectively; and the ion source temperature was 400 ˚C. Quadrupoles Q1 and Q3 were operating at unit mass resolution. The MRM transitions and optimized mass spectrometer parameters for each analyte for which authentic standards were available, along with their reference internal standards (ISs), are summarized in **Table 3-1**. In addition, the actual MS/MS method includes an additional 14 MRM transitions for analytes which were investigated but for which no standards were available. Specifically, these include C20:1-GlcCer (*m/z* 754.6→264.3), C20:0-GlcCer (*m/z* 756.6→264.3), C22:1-GlcCer (*m/z* 782.6→264.3), C26:1-GlcCer (*m/z* 838.6→264.3), C26:0-GlcCer (*m/z* 840.6→264.3), C12:0-Cer (*m/z* 482.3→264.3), C14:0-Cer (*m/z* 510.3→264.3), C16:1-Cer (*m/z* 536.3→264.3), C18:1-Cer (*m/z* 564.3→264.3), C20:1-Cer (*m/z* 592.3→264.3), C20:0-Cer (*m/z* 594.3→264.3), C22:1-Cer (*m/z* 620.3→264.3), C26:1-Cer (*m/z* 676.3→264.3) and C26:0-Cer (*m/z* 678.3→264.3). All 39 transitions (including all analytes plus ISs) were monitored throughout the run with an overall cycle time of 100 ms.

Table 3-1. MRM transitions and optimized parameters for each compound.

Compounds	MRM transitions (amu)	DP[a] (eV)	EP[a] (eV)	CEP[a] (eV)	CE[a] (eV)	RT[a] (min)
C2:0-Cer	342.3→264.3	31	3	15	23	6.2
C16:0-Cer	538.3→264.3	50	4	15	35	10.3
C18:0-Cer	566.3→264.3	40	4	18	35	11.7
C22:0-Cer	622.3→264.3	45	4.5	20	40	14.8

C24:1-Cer	648.3→264.3	50	4	15	40	14.6
C24:0-Cer	650.3→264.3	45	4.5	20	40	17.1
C16:0-dHCer	540.5→522.5	50	6	15	25	10.8
C24:0-dHCer	652.7→634.7	50	6	15	32	18.1
C16:0-GlcCer	700.6→264.3	35	6	12	45	9.5
C18:0-GlcCer	728.6→264.3	40	6	13	47	10.7
C18:1-GlcCer	726.6→264.3	40	5	15	47	9.9
C22:0-GlcCer	784.6→264.3	25	5	15	50	13.6
C24:1-GlcCer	810.6→264.3	40	5	13	55	13.4
C24:0-GlcCer	812.6→264.3	35	5	15	45	15.0
C16h:0-GlcCer	714.5→262.3	35	5	15	45	8.7
d18:1-So	300.3→282.3	30	4	12	15	2.9
d18:0-Sa	302.3→284.3	40	4	12	18	3.7
d18:1-So1P	380.3→264.3	35	4	12	22	5.5
d18:0-Sa1P	382.3→284.3	45	5	12	20	5.8
ISs: C17:0-Cer	552.3→264.5	50	3.5	15	35	11.0
C17:0-GlcCer	714.5→264.5	40	5	12	45	10.1
d17:1-So	286.3→268.3	20	7	12	15	1.9
d17:0-Sa	288.3→270.3	40	5	15	18	2.4
d17:1-So1P	366.3→250.3	35	4	15	20	4.7
d17:0-Sa1P	368.3→270.3	40	5	12	15	5.3

[a] DP, EP, CEP, CE and RT are declustering potential, entrance potential, collision cell entrance potential, collision energy and retention time.

3.2.5. Method validation

3.2.5.1. Calibration curves and linearity

Calibration curves were constructed with ranges of 5-10,000 nM for d18:1-So and d18:0-Sa; 10-10,000 nM for d18:1-So1P, d18:0-Sa1P, C16:0-dHCer and C24:0-dHCer; 2.5-10,000 nM for C16h:0-GlcCer, C16:0-GlcCer, C18:0-GlcCer, C18:1-GlcCer, C22:0-GlcCer, C24:1-GlcCer, C2:0-Cer, C16:0-Cer, C22:0-Cer, C24:1-Cer and C24:0-Cer. The mixed solution of d17:1-So, d17:0-Sa, d17:1-So1P, d17:0-Sa1P, C17:0-GlcCer and C17:0-Cer at a constant concentration of

100 nM was spiked as the ISs for d18:1-So, d18:0-Sa, d18:1-So1P, d18:0-Sa1P, GlcCer and Cer (including dHCer), respectively. Calibration curves were constructed by plotting the peak area ratios of analytes to their reference IS against the analyte concentrations. Calibration curve linearity was assessed by the correlation coefficient (R^2) value.

3.2.5.2. Sensitivity

Limits of detection (LOD) and quantification (LOQ) were defined as the lowest concentration with a signal-to-noise ratio (S/N) greater than 3 and 10, respectively. LOD and LOQ values for this method were estimated independently for each So, Sa, So1P, Sa1P, Cer, dHCer and GlcCer analyte in a standard solution with serial dilution. The LOQ values of the analytes were also used as the lower ends of their corresponding calibration curves.

The calibration curve equations, R^2 value, LODs, LOQs and linear dynamic range data for all sphingolipid standards used in this study were shown in **Table 3-2**.

3.2.5.3. Accuracy and precision

The precision and accuracy of the newly developed method were determined based on the analysis of triplicate preparation of 3 QC concentration points (high, medium and low) distributed throughout the calibration range for all So, Sa, So1P, Sa1P, Cer, dHCer and GlcCer analytes (see Section **3.2.2**). Each QC solution was analyzed by LC/MS/MS in triplicate. The results obtained were summarized in **Table 3-3**.

3.2.5.4. Extraction recovery

The optimized lipid extraction method was validated by evaluating the recovery rates of the analytes. In absence of a matrix blank, extraction recovery experiments were performed by spiking

into cell solutions at two different levels, a solution containing known amounts of 17 authentic standards. One of the samples from leukemia patients was used as an example for the recovery test. All recovery trials were carried out in triplicate. The selected sample was re-suspended in LC/MS-grade water and then 9 aliquots of 80 µL were taken out from the re-suspended samples. Of these aliquots, 6 were spiked with the authentic standards at high and low levels (see **Table 3-4** for the detailed amounts), each in triplicate. The remaining 3 blank aliquots and the 6 spiked aliquots were extracted under the same conditions and analyzed by the established LC/MS/MS method. The concentrations of the target analytes in all extracts were determined based on their corresponding calibration curves (**Table 3-2**). Extraction recoveries were reported as a ratio of the measured spiked amount to the actually spiked amount. **Table 3-4** shows the results of these recovery measurements.

3.3. Results and Discussion

3.3.1. LC/MS/MS method development

3.3.1.1. Fragmentation behaviors of all compounds under investigation

Sphingolipid compounds have been commonly detected by MS using ESI in the positive ion mode due to the facile protonation of their primary and secondary amine groups or in the case of the zwitterionic compounds, the preformed substituted ammonium groups in their molecular structures (**Figure 3-1**). Thus, protonated molecular ions $[M+H]^+$ are easily observed for all types of sphingolipid molecules.

In order to maximize the specificity and sensitivity of the proposed sphingolipid method, the optimal transitions for multiple reaction monitoring (MRM) experiments for all 7 subclasses of sphingolipids (**Figure 3-1**) must be established, along with that of the proposed ISs. First, for each

analyte, MS/MS experiments were carried out to demonstrate their fragmentation patterns, some examples of which are shown in **Figure 3-3** along with the proposed fragment pathways. In most cases, the MS/MS transitions giving fragment ions with the highest signal intensities, were ultimately selected for MRM detection. For example, the predominant product ion was *m/z* 264 (sphingoid base moiety) for Cer, GlcCer (**Figure 3-3**) (except for C16h:0-GlcCer) and So1P compounds (not shown) and corresponds to $[M+H\text{-FA chain-}2H_2O]^+$, $[M+H\text{-FA chain-glucose-}H_2O]^+$ and $[M+H\text{-}H_3PO_4\text{-}H_2O]^+$, respectively. The product ions at *m/z* 522 and *m/z* 634 were the most abundant fragment ions of protonated molecular ions for C16:0-dHCer (**Figure 3-3B**) and C24:0-dHCer (not shown). They were formed by the loss of water from their corresponding protonated parent ions. For d18:1-So and d18:0-Sa, the abundant product ions at *m/z* 282 and *m/z* 284 are also attributed to the dehydration of their pronated molecular ions. However, the major product ion at *m/z* 284 for d18:0-Sa1P (**Figure 3-3E**) arises through loss of phosphoric acid from the molecular structure.

Unlike the fragmentation pattern shown for C16:0-GlcCer in **Figure 3-3C** which shows the predominant product ion at *m/z* 264, as typically found for GlcCer compounds, for C16h:0-GlcCer, a fragment ion at *m/z* 262 was detected. C16h:0-GlcCer consists of an amide-linked FA chain with 16 carbon atoms, a sphingadiene ($d18:2^{\Delta 4,\ 8}$) as the sphingoid base and a glucose as the polar headgroup. This ion was also identified as $[M+H\text{-FA chain-glucose-}H_2O]^+$, but due to the presence of two double bonds in the sphingoid base (see **Figure 3-1**) compared to only one for the other GlcCer compounds, the product ion detected is *m/z* 262 in this case.

Instrumental parameters including DP, EP, CE, CEP and RT for each compound were optimized by infusing the individual standard solution into the Turbo Spray ion source of the QTRAP mass spectrometer using the syringe pump at a flow rate of 10 µL min^{-1}. The final

optimized data for all analytes and IS were described in **Table 3-1**.

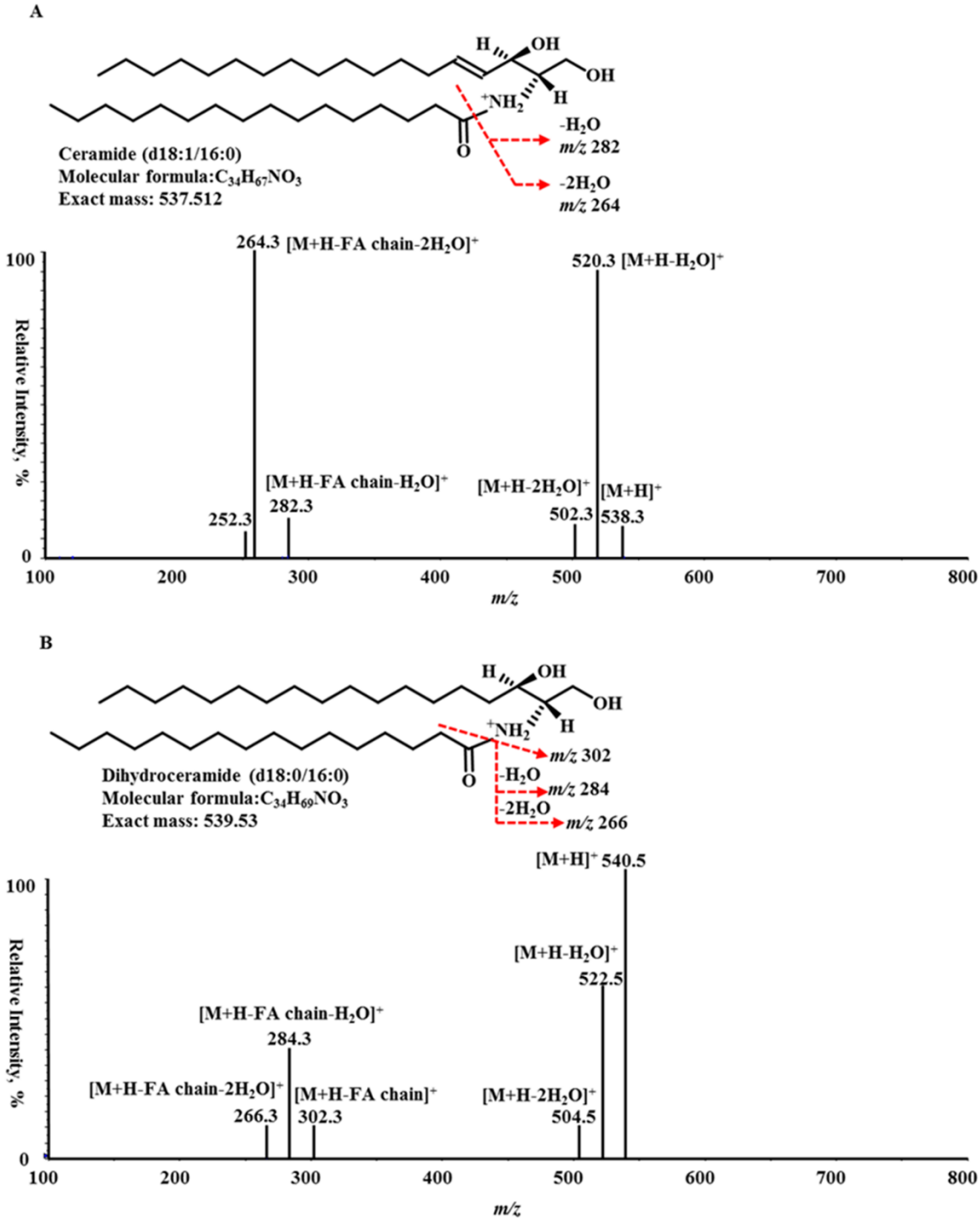

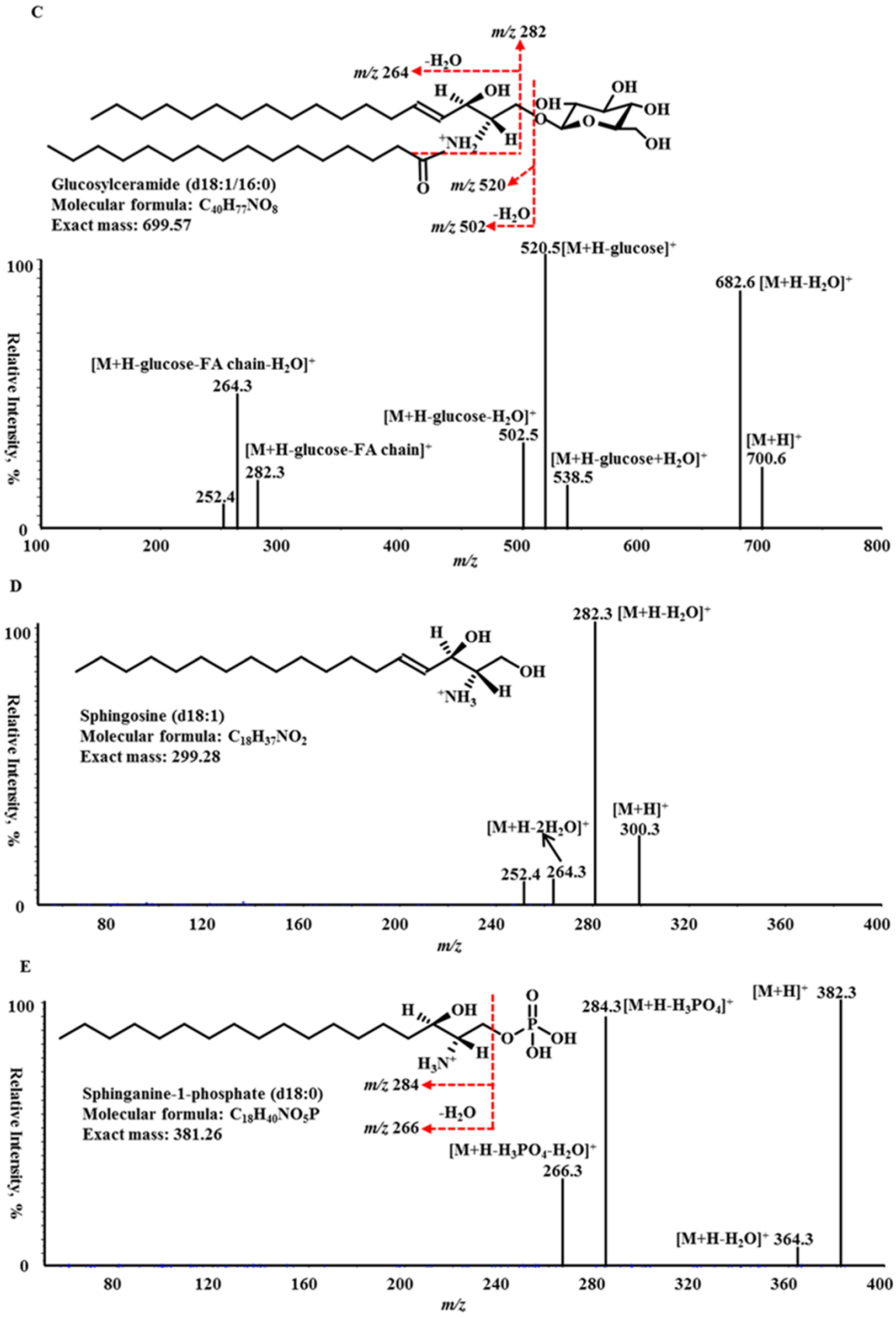
C
m/z 282
-H2O
m/z 264
Glucosylceramide (d18:1/16:0)
Molecular formula: C40H77NO8
Exact mass: 699.57
m/z 520
-H2O
m/z 502
520.5[M+H-glucose]+
682.6 [M+H-H2O]+
[M+H-glucose-FA chain-H2O]+
264.3
[M+H-glucose-H2O]+
502.5
[M+H-glucose-FA chain]+
282.3
[M+H-glucose+H2O]+
538.5
[M+H]+
700.6
252.4
Relative Intensity, %
m/z
D
282.3 [M+H-H2O]+
Sphingosine (d18:1)
Molecular formula: C18H37NO2
Exact mass: 299.28
[M+H]+
300.3
[M+H-2H2O]+
252.4
264.3
Relative Intensity, %
m/z
E
[M+H]+ 382.3
284.3[M+H-H3PO4]+
Sphinganine-1-phosphate (d18:0)
Molecular formula: C18H40NO5P
Exact mass: 381.26
m/z 284
-H2O
m/z 266
[M+H-H3PO4-H2O]+
266.3
[M+H-H2O]+ 364.3
Relative Intensity, %
m/z

Figure 3-3. ESI-MS/MS product ion spectra of (A) ceramide standard (C16:0-Cer as an example), (B) dihydroceramide standard (C16:0-dHCer as an example), (C) glucosylceramide standard (C16:0-GlcCer as an example), (D) d18:1-sphingosine and (E) d18:0-sphinganine-1-phosphate. The chemical structures, molecular information, fragmentation patterns, as well as masses of parent and fragment ions for each compound are also shown.

3.3.1.2. HPLC method development

Here, the separation of all target sphingolipid compounds was studied on the reversed-phase chromatography by using a C18 Ascentis Express Fused-Core Particle Column, which has been shown to give improved resolution compared to conventional porous C18 columns [18].

In order to achieve a fast, efficient and reproducible chromatographic separation, various combinations of organic phases, aqueous buffers and gradient programs were evaluated using a solution containing 19 standards plus 6 ISs (d17:1-So, d17:0-Sa, d17:1-So1P, d17:0-Sa1P, C17:0-GlcCer and C17:0-Cer).

Sullards *et al.* [19] concluded that solvent mixtures containing methanol-water are usually used as the mobile phase in the LC/MS/MS analysis of mammalian sphingolipids. Here, we tested the impact of methanol, acetonitrile and isopropanol on the retention time, resolution, peak shape and sensitivity of sphingolipids analyses. In this work, the stronger organic solvent isopropanol, was included in order to reduce retention times and improve the peak shapes of the later eluting sphingolipid compounds, such as GlcCer. However, the use of isopropanol also results in increased column backpressure due to greater solvent viscosity. To compensate for this problem, acetonitrile is also added.

Different concentrations of ammonium formate buffer (5 mM and 20 mM) in both mobile phase A and B were tested but a high level of ion suppression was observed for So and Sa

especially when using the buffer in a mobile phase A (aqueous phase). Ultimately, 0.1% formic acid (*v/v*) was added to both mobile phases A and B in order to improve the ionization efficiency.

The mobile phase composition at which an analyte elutes from the column and passes into the ESI ion source can have a significant impact on its ionization efficiency and the resulting signal response. Therefore, the LC gradient (increased levels of organic phase) finally selected in this work was a compromise between the LC separation efficiency and the detection sensitivity for the range of sphingolipid analytes investigated.

In summary, the optimal sensitivity and resolution was achieved on a short (7.5 cm) C18 Ascentis Express column with the binary solvent system comprising of water with 0.1% formic acid as mobile phase A and methanol/acetonitrile/isopropanol (4:1:1, *v/v/v*) with 0.1% formic acid as mobile phase B. Using the optimal LC conditions, all of the target analytes were resolved from each other in less than 20 min, slightly shorter than the 26 min run-time reported for the earlier method described by Bode and Gräler [20]. **Figure 3-4** shows the LC/MS/MS chromatogram of a mixture of the sphingolipid standards under investigation. Individual molecular species are separated by hydrophobicity, so species that vary by chain length, hydroxylation, or unsaturation will have different retention times. For example, GlcCer comes earlier than Cer due to the presence of polar headgroups linked to C-1 of the long-chain base ceramide; within each class of sphingolipids, compounds with shorter FA chain length elute earlier from the column than those with longer chain length. As a result of this, it is not possible to separate peaks arising from all possible combinations of FA substitutions and the 7 sphingolipid subclasses under investigation using reversed-phase separation. The adopted method shown in **Figure 3-4** does demonstrate good separation between most of the standards tested, which are representative of the anticipated analytes to be measured. However, it should be noted that there are clear overlaps between

sphingolipid subclasses. For example, the GlcCer compounds elute over a retention time window of around 8-15 min while the Cer compounds elute over retention times of around 11-17 min. Nonetheless, when combined with the additional specificity provided by MRM experiments, the separation achieved can be used as a general method for the analysis of sphingolipid metabolites, as shown below. Only minor modifications to the described LC/MS/MS method are necessary in order to apply it for sphingolipid analysis of a wide range of sample matrices, albeit with some modifications to the sample pretreatments.

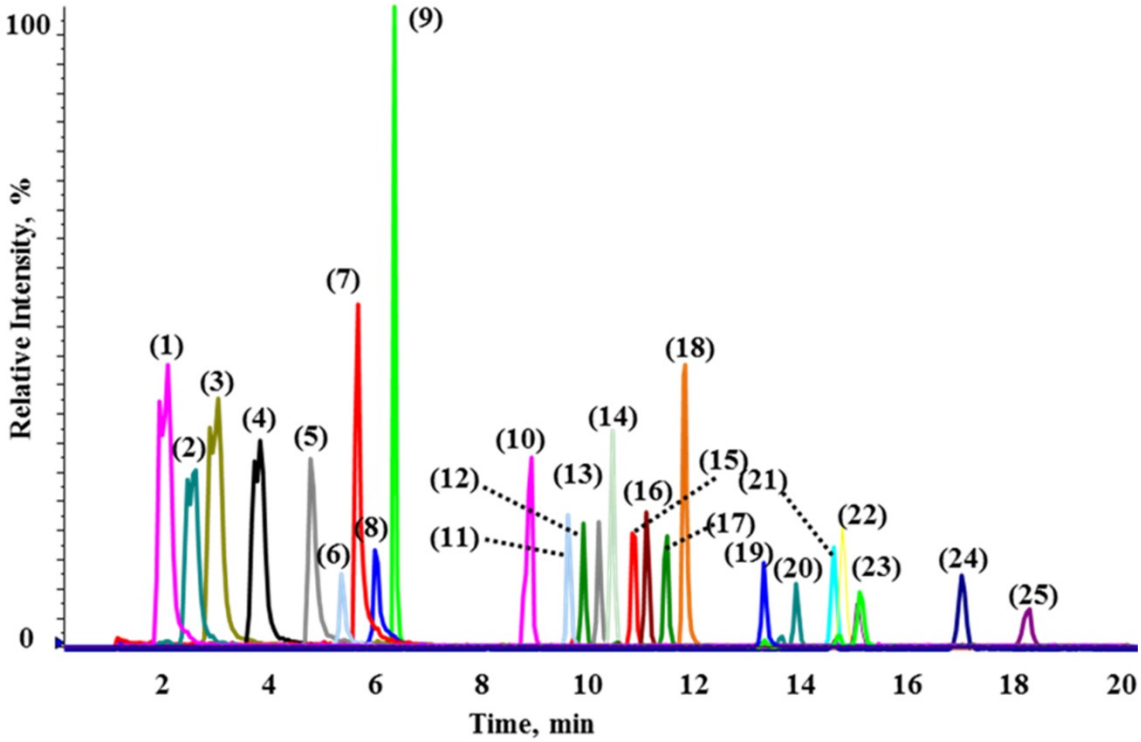

Figure 3-4. A representative chromatogram of sphingosine, sphinganine, sphingosine-1-phosphate, sphinganine-1-phosphate, ceramides, dihydroceramides and glucosylceramides in standard mixture solution at a concentration of 0.1 µM using an Ascentis Express C18 column with the established gradient elution. (1) d17:1-So; (2) d17:0-Sa; (3) d18:1-So; (4) d18:0-Sa; (5) d17:1-So1P; (6) d17:0-Sa1P; (7) d18:1-So1P; (8) d18:0-Sa1P; (9) C2:0-Cer; (10) C16h:0-GlcCer; (11) C16:0-GlcCer; (12) C18:1-GlcCer; (13) C17:0-GlcCer; (14) C16:0-Cer; (15) C18:0-GlcCer; (16) C16:0-dHCer; (17) C17:0-Cer; (18) C18:0-Cer; (19) C24:1-GlcCer; (20) C22:0-GlcCer; (21) C24:1-Cer; (22) C22:0-Cer; (23) C24:0-GlcCer; (24) C24:0-Cer; (25) C24:0-dHCer.

3.3.2. Method validation

3.3.2.1. Calibration curves and linearity

To compensate for variations in sample preparation and ionization efficiency, a set of non-naturally occurring sphingolipids, d17:1-So, d17:0-Sa, d17:1-So1P, d17:0-Sa1P, C17:0-GlcCer and C17:0-Cer, was used as ISs for calibration. **Table 3-2** shows the linear calibration parameters for all tested sphingolipid standards. The standard curves obtained displayed good linearity with R^2 values of >0.995 in the tested dynamic range over 3 orders of magnitude, demonstrating the capability of the method for measurement of large changes in sphingolipid contents. Subsequently, the calibration curves established in this manner were used for the quantification of So, Sa, So1P, Sa1P, Cer, dHCer and GlcCer in the B cell extract samples.

3.3.2.2. Limits of detection and quantification

The limit of detection (LOD) and quantification (LOQ) values for all standard compounds ranged from 0.5 to 5 nM (equivalent to 2.5 to 25 fmol on-column), and from 1 to 10 nM (5-50 fmol on-column), respectively (see **Table 3-2**). It is anticipated that the LOD and LOQ values achieved are sufficiently low to quantify most cellular extracts. For example, in the data reported by Scherer *et al.* [15], it was indicated that LOD values of <10 fmol would be sufficient for sphingolipid quantification in cell culture samples.

Table 3-2. Calibration curves, LODs, LOQs and linear dynamic ranges in the quantitative analysis.

Compounds	Calibration curves	R^2 value	LOD (nM)	LOQ (nM)	Tested linear dynamic range (nM)
C2:0-Cer	y=25.2x+0.032	0.9973	1.0	2.5	10,000-2.5
C16:0-Cer	y=14.9x+0.011	0.9987	1.0	2.5	10,000-2.5
C22:0-Cer	y=12.6x+0.023	0.9990	1.0	2.5	10,000-2.5
C24:1-Cer	y=9.22x+0.008	0.9990	1.0	2.5	10,000-2.5

C24:0-Cer	y=4.80x+0.022	0.9957	1.0	2.5	10,000-2.5
C16:0-dHCer	y=10.3x+0.004	0.9991	2.5	10.0	10,000-10
C24:0-dHCer	y=2.49x+0.007	0.9995	2.5	10.0	10,000-10
C16:0-GlcCer	y=9.32x+0.016	0.9980	0.5	1.0	10,000-2.5
C18:0-GlcCer	y=10.2x+0.016	0.9979	0.5	1.0	10,000-2.5
C18:1-GlcCer	y=8.22x+0.009	0.9989	0.5	1.0	10,000-2.5
C22:0-GlcCer	y=5.71x+0.007	0.9983	0.5	1.0	10,000-2.5
C24:1-GlcCer	y=6.66x+0.013	0.9986	0.5	1.0	10,000-2.5
C16h:0-GlcCer	y=18.9x+0.049	0.9970	0.5	1.0	10,000-2.5
d18:1-So	y=10.0x-0.016	0.9976	1.0	5.0	10,000-5
d18:0-Sa	y=11.2x-0.016	0.9978	1.0	5.0	10,000-5
d18:1-So1P	y=11.5x+0.088	0.9991	5.0	10.0	10,000-10
d18:0-Sa1P	y=14.3x+0.137	0.9984	5.0	10.0	10,000-10

3.3.2.3. Accuracy and precision

Three replicate samples were prepared for each QC level and three measurements were performed for each sample (n=9). The results obtained were summarized in **Table 3-3**. The accuracy of the measurements, defined as the percentage ratio of the measured *vs.* theoretical concentration, ranged from 92.5 to 109.4% for QC low (mean 100.8±4.4%), from 95.1 to 113.0% for QC medium (mean 104.2±4.7%), and from 94.1 to 109.3% for QC high (mean 101.3±4.9 %). The precision (for intraday triplicate measurements) of the method, indicated by the relative standard deviation (RSD), ranged from 0.3 to 8.0% for all QC samples. On a sphingolipid class basis, the overall average accuracies achieved were Cer (102.9±2.8%), dHCer (102.6±4.9%), GlcCer (102.9±5.6%), So (100.0±4.4%), Sa (105.9±3.7%), So1P (98.4±3.2%) and Sa1P (93.9±1.3%).

Table 3-3. Accuracy and precision for triplicate measurements of QC.

Compounds	QC-low		QC-medium		QC-high	
	Precision (RSD, %)	Accuracy (%)	Precision (RSD, %)	Accuracy (%)	Precision (RSD, %)	Accuracy (%)
C2:0-Cer	3.8	102.8	3.3	104.7	5.2	107.6
C16:0-Cer	8.0	103.5	2.4	101.1	2.1	96.2
C22:0-Cer	3.8	100.2	0.4	101.2	1.7	102.8
C24:1-Cer	4.2	104.5	1.0	101.1	1.4	106.6
C24:0-Cer	1.2	103.9	1.3	104.6	1.2	103.8
C16:0-dHCer	1.2	96.5	1.3	105.2	1.9	97.6
C24:0-dHCer	3.4	101.4	0.3	105.3	5.8	109.3
C16:0-GlcCer	1.7	101.1	1.5	109.6	0.9	97.3
C18:0-GlcCer	6.3	97.3	0.8	105.6	0.5	98.2
C18:1-GlcCer	0.9	104.7	0.9	111.3	1.3	100.1
C22:0-GlcCer	1.3	105.5	2.1	113.0	1.3	105.5
C24:1-GlcCer	5.5	97.2	2.2	107.4	1.1	102.1
C16h:0-GlcCer	4.7	94.6	1.3	106.2	1.1	95.4
d18:1-So	4.2	98.5	1.8	96.5	1.8	104.9
d18:0-Sa	1.3	109.4	2.1	102.0	0.3	106.3
C18:1-So1P	3.2	99.2	2.1	101.2	1.5	94.9
C18:0-Sa1P	1.4	92.5	0.5	95.1	0.8	94.1

3.3.2.4. Extraction efficiency

Table 3-4 provided the results of these recovery measurements. It was observed that the average recovery rate of the low-level spiked concentration was 102.6% and the average recovery rate of the high-level spiked concentration was 102.5%. On a sphingolipid class basis, the overall average recoveries achieved were Cer (102.3±5.0%), dHCer (100.0±3.1%), GlcCer (102.7±4.9%), So (108.3±1.4%), Sa (110.7±9.3%), So1P (94.5±4.6%) and Sa1P (106.4±1.8%). These recoveries are higher than those achieved by an earlier method using butanolic extraction in which mean recoveries were between 60% and 70% [15]. Overall, the results shown in Table 3-4 indicate that excellent recoveries were achieved for all of the analytes throughput the linear dynamic range of

the analysis.

Table 3-4. Extraction recovery of sphingolipid metabolites in cellular extracts.

Compounds	Spiked concentration (nM)		Measured concentration (nM)			Extraction recovery (%)	
	Low	High	Non	Low	High	Low	High
C2:0-Cer	20	200	ND	20.1±0.5	192.1±0.9	100.5	96.0
C16:0-Cer	20	200	104.6±3.5	129.8±5.4	322.9±8.8	104.2	106.0
C22:0-Cer	20	200	15.6±0.8	34.7±1.5	215.0±3.2	97.5	99.7
C24:1-Cer	100	1000	172.4±6.3	275.3±5.7	1197.0±33.2	101.1	102.1
C24:0-Cer	20	100	12.5±1.5	37.0±0.2	114.3±1.7	113.9	101.6
C16:0-dHCer	20	200	ND	19.2±0.3	205.9±3.5	96.0	102.9
C24:0-dHCer	20	200	ND	19.8±0.7	203.7±8.8	99.0	101.9
C16:0-GlcCer	20	200	31.9±2.5	59.2±4.7	234.8±2.5	114.1	101.3
C18:0-GlcCer	20	200	5.8±0.4	28.5±1.4	208.0±1.6	110.5	101.1
C18:1-GlcCer	20	200	<LOQ	20.7±1.0	198.7±6.2	103.5	99.4
C22:0-GlcCer	20	200	14.5±2.4	33.9±2.1	217.8±10.1	98.3	101.5
C24:1-GlcCer	100	1000	80.8±9.5	183.5±5.4	1094.4±29.8	101.5	101.3
C16h:0-GlcCer	20	200	ND	19.4±0.9	206.7±3.0	97.0	103.4
d18:1-So	10	100	14.3±0.3	26.6±0.7	122.7±0.9	109.3	107.3
d18:0-Sa	10	100	ND	10.4±0.5	117.3±2.9	104.1	117.3
d18:1-So1P	10	100	ND	9.1±0.7	97.7±3.7	91.2	97.7
d18:0-Sa1P	10	100	ND	10.51±0.9	107.7±1.9	105.1	107.7

Data were presented as mean±standard deviation (SD) in the unit of nM. ND, not detected.

3.3.3. Stability

The storage stability of solutions prepared for analysis was evaluated in 2 experiments, each over 3 days of storage at 15 °C or above. In the first, a solution in methanol containing all of the standards used was spiked into cell extract in duplicate. The second experiment involved 3 concentrations of the standard mixture solution in methanol (low, medium, high), each in duplicate. In both cases the average change in measured concentrations between day 1 and day 3 differed by less than 2.2% indicating that these solutions were stable under the storage conditions used for at

least 3 days.

3.3.4. Application to cell samples

In order to test the application of the validated method in a physical experimental example, it was used for the qualitative and quantitative determination of individual So, Sa, So1P, Sa1P, Cer, dHCer and GlcCer species in the B cells from both CLL patients (n=5) and healthy donors (n=4). As described above, lipids from these cell samples were first extracted using the single-phase extraction (chloroform/methanol/water, 1:2:0.8, *v/v/v*) procedure and then subjected to LC/MS/MS analysis.

Figure 3-5 shows the chromatograms of individual sphingolipid species detected in a typical B cell extract. As can be seen from the figure, 17 sphingolipid species were identified in the extracts out of the 33 MRM transitions monitored. All of these 17 compounds contain fatty acyl chains of ≥16 carbon atoms. With known molecular structures and fragmentation patterns, compounds whose authentic standards are not available can also be investigated in the samples. Thus, the MRM transitions relevant to Cer and GlcCer molecules containing short-chain FAs (2-14 carbon atoms) were also recorded in this study but none of these compounds were found to be present in the cell samples. In addition, we also examined looked for compounds with two double bonds in the sphingoid base, such as GlcCer (d18:2/C16:0), but these were not detected either. These findings are consistent with previous reports that GlcCer (d18:1) compounds are widely distributed in the mammalian cells, whereas GlcCer (d18:2) compounds are mainly present in cells and tissues of plant origin [1]. Other sphingolipids not found in the B cell extracts include Sa, dHCer and Sa1P, all of which are interconnected via a known metabolic pathway (see **Figure 3-2**).

Of the 17 analytes that were detected, 8 of them (d18:1-So, C16:0-GlcCer, C22:0-GlcCer, C24:1-GlcCer, C16:0-Cer, C22:0-Cer, C24:1-Cer and C24:0-Cer), whose authentic standards were available, were accurately quantified based on their corresponding calibration curves (see **Table 3-2**). For the other compounds (C20:0-GlcCer, C22:1-GlcCer, C24:0-GlcCer, C18:1-GlcCer, C18:0-GlcCer, C18:1-Cer, C18:0-Cer, C20:0-Cer and C22:1-Cer) for which authentic standards were not available, the best achievable quantification was performed by making use of the calibration curves for the standards with the most similar molecular structures. For instance, C20:0-GlcCer was quantified based on the calibration curve of C18:0-GlcCer.

Of the 17 sphingolipid compounds detected in lipid extracts from CLL patients (n=5) and healthy donors (n=4), 15 were quantified, as shown in **Figure 3-6**. The remaining 2 compounds (C18:1-GlcCer and C18:1-Cer) were detected below the LOQ values. From **Figure 3-6**, it can be seen that there was an altered sphingolipid composition (increased levels) observed in the B cells from the CLL patients compared to those from healthy donors. Hence, this method could be used in clinical research to study the connections between alterations in sphingolipid metabolism and the occurrence of cancer or other disease states. In turn, such findings can be used to understand the complex biology in CLL cells, and in turn may lead to the development of novel therapeutics strategies in CLL, such as drugs and physical treatments.

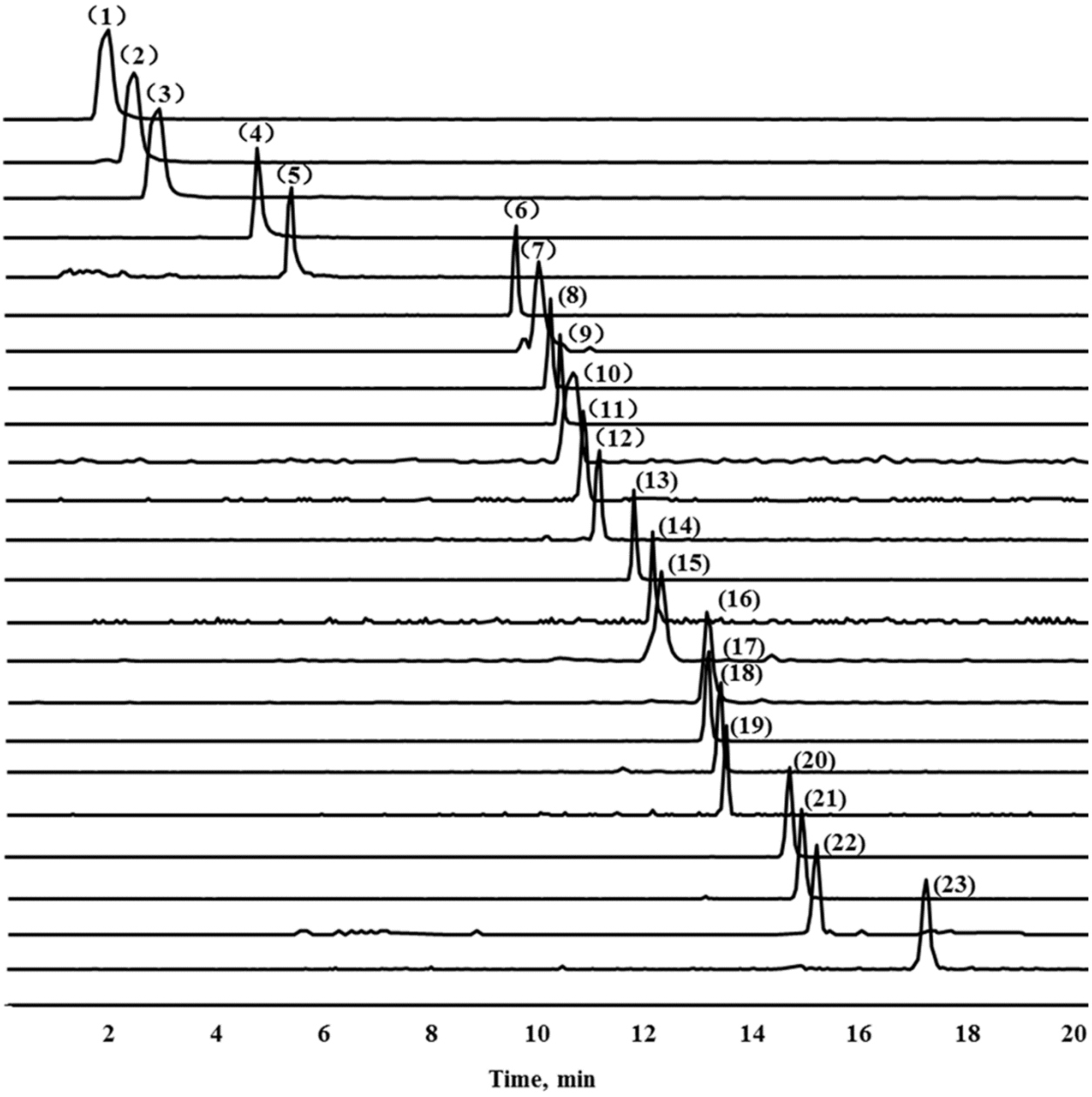

Figure 3-5. A representative LC chromatogram of sphingolipid metabolites detected in the B cell extracts under the established conditions. (1) d17:1-So; (2) d17:0-Sa; (3) d18:1-So; (4) d17:1-So1P; (5) d17:0-Sa1P; (6) C16:0-GlcCer; (7) C18:1-GlcCer; (8) C17:0-GlcCer (9) C16:0-Cer; (10) C18:1-Cer; (11) C18:0-GlcCer; (12) C17:0-Cer; (13) C18:0-Cer; (14) C20:0-GlcCer; (15) C22:1-GlcCer; (16) C22:1-Cer; (17) C20:0-Cer; (18) C24:1-GlcCer; (19) C22:0-GlcCer; (20) C24:1-Cer; (21) C22:0-Cer; (22) C24:0-GlcCer; (23) C24:0-Cer.

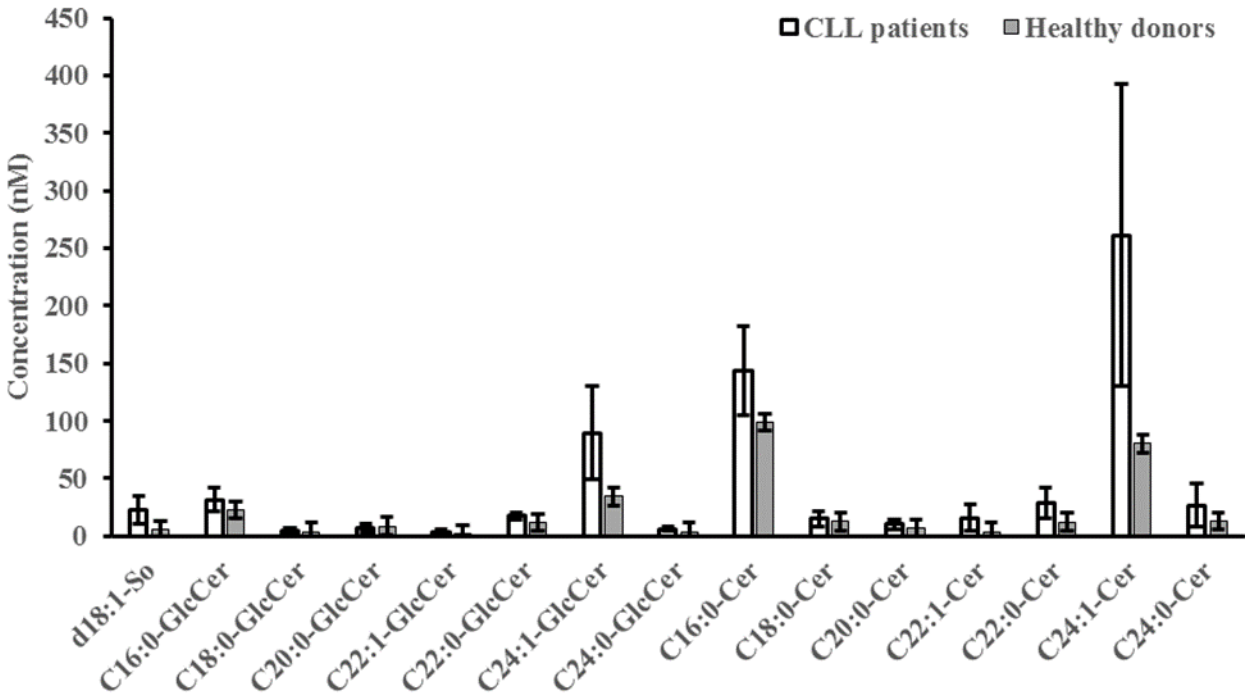

Figure 3-6. Contents of individual SPL species determined in B cells. *Note*, values were expressed as mean±standard deviation (SD) in the unit of nM.

3.4. Conclusions

In this study, a method was developed and validated for comprehensive profiling of individual sphingolipid molecular species covering 7 different subcategories. The method includes a modified single-phase extraction protocol using chloroform/methanol/water (1:2:0.8, *v/v/v*) and final analysis by LC/MS/MS using multiple reaction monitoring (MRM). This method allows for the simultaneous identification and quantification of 33 different sphingolipid species in a single chromatographic run of under 20 min. An LOD of between 0.5 and 5 nM was achieved for all 17 species tested in the method validation. It is anticipated that the method is able to provide sufficient sensitivity to accurately measure sphingolipid metabolites at levels appropriate for clinical studies, where sample volumes are limited.

The new method was successfully applied to the identification of 17 sphingolipid species extracted from the B cells of CLL patients and healthy donors. Of these, 15 sphingolipid species were quantified, allowing for direct comparison of sphingolipid profiles in healthy *vs.* CLL patients. It is likely that with minimal changes this method could be generally applied to the determination of or screening for many sphingolipid compounds in other biological matrices.

3.5. References

[1] V.E. Hubert, M. Schmelz, M.N. Nikolova-Karakashian, D.L. Dillehay, D.V. Lynch, A.H. Merrill Jr., Sphingolipids in food and the emerging importance of sphingolipids to nutrition, J Nutr. 129 (1999) 1239-1250.

[2] H. Farwanah, T. Kolter, K. Sandhoff, Mass spectrometric analysis of neutral sphingolipids: Methods, applications, and limitations, Biochim. Biophys. Acta (BBA)-Mol. Cell Biol. Lipids. 1811 (2011) 854-860.

[3] Y.Y. Zhao, Y.P. Xiong, J.M. Curtis, Measurement of phospholipids by hydrophilic interaction liquid chromatography coupled to tandem mass spectrometry: The determination of choline containing compounds in foods, J Chromatogr A. 32 (2011) 5470-5479.

[4] J. Bernal, J.A. Mendiola, E. Ibáñez, A. Cifuentes, Advanced analysis of nutraceuticals, J. Pharm. Biomed. Anal. 55 (2011) 758-774.

[5] A. Uphoff, M. Hermansson, P. Haimi, P. Somerharju, Analysis of complex lipidomes, in: K. Vékey, A. Telekes, A. Vertes (Eds.), Medical Applications of Mass Spectrometry, Elsevier, Amsterdam, 2008, pp. 223-249.

[6] M.C. Sullards, Analysis of sphingomyelin, glucosylceramide, ceramide, sphingosine, and sphingosine 1-phosphate by tandem mass spectrometry, Meth. Enzymol. 312 (2000) 32-45.

[7] G. Vielhaber, S. Pfeiffer, L. Brade, B. Lindner, T. Goldmann, E. Vollmer, U. Hintze, K. Wittern, R. Wepf, Localization of ceramide and glucosylceramide in human epidermis by immunogold electron microscopy, J. Invest. Dermatol. 117 (2001) 1126-1136.

[8] M.M. Mielke, W. Maetzler, N.J. Haughey, V.V.R. Bandaru, R. Savica, C. Deuschle, T. Gasser, A.K. Hauser, S. Gräber-Sultan, E. Schleicher, D. Berg, I. Liepelt-Scarfone, Plasma ceramide and glucosylceramide metabolism is altered in sporadic Parkinson's disease and associated with cognitive impairment: a pilot study, PLOS ONE. 8 (2013) e73094.

[9] E. Boslem, G. MacIntosh, A.M. Preston, C. Bartley, A.K. Busch, M. Fuller, D.R. Laybutt, P.J. Meikle, T.J. Biden, A lipidomic screen of palmitate-treated MIN6 β-cells links sphingolipid metabolites with endoplasmic reticulum (ER) stress and impaired protein trafficking, Biochem. J. 435 (2011) 267-276.

[10] T.B. Caligan, K. Peters, J. Ou, E. Wang, J. Saba, A.H. Merrill Jr, A high-performance liquid chromatographic method to measure sphingosine 1-phosphate and related compounds from sphingosine kinase assays and other biological samples, Anal Biochem. 281 (2000) 36-44.

[11] H. Farwanah, P. Nuhn, R. Neubert, K. Raith, Normal-phase liquid chromatographic separation of stratum corneum ceramides with detection by evaporative light scattering and atmospheric pressure chemical ionization mass spectrometry, Anal Chim Acta. 492 (2003) 233-239.

[12] R.L. Shaner, J.C. Allegood, H. Park, E. Wang, S. Kelly, C.A. Haynes, M.C. Sullards, A.H. Merrill Jr, Quantitative analysis of sphingolipids for lipidomics using triple quadrupole and quadrupole linear ion trap mass spectrometers, J Lipid Res. 50 (2009) 1692-1707.

[13] C.A. Haynes, J.C. Allegood, H. Park, M.C. Sullards, Sphingolipidomics: Methods for the comprehensive analysis of sphingolipids, J Chromatogr B. 877 (2009) 2696-2708.

[14] J.W. Lee, S. Nishiumi, M. Yoshida, E. Fukusaki, T. Bamba, Simultaneous profiling of polar lipids by supercritical fluid chromatography/tandem mass spectrometry with methylation, J Chromatogr A. 1279 (2013) 98-107.

[15] M. Scherer, K. Leuthäuser-Jaschinski, J. Ecker, G. Schmitz, G. Liebisch, A rapid and quantitative LC-MS/MS method to profile sphingolipids, J Lipid Res. 51 (2010) 2001-2011.

[16] R.F. Dielschneider, H. Eisenstat, S. Mi, J.M. Curtis, W. Xiao, J.B. Johnston, S.B. Gibson, Lysotropic agents selectively target chronic lymphocytic Leukemia cells due to altered sphingolipid metabolism, Leukemia. 30 (2016) 1290-1300.

[17] H. Shimoda, S. Terazawa, S. Hitoe, J. Tanaka, S. Nakamura, H. Matsuda, M. Yoshikawa, Changes in ceramides and glucosylceramides in mouse skin and human epidermal equivalents by rice-derived glucosylceramide, J Med Food. 15 (2012) 1064-1072.

[18] E.R. Badman, R.L. Beardsley, Z. Liang, S. Bansal, Accelerating high quality bioanalytical LC/MS/MS assays using fused-core columns, J Chromatogr B. 878 (2010) 2307-2313.

[19] M.C. Sullards, Y. Liu, Y. Chen, A.H. Merrill Jr, Analysis of mammalian sphingolipids by liquid chromatography tandem mass spectrometry (LC-MS/MS) and tissue imaging mass spectrometry (TIMS), Biochimica et Biophysica Acta. 1811 (2011) 838-853.

[20] C. Bode, M.H. Gräler, Quantification of sphingosine-1-phosphate and related sphingolipids by liquid chromatography coupled to tandem mass spectrometry, Methods Mol Biol. 874 (2012) 33-44.

Chapter 4*

Simultaneous Determination of Trimethylamine and Trimethylamine *N*-Oxide by HILIC LC/MS/MS: Quantification of Phospholipid Metabolites in Mouse Plasmas

4.1. Introduction

Trimethylamine (TMA) is a volatile and odorous compound derived from gut flora metabolism of glycine betaine, carnitine and choline, while trimethylamine *N*-oxide (TMAO) is an oxidation product of TMA formed by the enzymatic activity of flavin mono-oxygenase [1, 2]. Both TMA and TMAO are tertiary ammonium compounds and can be found in a wide variety of samples such as marine products [3], environmental samples (such as water and air) [4, 5, 6, 7] and human biological fluids (such as urine and plasma) [8, 9, 10, 11, 12]. It has been observed that the metabolic abnormalities of TMA and TMAO contribute to the incidence of certain diseases. For example, excess accumulation of TMA can cause trimethylaminuria (TMAU), which is characterized by an off-putting odor [13], while TMAO concentrations in plasma have been reported to be strongly related to atherosclerosis [2]. The metabolisms of TMA and TMAO are interrelated thus the simultaneous quantification of these two analytes in biological systems such as urine and plasma is of great importance in the discovery of disease biomarkers, elucidation of mechanisms underlying various diseases as well as investigation of nutritional status [14]. However, the simultaneous separation and accurate quantitation of TMA and TMAO in a single

* This chapter has been submitted to *Journal of Separation Science* as S. Mi, Y-Y Zhao, R.L. Jacobs and J.M. Curtis, "Simultaneous Determination of Trimethylamine and Trimethylamine *N*-Oxide in Mouse Plasma Samples by Hydrophilic Interaction Liquid Chromatography Coupled to Tandem Mass Spectrometry". I contributed to the experimental design, performance of experiments, data collection and analysis, as well as the manuscript composition.

liquid chromatographic (LC) run is challenging and this is made even worse by the high volatility of TMA and the low concentrations of TMA and TMAO present in target samples.

A number of analytical methods have been explored for the measurement of TMA and TMAO in various matrices. Gas chromatography (GC) coupled with detectors including mass spectrometry (MS) and flame ionization detection (FID) have been applied to the determination of both TMA and TMAO [4, 5, 8, 15]. However, the high volatility of TMA makes GC an applicable analytical method, which is not the case for TMAO. Hence, many GC methods that measure TMA alone have been reported [4, 5, 8]. Costa *et al.* [15] established a GC/MS method for the simultaneous measurement of dimethylamine (DMA), TMA and TMAO in tissues and biological fluids. In that work, TMAO was reduced to gaseous TMA using a titanium (III) chloride catalyst before analysis. However, this procedure compromises the ability to discriminate between TMA and TMAO, because they are detected as the same product. LC with ultraviolet (UV) or fluorescence detectors have also been applied to quantify TMA in environmental samples such as air and water [6, 7, 16], and these require chemical derivatization of the TMA prior to LC analysis due to the lack of suitable UV chromophores [16]. Usually, this derivatization procedure was carried out using 9-fluorenylmethylchloroformate (FMOC) as the derivatizing agent to improve the sensitivity of TMA towards the UV and fluorescence detectors [6, 7, 16]. Recently, MS has been used as a sensitive and selective detector in the analysis of TMA and/or TMAO either following LC separation [9, 10] or directly by flow injection [11, 12]. For example, Wang *et al.* [9] described the measurement of TMAO in plasma samples as a risk marker for cardiovascular diseases using an LC/MS/MS method with LC separation performed on a silica column. Lenky *et al*. [10] achieved the determination of marine osmolytes, including glycine betaine, TMAO, homarine, dimethylsulfoniopropionate and arsenobetaine in serum and plasma using LC-ESI-

MS/MS method. These studies indicate that LC/MS/MS can be an efficient and reliable approach to the quantification of TMAO in biological samples. However, in spite of the advantages of the LC/MS/MS method, published results on the combined HILIC separation and MS analysis of volatile TMA and TMAO are rather scarce to our knowledge. On the other hand, electrospray ionization tandem mass spectrometry (ESI-MS/MS) without prior chromatographic separation was examined for the simultaneous quantification of TMA and TMAO in urine samples [11, 12]. Although flow injection ESI-MS/MS and direct infusion ESI-MS/MS are straightforward and rapid analytical strategies, they are subject to various interferences. Firstly, there is the risk of ion suppression in which matrix compounds giving high response can suppress the formation of ions of low abundance analytes. Also, without chromatographic separation there are much more likely to be interferences from isobaric ions unless very high mass resolution is used.

The aim of our study is to establish and validate an LC/MS/MS method for the separation and accurate quantification of both TMA and TMAO in a single chromatographic run which is applicable to small volumes of plasma samples. The approach described here is to develop a simple derivatization reaction for TMA which converts it into a less volatile form that is more favorable towards chromatographic separation from TMAO and which yields unique fragment ions suitable for MRM experiments. We have also applied HILIC chromatography which has been shown to be especially suitable to the separation of small polar analytes [17] and is compatible with electrospray mass spectrometry.

4.2. Materials and Methods

4.2.1. Materials

The standards, trimethylamine hydrochloride (98%) and trimethylamine *N*-oxide dehydrate (≥99%)) were purchased from Sigma (St. Louis, MO). TMA-d_9 (^{2}HCl, 98% ^{2}H enrichment) and TMAO-d_9 (98% ^{2}H enrichment) were purchased from Cambridge Isotope Laboratories, Inc. (Andover, MA, USA). HPLC-grade ammonium formate (≥99%), formic acid and ethyl bromoacetate (reagent grade, 98%) were supplied by Sigma (St. Louis, MO). Water and acetonitrile were of LC/MS grade from Fisher Scientific Company (Ottawa, Ontario). All the other solvents were of HPLC grade and were obtained from Fisher Scientific Company (Ottawa, Ontario).

4.2.2. Preparation of stock, working and quality control standard solutions

TMA, TMAO, TMA-d_9 and TMAO-d_9 were precisely weighed to 0.01 mg and dissolved individually in LC/MS-grade water to make stock solutions of around 1 mg mL^{-1}. All stock solutions were stored in sealed vials at -20 ˚C until needed. Ethyl bromoacetate solution (4 mg mL^{-1}) was made in acetonitrile (LC/MS grade). Working standard solutions for calibration were prepared by diluting stock solutions in methanol. Triplicate low, medium and high quality control (QC) standards were separately prepared in methanol at 5 ng mL^{-1} (QC, L), 50 ng mL^{-1} (QC, M), 500 ng mL^{-1} (QC, H) for TMA; 2.5 ng mL^{-1} (QC, L), 25 ng mL^{-1} (QC, M), 500 ng mL^{-1} (QC, H) for TMAO.

4.2.3. Sample extraction

The University of Alberta Health Sciences Animal Care and Use Committee in accordance with the Canadian Council on Animal Care Guidelines and Polices approved all procedures. All

mice (male low-density lipoprotein receptor knockout) were food deprived for 12 h before being killed by exsanguination under isoflurane anesthesia. Plasma samples were collected from mice and frozen at -80 ˚C until analyzed. On the day of analysis, plasma samples were thawed to room temperature from -20 ˚C before use. Protein precipitation using an organic solvent was performed for sample clean-up. The three candidate solvent systems investigated in the present study were methanol with 0.1% formic acid, acetonitrile with 0.1% formic acid and acetonitrile/methanol/formic acid (90:10:0.1, *v/v/v*). The plasma sample (50 µL, accurately weighted) was spiked with internal standard solution (50 µL) and then the selected organic solvent system (150 µL) was added. After that, the mixture was vortexed for about 30 s, then centrifuged at 6,000 rpm at room temperature for 10 min. The supernatant was filtered through a 0.22 µm PVDF membrane, transferred into a separate glass vial and stored at -20 ˚C for further use.

4.2.4. Optimization of parameters for derivatization

A chemical derivatization procedure was optimized that would decrease TMA volatility and at the same time be beneficial for the detection and effective separation of TMA and TMAO on the HILIC column. The derivatization treatment selected for this study is the reaction between TMA and ethyl bromoacetate to form ethyl betaine [11], while TMAO remains the same during the reaction process. The obtained TMA derivative are specifically and sensitively determined by HILIC LC/MS/MS. The conditions for the derivatization reaction were optimized in order to find the shortest reaction time that gives quantitative conversion of volatile TMA into ethyl betaine. The parameters investigated to achieve this are listed in **Table 4-1**. Prior to the derivatization procedures, it has been checked that ethyl betaine is not originally present in the target plasma samples.

Table 4-1. Parameters assessed in the optimization of the derivatization reaction between TMA and ethyl bromoacetate.

Variables	Unit	Levels
Amount of 4 mg mL^{-1} ethyl bromoacetate	μL	10, 20, 50, 80, 100, 150, 200
Amount of conc. ammonium hydroxide	μL	2, 5, 8, 10, 15, 20
Reaction time	min	10, 20, 30, 40, 50, 60

4.2.5. HPLC/MS/MS analysis

An HPLC system equipped with binary pump and autosampler (Agilent Technologies, Palo Alto, CA, USA) coupled to a 3200 QTRAP mass spectrometer (AB SCIEX, Concord, ON, Canada) was used in this study. Data acquisition and analysis used the Sciex software Analyst version 1.4.2.

4.2.5.1. LC separation

LC separation was performed using an Ascentis Express HILIC column (10 cm×2.1 mm i.d., 2.7 μm in particle size) (Sigma, St. Louis, MO). The isocratic elution was carried out with a mobile phase composition of (A) 0.1% formic acid in acetonitrile and (B) 10 mM ammonium formate (70:30, *v/v*). The run time was 5 min with the flow rate set to 200 μL min^{-1}. The auto-sampler temperature was set to 15 ˚C and the injection volume was 5 μL. Since we applied only a simple sample clean-up procedure, an automated column valve system was used in this study to divert the column eluent to waste before and after the data acquisition window from 2.5 min to 4.5 min to prevent the contamination of mass spectrometer.

4.2.5.2. MS/MS conditions

A Turbo Spray ion source (electrospray ionization) was used under the positive ion mode. Four MRM transitions were selected in order to achieve quantification of the target analytes, as given

in Table 4-2. Nitrogen was used as curtain gas, nebulizing gas and drying gas. All other instrumental parameters used were as following: curtain gas at 20 arbitrary units; gas 1 at 50; gas 2 at 60; ion spray voltage at 5200 V. The cycle time was 300 ms and the ion source temperature was 400 ˚C. The MRM transitions and optimized mass spectrometer parameters for each analyte and their reference internal standards are shown in Table 4-2.

Table 4-2. MRM transitions and optimized parameters for each compound.

Compounds	MRM transitions (amu)	DP[a] (V)	EP[a] (V)	CEP[a] (V)	CE[a] (V)	CXP[a] (V)
Derivatized TMA	146→118	26	3	8	23	4
TMAO	76→58	26	10	12	25	4
Derivatized TMA-d_9	155→127	26	3	10	23	4
TMAO-d_9	85→68	31	9.5	8	17	4

[a] DP, EP, CEP, CE and CXP are declustering potential, entrance potential, collision cell entrance potential, collision energy and collision cell exit potential.

4.2.6. Method validation

4.2.6.1. Calibration curves and linearity

Calibration curves were constructed using ranges of 2.5-2500 ng mL^{-1} (seven points) for TMA and 0.5-2500 ng mL^{-1} (eight points) for TMAO. These ranges cover the normal concentrations of TMA and TMAO found in biological fluids and tissues. TMA-d_9 and TMAO-d_9 were spiked as the internal standards for TMA and TMAO, respectively to give a final concentration of 250 ng mL^{-1}. Calibration curves were made by plotting the peak area ratios of analytes to their reference internal standards against the analyte concentrations. The performance of the constructed calibration curves were assessed by linearity, slope stability and the accuracy of back-calculated concentrations of standards.

4.2.6.2. Sensitivity

In this study, the limit of quantification (LOQ) and detection (LOD) were taken as the lowest concentration with a signal-to-noise ratio (S/N) of ≥10:1 and ≥3:1, respectively. LOD and LOQ values were evaluated independently for TMA and TMAO in a standard solution with serial dilution.

4.2.6.3. Extraction recovery

Since a true blank matrix is not available, the recoveries of TMA and TMAO were evaluated by spiking known amounts of authentic standards into a mouse plasma sample at two different concentration levels in mouse plasma (high and low-see **Table 4-4**). The plasma sample was divided into 9 aliquots of 50 µL allowing for the triplicate analysis of unspiked (endogenous) plasma and plasma spiked at low and high levels. The 9 aliquots were treated under the same conditions and analyzed by the proposed LC/MS/MS method. The concentrations of TMA and TMAO in all extracts were determined based on their corresponding calibration curves (**Table 4-3**). The percentage recovery for each analyte (TMA or TMAO) was calculated by comparing the measured spiked amount (A) with the actually spiked amount (B) i.e., recovery (%)=A/B×100.

4.2.6.4. Intra- and inter-day accuracy and precision

The precision and accuracy of the newly established method were determined based on the analysis of triplicates of 3 QC solutions (see Section **4.2.2.**) having TMA and TMAO concentrations distributed throughout the calibrated ranges (low, medium and high). Accuracy was calculated as a percentage (%) of the nominal concentration, while precision was evaluated as the relative standard deviation for triplicate measurements. Accuracy and precision were also evaluated in a real sample matrix by spiking authentic standards (including TMA and TMAO) at

a concentration of 500 ng mL^{-1} into mouse plasma samples.

4.2.6.5. Stability

The storage stability of solutions prepared for analysis was evaluated in two experiments, each over 3 days of storage at 15 °C in the autosampler. In the first, standard solutions of TMA and TMAO in methanol at two concentration levels (50 and 500 ng mL^{-1}) were spiked into mouse plasma samples. The second experiment involved three concentrations of the standard mixture solutions (low, medium, high), each in duplicate.

4.3. Results and Discussion

4.3.1. Development of the derivatization procedure in standard solutions

A derivatization procedure was deemed necessary, due to the lack of any exploitable fragments of TMA in the ESI-MS/MS spectrum [11], to the similarity of LC elution times for TMA and TMAO and to the volatility of TMA limiting quantification accuracy. Ideally, this derivatization reaction would result in unique fragment ions in the MS/MS spectrum of a less volatile TMA derivative and be further beneficial for the detection and effective separation of TMA and TMAO by HILIC chromatography. This was achieved by converting TMA into ethyl betaine by the reaction between TMA and ethyl bromoacetate [11], see **Scheme 4-1**. In this reaction, TMAO remains unaltered so there is no change in TMAO MS/MS fragment ion patterns or sensitivity.

Optimization of the derivatization process was performed using a standard mixture solution of TMA and TMAO (50 µg mL^{-1} in HPLC-grade water) and an internal standard mixture solution of TMA-d_9 and TMAO-d_9 (5 µg mL^{-1} in HPLC-grade water).

Initially, the optimal amount of derivatizing agent added to the reaction solution was evaluated

at a fixed reaction time (40 min) and at room temperature. A fixed amount of concentrated ammonium hydroxide (10 µL) was also added since basic conditions are required. As shown in **Figure 4-1A**, an increasing trend of peak area of the derivatized TMA was observed with the addition of ethyl bromoacetate (4 mg mL^{-1}) from 10 to 50 µL. Beyond this, further increases in the amount of derivatizing agent added did not increase the abundance of the derivatized TMA. Therefore, for this condition 50 µL of ethyl bromoacetate (4 mg mL^{-1}) was selected as the optimal addition to maximize the formation of the derivatized TMA.

Then, using this condition, the amount of concentrated ammonium hydroxide was evaluated at six different levels, keeping the other parameters constant. Note that pH was varied via the amount of added base rather than standardized using a pH meter due to the low volumes (<100 µL) used. It was found from **Figure 4-1B** that the maximum peak area for the derivatized TMA was for a 10 µL addition of concentrated ammonium hydroxide, with higher amounts leading to a decrease in response.

Finally, the effect of reaction time was studied using the optimized parameters. The results shown in **Figure 4-1C** indicate that the peak area of the derivatized TMA increases for reaction times from 10 min to 40 min, but further increase of the reaction time (≥40 min) does not result in any appreciable change of the total amount of derivatized product.

On the basis of the above results, the final procedure selected for the chemical derivatization reaction of volatile TMA is therefore to add 50 µL ethyl bromoacetate (4 mg mL^{-1} in acetonitrile) to 25 µL of sample solution and vortex mix thoroughly. Then, the mixture is reacted at room temperature for 40 min along with 10 µL concentrated ammonium hydroxide. After the reaction is complete, HPLC-grade water (containing 0.5% formic acid) is added to obtain a final volume

of 500 µL. The purpose of adding this acidic solution is to neutralize the ammonium hydroxide and to terminate the reaction. The derivatized product is then ready for the following LC/MS/MS analysis.

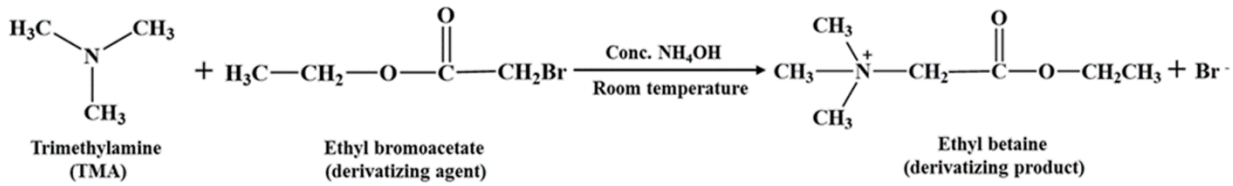

Scheme 4-1. The reaction of ethyl bromoacetate with trimethylamine.

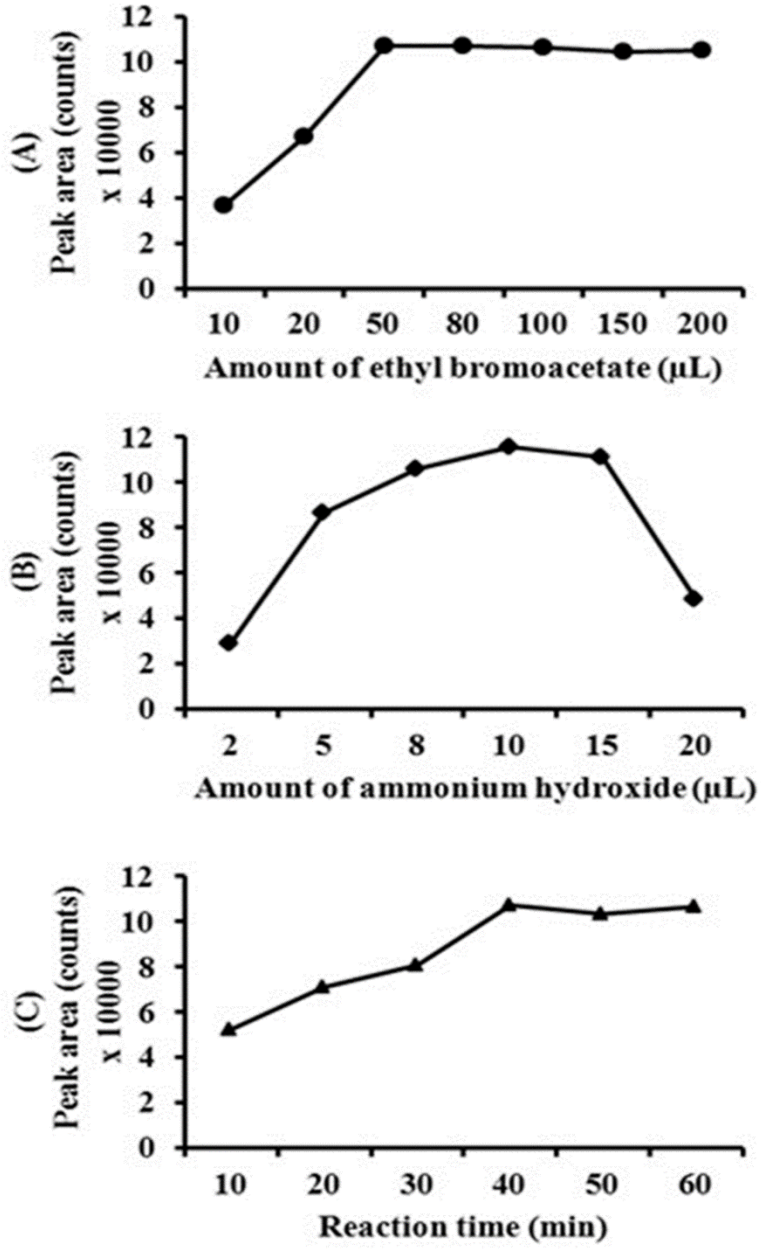

Figure 4-1. Effects of experimental variables on the peak area of derivatized TMA: (A) amount of ethyl bromoacetate (4 mg mL^{-1} in acetonitrile), (B) amount of concentrated ammonium hydroxide and (C) reaction time.

4.3.2. Mass detection and chromatographic separation of TMA and TMAO

TMA and TMAO are readily ionized and detected by ESI-MS in the positive ion mode, although the sensitivity for TMAO is >8 times higher than for TMA (data not shown). In addition, the low molecular weight and high volatility of TMA makes it less suitable for direct quantification. After derivatization with ethyl bromoacetate, the ESI-MS sensitivity for the TMA derivative is similar to that of TMAO.

In order to maximize the specificity and sensitivity of the proposed method, MRM experiments were carried out to investigate the fragmentation patterns for each analyte. Instrumental parameters for each compound were optimized by infusing a standard solution into the mass spectrometer using the syringe pump at a flow rate of 10 μL min^{-1}. The final optimized MS conditions for the derivatized TMA, TMAO and the internal standards are reported in **Table 4-2**. Using these conditions, ESI-MS/MS spectra were recorded in multichannel analyzer mode (MCA) to accumulate spectra from each scan and to enhance sensitivity for detection of low abundance ions. The optimized MS/MS spectra including molecular structures and their proposed fragment pathways are shown in **Figure 4-2**.

As can be seen from **Figure 4-2**, the protonated precursor molecular ions are visible for all of the analytes. TMAO and its reference internal standard (TMAO-d_9) are fragmented in two ways. For TMAO, the major product ion is at *m/z* 58 formed by loss of H_2O and the minor one is at *m/z* 59 corresponding to loss of "OH". TMAO-d_9 shows similar fragmentation pathways, but with *m/z* 68 as the major fragment ion which is generated by loss of a hydroxyl group. Of these two fragment ions, the one with higher intensity is selected for the subsequent quantitative analysis. In the case of the derivatized TMA and TMA-d_9, the major fragments are obtained by loss of $(CH_2)_2$, which

leads to the production of glycine betaine and glycine betaine-d_9, respectively. These observed transitions here resemble those reported in previous studies [9, 10, 11, 12].

Due to the relatively low level of TMA and TMAO present in the mouse plasma samples, a direct flow-injection analysis without LC separation may be hampered by ion suppression caused by other matrix components. Moreover, chromatographic separation could provide complementary retention time data for compound identification. Initially, we developed an LC method using a standard solution of TMAO and underivatized TMA. As mentioned above, HILIC is applicable to the separation of small polar analytes [17]. Therefore, various HILIC columns from different manufactures including Waters XBridge HILIC, Thermo Dionex HILIC-10, Superlco HILIC and Ascentis Express HILIC, were evaluated. At the same time, the effects of mobile phase composition and elution modes (isocratic or gradient) on the separation of the two target analytes were investigated. However, the co-elution of TMA and TMAO and considerable peak tailing were always observed under all the conditions studied. This was also true when switching to a Waters C18 column and an Ascentis C8 column. To address this problem, it was necessary to chemically derivatize TMA (**Scheme 4-1**). Then, using a derivatized standard solution, optimization of the chromatographic parameters was carried out on an Ascentis Express HILIC column. The mobile phase initially used for the HILIC was acetonitrile and water with 10 mM ammonium formate adjusted at pH 3.0 but the peaks for both TMA and TMAO were found to be very broad. The peak shapes improved when the mobile phase was modified with 0.1% formic acid added to acetonitrile and no pH adjustment for the aqueous phase. Considering the simple, rapid and efficient isocratic separation of the derivatized TMA and TMAO, 70% organic phase (acetonitrile with 0.1% formic acid) was used in the mobile phase for the following experiments. An MRM chromatogram of a standard mixture solution analyzed under the final chromatographic

conditions is shown in Figure 4-3. As is evident in Figure 4-3, the derivatized TMA and TMAO are successfully separated within 5 min with no equilibration time required due to the isocratic separation. In addition, the derivatization reaction enhanced the TMA signal intensity by >8 fold compare d to the underivatized form.

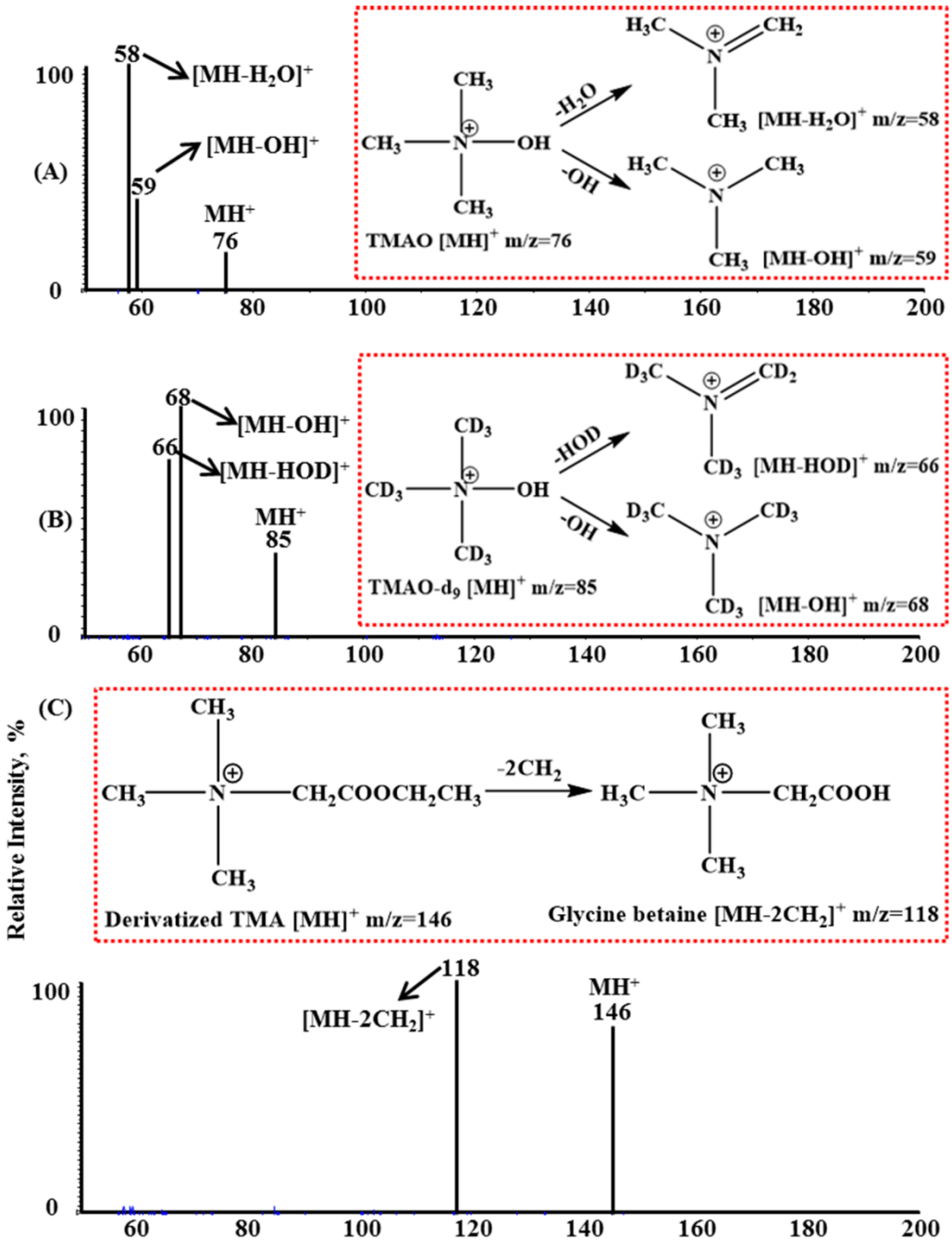

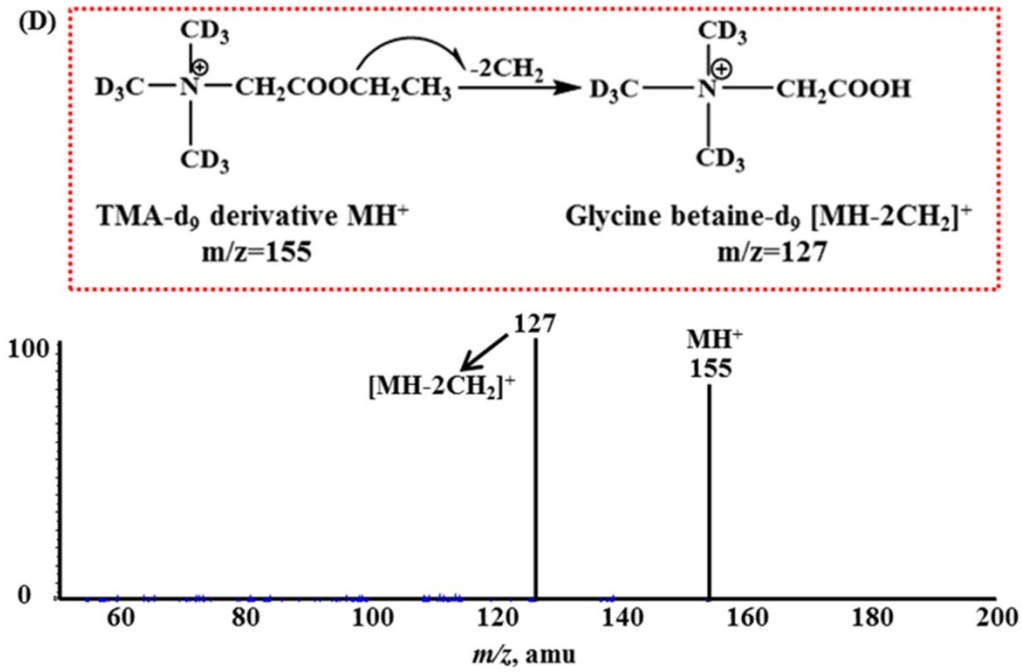

Figure 4-2. ESI-MS/MS spectra of (A) TMAO, (B) TMAO-d_9, (C) Derivatized TMA and (D) Derivatized TMA-d_9. The chemical structures, fragment patterns, as well as masses of parent and fragment ions for each compound are also shown.

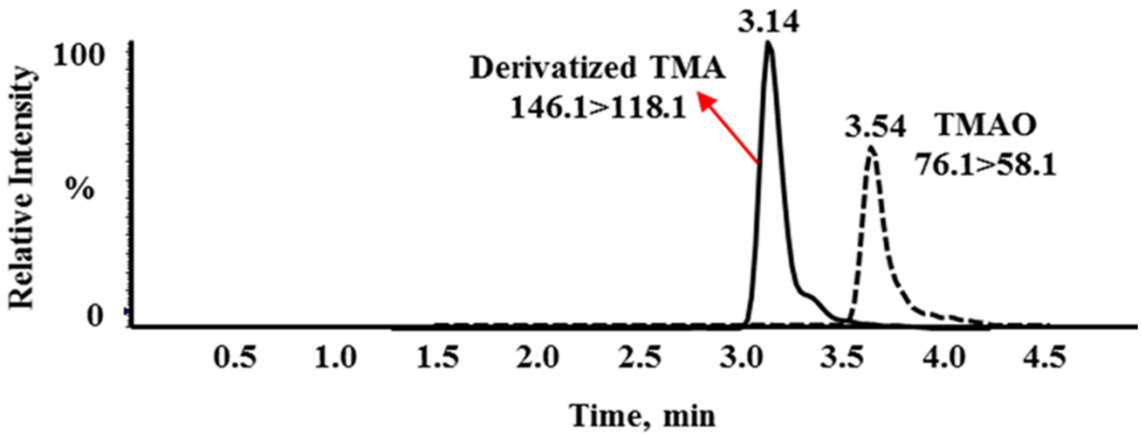

Figure 4-3. An MRM chromatogram of an authentic standard mixture at a level of 50 ng mL^{-1}. *Note,* prior to data collection, the eluent was diverted to waste for the initial 2.5 min and the last 0.5 min of the isocratic elution.

4.3.3. Method validation

4.3.3.1. Calibration curves, linearity, slope stability and carryover

The established calibration curves, R^2 value, and linear dynamic range data for TMA and TMAO are shown in **Table 4-3**. Both TMA and TMAO displayed good linearity over the test calibrator ranges with R^2 values of >0.998. The repeatability of the calibration curves were determined by running the standard solutions 3 times over the course of 1 day. For both TMA and TMAO, the slope of the calibration curves remained stable over the 3 separate runs, as indicated by the coefficient of variation (%CV) of the 3 slopes being 0.05% for TMA and 0.1% for TMAO. After storing the standard solutions at -20 ˚C for two years in glass vials, they were derivatised and the calibration curves were measured. It was found that the measured slopes changed by <5.3% for TMA and <0.9% for TMAO over two years. This indicats a long-term storage stability of the TMA and TMAO standard solutions over at least two years at -20 ˚C. Furthermore, the accuracy of back-calculated concentrations of all calibrators ranged from 91.9 to 109% for TMA and from 92.1 to 106% for TMAO. Subsequently, the calibration curves established in this manner were used for the quantification of TMA and TMAO in the mouse plasma samples.

In order to investigate carryover, a blank sample (methanol) was injected randomly during the analytical process and no carryover was observed for any of the analytes.

4.3.3.2. Limits of detection and quantification

For TMA and TMAO, the LOQ values (S/N ≥10:1) measured were 2.5 and 0.5 ng mL^{-1}, respectively (**Table 4-3**). These two concentrations were used as the lower limit of their corresponding calibration curves. The LOD values (S/N ≥3:1) obtained for the method was 0.25

ng mL^{-1} for TMAO which is well below the levels observed in the mouse plasma samples studied here.

Table 4-3. Calibration curves, LODs, LOQs and linear dynamic ranges.

Compounds	Calibration curves	R^2 value	LOD (ng mL^{-1})	LOQ (ng mL^{-1})	Linear dynamic range (ng mL^{-1})
TMA	y=39.5x-0.0857	0.9988	0.5	2.5	2.5-2500
TMAO	y=25x-0.0122	0.9996	0.25	0.5	0.5-2500

4.3.3.3. Analyte recoveries in mouse plasma

The ideal solvent to use for protein precipitation was selected based on the absence of interfering peaks in blank samples. Plasma blanks are unavailable because TMA and TMAO are always present in plasma and so for selection of the precipitation solvent, water was used as the blank sample. Three candidate solvent systems were investigated based on literature precedent including methanol with 0.1% formic acid, acetonitrile with 0.1% formic acid [18] and acetonitrile/methanol/formic acid (90:10:0.1, *v/v/v*) [10]. The inclusion of formic acid was to reduce the volatility of TMA and hence to minimize its loss during the extraction process. Prior to LC-ESI-MS/MS analysis, blank water samples were similarly treated using the optimized derivatization procedures. The results show that no interferences to TMAO were detected for all these three solvents, whereas an obvious interfering peak of the derivatized TMA was observed for both acetonitrile with 0.1% formic acid and acetonitrile/methanol/formic acid (90:10:0.1, *v/v/v*). Hence, methanol with 0.1% formic acid was selected as the sample extraction solvent in this work.

Table 4-4 summarized the results of the recovery measurements. It was found that the recovery of the TMA spikes varied from 90.4 to 98.4%, while TMAO recovery ranged from 99.2 to 108.4%. These results indicate that recoveries of 100%±10% for both TMA and TMAO were obtained

throughout the tested range when employing the extraction procedures described in Section 4.2.3.

Table 4-4. Extraction recoveries of TMA and TMAO in mouse plasma samples.

Compounds	Added amount (ng mL^{-1})		Measured amount (mean±SD) (ng mL^{-1})			Recovery (%)	
	Low-spiked	High-spiked	Non-spiked (endogenous)	Low-spiked	High-spiked	Low-spiked	High-spiked
TMA	4.5	45	3.8±0.2	8.3±0.8	44.5±1.9	98.4	90.4
TMAO	4.5	45	1.2±0.04	5.6±0.2	49.9±0.9	99.2	108.4

4.3.3.4. Accuracy and precision

The measured intraday accuracy (see Table 4-5A) ranged from 94.9 to 105.3% for TMA and from 91.4 to 103.7% for TMAO. These triplicate intraday measurements also indicate the precision of the method which ranged from 1.1 to 5.5% for TMA and 0.4 to 3.7% for TMAO. The interday (over 3 days) accuracy and precision data were described in Table 4-5B. For all of the 3 QC levels, the accuracy ranged from 98.1 to 102.4% for TMA and 96.6 to 102.7% for TMAO. The precision ranged from 1.7 to 6.6% for TMA and 1.8 to 3.5% for TMAO. The accuracy for the mouse plasma was 100% and 100.5% for TMA and TMAO, respectively. Correspondingly, the precision for the mouse plasma matrix was 3.5% and 4.1%.

These data demonstrate that the proposed method is sufficiently accurate and precise over the range studied in this work for both intraday and interday analysis of TMA and TMAO in mouse plasma samples. The method could be validated for other biological samples with some limited additional validation.

Table 4-5. (A) Intraday accuracy and precision for triplicate measurements of QC.

Compounds	QC-low		QC-medium		QC-high	
	Precision (RSD, %)	Accuracy (%)	Precision (RSD, %)	Accuracy (%)	Precision (RSD, %)	Accuracy (%)

TMA	3.1	105.3	1.1	94.9	5.5	100.7
TMAO	3.7	96.9	0.4	91.4	1.5	103.7

(B) Accuracy and precision for measurements of QC over 3 days.

Compounds	QC-low		QC-medium		QC-high		Mouse plasma	
	Precision (RSD, %)	Accuracy (%)	Precision (RSD, %)	Accuracy (%)	Precision (RSD, %)	Accuracy (%)	Precision (RSD, %)	Accuracy (%)
TMA	1.7	98.1	3.9	102.4	6.6	101.2	3.5	100.0
TMAO	2.4	96.6	1.8	102.7	3.5	98.4	4.1	100.5

4.3.3.5. Stability

In the prepared standard mixture solutions with high, medium and low concentration levels, the average change in measured concentrations between day 1 and day 3 differed by 2.0% for TMA and 0.1% for TMAO, which indicates that these solutions were stable under the storage conditions (15 °C) used for at least 3 days. For the stability experiments in mouse plasma samples, <6.6% variation of the measured concentrations (high and low) was observed for both TMA and TMAO, indicating the storage stability of mouse plasma samples in the autosampler for at least 3 days.

4.3.4. Application to mouse plasma samples

The validated method was applied to the quantitative analysis of TMA and TMAO in 7 fasting male mouse plasma samples. Each mouse plasma sample was collected, divided into two aliquots of 50 µL and stored at -20 ˚C until the time of analysis.

The plasma samples were treated according to the same procedures described in Section 4.2.3 and 4.2.4. Figure 4-4 illustrates the resulting LC/MS/MS chromatograms of derivatized TMA,

TMAO and their respective internal standards in mouse plasma samples. In order to make sure that the quantified TMA and TMAO were originally present in the target samples and there was no influences from choline, we also investigated choline (with mass transition 104→60) in this study together with TMA and TMAO. Results show that there was no change for the contents of choline before and after derivatization, proving that there was no conversion happening from choline to TMA.

The ranges of measured TMA and TMAO in fasting mouse plasma are indicated in **Figure 4-5** which shows that considerably higher levels of TMA were observed than TMAO. The measured TMA and TMAO levels in the tested samples ranged from 317.2 to 601.1 ng mL^{-1} and 70.1 to 189.0 ng mL^{-1}, respectively, which was in agreement with the results for male mice reported by other labs [2, 19].

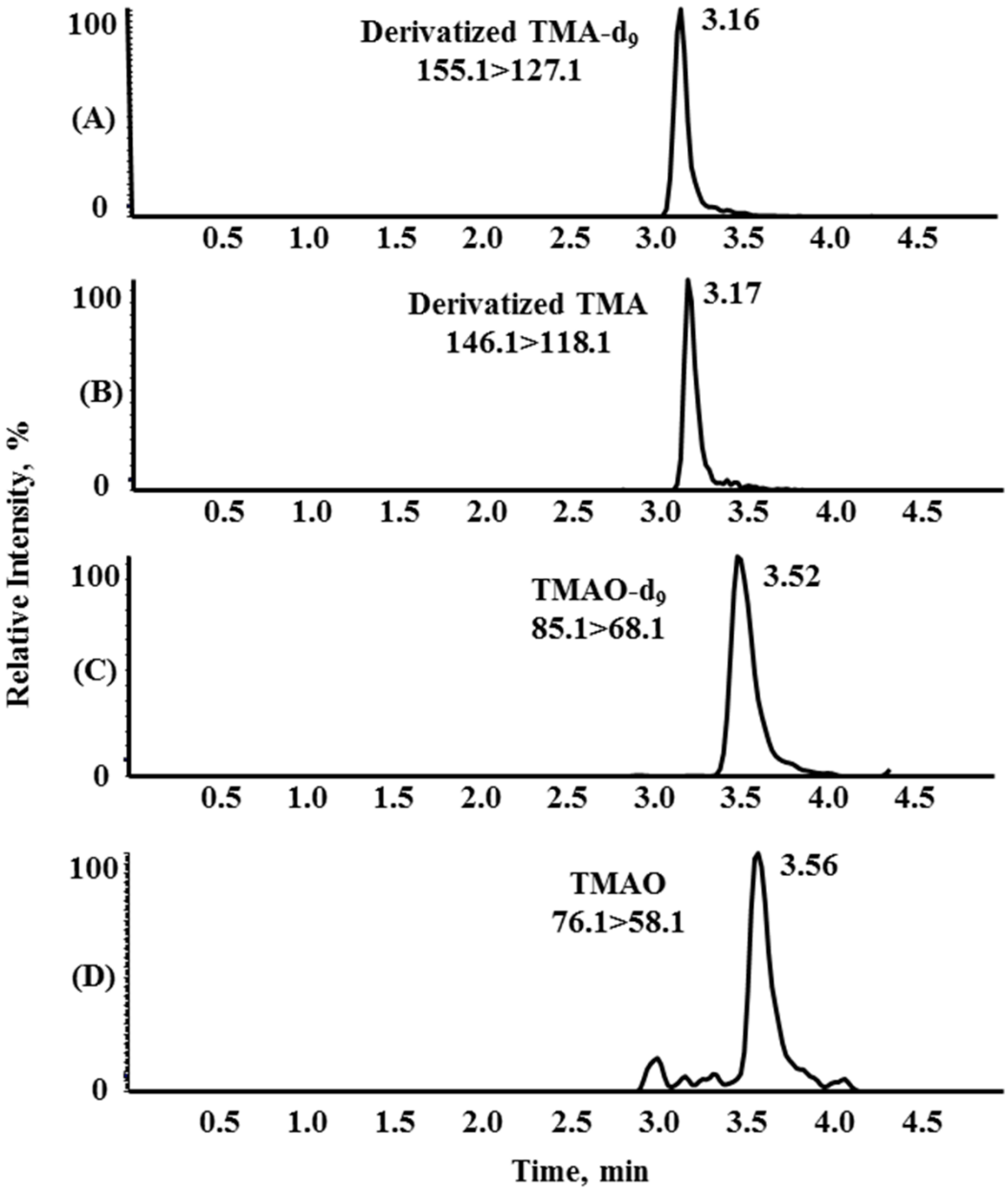

Figure 4-4. A representative MRM chromatogram of (A) Derivatized TMA-d_9, (B) Derivatized TMA, (C) TMAO-d_9 and (D) TMAO in fasting male mouse plasma samples under the established conditions.

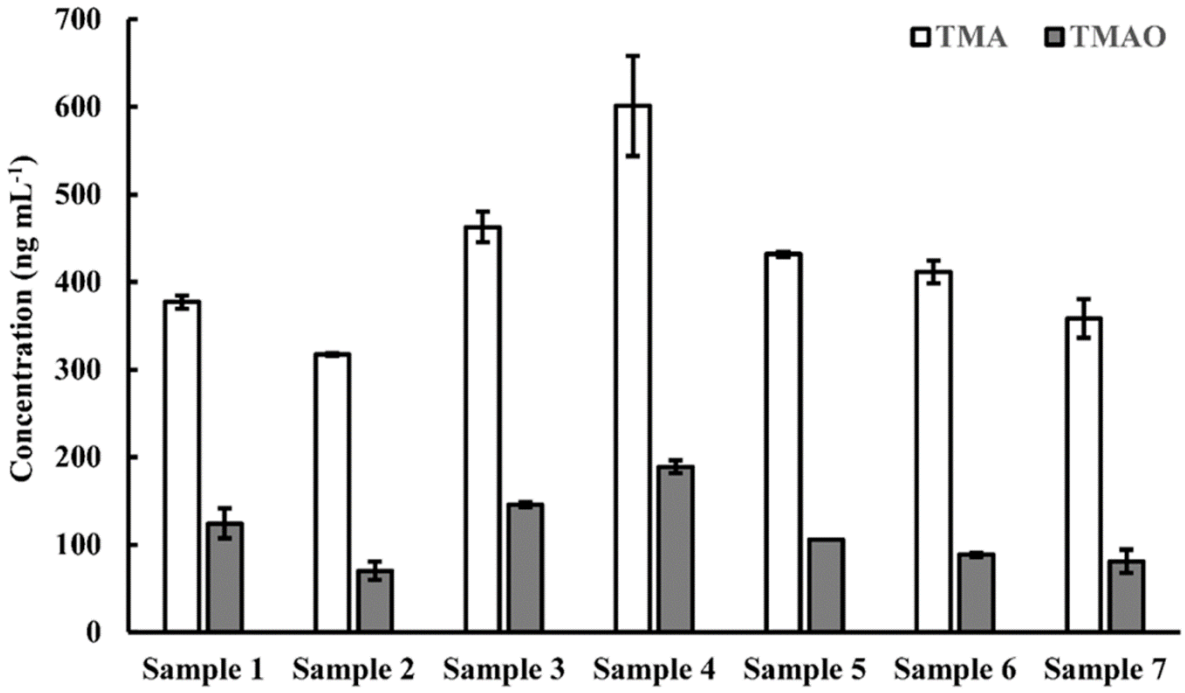

Figure 4-5. TMA and TMAO concentrations in fasting plasma samples taken from male mice. *Note*, all plasma samples were treated as 2× extraction and 2× derivatization for each extract (n=4); values were expressed as mean±standard deviation (SD) in ng mL^{-1}.

4.4. Conclusions

This study describes a new HILIC LC/MS/MS method for the simultaneous identification and quantification of TMA and TMAO in a single LC run within 5 min. This method enables the detection and chromatographic separation of TMA and TMAO by employing a simple and optimized derivatization procedure prior to HILIC LC/MS/MS analysis. The method validation has demonstrated levels of sensitivity, accuracy, precision and recovery that are suitable for clinical analyses, as illustrated by sample-limited measurements on mouse plasma. A recently-published method [18] also reports the use of HILIC LC/MS/MS for the measurement of choline, betaine, TMA, TMAO and creatinine in human plasma and urine. However, compared to that method, the one described in this work has considerably higher sensitivity with an LOD for TMA

that is 40 times lower and an LOD for TMAO that is 9 times lower. Application of the proposed method to the fasting mouse plasma samples shows that equivalent results can be obtained in the qualitative and quantitative determination of TMA and TMAO in comparison to the results in the literature [2, 19]. The method established here is expected to be adapted to the quantitative analysis of TMA and TMAO in other biological sources for nutritional, pharmaceutical and medical studies.

4.5. References

[1] I.D. Lidbury, J.C. Murrell, Y. Chen, Trimethylamine and trimethylamine *N*-oxide are supplementary energy sources for a marine heterotrophic bacterium: implications for marine carbon and nitrogen cycling, ISME J. 9 (2015) 760-769.

[2] B.J. Bennett, T.Q.deA. Vallim, Z. Wang, D. Shih, Y. Meng, J. Gregory, H. Allayee, R. Lee, M. Graham, R. Crooke, P. Edwards, S. Hazen, A. Lusis, Trimethylamine-N-oxide, a metabolite associated with atherosclerosis, exhibits complex genetic and dietary regulation, Cell Metab. 17 (2013) 49-60.

[3] A.Q. Zhang, S.C. Mitchell, R.L. Smith, Dietary precursors of trimethylamine in man: A pilot study, Food Chem. Toxicol. 37 (1999) 515-520.

[4] Y. Kim, K. Kim, An accurate and reliable analysis of trimethylamine using thermal desorption and gas chromatography–time of flight mass spectrometry, Anal Chim Acta. 780 (2013) 46-54.

[5] Y. Chien, S. Uang, C. Kuo, T. Shih, J. Jen, Analytical method for monitoring airborne trimethylamine using solid phase micro-extraction and gas chromatography-flame ionization detection, Anal Chim Acta. 419 (2000) 73-79.

[6] C. Cháfer-Pericás, P. Campíns-Falcó, R. Herráez-Hernández, Comparative study of the determination of trimethylamine in water and air by combining liquid chromatography and solid-phase microextraction with on-fiber derivatization, Talanta. 69 (2006) 716-723.

[7] C. Cháfer-Pericás, R. Herráez-Hernández, P. Campíns-Falcó, Liquid chromatographic determination of trimethylamine in water, J Chromatogr A. 1023 (2004) 27-31.

[8] G.A. Mills, V. Walker, H. Mughal, Quantitative determination of trimethylamine in urine by solid-phase microextraction and gas chromatography–mass spectrometry, J Chromatogr B. 723 (1999) 281-285.

[9] Z. Wang, B.S. Levison, J.E. Hazen, L. Donahue, X. Li, S.L. Hazen, Measurement of trimethylamine-N-oxide by stable isotope dilution liquid chromatography tandem mass spectrometry, Anal Biochem. 455 (2014) 35-40.

[10] C.C. Lenky, C.J. McEntyre, M. Lever, Measurement of marine osmolytes in mammalian serum by liquid chromatography–tandem mass spectrometry, Anal Biochem. 420 (2012) 7-12.

[11] D. W. Johnson, A flow injection electrospray ionization tandem mass spectrometric method for the simultaneous measurement of trimethylamine and trimethylamine *N*-oxide in urine, J. Mass Spectrom. 43 (2008) 495-499.

[12] O.A. Mamer, L. Choinière, A. Lesimple, Measurement of urinary trimethylamine and trimethylamime oxide by direct infusion electrospray quadrupole time-of-flight mass spectrometry, Anal Biochem. 406 (2010) 80-82.

[13] H. Yamazaki, M. Fujieda, M. Togashi, T. Saito, G. Preti, J.R. Cashman, T. Kamataki, Effects of the dietary supplements, activated charcoal and copper chlorophyllin, on urinary excretion of trimethylamine in Japanese trimethylaminuria patients, Life Sci. 74 (2004) 2739-2747.

[14] S.H. Zeisel, K.A. daCosta, M. Youssef, S. Hensey, Conversion of dietary choline to trimethylamine and dimethylamine in rats: dose-response relationship, J Nutr. 119 (1989) 800-804.

[15] K.A. daCosta, J.J. Vrbanac, S.H. Zeisel, The measurement of dimethylamine, trimethylamine, and trimethylamine *N*-oxide using capillary gas chromatography-mass spectrometry, Anal Biochem. 187 (1990) 234-239.

[16] M.A. Iqbal, J.E. Szulejko, K.H. Kim, Determination of methylamine, dimethylamine, and trimethylamine in air by high-performance liquid chromatography with derivatization using 9-fluorenylmethylchloroformate, Anal. Methods. 6 (2014) 5697-5707.

[17] J.M. Curtis, S. Mi, Hydrophilic interaction liquid chromatography for determination of betaine, in: Victor R. Preedy (Ed.), Betaine: Chemistry, Analysis, Function and Effects, RSC publishing, London, 2015, pp. 139-158.

[18] X. Zhao, S.H. Zeisel, S. Zhang, Rapid LC-MRM-MS assay for simultaneous quantification of choline, betaine, trimethylamine, trimethylamine *N*-oxide, and creatinine in human plasma and urine, Electrophoresis. 36 (2015) 2207-2214.

[19] Z. Wang, E. Klipfell, B.J. Bennett, R. Koeth, B.S. Levison, B. DuGar, A.E. Feldstein, E.B. Britt, X. Fu, Y.M. Chung, Y. Wu, P. Schauer, J.D. Smith, H. Allayee, W.H.W. Tang, J.A. DiDonato, A.J. Lusis, S.L. Hazen, Gut flora metabolism of phosphatidylcholine promotes cardiovascular disease, Nature. 472 (2011) 57-63.

Chapter 5*

A Method for the Identification of Conjugated Linolenic Acid isomers in Pomegranate and Tung Seed Oils by Silver Ion-LC/MS with In-Line Ozonolysis (Ag^+-LC/O_3-MS)

5.1. Introduction

Conjugated linolenic acid (CLnA) refers to a group of octadecatrienoic acid isomers (18:3) with a conjugated double bond system. These isomers can be further divided into positional isomers (e.g. 8,10,12-18:3; 9,11,13-18:3; 11,13,15-18:3, *etc*.) and geometric isomers (e.g. *trans, trans, trans*; *cis, trans, trans; cis, trans, cis*, *etc*.) [1].

CLnA isomers are naturally present in high levels in certain plant seed oils such as tung (*Aleurites fordii*), bitter ground (*Momordica charantia*), pomegranate (*Punica granatum*), trichosanthes (*Trichosanthes kirilowii*), pot marigold (*Calendula officinalis*), *Jacaranda (Jacaranda minosifolia)* and *Catalpa (Catalpa ovata)* [2]. Additionally, they can also be produced *in vitro* by strains of *butyrivibrio*, *propionibacterium*, *clostridia*, *lactobacillus* and *bifidobacterium* through the activity of linoleate isomerase (LAI) on linolenic acid [3, 4]. The naturally-occurring CLnA isomers mainly include *α*-eleostearic acid (*cis*9, *trans*11, *trans*13-18:3), catalpic acid (*trans*9, *trans*11, *cis*13-18:3), punicic acid (*cis*9, *trans*11, *cis*13-18:3), calendic acid (*trans*8, *trans*10, *cis*12-18:3) and jacaric acid (*cis*8, *trans*10, *cis*12-18:3). As for the produced CLnA isomers, only *cis*9, *trans*11, *cis*15-18:3 and *trans*9, *trans*11, *cis*15-18:3 were reported [3, 4].

* This chapter will be submitted to *European Journal of Lipid Science and Technology* as S. Mi, Y-Y Zhao and J.M. Curtis, "A Method for the Identification of Conjugated Linolenic Acid isomers in Pomegranate and Tung Seed Oils by Silver Ion-LC/MS with In-Line Ozonolysis (Ag^+-LC/O_3-MS)". I was responsible for the experimental design, performance of experiments, data collection and analysis, as well as the manuscript composition.

CLnA isomers are considered as health-enhancing compounds. Their protective biochemical functions have been intensively investigated, including anti-carcinogenesis [5, 6], lipid metabolism regulation [2], anti-inflammatory [7], anti-obesity [2, 3] and antioxidant activities [8, 9]. Therefore, natural sources and especially edible plant seeds rich in CLnA have the potential to be used as effective functional food ingredients and dietary supplements for use in disease management [2]. In addition to their biological activities, plant seed oils which contain high amounts of CLnA isomers are very important raw materials in the manufacture of organic coatings and polymers, as the conjugated unsaturation facilitates good polymerization and imparts adhesive properties when properly treated [9].

Due to the important health benefits, most of the work published on CLnA has focused on the investigation of their bioactive and nutritional properties and the corresponding underlying mechanisms [2, 3, 5, 6, 7, 8, 10], with fewer studies focusing on the method development for the comprehensive profiling of individual CLnA positional and geometric isomers in plant seed oils and other biological samples. However, in vivo and in vitro studies have observed that different CLnA isomers could exert different beneficial effects on the diseases such as cancer [2]. For example, punicic acid (*cis*9, *trans*11, *cis*13-18:3) was shown to reduce the incidence and multiplicity of chemically induced skin cancer significantly [2]. Considering their isomer-specific properties, an analytical strategy is required that can accurately identify the individual CLnA isomers in various sample sources.

The fatty acid compositions of seed oils are routinely determined by gas chromatography (GC). GC coupled with flame ionization detection (GC/FID) [9, 11] and with mass spectrometry (GC/MS) [7, 12, 13] has been used for the analysis of CLnA methyl esters in various types of samples. The

identification of individual CLnA isomers by GC/FID and GC/MS is usually achieved by comparing the retention times with those of the corresponding authentic standards [9], but only a limited number of pure CLnA standards are available. Using GC/MS, some additional information can be gained from mass spectral reference libraries [7], but the comprehensive profiling of all CLnA isomers in the target samples is still difficult to achieve due to the large number of possible isomers. In some cases, information on double bond locations can be gained by GC/MS following specific derivatization procedures, such as the formation of 2-alkenyl-4,4-dimethyloxazolines (DMOX) derivatives. This has been used to prepare derivatives of *β*-eleostearic acid, punicic acid and *α*-eleostearic acid, in order to confirm their double bonds positions [13].

High performance liquid chromatography (HPLC), thin layer chromatography (TLC), capillary electrophoresis (CE), and nuclear magnetic resonance (NMR) spectroscopy have also been explored for the analysis of CLnA isomers. Reversed-phase HPLC using C18 and C30 columns has been described for the separation of the methyl CLnA isomers from seed lipids of bitter gourd [11]. The incomplete separation of *c,t,t*-isomer and *t,t,c*-isomer was observed for both columns. Silver ion impregnated high performance liquid chromatography (Ag^+-HPLC) has been used as a complementary technique along with GC for better separation of CLnA isomers. In this way, CLnA isomer identification in bovine milk and muscle was studied by Plourde *et al.* [14] and by Yang *et al.* [15] in pomegranate seed oil (PSO) samples. Although the separation of geometric configuration groups can be achieved using Ag^+-HPLC, this is not the case for the positional isomers. The small differences in positional configuration of individual isomers make their separation and identification very difficult by using Ag^+-HPLC method [15], especially for the closely eluting peaks. Cao *et al.* [1] reported the identification and quantification of CLnA isomers using combined Ag^+-HPLC and ^{13}C-NMR techniques. The ^{13}C-^{1}H COSY correlation technique

was applied for the quantification of eight CLnA isomers. Notably, this technique also needs the commercially-available standards for the identification.

To date, none of these techniques individually could separate all CLnA isomers completely. Complementary techniques and reference standards are always required. Recently, Sun *et al.* [16] described a new method which combines ozonolysis on-line with silver ion LC/MS (Ag^+-LC/O_3-MS) in order to differentiate double bond positions in fatty acids without the use of authentic standards. In this method, the assignment of double bond positions was achieved based on the ozonolysis aldehyde products specific to the location of the initial double bonds. This approach has been successfully applied to an investigation of conjugated linoleic acid (CLA) isomers in nutraceutical products [17] and to an elucidation of phosphatidylcholine isomers in rat livers [18].

In the present study, we explore the feasibility of using in-line O_3-MS for the de novo identification of CLnA positional isomers, also making use of the ultra-high resolution capabilities of an Orbitrap mass spectrometer. We describe the development of the LC/O_3-MS method for the identification of CLnA isomers (both geometric and positional configuration) in complex lipid samples through the examples of pomegranate seed oil (PSO) and tung seed oil (TSO) samples.

5.2. Materials and Methods

5.2.1. Materials

HPLC grade hexanes, butyronitrile, acetonitrile, methanol and 2-propanol as well as sulfuric acid (95-98%) were purchased from Fisher Scientific Company (Ottawa, ON, Canada). All the CLnA standards (*trans*8, *trans*10, *cis*12-, *trans*8, *trans*10, *trans*12-, *cis*9, *trans*11, *cis*13-18:3) and CLnA methyl ester standard (*cis*9, *trans*11, *trans*13-18:3) were purchased from Larodan Inc. (Solna, Sweden). All of the CLA methyl ester standards (*cis*9, *trans*11-, *cis*9, *cis*11-, *trans*9,

*trans*11-, and *trans*10, *cis*12-18:2) were purchased from Matreya Inc. (Pleasant Gap, PA, USA). Fatty acid methyl ester (FAME) standards (*cis*9-18:1 and *trans*11-18:1) were purchased from Nu-Chek Prep Inc. (Elysian, MN, USA). Each standard stock solution was prepared in hexane at a concentration of 1 mg mL^{-1}. Ozone was generated using a Nano ozone generator (Absolute Systems Inc., Edmonton, AB, Canada). The Teflon AF-2400 tubing (0.020″ OD, 0.010″ ID) was purchased from Biogeneral Inc. (San Diego, CA, USA). The PSO and TSO samples were kindly provided by Dr. Randall Weselake (Department of Agricultural, Food and Nutritional Science, University of Alberta).

5.2.2. Preparation of CLnA methyl esters

Fatty acids were converted into their methyl esters before being analyzed by LC/MS. There have been many methods reported for the transesterification of oils to give fatty acids methyl esters [17, 19, 20]. It is important to optimize the temperature and time used in the methylation of CLnA isomers, since it has been shown that CLnA isomers (or conjugated triene structures) are even more susceptible to isomerization [19] and lipid oxidation [15] than conjugated linoleic acid (CLA), linoleic acid (LA) or α-linolenic acid (LN) especially under vigorous methylation conditions such as at elevated temperatures. Therefore, the influence of methylation temperature and time on the properties of the products was investigated. Three published methylation procedures [17, 19, 20] were compared in order to minimize artifacts derived from isomerization and lipid oxidation. These derivatization procedures were 1% (*v/v*) sulfuric acid in methanol at 50 °C for 12 h (**System 1**), 1% (*v/v*) sulfuric acid in methanol at 80 °C for 2 h with intermittent shaking (**System 2**) and 8% (*v/v*) sulfuric acid in methanol at 40 °C for 10 min (**System 3**).

5.2.3. Ag^+-LC/O_3-MS analysis of CLnA methyl esters

Silver ion chromatography (Ag^+-LC) was performed on FAME using two ChromSpher 5 Lipids columns (2 mm i.d.×250 mm, 5 μm in particle size) (Varian Inc., Palo Alto, CA) in series at room temperature. Isocratic elution was used with a mobile phase composition of 70% of hexane: isopropanol: butyronitrile (100:1:0.2, *v/v/v*) and 30% of hexane. The sample injection volume was 10 μL and the flow rate was 0.2 mL min^{-1}.

The in-line ozonolysis system consisted of a 0.5 L Omnifit solvent bottle, a two-valve bottle cap, and a variable length of gas permeable 0.5 mm o.d., 0.25 mm i.d. Teflon AF-2400 tubing (Biogeneral Inc., San Diego, CA). The Teflon tubing was inserted into the ozone filled solvent bottle, with one end connected to the LC autosampler and the other end directly coupled to the APCI ion source of the mass spectrometer (**Scheme 5-1**) as described previously [17]. The ozonolysis products were analyzed using an APCI ion source in the positive ion mode attached to a version of the Exactive™ benchtop Orbitrap mass spectrometer (Thermo Fisher Scientific, Waltham MA, USA). The MS system was calibrated with calibration solutions supplied by Thermo Fisher Scientific. Data was collected in profile data acquisition mode over the mass range *m/z* 50-350 based on a high resolution setting of 50,000 FWHM (scan speed, 2 Hz). The APCI ion source temperature was held at 350 °C, other parameters were as followings: sheath gas pressure at 20 arbitrary units, sheath gas flow at 5 arbitrary units and the capillary temperature was 270 °C. In all cases, high purity nitrogen (N_2) was the gas used. Data was processed by the Qual Browser Xcalibur software (Thermo Fisher).

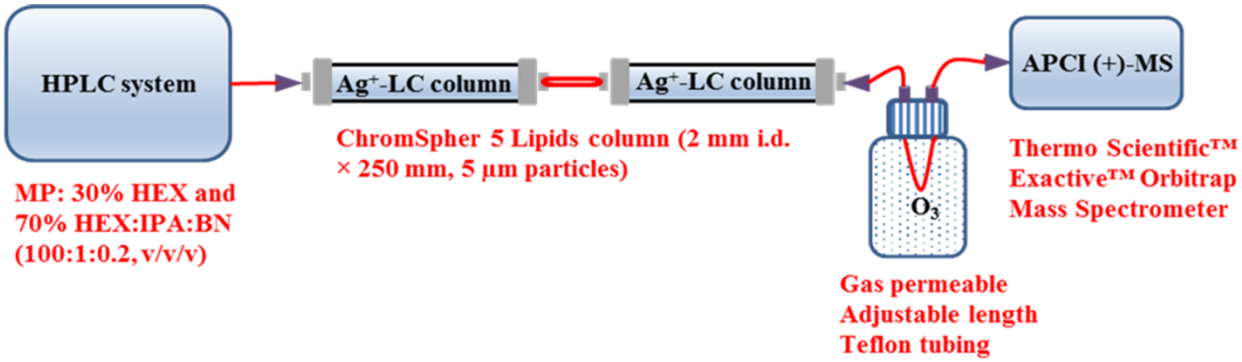

Scheme 5-1. Schematic of Ag^{+}-HPLC/O_3-MS system.

5.3. Results and Discussion

5.3.1. Preparation of CLnA methyl esters

CLnA standards (*trans*8, *trans*10, *cis*12-, *trans*8, *trans*10, *trans*12-, *cis*9, *trans*11, *cis*13-18:3) were converted to methyl esters using the three procedures described above. The resulting CLnA methyl esters were then subjected to O_3-MS analysis using the optimized conditions as described above. It was found that more than the expected three pairs of characteristic ozonolysis aldehyde ions were observed in the mass spectra of each of the CLnA-FAME produced from **Systems 1 and 2**. This indicates that the pure CLnA standard was isomerized at high temperatures (**System 2**, 80 °C) and long reaction times (**System 1**, 12 h). For example, the in-line O_3-MS spectrum of methylated *cis*9, *trans*11, *cis*13-CLnA shows that in addition to the three expected ion pairs, the ion pair at *m/z* 253 and 221 were also detected, indicating the presence of double bond at Δ^{14} position. However, when the **System 3** conditions were employed, no extra ozonolysis product ions were found in the mass spectrum. Hence, **System 3** was selected as the final procedure for methylation in this study. This result is consistent with *Chen et al.* [19] who found that these conditions avoid isomerization of CLnA during methylation.

Ultimately, the methylation procedure used was as follows. The oil sample (10 mg) was dissolved in 1 mL toluene and methylated using 2 mL of 8% (*v/v*) sulfuric acid in methanol at 40 °C for 10 min. After the reaction was complete, 5 mL of a 5% (w/w) sodium chloride solution was added and 5 mL of hexane was used to extract FAME twice. The hexane layer was washed with a 4 mL solution of 2% potassium bicarbonate (w/w). Then the hexane layer was collected, dried over anhydrous sodium sulfate and evaporated under nitrogen gas (N_2). Finally, FAMEs were re-suspended in hexane to obtain a concentration of 0.01 mg mL^{-1} (10 ppm) for Ag^+-LC/O_3-MS analysis.

5.3.2. Method development by Ag^+-LC/O_3-MS

5.3.2.1. Ag^+-LC separation

Silver ion chromatography (Ag^+-LC) was employed to separate the *cis* and *trans* geometric CLnA isomers. It is well-known that the interaction between silver ions and double bonds in the *trans* configuration are weaker than those with *cis* double bonds [21]. Thus, CLnA geometric configuration groups elute as the order of *t,t,t*-isomer<*c,t,t*-isomer <*c,t,c*-isomer<*c,c,c*-isomer [15].

Four individual CLnA FAME standards were used. Each was checked for authenticity by running Ag^+-LC/O_3-MS experiments which yielded single chromatographic peaks and the expected ozonolysis product ions. A mixture of the four methylated CLnA isomers, each at a concentration of 10 μg mL^{-1}, was used for the optimization of the Ag^+-LC conditions. Using a single Ag^+-LC column, it was found that the first peak which is *β*-calendic acid methyl ester (*trans*8, *trans*10, *trans*12-18:3) eluted at 5.7 min. Based on the separation principle above, along with the structural identification given by the supplier of the standards, the other three CLnA isomers followed closely eluting at 5.9, 6.0 and 6.1 min can be positively identified as *α*-eleostearic

acid methyl ester (*cis*9, *trans*11, *trans*13-18:3), *α*-calendic acid methyl ester (*trans*8, *trans*10, *cis*12-18:3) and punicic acid methyl ester (*cis*9, *trans*11, *cis*13-18:3), respectively. Since all of four isomers eluted so close together, two Ag^+-LC columns were connected in series in order to improve the peak resolution. In this way, three well-resolved peaks at retention times of 13. 6, 16.4 and 19.8 min were observed (**Figure 5-1**). However, there is still *a* co-elution of *cis*9, *trans*11, *trans*13-18:3 and *trans*8, *trans*10, *cis*12-18:3 isomers.

Mobile phase composition is another factor that can affect the chromatographic performance. Various mobile phase compositions were tested in this work to achieve the best separation. Initially, a binary system of 80% solvent A, 0.1% acetonitrile in hexane (*v/v*) and 20% solvent B, 100% hexane was used. However, a retention time drift was observed after several repeated running of the target analytes. This can be explained by the limited solubility of acetonitrile in hexane [22]. To address this problem, the acetonitrile was replaced by butyronitrile as a modifier in hexane and isopropanol (1%) was also added to the mobile phase system. Butyronitrile, as an alternate mobile-phase modifier, was proposed by R. G. Harfmann *et al.* [22] who found that butyronitrile was a more stable mobile-phase modifier compared to acetonitrile and propionitrile due to its higher solubility, resulting in more stable retention times. Furthermore, isopropanol has a polarity in-between hexane and butyronitrile and is miscible in many polar and non-polar solvents. Thus, isopropanol may effectively increase the solubility of butyronitrile in hexane and ultimately lead to more reproducible retention times in silver ion chromatography. Under the optimized mobile phase composition, three successive injections of the mixture of four CLnA isomers were made to test the stability of retention times. As an example, in three successive runs, the peak for *α*-eleostearic acid methyl ester (*cis*9, *trans*11, *trans*13-18:3) eluted at measured retention times of 16.4, 16.4 and 16.4 min. This indicates that within a sequence of injections on a given day,

sufficient retention time stability can be obtained with the optimized mobile phase systems. However, the day-to-day retention time stability of silver ion chromatography is poor.

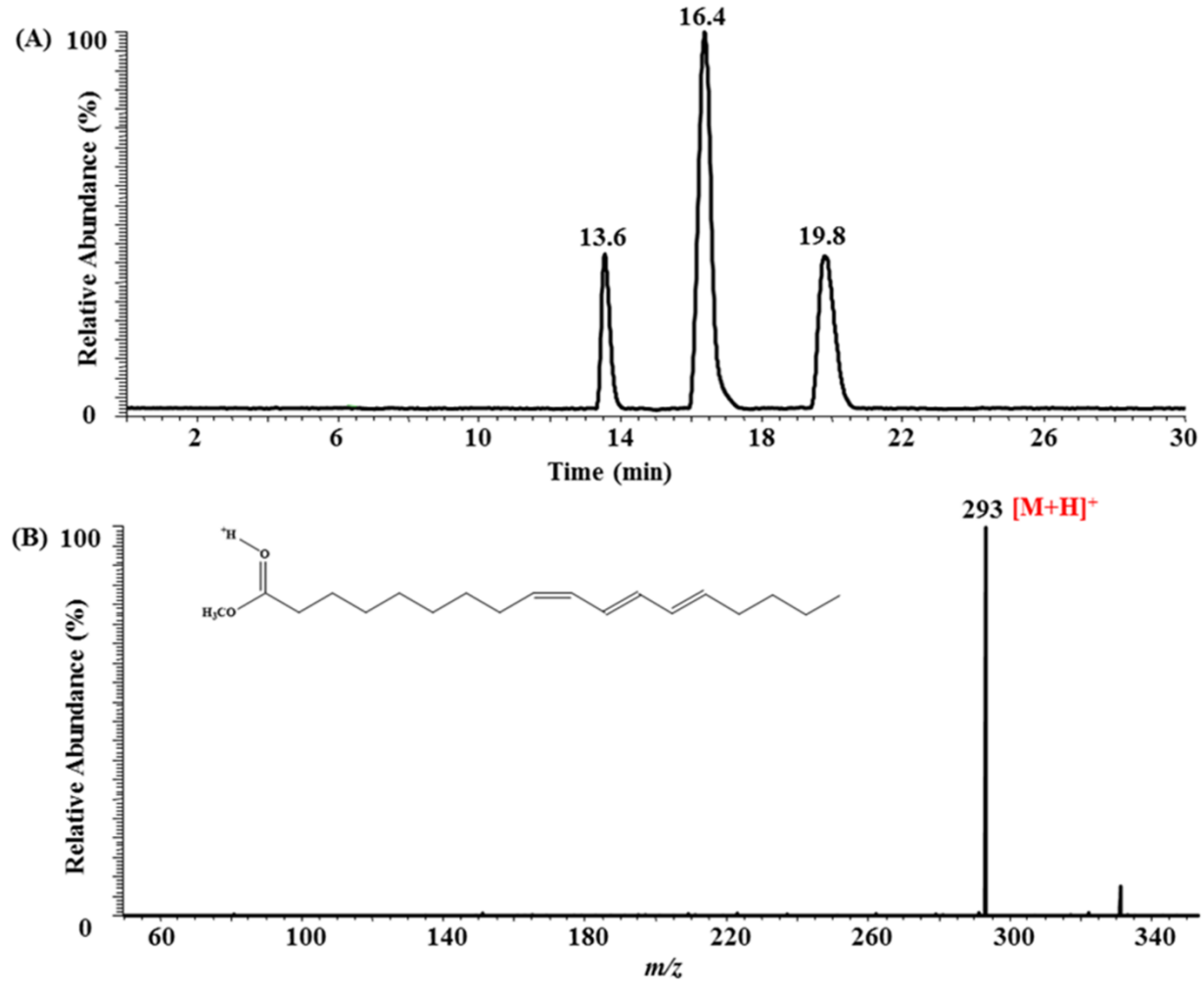

Figure 5-1. (A) the Ag^{+}-HPLC chromatogram of the conjugated linolenic acid methyl ester (CLnAMe) mixture (methylated using 8% (*v/v*) sulfuric acid at 40 ºC for 10 min): peaks at tR of 13.6, 16.4 and 19.8 min were identified as isomer 1 (8*t*, 10*t*, 12*t*-18:3), isomers 2 and 3 (9*c*, 11*t*, 13*t*-18:3 and 8*t*, 10*t*, 12*c*-18:3) and isomer 4 (9*c*, 11*t*, 13*c*-18:3), respectively; (B) the APCI(+)/MS spectrum of 9*c*, 11*t*, 13*t*-CLnAMe (example).

5.3.2.2. In-line O_3-MS analysis

In order to further identify the co-eluted peaks of *cis*9, *trans*11, *trans*13-18:3 and *trans*8, *trans*10, *cis*12-18:3 isomers, the LC effluent was passed through the in-line ozonolysis system prior to mass spectrometry (**Scheme 5-1**). In this way, each peak separated by silver ion chromatography is subjected to ozonolysis separately. The ozonolysis product aldehydes resulting from the oxidative cleavage at each double bond can then be used as indicators of double bond positions for monounsaturated and non-conjugated polyunsaturated FAME [17].

First, in-line O_3-MS analysis was performed on pure *cis*9, *trans*11, *cis*13- and *trans*8, *trans*10, *trans*12-CLnA methyl ester standards. The length of Teflon tubing within the ozone-filled solvent bottle was adjusted to make sure that the intact FAME molecular ion at *m/z* 293 could be detected simultaneously with the characteristic ozonolysis aldehyde ions. By doing so, both the number and position of the double bonds could be known in a single run.

From the in-line O_3-MS analysis of *cis*9, *trans*11, *cis*13-CLnA methyl ester, product ions at *m/z* 239, 207, 213, 181, 187 and 155 were observed (**Figure 5-2A**). The ions at *m/z* 239, 213 and 187 correspond to the protonated aldehyde ions from the ozonolysis cleavage at Δ^{13}, Δ^{11} and Δ^{9} positions, and the ions at *m/z* 207, 181 and 155 are due to methanol loss from *m/z* 239, 213 and 187. From the in-line O_3-MS analysis of the *trans*8, *trans*10, *trans*12-CLnA methyl ester, ions at *m/z* 225, 193, 199, 167, 173 and 141 were observed (**Figure 5-2B**). The ions at *m/z* 225, 199 and 173 are indicative of double bonds located at Δ^{12}, Δ^{10} and Δ^{8} positions, while the ions at *m/z* 193, 167 and 141 are due to the methanol loss from these ions. Hence, the in-line O_3-MS spectra of these two CLnA positional isomers demonstrate that the observed ozonolysis product aldehyde ion pairs are indicative of double bond locations even when there are three conjugated double

bonds. As a result, even though most CLnA isomers are not readily unavailable as standards, the pair of diagnostic aldehyde ions arising from ozonolysis cleavage at each double bond can be used to reliably identify and characterize CLnA positional isomers.

The mixture described above containing four CLnA methyl ester standards was analyzed by Ag^+-LC/O_3-MS under the optimized conditions. The extracted ion chromatogram (XIC) of the $[M + H]^+$ ion at *m/z* 293 and the O_3 mass spectrum of the unresolved peak eluting at 16.6 min are shown in **Figure 5-3A** and **B**, respectively. In **Figure 5-3B,** the ions at *m/z* 239, 213, 187, 225, 199 and 173 are the diagnostic aldehydes containing the methyl ester group formed due to ozonolysis cleavage of double bonds at Δ^{13}, Δ^{11}, Δ^{9}, Δ^{12}, Δ^{10} and Δ^{8} positions confirming the co-elution of *cis*9, *trans*11, *trans*13-18:3 and *trans*8, *trans*10, *cis*12-18:3 isomers. As expected, the aldehyde ions also lose methanol, giving rise to corresponding fragment ions at *m/z* 207, 181, 155, 193. 167 and 141. These results show how in-line O_3-MS method provides the additional dimension of information to Ag^+-LC needed to attempt the assignment of both the geometric and the positional isomers of CLnA. The predicted diagnostic aldehyde ions and their corresponding methanol loss fragment ions for common CLnA positional isomers are summarized in **Table 5-1**.

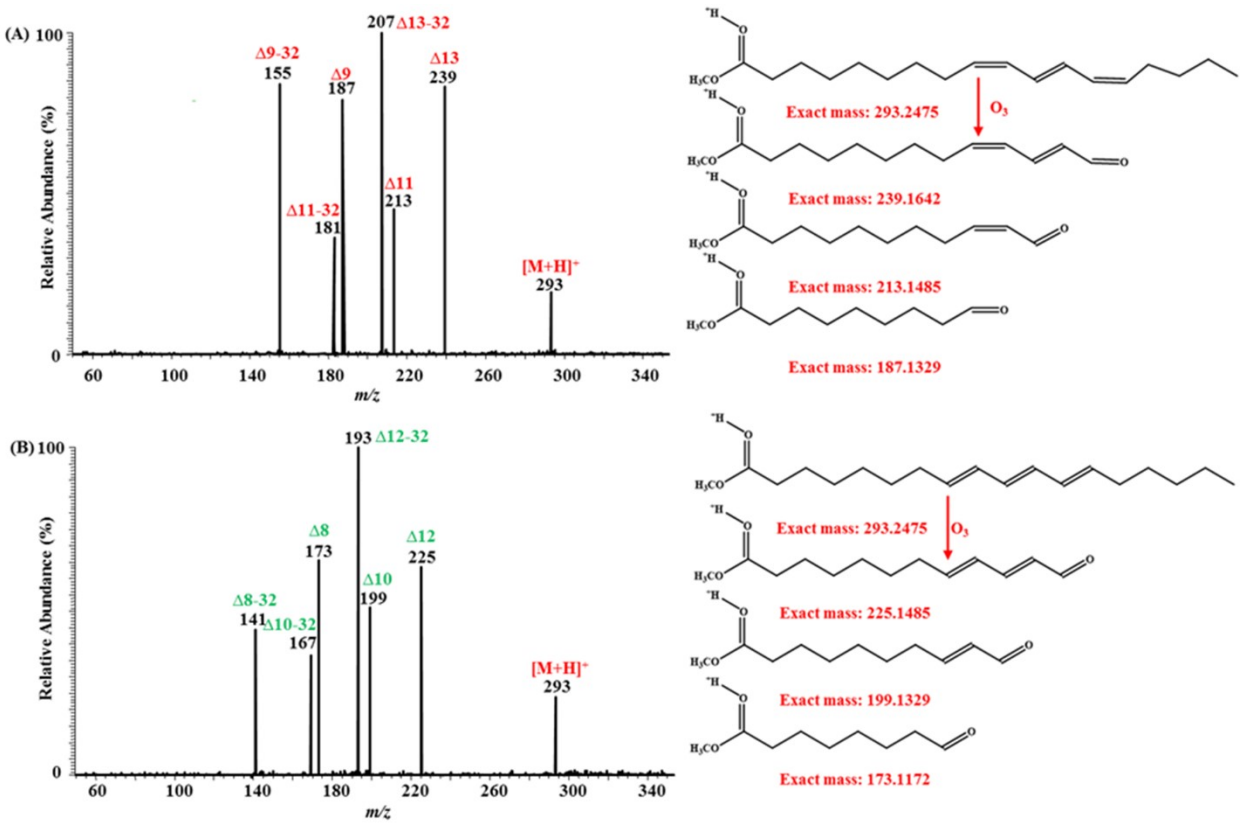

Figure 5-2. In-line O_3-APCI (+)-MS spectrum of (A) 9*c*, 11*t*, 13*c*-CLnA methyl ester and (B) 8*t*, 10*t*, 12*t*-CLnA methyl ester

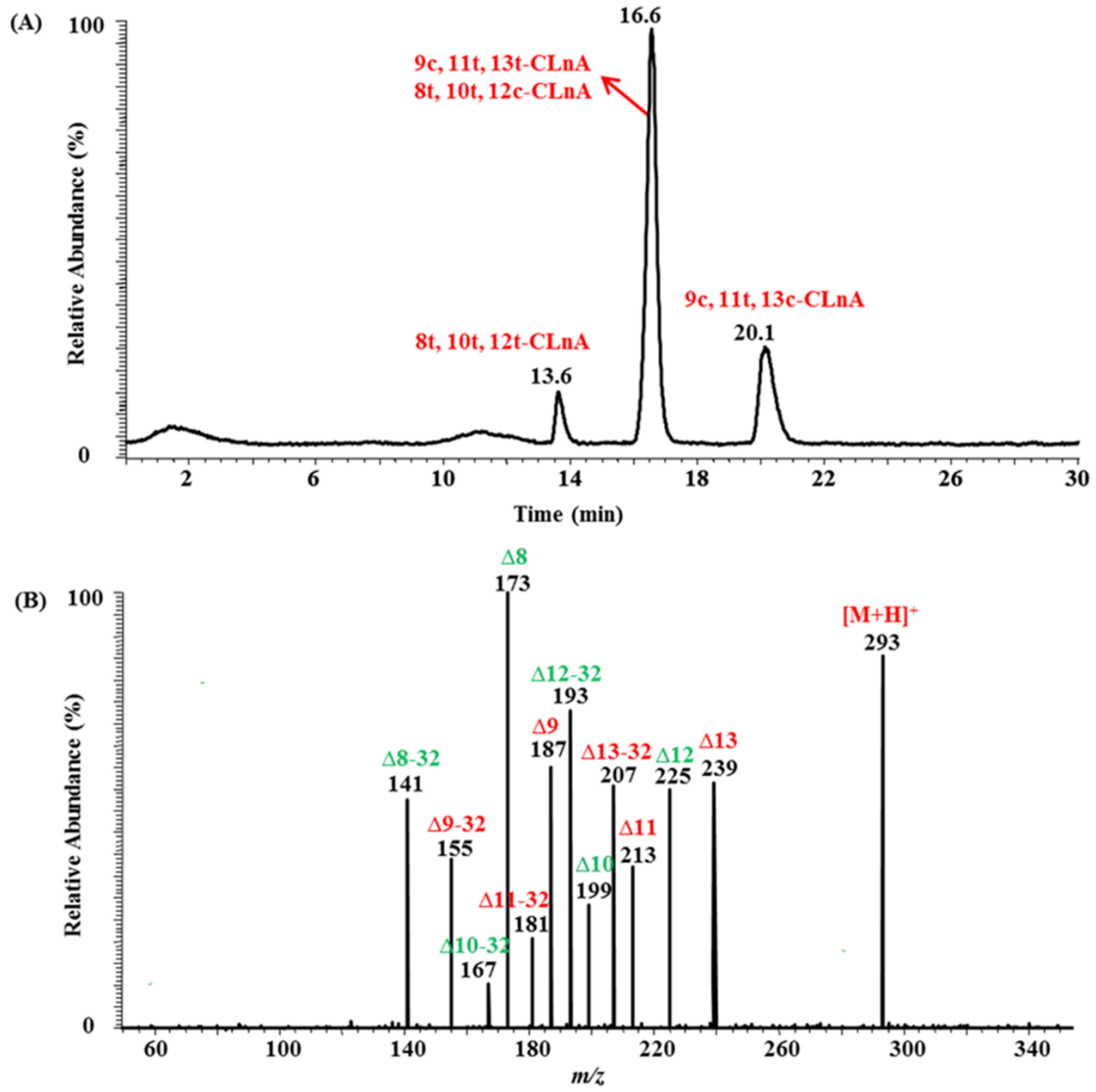

Figure 5-3. (A) Ag^{+}-LC/O_3-MS chromatogram of the conjugated linolenic acid methyl ester (CLnAMe) mixture (methylated using 8% (*v/v*) sulfuric acid at 40 ºC for 10 min): peaks at tR of 13.6, 16.6 and 20.1 min were identified as isomer 1 (8*t*, 10*t*, 12*t*-18:3), isomers 2 and 3 (9*c*, 11*t*, 13*t*-18:3 and 8*t*, 10*t*, 12*c*-18:3) and isomer 4 (9*c*, 11*t*, 13*c*-18:3), respectively; (B) the mass spectrum of peak at 16.6 min (2 isomers overlapped).

Table 5-1. Nominal m/z for in-line O_3/APCI(+)-MS diagnostic ions for CLnA positional isomer identification.

CLnA isomers	A. *m/z* of aldehyde ions from O_3 cleavage at Δ[a] position	*m/z* of ions due to methanol loss from A	B. *m/z* of aldehyde ions from O_3 cleavage at Δ+2 position	*m/z* of ions due to methanol loss from B	C. *m/z* of aldehyde ions from O_3 cleavage at Δ+3 position	*m/z* of ions due to methanol loss from C
8,10,12	173	141	199	167	225	193
9,11,13	187	155	213	181	239	207
10,12,14	201	169	227	195	253	221
11,13,15	215	183	241	209	267	235

[a] Position of double bond counted from the carboxyl group end.

5.3.3. Ag^+-LC/O_3-MS analysis of FAME mixtures from TSO samples

The Ag^+-LC/O_3-MS method for double bond assignment was applied to tung seed oil FAME. Figure 5-4 shows XIC trace obtained by Ag^+-LC/APCI(+)-MS (without ozonolysis) analysis of a TSO FAME mixture. Two major peaks at *m/z* 293 with retention times of 11.6 and 14.3 min were detected, showing the presence of C18:3 FAME (Figure 5-4). By comparing the retention times with those of the available standards, geometric configuration of these two peaks could be identified as *t,t,t*- and CLnA isomers which have 2 *trans* double bonds and 1 *cis* double bond.

In order to get positional information on these isomers, in-line ozonolysis was combined into the analytical system (Ag^+-LC/O_3-MS). In the XIC trace at *m/z* 293, there are two peaks detected at 12.1 and 14.7 min (Figure 5-5**A**). Figure 5-5**B** shows the O_3-MS spectrum of the peak at 12.1 min which contains six pairs of diagnostic ions. These ions, at *m/z* 239 (methanol loss ion at *m/z* 207), 213 (methanol loss ion at *m/z* 181), 187 (methanol loss ion at *m/z* 155), 225 (methanol loss ion at *m/z* 193), 199 (methanol loss ion at *m/z* 167) and 173 (methanol loss ion at *m/z* 141), can be used to unambiguously assign the double bond position at Δ^{13}, Δ^{11}, Δ^{9}, Δ^{12}, Δ^{10} and Δ^{8}. This

indicates the coelution of the two CLnA isomers $\Delta^{9,11,13}$ and $\Delta^{8,10,12}$. Furthermore, the mass spectrum of the peak at 14.7min (**Figure 5-5A**) is shown in **Figure 5-5C**, which identifies $\Delta^{9,11,13}$ CLnA isomer by detecting three pairs of diagnostic ions at *m/z* 239 (methanol loss ion at *m/z* 207), 213 (methanol loss ion at *m/z* 181) and 187 (methanol loss ion at *m/z* 155). In both of the mass spectra, the ion at *m/z* 293 is also detected, confirming the presence of protonated molecular ion of an 18:3 FAME isomer. Although the geometric configuration cannot be determined from the O_3-MS spectra, the available standards do indicate the region of the chromatogram where *trans, trans, trans*-C18:3 isomers elute and where 18:3 isomers containing 2 *trans* and 1 *cis* double bonds elute.

In summary, three CLnA isomers including *α*-eleostearic acid (*cis*9, *trans*11, *trans*13-18:3), *β*-calendic acid (*trans*8, *trans*10, *trans*12-18:3) and *β*-eleostearic acid (*trans*9, *trans*11, *trans*13-18:3) were detected in the TSO samples. It has been reported that TSO mainly contains two CLnA isomers: *α*-eleostearic acid (*cis*9, *trans*11, *trans*13-18:3) and *β*-eleostearic acid (*trans*9, *trans*11, *trans*13-18:3) [13]. Here, using combination of Ag^+-LC/O_3-MS and in-line ozonolysis techniques, *β*-calendic acid (*trans*8, *trans*10, *trans*12-18:3) was also identified in TSO samples, which provides supplementary information to the composition of CLnA isomers in TSO samples.

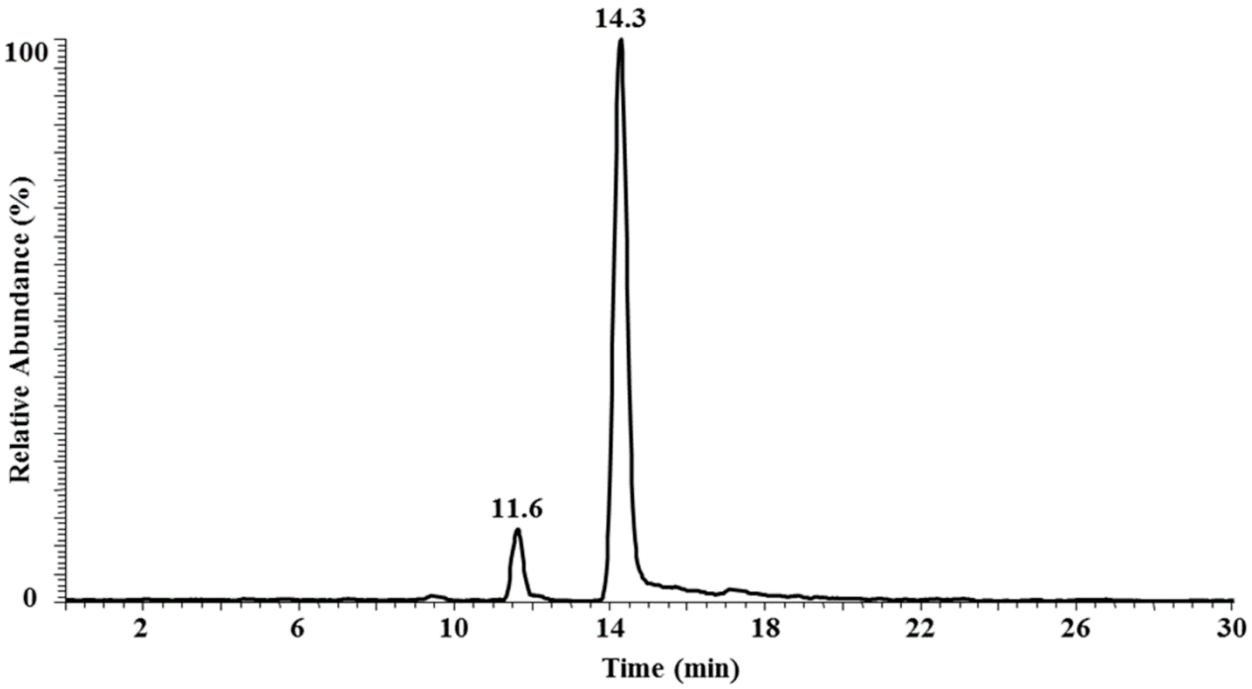

Figure 5-4. Extracted ion chromatograms of C18:3 FAME at *m/z* 293 (methylated using 0.8% (*v/v*) sulfuric acid at 40 ºC for 10 min) derived from TSO samples.

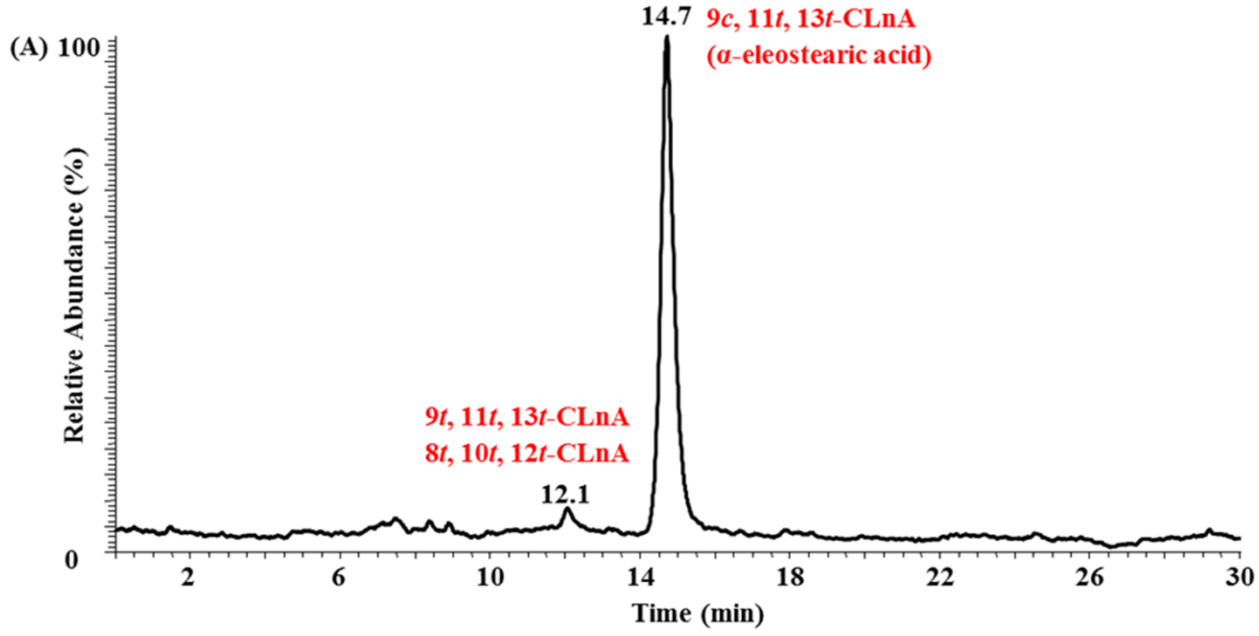

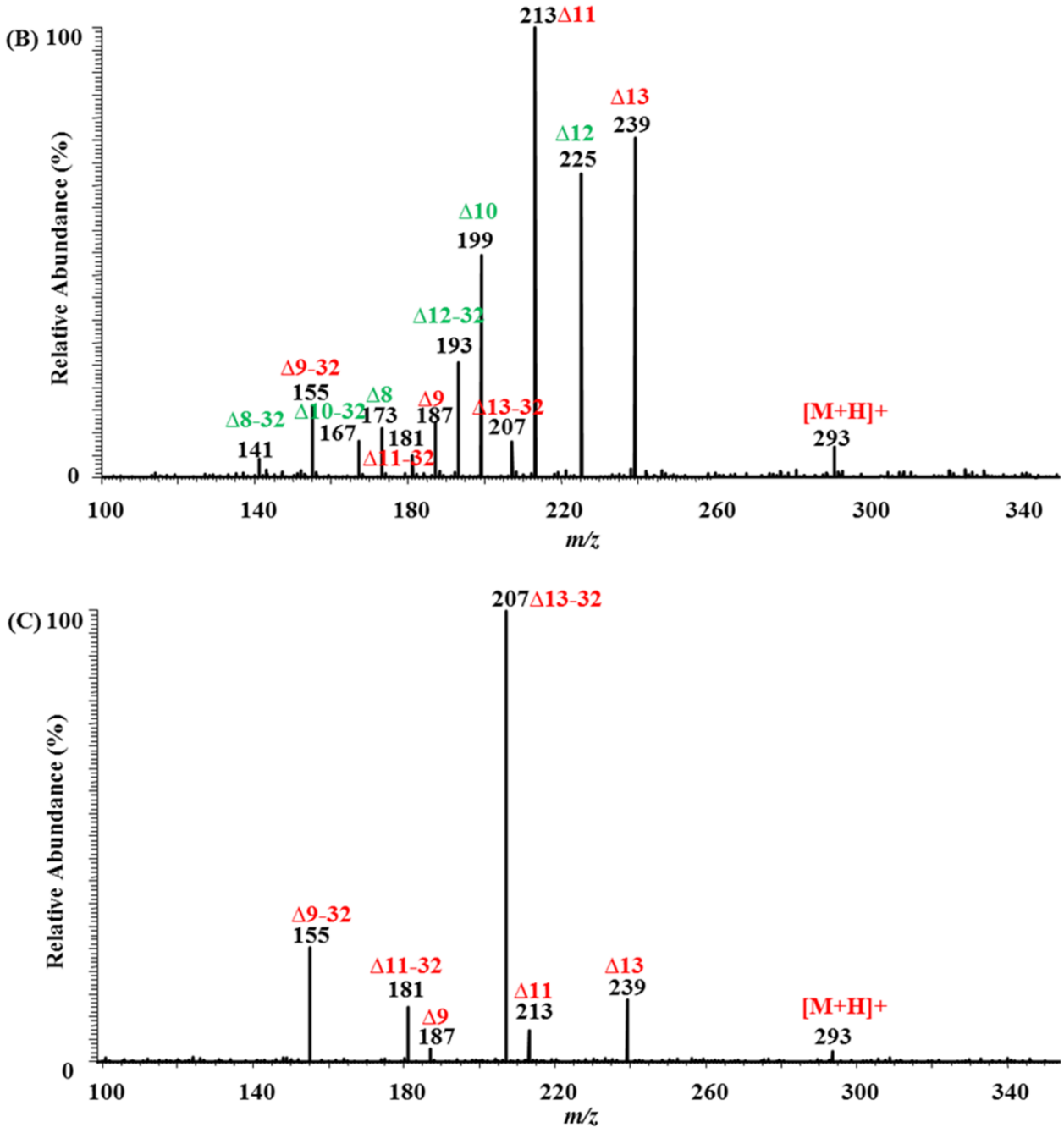

Figure 5-5. The Ag^{+}-LC/O_3-APCI(+)-MS analysis of CLnA components in TSO samples (methylated using 8% (*v/v*) sulfuric acid at 40 ºC for 10 min) (A) XIC of *m/z* 293; (B) mass spectrum averaged at 12.1 min and (C) mass spectrum averaged at 14.7 min.

5.3.4. Ag^+-LC/O_3-MS analysis of FAME mixtures from PSO samples

Another example showing the application of the Ag^+-LC/O_3-MS method is for profiling CLnA isomers in PSO, as shown in **Figure 5-6**. In **Figure 5-6**, the PSO CLnA isomers give rise to three peaks at 11.7, 14.4 and 17.3 min, respectively. By comparing with the retention times of the authentic CLnA standards, the geometric configuration of these three peaks could be identified as *t,t,t*-, *c,t,t*- and *c,t,c*-CLnA isomers. Using in-line ozonolysis/APCI-MS analysis, the positions of the double bonds of these CLnA isomers from PSO were determined. There are three peaks eluting at 12.1, 15.1 and 17.9 min in the XIC of *m/z* 293 from the Ag^+-LC/O_3-MS method (**Figure 5-7A**). Following the mass spectrum of the peak at 12.1 min (**Figure 5-7B**), 6 pairs of diagnostic ions at *m/z* 239 (methanol loss ion at *m/z* 207), 213 (methanol loss ion at *m/z* 181), 187 (methanol loss ion at *m/z* 155), 225 (methanol loss ion at *m/z* 193), 199 (methanol loss ion at *m/z* 167) and 173 (methanol loss ion at *m/z* 141) can be used to unambiguously assign the double bond position at Δ^{13}, Δ^{11}, Δ^{9}, Δ^{12}, Δ^{10} and Δ^{8}. In **Figure 5-7C and D**, the same pairs of diagnostic ions at *m/z* 239 (methanol loss ion at *m/z* 207), 213 (methanol loss ion at *m/z* 181) and 187 (methanol loss ion at *m/z* 155) can be seen, which identify these peaks as $\Delta^{9,11,13}$ CLnA isomers. Therefore, it can be concluded that four CLnA isomers including *β*-calendic acid (*trans*8, *trans*10, *trans*12-18:3), *β*-eleostearic acid (*trans*9, *trans*11, *trans*13-18:3), *α*-eleostearic acid (*cis*9, *trans*11, *trans*13-18:3) and punicic acid (*cis*9, *trans*11, *cis*13-18:3) were identified in PSO samples.

Previously, Alcaraz-Mármol *et al.* [12] reported that punicic acid (*cis*9, *trans*11, *cis*13-18:3), CLnA1, CLnA2 and CLnA3 (all conjugated linolenic acid, C18:3) were found in pomegranate seeds. But the identities of CLnA1, CLnA2 and CLnA3 were not further confirmed due to the lack of authentic standards. Here in our study, in addition to punicic acid (*cis*9, *trans*11, *cis*13-18:3), the other three CLnA isomers were also identified by combining the in-line ozonolysis into the

analytical system, which allows for the comprehensive CLnA profiling in the target oil samples even without the authentic standards.

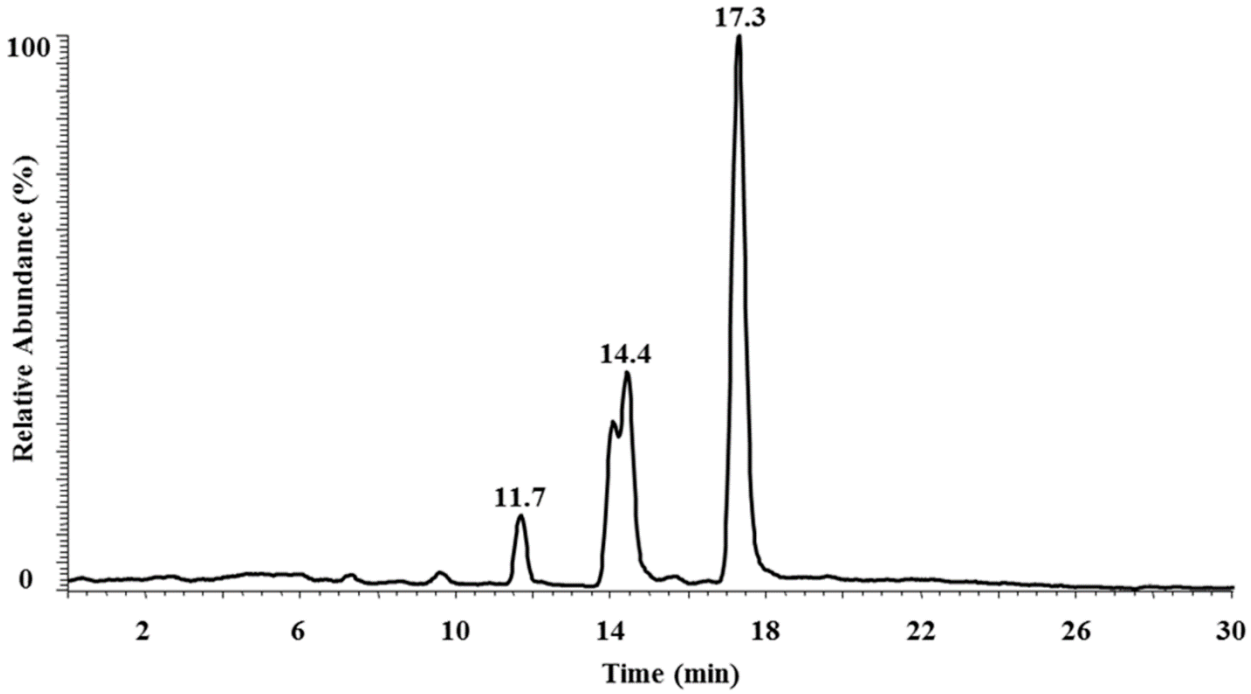

Figure 5-6. Extracted ion chromatogram of C18:3 FAME at *m/z* 293 (methylated using 8% (*v/v*) sulfuric acid at 40 ºC for 10 min) derived from PSO samples.

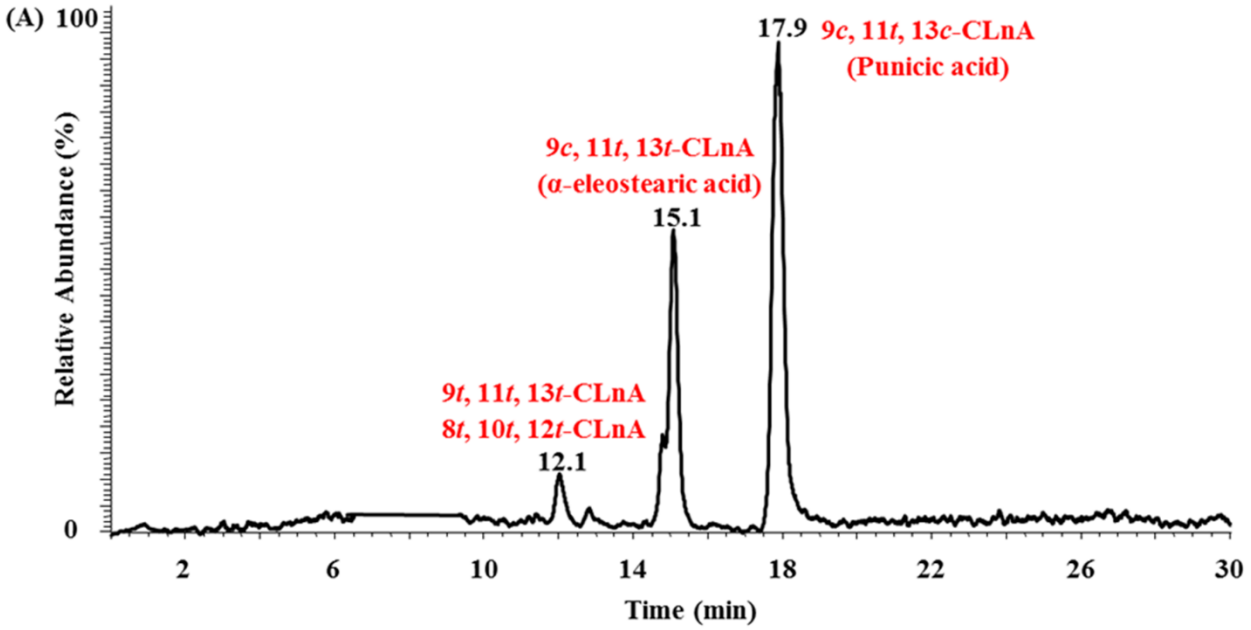

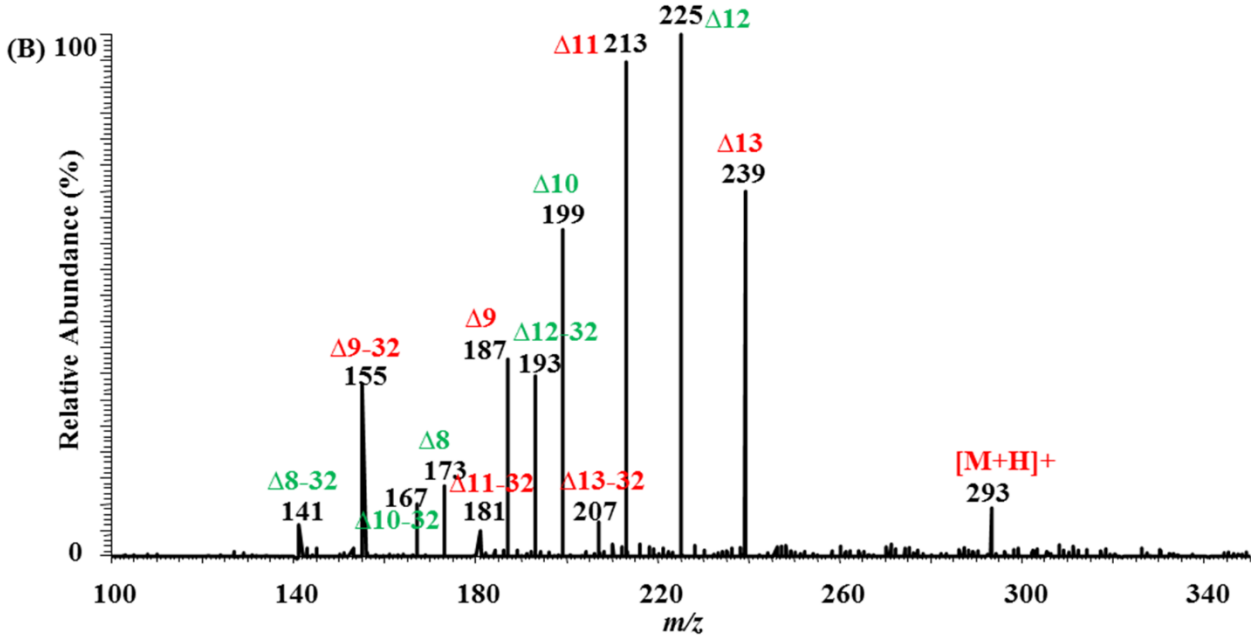
(B) 100
Relative Abundance (%)
0
100
140
180
220
260
300
340
m/z
225 Δ12
Δ11 213
Δ13
239
Δ10
199
Δ9
187
Δ12-32
193
Δ9-32
155
Δ8
173
Δ8-32
141
167
Δ10-32
Δ11-32
181
Δ13-32
207
[M+H]+
293

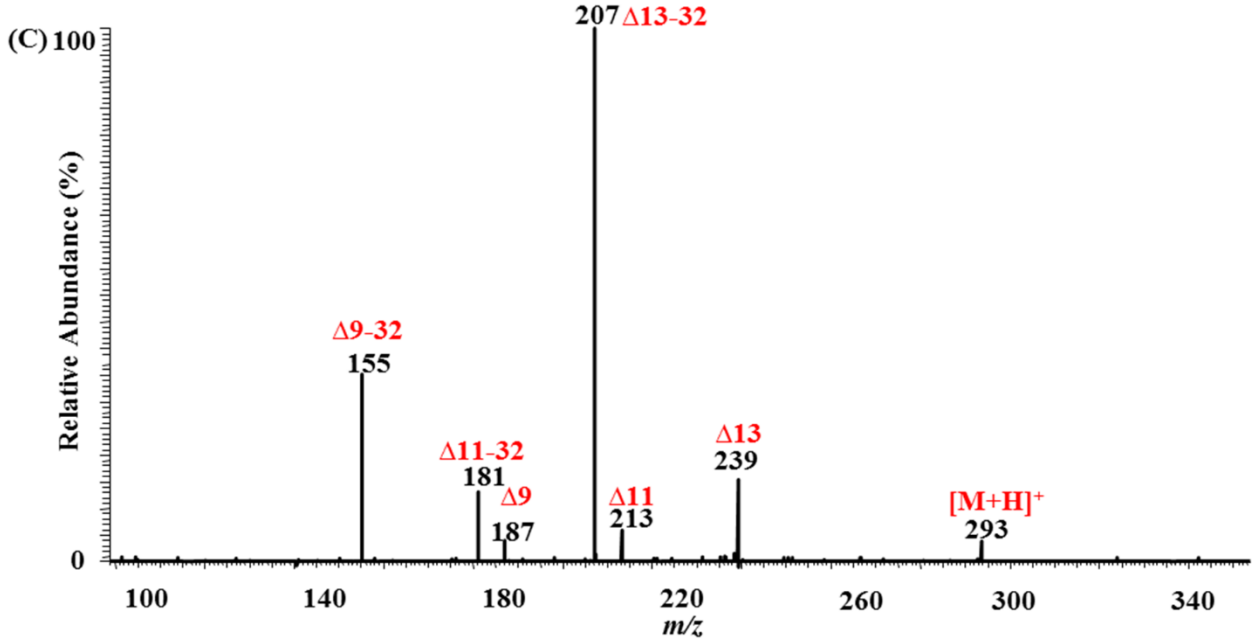
(C) 100
Relative Abundance (%)
0
100
140
180
220
260
300
340
m/z
207 Δ13-32
Δ9-32
155
Δ11-32
181
Δ9
187
Δ11
213
Δ13
239
[M+H]+
293

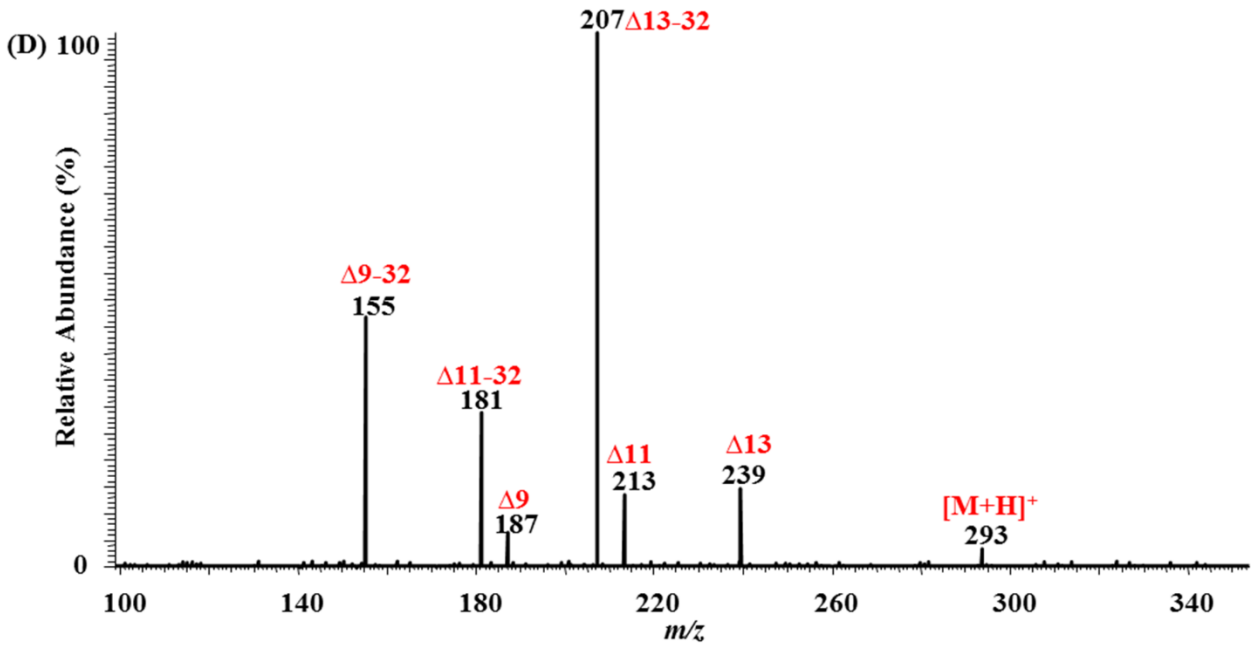

Figure 5-7. The Ag^+-LC/O_3-APCI(+)-MS analysis of CLnA components in PSO samples (methylated using 8% (*v/v*) sulfuric acid at 40 ºC for 10 min) (A) XIC of *m/z* 293; (B) mass spectrum averaged at 12.1 min; (C) mass spectrum averaged at 15.1 min and (D) mass spectrum averaged at 17.9 min.

5.4. Conclusions

In this study, a novel and straightforward strategy consisting of modified sample methylation conditions (including temperature and reaction time) and in-line ozonolysis reaction, coupled with Ag^+-LC/APCI(+)-MS, is demonstrated for the rapid analysis of CLnA compositions in the PSO and TSO samples. Ag^+-HPLC separated the CLnA mixture into different geometric groups, such as *ttt*, *ctt and ctc*. Within each group, the double bond positions (the positional isomers) were further identified using in-line O_3-MS. Using this approach, and from the high resolution/accurate mass (HR/AM) mass spectrum, we have achieved the most comprehensive CLnA profiles in PSO and TSO samples reported to date. These results facilitate a greater understanding of CLnA in studies involving its oxidative stability, functional properties and bioactivity which may be CLnA isomer specific. In summary, the Ag^+-LC/O_3-MS method described here provides a comprehensive

platform for the determination of the CLnA isomers present in lipid extracts.

5.5. References

[1] Y. Cao, H. Gao, J.N. Chen, Z.Y. Chen, L. Yang, Identification and characterization of conjugated linolenic acid isomers by Ag^{+}-HPLC and NMR, J Agric Food Chem. 54 (2006) 9004-9009.

[2] G.F. Yuan, X.E. Chen, D. Li, Conjugated linolenic acids and their bioactivities: a review, Food Funct. 5 (2014) 1360-1368.

[3] A.A. Hennessy, R.P. Ross, R. Devery, C. Stanton, The health promoting properties of the conjugated isomers of α-linolenic acid, Lipids. 46 (2011) 105-119.

[4] L. Gorissen, F. Leroy, L. De Vuyst, S. De Smet, K. Raes, Bacterial production of conjugated linoleic and linolenic acid in foods: a technological challenge, Crit Rev Food Sci Nutr. 55 (2015) 1561-1574.

[5] Y. Yasui, M. Hosokawa, T. Sahara, R. Suzuki, S. Ohgiya, H. Kohno, T. Tanaka, K. Miyashita, Bitter gourd seed fatty acid rich in 9*c*,11*t*,13*t*-conjugated linolenic acid induces apoptosis and up-regulates the GADD45, p53 and PPARγ in human colon cancer Caco-2 cells, Prostaglandins Leukot Essent Fatty Acids. 73 (2005) 113-119.

[6] H. Kohno, R. Suzuki, Y. Yasui, M. Hosokawa, K. Miyashita, T. Tanaka, Pomegranate seed oil rich in conjugated linolenic acid suppresses chemically induced colon carcinogenesis in rats, Cancer Sci. 95 (2004) 481-486.

[7] C. Zou, H. Shi, X. Liu, Y. Sheng, T. Ding, J. Yan, B. Gao, J. Liu, W. Lu, L. Yu, Conjugated linolenic acids and nutraceutical components in Jiaogulan (*Gynostemma pentaphyllum*) seeds, LWT-Food Sci Technol. 68 (2016) 111-118.

[8] S.S. Saha, M. Ghosh, Protective effect of conjugated linolenic acid isomers present in vegetable oils against arsenite-induced renal toxicity in rat model, Nutrition. 29 (2013) 903-910.

[9] S. Özgül-Yücel, Determination of conjugated linolenic acid content of selected oil seeds grown in Turkey, J Am Oil Chem. Soc. 82 (2005) 893-897.

[10] I.A.T.M. Meerts, C.M. Verspeek-Rip, C.A.F. Buskens, H.G. Keizer, J. Bassaganya-Riera, Z.E. Jouni, A.H.B.M. van Huygevoort, F.M. van Otterdijk, E.J. van de Waart, Toxicological evaluation of pomegranate seed oil, Food Chem Toxicol. 47 (2009) 1085-1092.

[11] R. Suzuki, S. Arato, R. Noguchi, K. Miyashita, O. Tachikawa, Occurrence of conjugated linolenic acid in flesh and seed of bitter gourd. J Oleo Sci. 50 (2001) 753-758.

[12] F. Alcaraz-Mármol, N. Nuncio-Jáuregui, Á. Calín-Sánchez, Á.A. Carbonell-Barrachina, J.J. Martínez, F. Hernández, Determination of fatty acid composition in arils of 20 pomegranates cultivars grown in Spain, Sci Hort. 197 (2015) 712-718.

[13] Y. Cao, L. Yang, H.L. Gao, J.N. Chen, Z.Y. Chen, Q.S. Ren, Re-characterization of three conjugated linolenic acid isomers by GC-MS and NMR. Chem Phys Lipids. 145 (2007) 128-133.

[14] M. Plourde, F. Destaillats, P.Y. Chouinard, P. Angers, Conjugated α-linolenic acid isomers in bovine milk and muscle, J Dairy Sci. 90 (2007) 5269-5275.

[15] L. Yang, Y. Cao, J.N. Chen, Z.Y. Chen, Oxidative stability of conjugated linolenic acids, J Agric Food Chem. 57 (2009) 4212-4217.

[16] C. Sun, J.M. Curtis, Locating double bonds in lipids-new approaches to the use of ozonolysis, Lipid Technol. 25 (2013) 279-282.

[17] C. Sun, B.A. Black, Y.Y. Zhao, M.G. Gänzle, J.M. Curtis, Identification of conjugated linoleic acid (CLA) isomers by silver ion-liquid chromatography/in-line ozonolysis/mass spectrometry (Ag^+-LC/O_3-MS), Anal Chem. 85 (2013) 7345-7352.

[18] C. Sun, Y.Y. Zhao, J.M. Curtis, Elucidation of phosphatidylcholine isomers using two dimensional liquid chromatography coupled in-line with ozonolysis mass spectrometry, J Chromatogr A. 1351(2014) 37-45.

[19] J. Chen, Y. Cao, H. Gao, L. Yang, Z.Y. Chen, Isomerization of conjugated linolenic acids during methylation, Chem Phys Lipids. 150 (2007) 136-142.

[20] B.A. Black, C. Sun, Y.Y. Zhao, M.G. Gänzle, J.M. Curtis, Antifungal lipids produced by lactobacilli and their structural identification by normal phase LC/atmospheric pressure photoionization-MS/MS. J Agric Food Chem. 61 (2013) 5338-5346.

[21] B. Nikolova-Damyanova, Retention of lipids in silver ion high-performance liquid chromatography: Facts and assumptions, J Chromatogr A. 1216 (2009) 1815-1824.

[22] R.G. Harfmann, S. Julka, H.J. Cortes, Instability of hexane-acetonitrile mobile phases used for the chromatographic analysis of triacylglycerides, J Sep Sci. 31 (2008) 6-7.

Chapter 6

General Conclusions and Future Work

Lipidomics research is fascinating and challenging due to their important functional roles and immense structural and chemical diversity. Lipidomics enables investigators to monitor changes of hundreads of thousands compounds during dynamic metabolic processes, which cannot be achieved by other lipid analysis projects.

In this dissertation, I established LC/MS-based analytical methods for identification and quantification of target lipid and lipid-related compounds in various biological systems. For targeted lipidomics, chromatographic separation techniques, such as GC or LC, are usually employed to isolate the target compounds from complex mixtures. The specificity and sensitivity of the LC/MS-based methods are greatly enhanced by the use of a triple quadrupole mass spectrometer, which enables quantitative analyses of high precision and accuracy with the multiple-reaction monitoring (MRM) mode [1, 2]. In the quantitative lipidomics, the major challenge faced by the analysts is the availability of commercial internal standards (such as isotope-labeled analogues, homologues or simple structural analogues) which can be used to generate calibration curves to convert abundance of ions into a quantitative measurement of concentrations for many lipid classes [3, 2]. It is also worth noticing that lipids of various types over a wide range of concentrations make it impractical to use a single uniform analytical platform to measure all of them [1, 4]. All studies herein focus on the qualitative and quantitative analysis of different molecular species within a lipid class in targeted samples. The proposed approaches have been validated and successfully applied for the measurement of bile acids (including the conjugated forms) in piglet bile samples, sphingolipids in cells, trimethylamine (TMA) and

trimethylamine *N*-oxide (TMAO) in mouse plasma samples. In addition to triple quadrupole mass spectrometer, Orbitrap mass spectrometer with better performance characteristics including high mass accuracy, resolving power and dynamic range [2, 4] was also utilized in this dissertation for comprehensive profiling of conjugated linolenic acid (CLnA) isomers in pomegranate seed oil (PSO) and tung seed oil (TSO) samples.

Bile acids and their conjugates belong to the sterols category [2]. An analytical strategy combining an optimized C18-based SPE protocol and a LC/MS/MS method was described for the large-scaled analysis of 19 target bile acids and their conjugates (taurine and glycine) in piglet bile samples. Using this approach, all 19 compounds were separated and quantified in a single 12 min chromatographic run. The validated method was successfully applied to the profiling of bile acids and their conjugates in the bile from piglets treated with exogenous glucagon-like peptide-2 (GLP-2) in a preclinical model of neonatal parenteral nutrition-associated liver disease (PNALD). Apart from taurine and glycine conjugates, there are also other conjugates present for bile acids, such as sulfuric acid and glucuronic acid conjugates. Continued work on developing more comprehensive method is required to guarantee that larger scale of bile acids and their conjugates can be incorporated and analysed.

In this work, cell-based high throughput screening of sphingolipids including ceramides, dihydroceramides, glucosylceramides, sphingosine, sphingosine-1-phosphate, sphinganine and sphinganine-1-phosphate were carried out for mechanism investigation of sphingolipid metabolic regulation in Chronic Lymphocytic Leukemia (CLL) disease. The targeted lipid analytes were determined according to the specific biological research objectives. The LC/MS/MS method described in the study enables the simultaneous identification and quantification of 33 individual

sphingolipid molecular species covering 7 subclasses in a single chromatographic run of under 20 min. Nonetheless, sphingomyelins (SM), sulfatides and gangliosides, as important sphingolipid types, were not investigated during analysis. SM is characterized by a phosphaticholine polar group in its molecular structure [2]. Thus, its characterization has been done together the phospholipids using HILIC LC/MS/MS method described by Zhao *et al.* [5]. In order to fully characterize the sphingolipids and their role in health and disease, further work will be given to development of analytical methods for sulfatides and gangliosides such as GM1, GM2 and GM3.

The absolute quantitation of TMA and TMAO was achieved in this work with ESI in the MRM mode of MS/MS operation. TMA and TMAO are known as choline metabolites and their analysis has always been a challenge because of the low quantities made within tissues or cells. In a separate study, Zhao *et al.* [5] established a hydrophilic interaction liquid chromatography–tandem mass spectrometry (HILIC LC/MS/MS) method using multiple scan modes to separate and quantify 11 compounds including acetylcholine (AcCho), betaine (Bet), choline (Cho), glycerophosphocholine (GPC), lysophosphatidylcholine (LPC), lysophosphatidylethanolamine (LPE), phosphatidylcholine (PC), phosphatidylethanolamine (PE), phosphatidylinositol (PI), phosphocholine (PCho) and sphingomyelin (SM). This covers all of the major phospholipid compounds found in biological systems. Herein, the extended application of the HILIC LC/MS/MS method has been shown for simultaneous analysis of TMA and TMAO in the fasting mouse plasma samples. A simple and optimized derivatization procedure for TMA was performed in order to facilitate its separation from TMAO and obtain unique fragment ions suitable for MRM experiments. Finally, the derivatized TMA and TMAO are successfully separated within 5 min with no equilibration time required due to the isocratic separation.

Ozonolysis has been used for positional analysis of double bonds in fatty acid methyl esters (FAME) for many years [2, 6]. The 3-step reaction mechanism involved has been explained by Criegee [6]. Recently, the University of Alberta Lipid Chemistry Group (LCG) has published a series of papers describing a method of in-line ozonolysis coupled to MS (O_3-MS) to identify the location of the double bonds on unsaturated fatty acyl chain. Compared to off-line ozonolysis and in-situ O_3-MS (also known as OzESI-MS) methods, the key innovation of this technique was using ozonolysis in-line with MS, after the LC separation system but before the analytes reach the mass spectrometer ion source [6]. The utility of this methodology has been demonstrated by the successful identification of double bond positions in conjugated linoleic acid (CLA) isomers in nutraceutical products [7] and in phosphatidylcholine (PC) isomers in rat livers [8]. In this work, a hyphenated technique of Ag^+-LC and O_3-MS (Ag^+-LC/O_3-MS) are adopted to achieve the goal of comprehensive screening of all positional and geometric CLnA isomers. As a proof of its applicable capacity, the most comprehensive CLnA profiles in PSO and TSO samples reported to date were achieved. However, quantitative data of these identified CLnA isomers is still lacking and more efforts are still required to complete the quantitation, dependent upon the availability of suitable isotopically labelled internal standards. Quantitative results can provide further insight into discovery of interesting new ways that CLnA isomers are involved, and possibly in extending the application of natural PSO and TSO resources.

LC/MS-based methods established in this work were shown to be rapid, reliable and informative. It is important to note that each new application of these methodologies in the future will require some degree of re-validation of the parameters, and they should be periodically re-checked with even routine analyses. If they are applied to different sample types, minimal but necessary modifications need to be made to sample preparation procedures.

CHAPTER 6

Development of novel methodologies for lipidomics relies heavily upon the advances of analytical instrumentation such as high performance chromatography combined with MS. There is no one standard extraction protocol or analytical approach suitable for global lipidomic analysis due to the enormous complexity of lipids. That is why in this thesis we established four separate LC/MS-based methods for targeted lipid research.

In the future, efforts will be put on developing more efficient method for the large-scale analysis of lipids in a single experiment. This will lead to the production of an overwhelming amount of data that requires novel bioinformatic tools for automated data processing. With the widespread applications of lipidomics, creation of databases is essential to profile the lipidome of biofluids, cells and tissues. Unlike the already-present databases or online resources, such as LIPID MAPS and LIPID BANK, the newly-established databases will concentrate on the collection of information on lipid composition in model systems instead of providing general information on lipid nomenclature, classification, structures and other chemical properties. Lipidomics is an interdisciplinary program. Thus, another trend in this area is the establishment of large research units in the same way as proteomics and genomics, which involve collaboration of laboratories and researchers in biosciences, analytical chemistry and medicine to collect, analyse, compare and illustrate lipidomic data for future research. At the same time, the integration of lipidomics into proteomics, genomics, transcriptomics and metabolomics will facilitate elucidation of the essential roles of lipids in defining the biochemical mechanisms of lipid-related diseases such as cardiovascular disease, diabetes, brain disorders, multiple sclerosis and obesity [2, 9], in generating novel approaches to disease diagnostics [3] as well as in discovering potential lipid biomarkers. Overall, lipidomics, as a powerful tool, will be expected to generate breakthroughs and innovations in biosciences.

6.1. References

[1] S.J. Blanksby, T.W. Mitchell, Advances in mass spectrometry for lipidomics, Annu Rev Anal Chem. 3 (2010) 433-465.

[2] M. Bou Khalil, W. Hou, H. Zhou, F. Elisma, L.A. Swayne, A.P. Blanchard, Z. Yao, S.A. Bennett, D. Figeys, Lipidomics era: accomplishments and challenges, Mass Spectrom Rev. 29 (2010) 877-929.

[3] R.C. Murphy, S.J. Gaskell, New applications of mass spectrometry in lipid analysis, J Biol Chem. 286 (2011) 25427-25433.

[4] Q. Hu, R.J. Noll, H. Li, A. Makarov, M. Hardman, R. Graham Cooks, The Orbitrap: a new mass spectrometer, J Mass Spectrom. 40 (2005) 430-443.

[5] Y.Y. Zhao, Y.P. Xiong, J.M. Curtis, Measurement of phospholipids by hydrophilic interaction liquid chromatography coupled to tandem mass spectrometry: The determination of choline containing compounds in foods, J Chromatogr A. 1218 (2011) 5470-5479.

[6] C. Sun, J.M. Curtis, Locating double bonds in lipids-new approaches to the use of ozonolysis, Lipid Technol. 25 (2013) 279-282.

[7] C. Sun, B.A. Black, Y.Y. Zhao, M.G. Gänzle, J.M. Curtis, Identification of conjugated linoleic acid (CLA) isomers by silver ion-liquid chromatography/in-line ozonolysis/mass spectrometry (Ag^+-LC/O_3-MS), Analytical chemistry. 85 (2013) 7345-7352.

[8] C. Sun, Y.Y. Zhao, J.M. Curtis, Elucidation of phosphatidylcholine isomers using two dimensional liquid chromatography coupled in-line with ozonolysis mass spectrometry, J Chromatogr A. 1351 (2014) 37-45.

[9] A. Nicolaou, Lipidomics: What does the future hold?, Eur. J. Lipid Sci. Technol. 113 (2011) 537-538.

Bibliography

[1] C.C. Akoh, D.B. Min, (2008). *Food lipids: chemistry, nutrition, and biotechnology*. New York: CRC press.

[2] J.L. Bernal, M.T. Martín, L. Toribio, Supercritical fluid chromatography in food analysis, J Chromatogr A. 1313 (2013) 24-36.

[3] M. Orešič, V.A. Hänninen, A. Vidal-Puig, Lipidomics: a new window to biomedical frontiers, Trends Biotechnol. 26 (2008) 647-652.

[4] P.D. Rainville, C.L. Stumpf, J.P. Shockcor, R.S. Plumb, J.K. Nicholson, Novel application of reversed-phase UPLC-oaTOF-MS for lipid analysis in complex biological mixtures: A new tool for lipidomics, J Proteome Res. 6 (2007) 552-558.

[5] A. Shevchenko, K. Simons, Lipidomics: coming to grips with lipid diversity, Nat Rev Mol Cell Biol. 11 (2010) 593-598.

[6] M. Orešič, Informatics and computational strategies for the study of lipids, Biochim Biophys Acta. 1811 (2011) 991-999.

[7] S.M. Lam, G. Shui, Lipidomics as a principal tool for advancing biomedical research, J Genet Genomics. 40 (2013) 375-390.

[8] B.M. Kenwood, A.H. Merrill Jr. Lipidomics, Encyclopedia of Cell Biology. 1 (2016) 147-159.

[9] M.A.L. de Oliveira, B.L.S. Porto, I.D.L. Faria, P.L. de Oliveira, P.M. de Castro Barra, R.D.J.C. Castro, R.T. Sato, 20 years of fatty acid analysis by capillary electrophoresis, Molecules. 19 (2014) 14094-14113.

[10] S.H. Chen, Y.J. Chuang, Analysis of fatty acids by column liquid chromatography, Anal Chim Acta. 465 (2002) 145-155.

[11] I. Brondz, Development of fatty acid analysis by high-performance liquid chromatography, gas chromatography, and related techniques, Anal Chim Acta. 465 (2002) 1-37.

[12] S.A. Mjøs, B.O. Haugsgjerd, Trans fatty acid analyses in samples of marine origin: the risk of false positives, J Agric Food Chem. 59 (2011) 3520-3531.

[13] C. Wolf, P.J. Quinn, Lipidomics: Practical aspects and applications, Prog Lipid Res. 47 (2008) 15-36.

[14] M. Wang, R.H. Han, X. Han, Fatty acidomics: global analysis of lipid species containing a carboxyl group with a charge-remote fragmentation-assisted approach. Anal Chem. 85 (2013) 9312-9320.

[15] T. Hyötyläinen, I. Bondia-Pons, M. Orešič, Lipidomics in nutrition and food research, Mol Nutr Food Res. 57 (2013) 1306-1318.

[16] S. Qu, Z. Du, Y. Zhang, Direct detection of free fatty acids in edible oils using supercritical fluid chromatography coupled with mass spectrometry, Food Chem. 170 (2015) 463-469.

[17] S. Ng, Quantitative analysis of partial acylglycerols and free fatty acids in palm oil by 13C nuclear magnetic resonance spectroscopy, J Am Oil Chem Soc. 77 (2000) 749-755.

[18] J. Bian, Y. Xue, K. Yao, X. Gu, C. Yan, Y. Wang, Solid-phase extraction approach for phospholipids profiling by titania-coated silica microspheres prior to reversed-phase liquid chromatography-evaporative light scattering detection and tandem mass spectrometry analysis, Talanta. 123 (2014) 233-240.

[19] A. Uphoff, M. Hermansson, P. Haimi, P. Somerharju, (2007). Analysis of complex lipidomes. *Medical Applications of Mass Spectrometry*, pp. 217-243. Amsterdam: Elsevier.

[20] H. Farwanah, T. Kolter, K. Sandhoff, Mass spectrometric analysis of neutral sphingolipids: methods, applications, and limitations, Biochim Biophys Acta. 1811 (2011) 854-860.

[21] H. Vesper, E.M. Schmelz, M.N. Nikolova-Karakashian, D.L. Dillehay, D.V. Lynch, A.H. Merrill, Sphingolipids in food and the emerging importance of sphingolipids to nutrition, J Nutr. 129 (1999) 1239-1250.

[22] J. Bernal, A. Mendiola, E. Ibáñez, A. Cifuentes, Advanced analysis of nutraceuticals, J Pharm Biomed Anal. 55 (2011) 758-774.

[23] S.L. Abidi, Chromatographic analysis of plant sterols in foods and vegetable oils, J Chromatogr A. 935 (2001)173-201.

[24] M.J. Lagarda, G. García-Llatas, R. Farré, Analysis of phytosterols in foods, J Pharm Biomed Anal. 41 (2006) 1486-1496.

[25] Š. Horník, M. Sajfrtová, J. Karban, J. Sýkora, A. Březinová, Z. Wimmer, LC-NMR technique in the analysis of phytosterols in natural extracts, J Anal Methods Chem. 2013 (2013) 1-7.

[26] E. Fahy, S. Subramaniam, H.A.C. Brown, K. Glass, A.H. Merrill, R.C. Murphy, C.R.H. Raetz, D.W. Russell, Y. Seyama, W. Shaw, T. Shimizu, F. Spener, G. van Meer, M.S. VanNieuwenhze, S.H. White, J.L. Witztum, E.A. Dennis, A comprehensive classification system for lipids, J Lipid Res. 46 (2005) 839-862.

[27] M.R. Wenk, The emerging field of lipidomics, Nat Rev Drug Discov. 4 (2005) 594-610.

[28] E. Fahy, S. Subramaniam, R.C. Murphy, M. Nishijima, C.R.H. Raetz, T. Shimizu, F. Spener, G. van Meer, M.J. Wakelam, E.A. Dennis, Update of the LIPID MAPS comprehensive classification system for lipids, J Lipid Res. 50 (2009) S9-S14.

[29] C. Hu, R. van der Heijden, M. Wang, J. van der Greef, T. Hankemeier, G. Xu, Analytical strategies in lipidomics and applications in disease biomarker discovery, J Chromatogr B. 877 (2009) 2836-2846.

[30] T. Hyötyläinen, M. Orešič, Analytical lipidomics in metabolic and clinical research, Trends Endocrinol Metab. 26 (2015) 671-673.

[31] G. van Meer, Cellular lipidomics, EMBO J. 24 (2005) 3159-3165.

[32] M.R. Wenk, Lipidomics: new tools and applications, Cell. 143 (2010) 888-895.

[33] M. Wang, C. Wang, R.H. Han, X. Han, Novel advances in shotgun lipidomics for biology and medicine, Prog Lipid Res. 61 (2016) 83-108.

[34] K. Schmelzer, E. Fahy, S. Subramaniam, E.A. Dennis, The lipid maps initiative in lipidomics, Methods Enzymol. 432 (2007) 171-183.

[35] M. Herrero, M. Castro-Puyana, E. Ibanez, A. Cifuentes, (2013). Compositional analysis of foods. *Liquid Chromatography: Applications*, pp. 295-317. Amsterdam: Elsevier.

[36] D.S. Nichols, (2003). Principles of lipid analysis. *Chemical and Functional Properties of Food Lipids*, pp. 167-188. New York: CRC Press.

[37] Y.Y. Zhao, S.P. S. Wu, Liu, Y. Zhang, R.C. Lin, Ultra-performance liquid chromatography-mass spectrometry as a sensitive and powerful technology in lipidomic applications, Chem Biol Interact. 220 (2014) 181-192.

[38] J. Folch, M. Lees, G.H. Sloane-Stanley, A simple method for the isolation and purification of total lipids from animal tissues, J Biol Chem. 226 (1957) 497-509.

[39] R.A. Moreau, J.K. Winkler-Moser, (2012). Extraction and analysis of food lipids. *Methods of Analysis of Food Components and Additives,* pp. 115-134. New York: CRC Press.

[40] E.G. Bligh, W.J. Dyer, A rapid method of total lipid extraction and purification, Can J Biochem Physiol. 37 (1959) 911-917.

[41] J.D. EbeIer, SPE methodologies for the separation of lipids, Lipids. 8 (1996) 1094-1103.

[42] E. Bravi, P. Benedetti, O. Marconi, G. Perretti, Determination of free fatty acids in beer wort, Food Chem. 151 (2014) 374-378.

[43] F.J. Eller, J.W. King, Determination of fat content in foods by analytical SFE, Seminars in food analysis. 1 (1996) 145-165.

[44] S. Armenta, S. Garrigues, M. de la Guardia, The role of green extraction techniques in Green Analytical Chemistry, Trends Anal Chem. 71 (2015) 2-8.

[45] A. Zgoła-Grześkowiak, T. Grześkowiak, Dispersive liquid-liquid microextraction, Trends Anal Chem. 30 (2011) 1382-1399.

[46] H. Zhang, C. Wolf-Hall, C. Hall, Modified microwave-assisted extraction of ergosterol for measuring fungal biomass in grain cultures, J Agric Food Chem. 56 (2008) 11077-11080.

[47] A.H. Metherel, A.Y. Taha, H. Izadi, K.D. Stark, The application of ultrasound energy to increase lipid extraction throughput of solid matrix samples (flaxseed), Prostaglandins Leukot Essent Fatty Acids. 81 (2009) 417-423.

[48] C. Dejoye, M.A. Vian, G. Lumia, C. Bouscarle, F. Charton, F. Chemat, Combined extraction processes of lipid from Chlorella vulgaris microalgae: microwave prior to supercritical carbon dioxide extraction, Int J Mol Sci. 12 (2011) 9332-9341.

[49] J.G. McDonald, P.T. Ivanova, H.A. Brown, (2015). Approaches to lipid analysis. *Biochemistry of Lipids, Lipoproteins and Membranes*, pp. 41-71. Amsterdam: Elsevier.

[50] J.J. Myher, A. Kuksis, General strategies in chromatographic analysis of lipids, J Chromatogr B. 671 (1995) 3-33.

[51] M. Buchgraber, F. Ulberth, H. Emons, E. Anklam, Triacylglycerol profiling by using chromatographic techniques, Eur J Lipid Sci Technol. 106 (2004) 621-648.

[52] A.J. Alpert, Hydrophilic-interaction chromatography for the separation of peptides, nucleic acids and other polar compounds, J Chromatogr A. 499 (1990) 177-196.

[53] Y. Guo, S. Gaiki, Retention and selectivity of stationary phases for hydrophilic interaction chromatography, J Chromatogr A. 35 (2011) 5920-5938.

[54] J.M. Curtis, S. Mi, (2015). Hydrophilic interaction liquid chromatography for determination of betaine. *Betaine: Chemistry, Analysis, Function and Effects*, pp. 139-158. Royal Society of Chemistry (Great Britain).

[55] Y.Y. Zhao, Y. Xiong, J.M. Curtis, Measurement of phospholipids by hydrophilic interaction liquid chromatography coupled to tandem mass spectrometry: The determination of choline containing compounds in foods, J Chromatogr A. 1218 (2011) 5470-5479.

[56] V. Verardo, A.M. Gómez-Caravaca, C. Montealegre, A. Segura-Carretero, M.F. Caboni, A. Fernández-Gutiérrez, A. Bendini, Optimization of a solid phase extraction method and hydrophilic interaction liquid chromatography coupled to mass spectrometry for the determination of phospholipids in virgin olive oil, Food Res Int. 54 (2013) 2083-2090.

[57] W.J. Griffiths, Y. Wang, Mass spectrometry: from proteomics to metabolomics and lipidomics, Chem Soc Rev. 38 (2009) 1882-1896.

[58] F.J. Senorans, E. Ibanez, Analysis of fatty acids in foods by supercritical fluid chromatography, Anal Chim Acta. 465 (2002) 131-144.

[59] C. Turner, J.W. King, L. Mathiasson, Supercritical fluid extraction and chromatography for fat-soluble vitamin analysis, J Chromatogr A. 936 (2001) 215-237.

[60] S.M. Momchilova, B.M. Nikolova-Damyanova, Advances in silver ion chromatography for the analysis of fatty acids and triacylglycerols-2001 to 2011, Anal Sci. 28 (2012) 837-844.

[61] C. Sun, B.A. Black, Y.Y. Zhao, M.G. Gänzle, J.M. Curtis, Identification of conjugated linoleic acid (CLA) isomers by silver ion-liquid chromatography/in-line ozonolysis/mass spectrometry (Ag^+-LC/O_3-MS), Anal Chem. 85 (2013) 7345-7352.

[62] A. Kaufmann, Combining UHPLC and high-resolution MS: A viable approach for the analysis of complex samples, Trends Anal. Chem. 63 (2014) 113-128.

[63] M. Lísa, K. Netušilová, L. Franěk, H. Dvořáková, V. Vrkoslav, M. Holčapek, Characterization of fatty acid and triacylglycerol composition in animal fats using silver-ion and non-aqueous reversed-phase high-performance liquid chromatography/mass spectrometry and gas chromatography/flame ionization detection, J Chromatogr A. 1218 (2011) 7499-7510.

[64] B. Tang, K.H. Row, Development of gas chromatography analysis of fatty acids in marine organisms, J Chromatogr Sci. 51 (2013) 599-607.

[65] Q. Gu, F. David, F. Lynen, P. Vanormelingen, W. Vyverman, K. Rumpel, G. Xu, P. Sandra, Evaluation of ionic liquid stationary phases for one dimensional gas chromatography–mass spectrometry and comprehensive two dimensional gas chromatographic analyses of fatty acids in marine biota, J Chromatogr A. 1218 (2011) 3056-3063.

[66] Y. Hirata, I. Sogabe, Separation of fatty acid methyl esters by comprehensive two-dimensional supercritical fluid chromatography with packed columns and programming of sampling duration, Anal Bioanal Chem. 378 (2004) 1999-2003.

[67] R. Esche, B. Scholz, K.H. Engel, Online LC–GC analysis of free sterols/stanols and intact steryl/stanyl esters in cereals, J Agric Food Chem. 61 (2013) 10932-10939.

[68] R.M. Toledano, J.M. Cortés, Á. Rubio-Moraga, J. Villén, A. Vázquez, Analysis of free and esterified sterols in edible oils by online reversed phase liquid chromatography-gas chromatography (RPLC-GC) using the through oven transfer adsorption desorption (TOTAD) interface, Food Chem. 135 (2012) 610-615.

[69] R.M. Toledano, J.M. Cortés, J.C. Andini, A. Vázquez, J. Villén, On-line derivatization with on-line coupled normal phase liquid chromatography-gas chromatography using the through oven

transfer adsorption desorption interface: Application to the analysis of total sterols in edible oils, J Chromatogr A. 1256 (2012) 191-196.

[70] C. Sun, Y.Y. Zhao, J.M. Curtis, Elucidation of phosphatidylcholine isomers using two dimensional liquid chromatography coupled in-line with ozonolysis mass spectrometry, J Chromatogr A. 1351 (2014) 37-45.

[71] J. Vongsvivut, M.R. Miller, D. McNaughton, P. Heraud, C.J. Barrow, Rapid discrimination and determination of polyunsaturated fatty acid composition in marine oils by FTIR spectroscopy and multivariate data analysis, Food Bioprocess Tech. 7 (2014) 2410-2422.

[72] R. Miglio, S. Palmery, M. Salvalaggio, L. Carnelli, F. Capuano, R. Borrelli, Microalgae triacylglycerols content by FT-IR spectroscopy, J Appl Phycol. 25 (2013) 1621-1631.

[73] X. Meng, Q. Ye, Q. Pan, Y. Ding, M. Wei, Y. Liu, F.R. van de Voort, Total phospholipids in edible oils by in-vial solvent extraction coupled with FTIR analysis, J Agric Food Chem. 62 (2014) 3101-3107.

[74] M. Janssens, G.S. Gooris, J.A. Bouwstra, Infrared spectroscopy studies of mixtures prepared with synthetic ceramides varying in head group architecture: coexistence of liquid and crystalline phases, Biochim Biophys Acta. 1788 (2009) 732-742.

[75] T.M. Greve, K.B. Andersen, O.F. Nielsen, A. Engdahl, FTIR imaging and ATR-FT-Far-IR synchrotron spectroscopy of pig ear skin, J Spectrosc. 24 (2010) 105-111.

[76] E. Mandak, D. Zhu, T.A. Godany, L. Nyström, Fourier transform infrared spectroscopy and Raman spectroscopy as tools for identification of steryl ferulates, J Agric Food Chem. 61 (2013) 2446-2452.

[77] E. Rozema, R. Popescu, H. Sonderegger, C.W. Huck, J. Winkler, G. Krupitza, E. Urban, B. Kopp, Characterization of glucocerebrosides and the active metabolite 4, 8-sphingadienine from arisaema amurense and pinellia ternata by NMR and CD spectroscopy and ESI-MS/CID-MS, J Agric Food Chem. 60 (2012) 7204-7210.

[78] S. Kaffarnik, I. Ehlers, G. Gröbner, J. Schleucher, W. Vetter, Two-dimensional 31P, 1H NMR spectroscopic profiling of phospholipids in cheese and fish, J Agric Food Chem. 61 (2013) 7061-7069.

[79] J. Sýkora, P. Bernášek, M. Zarevúcká, M. Kurfürst, H. Sovová, J. Schraml, High-performance liquid chromatography with nuclear magnetic resonance detection-A method for quantification of α-and γ-linolenic acids in their mixtures with free fatty acids, J Chromatogr A. 1139 (2007) 152-155.

[80] H. Wu, J.V. Volponi, A.E. Oliver, A.N. Parikh, B.A. Simmons, S. Singh, In vivo lipidomics using single-cell Raman spectroscopy, Proc Natl Acad Sci. 108 (2011) 3809-3814.

[81] E. Sosińska, R. Przybylski, F. Aladedunye, P. Hazendonk, Spectroscopic characterisation of dimeric oxidation products of phytosterols, Food Chem. 151 (2014) 404-414.

[82] B. Fong, L. Ma, C. Norris, Analysis of phospholipids in infant formulas using high performance liquid chromatography-tandem mass spectrometry, J Agric Food Chem. 61 (2013) 858-865.

[83] A.M. Porcari, G.D. Fernandes, K.R.A. Belaz, N.V. Schwab, V.G. Santos, R.M. Alberici, V.A. Gromova, M.N. Eberlin, A.T. Lebedev, A. Tata, High throughput MS techniques for caviar lipidomics, Anal Methods. 6 (2014) 2436-2443.

[84] X. Han, K. Yang, R.W. Gross, Multi-dimensional mass spectrometry-based shotgun lipidomics and novel strategies for lipidomic analyses, Mass Spectrom Rev. 31 (2012) 134-178.

[85] A. Carrasco-Pancorbo, N. Navas-Iglesias, L. Cuadros-Rodriguez, From lipid analysis towards lipidomics, a new challenge for the analytical chemistry of the 21st century. Part I: Modern lipid analysis, Trends Anal Chem. 28 (2009) 263-278.

[86] M. Ståhlman, C.S. Ejsing, K. Tarasov, J. Perman, J. Borén, K. Ekroos, High-throughput shotgun lipidomics by quadrupole time-of-flight mass spectrometry, J Chromatogr B. 877 (2009) 2664-2672.

[87] K. Schuhmann, R. Almeida, M. Baumert, R. Herzog, S.R. Bornstein, A. Shevchenko, Shotgun lipidomics on a LTQ Orbitrap mass spectrometer by successive switching between acquisition polarity modes, J Mass Spectrom. 47 (2012) 96-104.

[88] K. Yang, H. Cheng, R.W. Gross, X. Han, Automated lipid identification and quantification by multidimensional mass spectrometry-based shotgun lipidomics, Anal Chem. 81 (2009) 4356-4368.

[89] X. Han, R.W. Gross, Shotgun lipidomics: multidimensional MS analysis of cellular lipidomes, Expert Rev Proteomics. 2 (2005) 253-264.

[90] X. Han, Multi-dimensional mass spectrometry-based shotgun lipidomics and the altered lipids at the mild cognitive impairment stage of Alzheimer's disease, Biochim Biophys Acta. 1801 (2010) 774-783.

[91] N. Zehethofer, D.M. Pinto, Recent developments in tandem mass spectrometry for lipidomic analysis, Anal Chim Acta. 627 (2008) 62-70.

[92] W.C. Byrdwell, Quadruple parallel mass spectrometry for analysis of vitamin D and triacylglycerols in a dietary supplement, J Chromatogr A. 1320 (2013) 48-65.

[93] S.J. Blanksby, T.W. Mitchell, Advances in mass spectrometry for lipidomics, Annu Rev Anal Chem. 3 (2010) 433-465.

[94] R. Cozzolino, B. De Giulio, Application of ESI and MALDI-TOF MS for triacylglycerols analysis in edible oils, Eur J Lipid Sci Tech. 113 (2011) 160-167.

[95] C. Montealegre, V. Verardo, M. Luisa Marina, M.F. Caboni, Analysis of glycerophospho-and sphingolipids by CE, Electrophoresis. 35 (2014) 779-792.

[96] S. Flor, S. Lucangioli, M. Contin, V. Tripodi, Simultaneous determination of nine endogenous steroids in human urine by polymeric-mixed micelle capillary electrophoresis, Electrophoresis. 31 (2010) 3305-3313.

[97] C. Montealegre, L. Sanchez-Hernandez, A.L. Crego, M.L. Marina, Determination and characterization of glycerophospholipids in olive fruit and oil by nonaqueous capillary electrophoresis with electrospray-mass spectrometric detection, J Agric Food Chem. 61 (2013) 1823-1832.

[98] M.J. Lerma-García, M. Vergara-Barberán, J.M. Herrero-Martínez, E.F. Simó-Alfonso, Acrylate ester-based monolithic columns for capillary electro chromatography separation of triacylglycerols in vegetable oils, J Chromatogr A. 1218 (2011) 7528-7533.

[99] P.J. Crick, X.L. Guan, Lipid metabolism in mycobacteria-Insights using mass spectrometry-based lipidomics, Biochim Biophys Acta. 1861 (2016) 60-67.

[100] K. Yang, X. Han, Accurate quantification of lipid species by electrospray ionization mass spectrometry-meets a key challenge in lipidomics, Metabolites, 1 (2011) 21-40.

[101] M. Wang, C. Wang, X. Han, Selection of internal standards for accurate quantification of complex lipid species in biological extracts by electrospray ionization mass spectrometry-What, how and why?, Mass Spectrom. Rev. 9999 (2016) 1-22.

[102] M.J. Monte, J.J. Marin, A. Antelo, J. Vazquez-Tato, Bile acids: chemistry, physiology, and pathophysiology, World J Gastroenterol. 15 (2009) 804-816.

[103] J. Sjövall, Fifty years with bile acids and steroids in health and disease, Lipids. 39 (2004) 703-722.

[104] I. Bobeldijk, M. Hekman, J. de Vries-van der Weij, L. Coulier, R. Ramaker, R. Kleemann, T. Kooistra, C. Rubingh, A. Freidig, E. Verheij, Quantitative profiling of bile acids in biofluids and tissues based on accurate mass high resolution LC-FT-MS: compound class targeting in a metabolomics workflow, J Chromatogr B. 871 (2008) 306-313.

[105] Y. Alnouti, I.L. Csanaky, C.D. Klaassen, Quantitative-profiling of bile acids and their conjugates in mouse liver, bile, plasma, and urine using LC-MS/MS, J Chromatogr B. 873 (2008) 209-217.

[106] P. Shahid, M. Diane, T. Beatriz, M.Y. Ibrahim, Rapid and improved method for the determination of bile acids in human feces using MS, Lipids. 37 (2002) 1093-1100.

[107] R.S. Kirti, Review on bile acid analysis, Int J Pharm Biomed Sci. 3 (2012) 28-34.

[108] D.W. Lim, P.W. Wales, S. Mi, J.Y. Yap, J.M. Curtis, D.R. Mager, V.C. Mazurak, P.R. Wizzard, D.L. Sigalet, J.M. Turner, Glucagon-like peptide-2 alters bile acid metabolism in parenteral nutrition-associated liver disease, J Parenter Enteral Nutr. 40 (2016) 22-35.

[109] B.S. Kumar, B.C. Chung, Y.J. Lee, H.J. Yi, B.H. Lee, B.H. Jung, Gas chromatography–mass spectrometry-based simultaneous quantitative analytical method for urinary oxysterols and bile acids in rats, Anal Biochem. 408 (2011) 242-252.

[110] X. Qiao, M. Ye, C. Xiang, T. Bo, W. Yang, C. Liu, W. Miao, D. Guo, Metabolic regulatory effects of licorice: a bile acid metabonomic study by liquid chromatography coupled with tandem mass spectrometry, Steroids. 77 (2012) 745-755.

[111] E.J. Want, M. Coen, P. Masson, H.C. Keun, J.T. Pearce, M.D. Reily, D.G. Robertson, C.M. Rohde, E. Holmes, J.C. Lindon, R.S. Plumb, J.K. Nicholson, Ultra performance liquid chromatography mass spectrometry profiling of bile acid metabolites in biofluids: application to experimental toxicology studies, Anal Chem. 82 (2010) 5282-5289.

[112] K. Taguchi, E. Fukusaki, T. Bamba, Simultaneous and rapid analysis of bile acids including conjugates by supercritical fluid chromatography coupled to tandem mass spectrometry, J Chromatogr A. 1299 (2013) 103-109.

[113] Z. Hu, L. He, J. Zhang, G. Luo, Determination of three bile acids in artificial Calculus bovis and its medicinal preparations by micellar electrokinetic capillary electrophoresis, J Chromatogr B. 837 (2006) 11-17.

[114] C.A. Bloch, J.B. Watkins, Determination of conjugated bile acids in human bile and duodenal fluid by reverse-phase high performance liquid chromatography, J Lipid Res. 19 (1978) 510-513.

[115] R.S. Plumb, P.D. Rainville, W.B. Potts, K.A. Johnson, E. Gika, I.D. Wilson, Application of ultra-performance liquid chromatography-mass spectrometry to profiling rat and dog bile, J Proteome Res. 8 (2009) 2495-2500.

[116] Y. Siow, A. Schurr, G.C. Vitale, Diabetes-induced bile acid composition changes in rat bile determined by high performance liquid chromatography, Life Sci. 49 (1991) 1301-1308.

[117] S. Perwaiz, B. Tuchweber, D. Mignault, T. Gilat, I.M. Yousef, Determination of bile acids in biological fluids by liquid chromatography-electrospray tandem mass spectrometry, J Lipid Res. 42 (2001) 114-119.

[118] D.W. Lim, P.W. Wales, J.K. Josephson, P.N. Nation, P.R. Wizzard, C.M. Sergi, C.J. Field, D.L. Sigalet, J.M. Turner, Glucagonlike peptide 2 improves cholestasis in parenteral nutrition-associated liver disease, J Parenter Enteral Nutr. 40 (2014) 14-21.

[119] E.R. Badman, R.L. Beardsley, Z. Liang, S. Bansal, Accelerating high quality bioanalytical LC/MS/MS assays using fused core columns, J Chromatogr B. 878 (2010) 2307-2313.

[120] M. Sergi, C. Montesano, S. Napoletano, D. Pizzoni, C. Manetti, F. Colistro, R. Curini, D. Compagnone, Analysis of bile acids profile in human serum by ultrafiltration clean-up and LC-MS/MS, Chromatographia. 75 (2012) 479-489.

[121] D. Haas, H. Gan-Schreier, C.D. Langhans, T. Rohrer, G. Engelmann, M. Heverin, D.W. Russell, P.T. Clayton, G.F. Hoffmann, J.G. Okun, Differential diagnosis in patients with suspected bile acid synthesis defects, World J Gastroenterol. 18 (2012) 1067-1076.

[122] V.E. Hubert, M. Schmelz, M.N. Nikolova-Karakashian, D.L. Dillehay, D.V. Lynch, A.H. Merrill Jr., Sphingolipids in food and the emerging importance of sphingolipids to nutrition, J Nutr. 129 (1999) 1239-1250.

[123] H. Farwanah, T. Kolter, K. Sandhoff, Mass spectrometric analysis of neutral sphingolipids: Methods, applications, and limitations, Biochim. Biophys. Acta (BBA)-Mol. Cell Biol. Lipids. 1811 (2011) 854-860.

[124] Y.Y. Zhao, Y.P. Xiong, J.M. Curtis, Measurement of phospholipids by hydrophilic interaction liquid chromatography coupled to tandem mass spectrometry: The determination of choline containing compounds in foods, J Chromatogr A. 32 (2011) 5470-5479.

[125] J. Bernal, J.A. Mendiola, E. Ibáñez, A. Cifuentes, Advanced analysis of nutraceuticals, J. Pharm. Biomed. Anal. 55 (2011) 758-774.

[126] A. Uphoff, M. Hermansson, P. Haimi, P. Somerharju, Analysis of complex lipidomes, in: K. Vékey, A. Telekes, A. Vertes (Eds.), Medical Applications of Mass Spectrometry, Elsevier, Amsterdam, 2008, pp. 223-249.

[127] M.C. Sullards, Analysis of sphingomyelin, glucosylceramide, ceramide, sphingosine, and sphingosine 1-phosphate by tandem mass spectrometry, Meth. Enzymol. 312 (2000) 32-45.

[128] G. Vielhaber, S. Pfeiffer, L. Brade, B. Lindner, T. Goldmann, E. Vollmer, U. Hintze, K. Wittern, R. Wepf, Localization of ceramide and glucosylceramide in human epidermis by immunogold electron microscopy, J. Invest. Dermatol. 117 (2001) 1126-1136.

[129] M.M. Mielke, W. Maetzler, N.J. Haughey, V.V.R. Bandaru, R. Savica, C. Deuschle, T. Gasser, A.K. Hauser, S. Gräber-Sultan, E. Schleicher, D. Berg, I. Liepelt-Scarfone, Plasma

ceramide and glucosylceramide metabolism is altered in sporadic Parkinson's disease and associated with cognitive impairment: a pilot study, PLOS ONE. 8 (2013) e73094.

[130] E. Boslem, G. MacIntosh, A.M. Preston, C. Bartley, A.K. Busch, M. Fuller, D.R. Laybutt, P.J. Meikle, T.J. Biden, A lipidomic screen of palmitate-treated MIN6 β-cells links sphingolipid metabolites with endoplasmic reticulum (ER) stress and impaired protein trafficking, Biochem. J. 435 (2011) 267-276.

[131] T.B. Caligan, K. Peters, J. Ou, E. Wang, J. Saba, A.H. Merrill Jr, A high-performance liquid chromatographic method to measure sphingosine 1-phosphate and related compounds from sphingosine kinase assays and other biological samples, Anal Biochem. 281 (2000) 36-44.

[132] H. Farwanah, P. Nuhn, R. Neubert, K. Raith, Normal-phase liquid chromatographic separation of stratum corneum ceramides with detection by evaporative light scattering and atmospheric pressure chemical ionization mass spectrometry, Anal Chim Acta. 492 (2003) 233-239.

[133] R.L. Shaner, J.C. Allegood, H. Park, E. Wang, S. Kelly, C.A. Haynes, M.C. Sullards, A.H. Merrill Jr, Quantitative analysis of sphingolipids for lipidomics using triple quadrupole and quadrupole linear ion trap mass spectrometers, J Lipid Res. 50 (2009) 1692-1707.

[134] C.A. Haynes, J.C. Allegood, H. Park, M.C. Sullards, Sphingolipidomics: Methods for the comprehensive analysis of sphingolipids, J Chromatogr B. 877 (2009) 2696-2708.

[135] J.W. Lee, S. Nishiumi, M. Yoshida, E. Fukusaki, T. Bamba, Simultaneous profiling of polar lipids by supercritical fluid chromatography/tandem mass spectrometry with methylation, J Chromatogr A. 1279 (2013) 98-107.

[136] M. Scherer, K. Leuthäuser-Jaschinski, J. Ecker, G. Schmitz, G. Liebisch, A rapid and quantitative LC-MS/MS method to profile sphingolipids, J Lipid Res. 51 (2010) 2001-2011.

[137] R.F. Dielschneider, H. Eisenstat, S. Mi, J.M. Curtis, W. Xiao, J.B. Johnston, S.B. Gibson, Lysotropic agents selectively target chronic lymphocytic Leukemia cells due to altered sphingolipid metabolism, Leukemia. 30 (2016) 1290-1300.

[138] H. Shimoda, S. Terazawa, S. Hitoe, J. Tanaka, S. Nakamura, H. Matsuda, M. Yoshikawa, Changes in ceramides and glucosylceramides in mouse skin and human epidermal equivalents by rice-derived glucosylceramide, J Med Food. 15 (2012) 1064-1072.

[139] E.R. Badman, R.L. Beardsley, Z. Liang, S. Bansal, Accelerating high quality bioanalytical LC/MS/MS assays using fused-core columns, J Chromatogr B. 878 (2010) 2307-2313.

[140] M.C. Sullards, Y. Liu, Y. Chen, A.H. Merrill Jr, Analysis of mammalian sphingolipids by liquid chromatography tandem mass spectrometry (LC-MS/MS) and tissue imaging mass spectrometry (TIMS), Biochimica et Biophysica Acta. 1811 (2011) 838-853.

[141] C. Bode, M.H. Gräler, Quantification of sphingosine-1-phosphate and related sphingolipids by liquid chromatography coupled to tandem mass spectrometry, Methods Mol Biol. 874 (2012) 33-44.

[142] I.D. Lidbury, J.C. Murrell, Y. Chen, Trimethylamine and trimethylamine *N*-oxide are supplementary energy sources for a marine heterotrophic bacterium: implications for marine carbon and nitrogen cycling, ISME J. 9 (2015) 760-769.

[143] B.J. Bennett, T.Q.deA. Vallim, Z. Wang, D. Shih, Y. Meng, J. Gregory, H. Allayee, R. Lee, M. Graham, R. Crooke, P. Edwards, S. Hazen, A. Lusis, Trimethylamine-N-oxide, a metabolite associated with atherosclerosis, exhibits complex genetic and dietary regulation, Cell Metab. 17 (2013) 49-60.

[144] A.Q. Zhang, S.C. Mitchell, R.L. Smith, Dietary precursors of trimethylamine in man: A pilot study, Food Chem. Toxicol. 37 (1999) 515-520.

[145] Y. Kim, K. Kim, An accurate and reliable analysis of trimethylamine using thermal desorption and gas chromatography–time of flight mass spectrometry, Anal Chim Acta. 780 (2013) 46-54.

[146] Y. Chien, S. Uang, C. Kuo, T. Shih, J. Jen, Analytical method for monitoring airborne trimethylamine using solid phase micro-extraction and gas chromatography-flame ionization detection, Anal Chim Acta. 419 (2000) 73-79.

[147] C. Cháfer-Pericás, P. Campíns-Falcó, R. Herráez-Hernández, Comparative study of the determination of trimethylamine in water and air by combining liquid chromatography and solid-phase microextraction with on-fiber derivatization, Talanta. 69 (2006) 716-723.

[148] C. Cháfer-Pericás, R. Herráez-Hernández, P. Campíns-Falcó, Liquid chromatographic determination of trimethylamine in water, J Chromatogr A. 1023 (2004) 27-31.

[149] G.A. Mills, V. Walker, H. Mughal, Quantitative determination of trimethylamine in urine by solid-phase microextraction and gas chromatography–mass spectrometry, J Chromatogr B. 723 (1999) 281-285.

[150] Z. Wang, B.S. Levison, J.E. Hazen, L. Donahue, X. Li, S.L. Hazen, Measurement of trimethylamine-N-oxide by stable isotope dilution liquid chromatography tandem mass spectrometry, Anal Biochem. 455 (2014) 35-40.

[151] C.C. Lenky, C.J. McEntyre, M. Lever, Measurement of marine osmolytes in mammalian serum by liquid chromatography–tandem mass spectrometry, Anal Biochem. 420 (2012) 7-12.

[152] D. W. Johnson, A flow injection electrospray ionization tandem mass spectrometric method for the simultaneous measurement of trimethylamine and trimethylamine *N*-oxide in urine, J. Mass Spectrom. 43 (2008) 495-499.

[153] O.A. Mamer, L. Choinière, A. Lesimple, Measurement of urinary trimethylamine and trimethylamime oxide by direct infusion electrospray quadrupole time-of-flight mass spectrometry, Anal Biochem. 406 (2010) 80-82.

[154] H. Yamazaki, M. Fujieda, M. Togashi, T. Saito, G. Preti, J.R. Cashman, T. Kamataki, Effects of the dietary supplements, activated charcoal and copper chlorophyllin, on urinary excretion of trimethylamine in Japanese trimethylaminuria patients, Life Sci. 74 (2004) 2739-2747.

[155] S.H. Zeisel, K.A. daCosta, M. Youssef, S. Hensey, Conversion of dietary choline to trimethylamine and dimethylamine in rats: dose-response relationship, J Nutr. 119 (1989) 800-804.

[156] K.A. daCosta, J.J. Vrbanac, S.H. Zeisel, The measurement of dimethylamine, trimethylamine, and trimethylamine *N*-oxide using capillary gas chromatography-mass spectrometry, Anal Biochem. 187 (1990) 234-239.

[157] M.A. Iqbal, J.E. Szulejko, K.H. Kim, Determination of methylamine, dimethylamine, and trimethylamine in air by high-performance liquid chromatography with derivatization using 9-fluorenylmethylchloroformate, Anal. Methods. 6 (2014) 5697-5707.

[158] J.M. Curtis, S. Mi, Hydrophilic interaction liquid chromatography for determination of betaine, in: Victor R. Preedy (Ed.), Food and Nutritional Components in Focus, RSC publishing, London, 2015, pp. 139-158.

[159] X. Zhao, S.H. Zeisel, S. Zhang, Rapid LC-MRM-MS assay for simultaneous quantification of choline, betaine, trimethylamine, trimethylamine *N*-oxide, and creatinine in human plasma and urine, Electrophoresis. 36 (2015) 2207-2214.

[160] Z. Wang, E. Klipfell, B.J. Bennett, R. Koeth, B.S. Levison, B. DuGar, A.E. Feldstein, E.B. Britt, X. Fu, Y.M. Chung, Y. Wu, P. Schauer, J.D. Smith, H. Allayee, W.H.W. Tang, J.A. DiDonato, A.J. Lusis, S.L. Hazen, Gut flora metabolism of phosphatidylcholine promotes cardiovascular disease, Nature. 472 (2011) 57-63.

[161] Y. Cao, H. Gao, J.N. Chen, Z.Y. Chen, L. Yang, Identification and characterization of conjugated linolenic acid isomers by Ag^{+}-HPLC and NMR, J Agric Food Chem. 54 (2006) 9004-9009.

[162] G.F. Yuan, X.E. Chen, D. Li, Conjugated linolenic acids and their bioactivities: a review, Food Funct. 5 (2014) 1360-1368.

[163] A.A. Hennessy, R.P. Ross, R. Devery, C. Stanton, The health promoting properties of the conjugated isomers of α-linolenic acid, Lipids. 46 (2011) 105-119.

[164] L. Gorissen, F. Leroy, L. De Vuyst, S. De Smet, K. Raes, Bacterial production of conjugated linoleic and linolenic acid in foods: a technological challenge, Crit Rev Food Sci Nutr. 55 (2015) 1561-1574.

[165] Y. Yasui, M. Hosokawa, T. Sahara, R. Suzuki, S. Ohgiya, H. Kohno, T. Tanaka, K. Miyashita, Bitter gourd seed fatty acid rich in 9*c*,11*t*,13*t*-conjugated linolenic acid induces apoptosis and up-regulates the GADD45, p53 and PPARγ in human colon cancer Caco-2 cells, Prostaglandins Leukot Essent Fatty Acids. 73 (2005) 113-119.

[166] H. Kohno, R. Suzuki, Y. Yasui, M. Hosokawa, K. Miyashita, T. Tanaka, Pomegranate seed oil rich in conjugated linolenic acid suppresses chemically induced colon carcinogenesis in rats, Cancer Sci. 95 (2004) 481-486.

[167] C. Zou, H. Shi, X. Liu, Y. Sheng, T. Ding, J. Yan, B. Gao, J. Liu, W. Lu, L. Yu, Conjugated linolenic acids and nutraceutical components in Jiaogulan (*Gynostemma pentaphyllum*) seeds, LWT-Food Sci Technol. 68 (2016) 111-118.

[168] S.S. Saha, M. Ghosh, Protective effect of conjugated linolenic acid isomers present in vegetable oils against arsenite-induced renal toxicity in rat model, Nutrition. 29 (2013) 903-910.

[169] S. Özgül-Yücel, Determination of conjugated linolenic acid content of selected oil seeds grown in Turkey, J Am Oil Chem. Soc. 82 (2005) 893-897.

[170] I.A.T.M. Meerts, C.M. Verspeek-Rip, C.A.F. Buskens, H.G. Keizer, J. Bassaganya-Riera, Z.E. Jouni, A.H.B.M. van Huygevoort, F.M. van Otterdijk, E.J. van de Waart, Toxicological evaluation of pomegranate seed oil, Food Chem Toxicol. 47 (2009) 1085-1092.

[171] R. Suzuki, S. Arato, R. Noguchi, K. Miyashita, O. Tachikawa, Occurrence of conjugated linolenic acid in flesh and seed of bitter gourd. J Oleo Sci. 50 (2001) 753-758.

[172] F. Alcaraz-Mármol, N. Nuncio-Jáuregui, Á. Calín-Sánchez, Á.A. Carbonell-Barrachina, J.J. Martínez, F. Hernández, Determination of fatty acid composition in arils of 20 pomegranates cultivars grown in Spain, Sci Hort. 197 (2015) 712-718.

[173] Y. Cao, L. Yang, H.L. Gao, J.N. Chen, Z.Y. Chen, Q.S. Ren, Re-characterization of three conjugated linolenic acid isomers by GC-MS and NMR. Chem Phys Lipids. 145 (2007) 128-133.

[174] M. Plourde, F. Destaillats, P.Y. Chouinard, P. Angers, Conjugated α-linolenic acid isomers in bovine milk and muscle, J Dairy Sci. 90 (2007) 5269-5275.

[175] L. Yang, Y. Cao, J.N. Chen, Z.Y. Chen, Oxidative stability of conjugated linolenic acids, J Agric Food Chem. 57 (2009) 4212-4217.

[176] C. Sun, J.M. Curtis, Locating double bonds in lipids-new approaches to the use of ozonolysis, Lipid Technol. 25 (2013) 279-282.

[177] C. Sun, B.A. Black, Y.Y. Zhao, M.G. Gänzle, J.M. Curtis, Identification of conjugated linoleic acid (CLA) isomers by silver ion-liquid chromatography/in-line ozonolysis/mass spectrometry (Ag^+-LC/O_3-MS), Anal Chem. 85 (2013) 7345-7352.

[178] C. Sun, Y.Y. Zhao, J.M. Curtis, Elucidation of phosphatidylcholine isomers using two dimensional liquid chromatography coupled in-line with ozonolysis mass spectrometry, J Chromatogr A. 1351(2014) 37-45.

[179] J. Chen, Y. Cao, H. Gao, L. Yang, Z.Y. Chen, Isomerization of conjugated linolenic acids during methylation, Chem Phys Lipids. 150 (2007) 136-142.

[180] B.A. Black, C. Sun, Y.Y. Zhao, M.G. Gänzle, J.M. Curtis, Antifungal lipids produced by lactobacilli and their structural identification by normal phase LC/atmospheric pressure photoionization-MS/MS. J Agric Food Chem. 61 (2013) 5338-5346.

[181] B. Nikolova-Damyanova, Retention of lipids in silver ion high-performance liquid chromatography: Facts and assumptions, J Chromatogr A. 1216 (2009) 1815-1824.

[182] R.G. Harfmann, S. Julka, H.J. Cortes, Instability of hexane-acetonitrile mobile phases used for the chromatographic analysis of triacylglycerides, J Sep Sci. 31 (2008) 6-7.

[183] S.J. Blanksby, T.W. Mitchell, Advances in mass spectrometry for lipidomics, Annu Rev Anal Chem. 3 (2010) 433-465.

[184] M. Bou Khalil, W. Hou, H. Zhou, F. Elisma, L.A. Swayne, A.P. Blanchard, Z. Yao, S.A. Bennett, D. Figeys, Lipidomics era: accomplishments and challenges, Mass Spectrom Rev. 29 (2010) 877-929.

[185] R.C. Murphy, S.J. Gaskell, New applications of mass spectrometry in lipid analysis, J Biol Chem. 286 (2011) 25427-25433.

[186] Q. Hu, R.J. Noll, H. Li, A. Makarov, M. Hardman, R. Graham Cooks, The Orbitrap: a new mass spectrometer, J Mass Spectrom. 40 (2005) 430-443.

[187] Y.Y. Zhao, Y.P. Xiong, J.M. Curtis, Measurement of phospholipids by hydrophilic interaction liquid chromatography coupled to tandem mass spectrometry: The determination of choline containing compounds in foods, J Chromatogr A. 1218 (2011) 5470-5479.

[188] C. Sun, J.M. Curtis, Locating double bonds in lipids-new approaches to the use of ozonolysis, Lipid Technol. 25 (2013) 279-282.

[189] C. Sun, B.A. Black, Y.Y. Zhao, M.G. Gänzle, J.M. Curtis, Identification of conjugated linoleic acid (CLA) isomers by silver ion-liquid chromatography/in-line ozonolysis/mass spectrometry (Ag^+-LC/O_3-MS), Analytical chemistry. 85 (2013) 7345-7352.

[190] C. Sun, Y.Y. Zhao, J.M. Curtis, Elucidation of phosphatidylcholine isomers using two dimensional liquid chromatography coupled in-line with ozonolysis mass spectrometry, J Chromatogr A. 1351 (2014) 37-45.

[191] A. Nicolaou, Lipidomics: What does the future hold?, Eur. J. Lipid Sci. Technol. 113 (2011) 537-538.

Appendix 1*

Hydrophilic Interaction Liquid Chromatography for Determination of Betaine

A1.1. Introduction

A1.1.1. Basics of HILIC

Hydrophilic interaction liquid chromatography (HILIC) was first introduced by Andrew Alpert in 1990. The HILIC method was originally proposed as an alternative to the more conventional normal-phase (NP) and reversed-phase (RP) LC methods to separate extremely polar and hydrophilic compounds [1]. Since its development, HILIC has been widely used in many research fields including food, environmental, pharmaceutical and clinical analyses [2, 3, 4, 5, 6]. Through these applications, HILIC has been shown to be a valuable separation method for the analysis of both polar and ionic compounds [7].

A typical HILIC system is usually comprised of a hydrophilic stationary phase and a binary mobile phase system (**Figure A1-1**). In comparison with the widely used RPLC techniques, HILIC has the advantage of providing high retention of highly hydrophilic and polar molecules but with less requirement for ion-pair reagents. The typical elution order is similar to that found in NPLC with the less polar compounds eluting ahead of the more polar ones.

* This appendix has been published as J.M. Curtis, S. Mi, "Hydrophilic Interaction Liquid Chromatography for Determination of Betaine" (Chapter 10) in: Victor R. Preedy (Ed.), *Betaine: Chemistry, Analysis, Function and Effects*, RSC publishing, London, 2015, pp. 139-158. I was responsible for the literature review and manuscript composition.

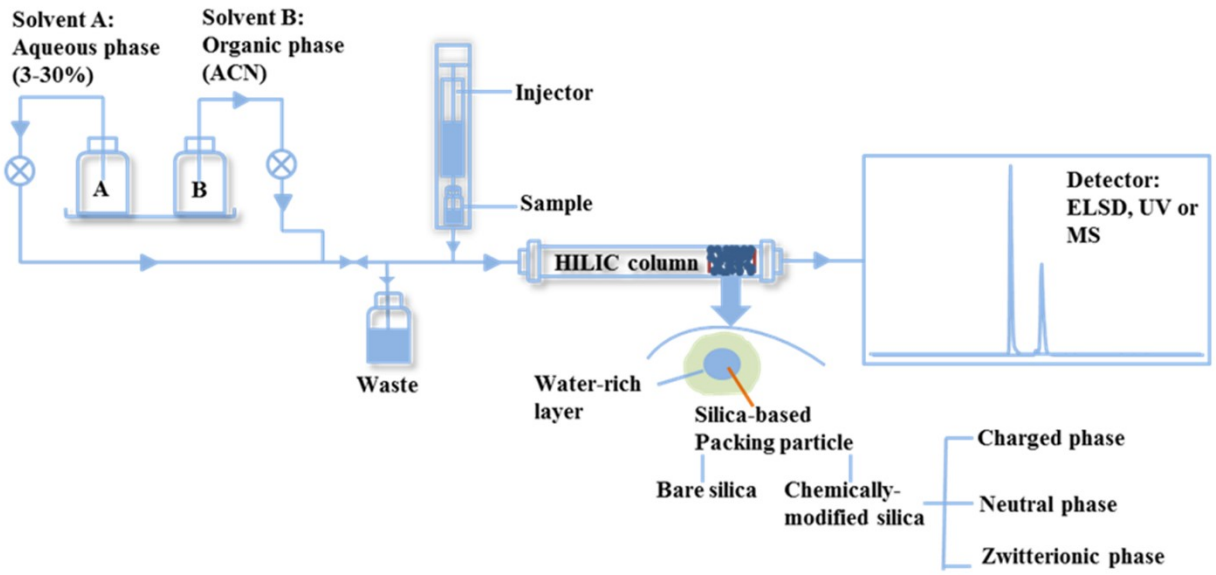

Figure A1-1. The HILIC chromatography apparatus. This figure shows the LC components used in HILIC separations. A binary system of water (solvent A) and ACN (solvent B) is mixed as indicated. The mobile phase and injected sample is passed into a HILIC column that is packed with the stationary-phase particles. Under HILIC conditions, a water-enriched layer forms around each particle as shown. This layer plays a crucial role in the HILIC separation.

A1.1.1.1. Separation Mechanisms of HILIC

Although HILIC chromatography has been developed and widely applied over several decades, the relevant mechanisms of separation are still not well clarified. Since the pattern of separation in HILIC mode may be a result of multiple types of interactions between the analyte and stationary phase, it can be influenced by many chromatographic conditions, such as the stationary phase type, the mobile phase composition and the structural properties of the target solutes [8]. There are two accepted retention mechanisms that are believed to operate under HILIC conditions.

First, as with RPLC, partition is considered to be one of the primary separation mechanisms in HILIC. This mechanism was proposed by Andrew Alpert who suggested that the retention on HILIC columns is based upon the partitioning of analytes between a water-enriched layer adsorbed

onto the surface of the hydrophilic stationary phase and the relatively less polar organic eluent [9]. In this model, the partially immobilized water-rich layer is formed via attractive interactions between the polar functional groups on the stationary phase and water molecules in the mobile phase. Thus, hydrophilic analytes carried in the mobile phase preferentially partition into the immobilized water-rich layer leading to strong retention on the column. This explains the elution order in HILIC since the less polar compounds elute from the column earlier than the more polar ones. However, it should be noted that there is a saturation limit for the amount of water that can be adsorbed on the surface of the stationary phase [8, 10]. Beyond this limit, excess water molecules would stay in the organic-enriched eluent, which makes the water-rich layer and the organic bulk phase more similar to each other. Consistent with this idea, Hemström and Irgum [11] discussed the results obtained by Orth and Engelhardt, which noted that the retention of solutes decreased along with the decrease of the difference in polarity between the two phases [10]. Therefore, there is a defined range of water content required for the HILIC mobile phase. A lower limit of 3% water is generally sufficient to guarantee the formation of a water layer around the stationary phase particles, whereas an upper limit of 30% water ensures that there is sufficient retention of polar solutes. The partition mechanism has been discussed extensively and is supported experimentally in many publications [8, 12, 13, 14].

However, some separation results in HILIC cannot be explained by the partition mechanism alone. For example, different retention properties of four HILIC stationary phases were observed for analysis of the same group of model compounds under identical chromatographic conditions [15]. This suggests that other retention mechanisms besides simple partitioning must also occur in HILIC. It was reported that the elution pattern of peptides achieved in HILIC was similar to that in NPLC [11]. The retention mechanism in NPLC is known to be controlled by surface adsorption

[16] and hence the adsorptive retention model may also play a role in HILIC separations. The adsorption mechanism requires direct contact or interaction between the analytes and the stationary phase [17]. These interactions have been investigated in many publications and mostly involve hydrogen bonding, electrostatic forces and dipole-dipole interactions [7, 11, 14, 16]. Notably, the adsorption mechanism usually involves multiple weak interactions between the analytes and the stationary phase, hence in some publications it is also referred to as a multimodal mechanism [14]. In some cases, the predominant separation mechanism may even vary during the separation process as chromatographic conditions change [17].

A1.1.1.2. Components of HILIC-Mobile and Stationary Phases

A1.1.1.2.1 Mobile Phases. In general, the mobile phase in HILIC chromatography is composed of a binary system of water with a higher percentage of a water-miscible polar organic solvent. Thus, compared with NPLC, the aqueous-organic mobile phase in HILIC provides greater solubility for the polar and hydrophilic analytes [12]. Importantly, the polar mobile phase makes HILIC highly compatible with the electrospray-mass spectrometry (ESI-MS) detection allowing for high ionization efficiency and sensitivity.

Acetonitrile (ACN) is commonly employed, being an aprotic organic solvent with low viscosity, so that separations can be optimized at low backpressures [8]. Other water-miscible solvents including methanol, ethanol, isopropanol (IPA) and tetrahydrofunan (THF) have also been utilized as components of the HILIC mobile phase. However, it is worth mentioning that alcohols are both protic and stronger eluting solvents than ACN [8, 18]. These characteristics may result in lower retention and decreased separation efficiency. Moreover, since THF is a better hydrogen-bond acceptor than ACN, its inclusion in place of ACN will result in competition with

water for the active sites on stationary phase. This will affect the formation of the immobilized water layer on the surface of stationary phase [19]. Hence, in general it is found that ACN is the preferred choice of organic modifier in HILIC mobile phase.

The aqueous phase, which may contain volatile salts or weak acids (e.g. ammonium acetate, ammonium formate, trifluoroacetic acid), is the stronger eluting solvent in the HILIC mobile phase [20, 21]. The salts or weak acids are added in low amounts to manipulate the separation [22] or the ionization efficiency for MS detection. Differences in both selectivity and retention due to choice of additive have been investigated in detail [7] and been shown to be important for optimizing HILIC separations.

A1.1.1.2.2 Stationary Phases. In recent years, a very large number of stationary phases have been employed in HILIC experiments. Generally, these can be divided into silica-based stationary phases and polymer-based stationary phases. Of these two kinds of stationary phases, silica-based columns are far more commonly used in HILIC, either bare silica columns or chemically modified silica columns with functionalities including amide, cyano, sulfobetaine and diol. Chemically modified silica columns can be divided into categories depending on the surface charge properties of the silica. Thus neutral phases carry no net charge over the pH range of the mobile phase used for HILIC as may be the case for amide, cyano, diol and cyclodextrin modified silica [1]. Phases carrying a net positive or negative charge over the mobile phase pH range for HILIC include the widely used amino phase [1]. Examples of zwitterionic phases used in HILIC separations include sulfobetaine phases and phosphocholine phases [1]. In addition, many other novel HILIC phases have been developed, such as those modified with polysaccharides [22].

A1.1.2. Summary and comparison to other analytical techniques used for analysis of betaine

Betaine is present in many samples of both plant and animal origins, as described elsewhere in this book. Consequently, a wide variety of analytical techniques have been developed for the measurement of betaine in various matrices.

RPLC is an efficient and widely used separation technique, but betaine is poorly retained due to its high polarity. The use of RPLC for betaine analysis in *Lycium chinense* was reported by Lee *et al.* [23]. In order to obtain sufficient retention, an ion-pairing reagent, in this case perfluoropentanoic acid (PFPA), was used. A disadvantage of this approach is that many ion-pairing reagents are not compatible with MS detection due to potential ion-suppression effects and/or possible ion-source contamination. NPLC separations have been discussed for betaine analysis [5] in the context of a method to analyze choline-containing compounds in food samples. The use of typical normal phase organic solvents is less desirable in a laboratory setting, less compatible with ESI-MS compared to RP-LC or HILIC mobile phases and not ideal for polar analytes such as betaine.

Ion chromatography (IC) with different detectors has been tested for betaine measurement. Multiple ion exchange columns were tested to separate betaine in feed ingredients [24]. However, good separation of betaine from other impurities present in the feed and subsequent quantification of betaine could only be achieved after the development of suitable extraction procedures and further clean-up using ion-exchange resins. The application of gas chromatography (GC) in betaine analysis requires the conversion of nonvolatile betaine into more volatile derivatives. For example, Hitz and Hanson [25] described the pyrolytic conversion of betaine from plants to trimethylamine (TMA), whereas Allen *et al.* [26] measured betaine in serum by enzymatically converting it to

dimethylglycine (DMG) including a stable isotope dilution procedure for quantification by GC/MS. The requirement for derivatization in GC analysis may increase the uncertainty in quantitative analysis. Capillary electrophoresis (CE) is another possible separation technique for betaine that has been used for quantification in plants [27] and in various seed oils [28]. Prior esterification of betaine was used to reduce interferences from other compounds and to provide a chromophore for UV detection.

The use of the HILIC method in betaine analysis may overcome many of the problems associated with the analytical methods described above. For example, the polar stationary phases employed can strongly retain betaine molecules without the need for ion-pairing reagents or derivatization. At the same time, the HILIC mobile phase is typically a mixture of water with a high content of ACN, which can solubilize betaine and is compatible with ESI-MS detection.

A1.2. The Use of HILIC in the Determination of Betaine Concentrations

A1.2.1. Betaine in standard mixtures

The analysis of a mixture of quaternary amine standards of biological and environmental importance (acetylcholine, choline, betaine, chlormequat and mepiquat) by HILIC/MS was described by Guo [29]. Two HILIC columns were compared for this separation, a YMC-Pack NH_2 (YMC Co.), containing aminopropyl groups attached to the silica surface and a TSKgel Amide-80 (Tosoh Bioscience), an amide phase containing amide groups bound to silica via a hydrocarbon chain. The effects of ACN content, column temperature, buffer salt type (ammonium acetate or formate) and its concentration on the retention behavior were investigated for both columns. Under most conditions betaine was more strongly retained on the amide column compared to the amino column. All five of the model compounds gave rise to peak tailing on the amide phase, which was

explained as a result of interactions between the positively charged amines and negatively charged surface silanols. Increasing the ACN content of the mobile phase gave rise to greater betaine retention. However, plots of ln k' (the capacity factor) against ACN content of betaine deviated from linearity indicating that secondary interactions contribute to retention in addition to HILIC mode. With the amino column, use of low concentrations of ammonium formate (~10 mM) resulted in better peak shapes than with similar concentrations of ammonium acetate in the mobile phase. Although betaine quantification was not described, under optimized HILIC conditions using the YMC-Pack NH_2 column and coupled with ESI-MS in SIM mode, the LOD for choline was 0.4 fmol (S/N=4). This is considerably lower than the LOD of 30 fmol previously reported for a RPLC-MS method [30]. This difference in sensitivity is attributed to avoiding the use of ion-pairing reagents and the use of higher levels of organic solvent in the mobile phase that is closer to optimal for ESI. The HILIC separation had a run time of less than 5 min and exhibited at least 2 orders of magnitude of linearity. Although this discussion of sensitivity refers to choline, it can be assumed that similar arguments would apply to betaine analysis.

A1.2.2. Betaine in samples of plant origin

Fructus Lycii is a commonly used traditional Chinese herbal medicine that is said to have many functional properties as a tonic including as an antioxidant and antitumor agent. Betaine is reported to be a major bioactive component and therefore quantitative determination of betaine is of importance in quality control of products derived from Fructus Lycii. Furthermore, both the Korean and Chinese Pharmacopoeia specify the required minimum betaine concentrations. Three HILIC-based methods for the quantification of betaine in Fructus Lycii have been reported [31, 32, 33].

APPENDIX 1

In 1999, Shin *et al.* extracted the dried Lycium *chinense* fruit samples at room temperature with methanol using sonication, followed by centrifugation [31]. The supernatant was dried under nitrogen and reconstituted with water. The final extract was then directly injected for HILIC analysis on a YMC NH_2-phase column (4.6 mm i.d.×250 mm, 5 μm in particle size) with an isocratic mobile phase composition of water and ACN (25:75, *v/v*) followed by both UV (210 nm) and ESI-MS detection in both selected ion monitoring (SIM) and full scan modes. Protonated molecular ions of betaine at *m/z* 118 were observed but no molecular species could be seen in negative-ion mode. Although the HILIC LC-UV trace was complex and the betaine peak not completely resolved, there were no apparent interferences seen for the betaine SIM trace at *m/z* 118. A linear betaine calibration curve was constructed over the 0.02 to 1 mg mL^{-1} range and used to demonstrate an LOD (S/N=3) of 0.2 ng ml^{-1} for ESI-MS (SIM) compared to 0.1 μg ml^{-1} by LC-UV. The HILIC LC-MS method was validated and showed acceptable levels of precision and accuracy. Levels of betaine in Lycium *chinense* fruits were found to lie at between 0.15 and 0.21%. In summary, the HILIC LC-MS (SIM) method described in this work is a simple and effective way of measuring the high betaine levels present in Fructus Lycii but may not be sufficiently specific for use in other cases where much lower concentrations of betaine are present.

A later publication by Shin *et al.* in 2012 also described a quantitative assay for betaine in Fructus Lycii but made use of evaporative light-scattering detection (ELSD) instead of MS [32]. Extraction was simply carried out by sonication in 70% methanol (25 °C, 40 min) followed by centrifugation, filtration and the addition of a solution of the internal standard stachydrine in methanol. Three HILIC columns were tested including a Phenomenex Kinetex HILIC (2.1 mm× 100 mm, 2.6 μm), a Waters Atlantis HILIC (3.0 mm×100 mm, 5 μm) and a HALO HILIC (2.1 mm×100 mm, 2.7 μm). The optimal separation was achieved using the Phenomenex Kinetex

HILIC column with a gradient elution of (A) ACN and (B) 10 mM ammonium formate (pH 3.0)/ACN (90/10, *v/v*). The gradient used was 15% B at 0-1 min, 25% B at 16 min and 40% B at 17 min. It is apparent from the chromatograms in the paper that a final hold to 35 min was used, although this was not specified in the experimental section of the paper. The ELSD was operated at an optimized temperature and nebulizing gas pressure of 50 °C and 3.0 bar. The method LOQ (S/N=10) and LOD (S/N=3) were 10 and 3 μg ml^{-1}, respectively. Hence, the HILIC LC-ELSD method is less sensitive than the HILIC LC-MS (SIM) method described by Shin *et al.* [31], but this is unimportant due to the high content of betaine in Fructus Lycii samples. Replacement of the more sophisticated and specific MS method by ELSD detection has the advantages of lower cost and simplicity. The HILIC LC-ELSD method achieved recoveries of greater than 96.5%, intra- and interday precision of less than 5.3% (n=5) and accuracy in the range of 94-107%. The validated HILIC LC-ELSD method was successfully applied to 14 Fructus Lycii samples (one originated from L. *barbarum* and 13 from L. *chinense*) that contained betaine at weight percentages of between ~0.5-1.0%.

The most recent HILIC-based method for betaine quantification in Fructus Lycii samples was published by Zhao *et al.* in 2013 [33]. In this case betaine was extracted directly into water containing the *β*-alanine internal standard. Water was said to give higher extraction amounts compared to 70% methanol or 50 or 70% ethanol, with 60 min sonication at room temperature in each case. Extraction into water was followed by filtration prior to analysis by HILIC LC-ELSD. Two HILIC columns were tested: Atlantis silica HILIC column 100 Å (4.6 mm×150 mm, 5 μm), and Phenomenex Luna HILIC column 200 Å (4.6 mm×150 mm, 5 μm). The elution was carried out under isocratic conditions with a mobile phase composition of 30 mM ammonium acetate buffer and ACN (20:80, *v/v*), at a flow rate of 1.0 mL min^{-1} for 30 min. For this particular separation,

the Atlantis HILIC column was selected since it was shown to have slightly better performance, including higher plate count and capacity factor. Using this simple isocratic HILIC LC-ELSD method an LOD (S/N=3) and LOQ (S/N=10) of 2 and 7 μg ml^{-1} were obtained, similar to the earlier study by Shin *et al.* [32]. However, this study had the advantage of an isocratic separation, thereby avoiding the need for column re-equilibration. Using this method, 92 Fructus Lycii samples (29 from L. *barbarum* L. and 63 from L. *chinense* Miller) with betaine weight percentages of ~0.6-0.8% were quantitatively analyzed. This simple and stable method was suggested to be used as an official analytical method for Fructus Lycii in the Korean Pharmacopoeia (K.P.) and the results used in specifying the content regulation of betaine for Lycii Fructus.

A1.2.3. Betaine in samples of animal origin

Betaine is present in a wide variety of animal tissues and fluids including plasma, urine and liver. Betaine is produced by the enzymatic oxidation of choline and acts as a methyl donor in the homocysteine-methionine reaction in the presence of betaine: homocysteine methyltransferase (BHMT). The quantification of betaine in tissues and other biological fluids has great significance in clinical studies. This requires a sensitive and specific method due to the low content of betaine in these highly complex matrices.

A method based on LC-MS/MS for the combined determination of free choline, betaine and dimethylglycine (DMG) in human EDTA plasma and serum was proposed by Holm *et al*. in 2003 [2]. The LC separation in this work was conducted on a normal-phase Hypersil silica column (100 mm×2.1 mm, 5 μm). The target analytes were eluted from the column at a flow rate of 0.6 mL min^{-1} with the mobile phase consisting of 15 mM ammonium formate (pH 3.5) and ACN, in gradient. Thus, the starting conditions (25% aqueous) could be considered HILIC conditions

although the rapid gradient to high aqueous content indicates normal phase separation. This allows for a short run time but with little or no separation between betaine and DMG. It is probable that a superior separation could be achieved purely in HILIC mode but at the expense of run time. MS detection was performed on a triple-quadrupole tandem mass spectrometer with an ESI interface operated in positive-ion mode. Human plasma and serum samples were treated with three volumes of ACN containing the stable isotopically labeled internal standards (d_9-choline and d_9-betaine), to precipitate protein. The samples were centrifuged and the supernatant was then directly used for analysis by LC-MS/MS. Betaine was quantified by multiple reaction monitoring (MRM) using the transition *m/z* 118 ($[M + H]^+$)→*m/z* 59 ($[M + H\text{-}CH_2COOH]^+$) and the corresponding transition for the d_9 labeled internal standard (*i.e. m/z* 127→*m/z* 68). Linearity was demonstrated by standard additions to dialyzed plasma over the range of concentrations 0.01-400 μmol L^{-1} with an LOD for betaine of 0.3 μmol L^{-1} (S/N=5). Similar results were obtained for the other two analytes. The method achieved recoveries and precision for betaine of 93-103% and <6%, respectively. This was claimed to be the first published method enabling the simultaneous analysis of three target compounds from a single preparation procedure. The method is suitable for large-scale clinical and epidemiologic studies due to the short analysis time of 6 min (including equilibration) and the simple extraction procedure that is amenable to robotic automation. The method was used to determine the choline, betaine and DMG levels in plasma and serum of 60 fasting and non-fasting donors. The betaine levels in the combined groups were found to be in the range of 27-47 μmol L^{-1} in plasma and 28-48 μmol L^{-1} in serum; thus plasma and serum betaine levels did not differ significantly.

To better understand choline metabolism, Kirsch *et al.* [4] described a stable-isotope dilution ultra performance liquid chromatography-mass spectrometry (UPLC-MS) method for the

determination of choline and related metabolites including betaine, DMG and acetylcholine (ACh). This allowed the presence of these compounds in EDTA plasma, urine, amniotic fluid (AF), and cerebrospinal fluid (CSF) to be measured. Sample pretreatment included protein precipitation by ACN for all samples proceeded by a 5-fold dilution with water in the case of urine samples due to the presence of a high concentration of biological salts. The chromatographic separation used an Acquity UPLC BEH HILIC column (100 mm×2.1 mm i.d., 1.7 µm) at 30 °C. A run time of only 6.5 min was used with a gradient of between 12.5% and 20% 15 mmol L^{-1} ammonium formate (pH 3.5) and the remainder ACN. Similar to the earlier method [2], positive-ion ESI-MS/MS in MRM mode was used for the quantification of the four target compounds and their corresponding stable-isotope labeled internal standards (d_9-ACh, d_9-choline, d_6-DMG and d_9-betaine). The LODs in this study ranged from 0.11 to 0.34 µmol L^{-1}, which was similar to that obtained by Holm *et al.* [2], but the range of tested materials and analytes was extended. Analysis of biological fluids in volumes of <100 µL was demonstrated, suggesting that the method is feasible both when sample size is a limitation (e.g. CSF) and for high-throughput analysis in clinical studies.

In 2010, a closely related UPLC-MS/MS method was reported by Bruce *et al.* [3] for the determination of betaine and free choline in plasma as well as in cereal and cereal-related products that are discussed in Section **A1.2.4**. In this work, the sample-preparation procedure was optimized based on previously reported methods [2, 34, 35]. For plasma samples, this involved protein precipitation and extraction into methanol (in place of ACN in other methods) followed by centrifugation. LC separation used a UHPLC HILIC column (2.1 mm×150 mm, 1.7 µm) with a mobile phase gradient of 10 mM ammonium acetate in water containing 0.005% acetic acid and ACN. However, since the gradient used was between 20% and 100% aqueous, this method is not strictly in HILIC mode. In fact, the LC eluent only flowed to the mass spectrometer at between 1

and 3.65 min at which points in time the aqueous content of the mobile phase was ~50% and 100%, respectively. Nevertheless, the published chromatograms do show separation between the choline and betaine analytes that each elute at around 2 min. The triple-quadrupole MS/MS system was operated in positive ESI in the MRM mode, monitoring the two transitions for each analyte (*m/z* 118→58, 59 for betaine and *m/z* 104→60, 58 for choline). Quantitative results were achieved by relying on the signal ratios between the analytes in the sample and the corresponding isotope-labeled standards (d_{11}-betaine and d_9-choline). This method was applied to the plasma of 47 subjects who were found to have average plasma levels of betaine of 40 μmol L^{-1}.

A1.2.4. Betaine in food samples

Interest in the analysis of betaine in foods has been increased considerably in the past few years because of the potential health benefits associated with betaine intake. Many types of food, such as eggs, milk, cheese, whole grains and yogurt, are known to be important sources of betaine [36] and in addition, betaine is produced via enzymatic oxidation of choline. A dietary deficiency of betaine might result in increased risk of diseases such as fatty liver disease and bone abnormalities [37]. Hence, the measurement of betaine and related compounds in food is important in order to track dietary intake.

In 1981, Vialle and Kolosky published a paper in which betaine in commercial refined sugar and wine was measured by refractive index detection using amino-bonded silica as the stationary phase and a mobile phase of ACN and water (75:25, *v/v*), as is customary for sugar analysis [38]. In this way, a mixture of betaine and several sugars was separated with betaine eluting first in the chromatogram ahead of the monosaccharides fructose and glucose. Before chromatographic separation, sample preparation was performed using two ion-exchange columns. Acidified

solutions of commercial refined sugar were passed through a cation-exchange resin to concentrate betaine, which was subsequently eluted by an ammonia solution. Wine samples were additionally passed through a second column (a mixed bed of cation- and anion-exchange resins) for further clean-up. Using quantification against an external standard calibration, it was found that the betaine content of refined beet sugar was in the range of 30-37 mg kg^{-1}. Wine samples were found to contain 0.8-5.7 mg betaine/liter, which may reflect the level of addition of beet sugar to the wine. Although this paper predates the first description of HILIC, its use of a hydrophilic stationary phase and a mobile phase of 3-30% water plus ACN, indicates that the chromatography was operating in HILIC mode. Thus, amongst all of the papers cited in this chapter, this was the earliest one concerning the application of HILIC to betaine analysis.

Betaine and free choline measurement in a broad range of cereal flours and cereal food products was reported by Bruce *et al.* [3] using the UPLC-MS/MS method employing a HILIC column, as described above in Section **A1.2.3**. The range of betaine concentration in the 8 white wheat flours analyzed was 166-326 µg g^{-1}, while for 6 whole-grain wheat flours it was 747-1503 µg g^{-1}. In contrast, corn and rice flours contained barely measurable amounts, while whole grain oats and barley contained amounts in the range of 114-760 µg g^{-1}. Some correlation was found between betaine and free choline levels in cereals.

There have been many reports of the use of HILIC chromatography in phospholipid class separations. Zhao *et al.* in 2011 [5] reported on an LC-MS/MS experiment using multiple scan modes to simultaneously identify and quantify 11 choline-related compounds–acetylcholine (AcCho), betaine (Bet), choline (Cho), glycerophosphocholine (GPC), lysophosphatidylcholine (LPC), lysophosphatidylethanolamine (LPE), phosphatidylcholine (PC),

phosphatidylethanolamine (PE), phosphatidylinositol (PI), phosphocholine (PCho) and sphingomyelin (SM). This work used a modification to the Bligh and Dyer method of lipid extraction to ensure collection of the more polar components. In this paper, HILIC separation with an Ascentis Express HILIC column (150 mm×2.1 mm i.d., 2.7 μm) was compared with normal-phase HPLC separation with an Ascentis silica column (150 mm×2.1 mm i.d., 3 μm). An important difference between the 2 chromatographic modes is the simplicity of the HILIC method that used an ACN/water (10 mM ammonium formate, pH 3) gradient compared to the normal phase method that used a gradient of two complicated solvent mixtures, each containing ACN/water/ethanol/1 M ammonium acetate/glacial acetic acid in different proportions. It was found that the HILIC mode generally resulted in better peak shapes and higher ionization efficiency in LC-MS, along with a shorter run time and better sensitivity. This applied to both phospholipids and to betaine analysis, where the *m/z* 118→*m/z* 58 MRM transition was monitored and choline-d_9 was used as the internal standard. Although the focus of this work was to quantify total choline in foods from all sources (*i.e.* free choline and bound), it does demonstrate how in a single HILIC LC run, betaine can be measured alongside many other diverse species.

Later, this work was extended to include 14 compounds or compounds classes comprised of 6 aqueous choline-related compounds (Cho, Bet, AcCho, PCho, GPC, CDP-Cho) and 8 phospholipid classes (PC, LPC, PE, LPE, SM, PI, PS and PG) [6]. For betaine, a working linear dynamic range of 0.05-5 μg mL^{-1}, an LOD of 0.02 μg mL^{-1} (S/N>3) and an LOQ of 0.05 μg mL^{-1} (S/N>10) were established. However, it should be noted that these values could be improved on in a method that focused only on the analysis of compounds similar to betaine, rather than one developed to quantify a wide range of phospholipids and choline-related compounds in a single run. The method recoveries were excellent (99-102%) for betaine spiked into food at 20-40 mg/100

g levels. Intraday triplicate measurement precision for betaine quantified in standards and egg yolk was <10%, which is adequate for food and tissue analysis. Thus, betaine analysis as part of a wider nutritional analysis that measures phospholipids and other choline-related metabolites can be achieved by HILIC LC-MS/MS methods.

APPENDIX 1

Table A1-1. The determination of betaine from HILIC-based methods. A summary of published HILIC-based methods used for betaine analysis in a variety of samples.

Matrix	Target compound (s)	Stationary phase	Mobile phase	Detection	References
Plasma, cereals, cereal products	Betaine, free choline	UHPLC HILIC (waters) (2.1 mm×150 mm, 1.7 µm)	10 mM aqueous ammonium acetate-0.005% acetic acid+ ACN; gradient	ESI-MS/MS	[3]
Mixture of standards	Acetylcholine, choline, betaine, chlormequat, mepiquat	YMC-Pack NH_2 (waters) (150 mm×4.6 mm, 3 µm) TSKgel Amide-80 (Tosoh Bioscience) (250 mm×4.6 mm, 5 µm)	ACN + 10 mM aqueous ammonium acetate (81:19, *v/v*); isocratic	ESI-MS/MS	[29]
Plasma	Choline, betaine, dimethylglycine	Hypersil silica column (100 mm×2.1 mm, 5 µm)	15 mM ammonium formate (pH 3.5)+ACN; gradient	ESI-MS/MS	[2]
EDTA plasma, urine, amniotic fluid, cerebrospinal fluid	Acetylcholine, choline, betaine, dimethylglycine	Acquity UPLC BEH HILIC (100 mm×2.1 mm, 1.7 µm)	15 mM ammonium formate (pH 3.5)+ACN; gradient	ESI-MS/MS	[4]
Lycium chinense fruits	Betaine	YMC-Pack NH_2 (250 mm×4.6 mm, 5 µm)	water+ACN (25:75, *v/v*); isocratic	ESI-MS/MS	[31]
Lycii fructus	Betaine	Phenomenex Kinetex HILIC (2.1 mm×100 mm, 2.6 µm) Waters Atlantis HILIC (3.0 mm×100 mm, 5 µm) HALO HILIC (2.1 mm×100 mm, 2.7 µm)	ACN+10 mM ammonium formate (pH 3.0)-ACN (90/10, *v/v*); isocratic	ELSD	[32]
Refined sugar, wine	Betaine	Amino-bonded silica (150 mm×4.7 mm, 10 µm)	water+ACN (25:75, *v/v*); isocratic	Refractive index detection	[38]

Egg yolk extracts, human diets, rat livers, stomach contents	Acetylcholine, betaine, choline, glycerophosphocholine, lysophosphatidylcholine, lysophosphatidylethanolamine, phosphatidylcholine, phosphatidylethanolamin, phosphatidylinositol, phosphocholine, sphingomyelin, cytidine diphosphocholine, phosphatidylserine, phosphatidylglycerol	Ascentis Express HILIC (150 mm×2.1 mm, 2.7 μm)	ACN+10 mM aqueous ammonium formate (pH 3); gradient	ESI-MS/MS	[6]
Egg yolk extracts	Acetylcholine, betaine, choline, glycerophosphocholine, lysophosphatidylcholine, lysophosphatidylethanolamine, phosphatidylcholine, phosphatidylethanolamin, phosphatidylinositol, phosphocholine, sphingomyelin	Ascentis Express HILIC (150 mm×2.1 mm, 2.7 μm)	ACN+10 mM aqueous ammonium formate (PH 3); gradient	ESI-MS/MS	[5]
Lycii fructus	Betaine	Atlantis HILIC silica (4.6 mm×150 mm, 5 μm); Phenomenex Luna HILIC (4.6 mm×150 mm, 5 μm)	30 mM ammonium acetate+ACN (20:80, *v/v*); isocratic	ELSD	[33]

A1.3. Conclusions and Future Perspectives

The HILIC method is becoming increasingly popular for the analysis of polar, hydrophilic and ionic compounds. In this chapter, a number of HILIC-based methods that include betaine determination are summarized. In general, these methods were developed to analyze a range of related or unrelated compounds in addition to betaine. The methods discussed employ the HILIC technique in conjunction with several types of detectors including UV, ELSD, refractive index, MS or MS/MS for betaine analysis. Some key developments in the use of the HILIC method in betaine characterization include the simplification of sample preparation procedures, the optimization of mobile-phase composition and selection of the HILIC column from the continually increased number of commercially available columns. Since HILIC chromatography can involve multimodal interactions, the selection of the stationary phase to achieve an optimal separation may vary depending on the nature of the analytes and sample matrix.

Of the ten papers reviewed in this chapter that describe the use of HILIC methods for betaine analyses, six of them were published in the past five years. Hence, this is still an emerging area of study and it is expected that improvements in sensitivity and selectivity will be forthcoming based on newer HILIC phases and more targeted analyses. This would be desirable, especially for biomedical type analyses where the use of limited sample amounts and betaine concentrations are important.

A1.4. References

[1] Y. Guo, S. Gaiki, Retention and selectivity of stationary phases for hydrophilic interaction chromatography, J Chromatogr A. 35 (2011) 5920-5938.

[2] P.I. Holm, P.M. Ueland, G. Kvalheim, E.A. Lien, Determination of choline, betaine, and dimethylglycine in plasma by a high-throughput method based on normal-phase chromatography-

tandem mass spectrometry, Clin. Chem. 49 (2003) 286-294.

[3] S.J. Bruce, P.A. Guy, S. Rezzi, A.B. Ross, Quantitative measurement of betaine and free choline in plasma, cereals and cereal products by isotope dilution LC-MS/MS, J Agric Food Chem. 58 (2010) 2055-2061.

[4] S.H. Kirsch, W. Herrmann, Y. Rabagny, R. Obeid, Quantification of acetylcholine, choline, betaine, and dimethylglycine in human plasma and urine using stable-isotope dilution ultra performance liquid chromatography-tandem mass spectrometry, J Chromatogr B. 878 (2010) 3338-3344.

[5] Y.Y. Zhao, Y.P. Xiong, J.M. Curtis, Measurement of phospholipids by hydrophilic interaction liquid chromatography coupled to tandem mass spectrometry: The determination of choline containing compounds in foods, J Chromatogr A. 1218 (2011) 5470-5479.

[6] Y.P. Xiong, Y.Y. Zhao, S. Goruk, K. Oilund, C.J. Field, R.L. Jacobs, J.M. Curtis, Validation of an LC-MS/MS method for the quantification of choline-related compounds and phospholipids in foods and tissues, J Chromatogr B. 911 (2012) 170-179.

[7] D.V. McCalley, Is hydrophilic interaction chromatography with silica columns a viable alternative to reversed-phase liquid chromatography for the analysis of ionisable compounds? J Chromatogr A. 1171 (2007) 46-55.

[8] M.R. Gama, R.G. da Costa Silva, C.H. Collins, C.B.G. Bottoli, Hydrophilic interaction chromatography, Trends Anal Chem. 37 (2012) 48-60.

[9] A.J. Alpert, Hydrophilic-interaction chromatography for the separation of peptides, nucleic acids and other polar compounds, J Chromatogr A. 499 (1990) 177-196.

[10] P. Orth, H. Engelhardt, Separation of sugars on chemically modified silica gel, Chromatographia. 15 (1982) 91-96.

[11] P. Hemström, K. Irgum, Hydrophilic interaction chromatography, J Sep Sci. 29 (2006) 1784-1821.

[12] B. Dejaegher, D. Mangelings, Y. Vander Heyden, Method development for HILIC assays, J Sep Sci. 31 (2008) 1438-1448.

[13] B. Dejaegher, Y. Vander Heyden, HILIC methods in pharmaceutical analysis, J Sep Sci. 33 (2010) 698-715.

[14] A. Cavazzini, A. Felinger, 2013. Liquid Chromatography: Fundamentals and Instrumentation. Elsevier Science Publishers, Amsterdam, Netherlands. 520 pp.

[15] Y. Guo, S. Gaiki, Retention behavior of small polar compounds on polar stationary phases in hydrophilic interaction chromatography, J Chromatogr A. 1074 (2005) 71-80.

[16] T. Yoshida, Peptide separation by hydrophilic-interaction chromatography: A review, J. Biochem. Biophys. Methods. 60 (2004) 265-280.

[17] Z. Hao, B. Xiao, N. Weng, Impact of column temperature and mobile phase components on selectivity of hydrophilic interaction chromatography HILIC, J Sep Sci. 31 (2008) 1449-1464.

[18] J. Bernal, A.M. Ares, J. Pól, S.K. Wiedmer, Hydrophilic interaction liquid chromatography in food analysis, J Chromatogr A. 1218 (2011) 7438-7452.

[19] R. Li, J. Huang, Chromatographic behavior of epirubicin and its analogues on high-purity silica in hydrophilic interaction chromatography, J Chromatogr A. 1041 (2004) 163-169.

[20] W. Jian, R.W. Edom, Y. Xu, N. Weng, Recent advances in application of hydrophilic interaction chromatography for quantitative bioanalysis, J Sep Sci. 33 (2010) 681-697.

[21] G. Kahsay, H. Song, A. Van Schepdael, D. Cabooter, E. Adams, Hydrophilic interaction chromatography HILIC in the analysis of antibiotics, J Pharm Biomed Anal. 87 (2014) 142-154.

[22] P. Lehnert, M. Douša, K. Lemr, Underivatized amylose and cellulose as new stationary phases for hydrophilic interaction chromatography, J Sep Sci. 36 (2013) 3345-3350.

[23] S.M. Lee, C.K. Park, B.G. Cho, K.S. Cho, B.S. Min, K.H. Bae, A convenient HPLC/ELSD method for the quantitative analysis of betaine in lycium *chinense*, Nat Prod Sci. 17 (2011) 104-107.

[24] T.P. Chendrimada, M.G. Neto, G.M. Pesti, A.J. Davis, R.I. Bakalli, Determination of the betaine content of feed ingredients using high-performance liquid chromatography, J Sci Food Agr. 82 (2002) 1556-1563.

[25] W.D. Hitz, A.D. Hanson, Determination of glycine betaine by pyrolysis-gas chromatography

in cereals and grasses, Phytochemistry. 19 (1980) 2371-2374.

[26] R.H. Allen, S.P. Stabler, J. Lindenbaum, Serum betaine, *N, N*-dimethylglycine and *N*-methylglycine levels in patients with cobalamin and folate deficiency and related inborn errors of metabolism, Metabolism. 42 (1993) 1448-1460.

[27] J. Zhang, N. Nishimura, A. Okubo, S. Yamazaki, Development of an analytical method for the determination of betaines in higher plants by capillary electrophoresis at low pH, Phytochem Anal. 13 (2002) 189-194.

[28] L. Sánchez-Hernández, M. Castro-Puyana, M. Luisa Marina, A.L. Crego, Determination of betaines in vegetable oils by capillary electrophoresis tandem mass spectrometry-application to the detection of olive oil adulteration with seed oils, Electrophoresis. 32 (2011) 1394-1401.

[29] Y. Guo, Analysis of quaternary amine compounds by hydrophilic interaction chromatography/mass spectrometry HILIC/MS, J Liq Chrom Relat Tech. 28 (2005) 497-512.

[30] R. Dunphy, D.J. Burinsky, Detection of choline and acetylcholine in a pharmaceutical preparation using high-performance liquid chromatography/electrospray ionization mass spectrometry, J Pharm Biomed Anal. 31 (2003) 905-915.

[31] Y.G. Shin, K.H. Cho, J.M. Kim, M.K. Park, J.H. Park, Determination of betaine in lycium *chinense* fruits by liquid chromatography-electrospray ionization mass spectrometry, J Chromatogr A. 857 (1999) 331-335.

[32] H.D. Shin, J.H. Suh, J. Kim, H. Lee, H.Y. Eom, U. Kim, D.H. Yang, S.B. Han, J.R. Youm, Determination of betaine in fructus lycii using hydrophilic interaction liquid chromatography with evaporative light scattering detection, Bull Korean Chem Soc. 33 (2012) 553-558.

[33] B.T. Zhao, S.Y. Jeong, K. Hwangbo, D.C. Moon, E.K. Seo, D. Lee, J.H. Lee, B.S. Min, E.S. Ma, J.K. Son, M.H. Woo, Quantitative analysis of betaine in lycii fructus by HILIC-ELSD, Arch Pharmacal Res. 36 (2013) 1231-1237.

[34] H. Koc, M.H. Mar, A. Ranasinghe, J.A. Swenberg, S.H. Zeisel, Quantitation of choline and its metabolites in tissues and foods by liquid chromatography/electrospray ionization-isotope dilution mass spectrometry, Anal Chem. 74 (2002) 4734-4740.

[35] F.J. De Zwart, S. Slow, R.J. Payne, M. Lever, P.M. George, J.A. Gerrard, S.T. Chambers, Glycine betaine and glycine betaine analogues in common foods, Food Chem. 83 (2003) 197-204.

[36] K.Y. Patterson, S.A. Bhagwat, J.R. Williams, J.C. Howe, J.M. Holden, 2008. USDA Database for the Choline Content of Common Foods. Available at: http://www.ars.usda.gov/SP2UserFiles/Place/12354500/Data/Choline/Choln02.pdf. Accessed 23 December, 2013.

[37] S.H. Zeisel, M.H. Mar, J.C. Howe, J.M. Holden, Concentrations of choline-containing compounds and betaine in common foods, J Nutr. 133 (2003) 1302-1307.

[38] J. Vialle, M. Kolosky, J.L. Rocca, Determination of betaine in sugar and wine by liquid chromatography, J Chromatogr A. 204 (1981) 429-435.

Appendix 2*

Glucagon-Like Peptide-2 Alters Bile Acid Metabolism in Parenteral Nutrition-Associated Liver Disease

Clinical Relevancy Statement

We recently reported the novel finding that glucagon-like peptide-2 (GLP-2) therapy is associated with improvement in parenteral nutrition–associated liver disease (PNALD) in a preclinical model. In the following, we show that GLP-2 therapy is associated with alterations in bile acid synthetic and transport pathways, which may mediate the improvement in PNALD. Such revelations shed further light on the mechanisms of PNALD and a novel effect of GLP-2, with potential additional benefits of this therapy for all infants receiving long-term parenteral nutrition therapy.

A2.1. Introduction

Each year in the United States, more than a half-million hospitalized infants require parenteral nutrition (PN) therapy for support [1]. While PN remains a lifesaving measure for these children, the dreaded complication of PN-associated liver disease (PNALD) is still observed with extended PN therapy, especially for high-risk groups such as premature and low-birth-weight infants and infants with short bowel syndrome (SBS) [2]. The incidence of PNALD can be as high as 50% in infants receiving PN for >2 months, with 25% further progressing to end-stage liver disease and

* This appendix has been published as D.W. Lim, P.W. Wales, S. Mi, J.Y. Yap, J.M. Curtis, D.R. Mager, V.C. Mazurak, P.R. Wizzard, D.L. Sigalet, J.M. Turner, "Glucagon-Like Peptide-2 Alters Bile Acid Metabolism in Parenteral Nutrition-Associated Liver Disease", *Journal of Parenteral and Enteral Nutrition*, 40 (2016) 22-35. I contributed to conception and design of the tandem spectrometry work, and the acquisition, analysis of the tandem spectrometry data, interpretation of the bile acid composition in bile samples as well as the revision of the manuscript.

requiring liver transplantation [3, 4]. The development of PNALD is associated with several risk factors: developmental immaturity with regard to hepatic bile acid metabolism and transport, lack of enteral feeding, recurrent infection and sepsis, and specific PN lipid emulsion formulations [5]. Currently, no established pharmacological treatments are available. A significant part of the problem lies in a lack of understanding of the cellular and molecular mechanisms underlying PNALD [6]. Therapeutic interventions have so far been aimed at introducing enteral feeding as early as possible and using new-generation lipid emulsions containing beneficial ω-3 polyunsaturated fatty acids [7, 8].

Our group recently reported the novel finding that intravenous administration of the trophic factor, glucagon-like peptide-2 (GLP-2), in a preclinical model of neonatal PNALD was associated with improved bile flow and serum and histologic markers of cholestasis.9 While GLP-2 is being studied for a potential therapeutic application in SBS, we hypothesized that GLP-2 therapy may also benefit liver function in the setting of PNALD for several reasons. Inflammatory stress commonly occurs in PN-fed infants secondary to the high occurrence of bacterial sepsis from catheter-related line sepsis or intestinal translocation [1]. GLP-2 itself has local enteric anti-inflammatory activity and is known to strengthen the intestinal barrier, which is compromised with extended PN therapy, both significant factors that may prove beneficial in the setting of PNALD [10, 11]. The study objective was to delineate the cellular and molecular mechanisms occurring in the liver that may account for our previously reported observations. Several recent reports have highlighted dysfunction in the regulation of bile acid synthesis and transport in PNALD and SBS-associated liver disease and have suggested potential therapeutic interventions (such as new-generation lipid emulsions and enteral bile acid treatment) to alter these pathways [12, 13, 14]. Given these findings, we hypothesized that intravenous GLP-2 administration in our preclinical

neonatal piglet model of PNALD improved the clinical phenotype by altering bile acid synthesis and transport pathways in the liver. In turn, we further hypothesized that there may be differences in the composition of bile acids in bile that reflect differences in synthesis and transport pathways with GLP-2 therapy.

A2.2. Materials and Methods

A2.2.1. Animals and surgical procedures

All protocols and study design were approved by the University of Alberta Animal Care and Use Committee for Livestock. Neonatal male Landrace/Large White cross piglets (Hypor, Regina, SK, Canada), aged 2-6 days old, were obtained from the University of Alberta Swine Research and Technology Center (SRTC, University of Alberta, Edmonton, AB, Canada). At study day 0, piglets underwent general anesthesia with isoflurane (2%-3%; Bensen Medical Industries Inc, Markham, ON, Canada). As previously described, a 5F central venous catheter (Dow Corning, Midland, MI, USA) was inserted into the left external jugular vein via venous cutdown technique in order to provide PN and intravenous GLP-2 or vehicle therapy during the trial [9].

A2.2.2. Postsurgical animal care

Postoperatively, piglets received an intravenous narcotic, buprenorphine hydrochloride (0.02 mg kg^{-1}; Buprenex; Rekitt and Colman Pharmaceutical, Richmond, VA, USA), followed by buprenorphine hydrochloride (0.005 mg kg^{-1}) every 8 hours for 2 consecutive days. Piglets also received oral meloxicam (0.1 mg kg^{-1}; Metacam; Boehringer Ingelheim, Burlington, ON, Canada) for 3 consecutive days for analgesic support. Routine intravenous antibiotics were administered on study days 0-3 and 8-11, which included ampicillin sodium (10 mg kg^{-1}; Sandoz, Boucherville, QC, Canada) and trimethoprim-sulfadoxine 40/200 (0.5 mL; Borgal; Merck Animal Health,

Kirkland, QC, Canada), for line sepsis prevention.

Piglets were housed in individual animal cages lined with Plexiglas, in which they were secured to a tether-swivel system (Alice King Chatman Medical Arts, Los Angeles, CA, USA) to allow for freedom of movement while receiving PN. Room temperature was maintained at 25°C with the aid of a heat lamp, and lighting was established at a 12-hour light-dark cycle. Daily piglet weight, nutrient intake, and urine output measurements were recorded.

A2.2.3. Parenteral nutrition

Total PN (without enteral nutrition) was infused via the external jugular central venous catheter by a pressure-sensitive Alaris infusion pump (CareFusion Corporation, San Diego, CA, USA). Target energy intake was 1100 kJ kg^{-1} d^{-1}, with amino acids providing 27% of energy, carbohydrate 37%, and fat 36%. Target nutrient intakes were amino acids, 18.0 g kg^{-1} d^{-1}; glucose, 29.0 g kg^{-1} d^{-1}; and fat, 10.4 g kg^{-1} d^{-1}. These targets were estimated from daily nutrition requirements for sow-fed piglets, previously reported by Wykes *et al.* [15]. The PN solution consisted of an amino acid-based solution prepared in our laboratory based on human milk protein (Vaminolact; Fresenius Kabi, Bad Homburg, Germany). The amino acid profile of our PN solutions is presented in Table A2-S1 (available online). As previously described [9], crystalline amino acids (Ajinomoto, Fort Lee, NJ, USA) were dissolved in sterile water under a blanket of nitrogen, to which glucose (Dextrose; 90 g L^{-1} Sigma-Aldrich, St. Louis, MO, USA) and minerals (calcium, phosphate, potassium, manganese, sodium, and zinc; Sigma-Aldrich, St. Louis, MO, USA) were added. This mixture was filtered through a 0.22-μm filter (Millipore, Etobicoke, ON, Canada) into 1-L sterile bags (Baxter Corp, Toronto, ON, Canada). The final solution was prepared with the addition of iron dextran (FerroForte; Bimeda-MTC, Cambridge, ON, Canada), cobalamin (Abbott,

Mississauga, ON, Canada), multivitamins (Multi-12/K1 Pediatric; Sabex, Boucherville, QC, Canada), additional trace minerals (Sigma-Aldrich, St. Louis, MO, USA), famotidine (5 mg L^{-1}; Omega, Montreal, QC, Canada), and lipid (Intralipid 20%; 145 mL L^{-1}; Fresenius Kabi, Bad Homburg, Germany).

Delivery of PN commenced immediately following surgery at an initial rate of 50% of the targeted rate. The rate was increased to 75% of the total targeted rate 8 hours after surgery and then increased to the full rate (13.5 mL kg^{-1} h^{-1}) 16 hours after surgery for the remainder of the study period.

A2.2.4. Study design

Piglets were randomized to receive either saline control (PN/Saline group, n = 8) or GLP-2 therapy (PN/GLP-2 group, n = 7) at a dose of 11 nmol kg^{-1} d^{-1}. This dose was selected because previous studies have reported a positive effect on intestinal adaptation at 11 nmol kg^{-1} d^{-1}, as previously described [9, 16]. As previously described [16], intravenous human GLP-2 (Human GLP-2(1-33); CS9065; Lot I074 with 96.83% purity confirmed by HPLC; CS Bio, Menlo Park, CA, USA) was delivered using normal saline (0.9% sodium chlorine; Baxter Corp, Mississauga, ON, Canada) as a carrier solution to all piglets randomized to receive GLP-2. Piglets randomized to the PN/Saline group received normal saline (0.9% sodium chloride; Baxter, Mississauga, ON, Canada). GLP-2 or vehicle therapy was administered to piglets beginning on postoperative day 2 through the jugular venous catheter as a continuous 24-hour infusion at a rate of 0.42 mL kg^{-1} h^{-1} via a syringe pump (NE-300 Just Infusion Syringe Pump; New Era Pump Systems, Farmingdale, NY, USA) separate from the PN infusion. To provide a normal expected range for all data, a healthy sow-reared group of piglets (Sow-reared group, n = 8) were studied, representing the gold

standard for postnatal growth and development of preweaned piglets. Sow-reared piglets were chosen from the same litters as experimental piglets, when possible, and were raised under standard farm conditions until undergoing terminal laparotomy at the equivalent age of experimental piglets. Sow-reared piglets did not receive a catheter, PN or treatment, or antibiotics.

At study day 17, piglets underwent general anesthesia and terminal laparotomy. Terminal blood samples were drawn, bile flow was measured, and formalin-fixed liver samples for histologic analysis were collected as previously described, the results of which have been previously reported.9 Piglets were euthanized with pentobarbital sodium (Schering, Pointe-Claire, QC, Canada). Liver specimens were flash frozen in liquid nitrogen for real-time polymerase chain reaction (PCR) analysis. Bile samples collected from bile flow measurements were stored at –80°C for bile acid identification and quantification.

A2.2.5. Data collection

Real-time PCR. Total RNA from 30 mg of frozen liver was extracted using an RNeasy Plus Mini Kit (Qiagen, Germantown, MD, USA) and quantified by spectrophotometric assay. Reverse transcription was performed using the High Capacity cDNA Reverse Transcription Kit (Applied Biosystems, Foster City, CA, USA), and real-time semi-quantitative PCR was performed using TaqMan assays (Life Technologies, Carlsbad, CA, USA) (porcine-specific primers listed in Table A2-S2) with TaqMan Universal Master Mix (Invitrogen, Burlington, ON, Canada). For each sample, DNA amplification was performed in duplicate with the 7900HT Fast Real-time PCR System (Applied Biosystems) under the following thermal cycling conditions: 95 °C for 20 seconds, followed by 40 cycles of 95 °C for 1 second and 60 °C for 20 seconds. Amplification efficiency was controlled by the use of *HPRT1* (hypoxanthine-guanine phosphoribosyltransferase-

1 gene) as an internal control. Data were analyzed using the 7900HT Fast Real-time PCR System SDS v2.3 software (Applied Biosystems, Foster City, CA, USA). Relative expression was determined using the $2^{-\Delta\Delta C(t)}$ method.

Bile acid identification and quantification. Piglet bile samples were prepared for analysis with high-performance liquid chromatography (HPLC) with tandem mass spectrometry by solid phase extraction (SPE) using a Maxi-Clean C18 cartridge preconditioned with methanol followed by HPLC-grade water. A 10-fold diluted piglet bile sample solution (250 µL) was mixed with 250 µL of internal standard (IS) solution and 250 µL of 1% formic acid solution and then loaded onto the column. The column was washed with HPLC-grade water (5 mL), and bile acids were recovered by elution with 7 mL of methanol and finally dried under nitrogen and re-dissolved in 500 µL of methanol. Analysis of individual bile acids was achieved using an Agilent 1200 series HPLC (Agilent Technologies, Palo Alto, CA, USA) coupled to a 3200 QTRAP mass spectrometer (AB SCIEX, Concord, ON, Canada) with Analyst 1.4.2 software. The method and internal standards used in the bile acid analyses are outlined in supplemental material (Table A2-S3); the development and validation of this method will be the subject of a separate publication. Individual bile acids in the piglet bile samples were identified by comparison of their retention times to the known standards, accurate mass measurements, and fragmentation patterns. The method of quantification used a deuterated recovery standard and calibration curves constructed for 19 individual bile acid standards. All measurements were duplicate extractions and single analyses.

We also performed a pig total bile acid enzyme-linked immunosorbent assay (ELISA) (Catalog No. abx052581, Abbexa, Cambridge, UK) on liver tissue to determine the liver tissue bile acid concentration. The ELISA was performed on liver tissue homogenized in phosphate-buffered

saline according to the instructions provided. We then calculated an estimate of the total liver bile acid content by multiplying the liver tissue bile acid concentration by liver mass (adjusted per kilogram of body weight).

A2.2.6. Data analysis and statistics

Data are presented as mean±standard deviation. Results were analyzed using 1-way analysis of variance (ANOVA) followed by Bonferroni's post hoc analysis. For data with unequal variances between groups, as determined by Bartlett's test for equal variance, the Kruskal-Wallis analysis of variance was used instead followed by Mann-Whitney *U* test for post hoc analysis. Significance was set at $P < .05$.

A2.3. Results

A2.3.1. Bile acid synthesis

To determine potential mechanisms for a GLP-2-mediated improvement in cholestasis, we measured the expression of genes involved in the regulation, synthesis, and transport of bile acids (**Figure A2-1**). We first measured the expression of the bile acid receptor, Farnesoid X receptor (FXR), the key regulator of bile acid homeostasis, encoded by the *NR1H4* (nuclear receptor subfamily 1, group H, member 4) gene [17]. We found that *NR1H4* expression was significantly increased in the PN/GLP-2 group by 1-fold compared with the PN/Saline ($P = .001$) and Sowreared groups ($P = .002$); $P < .001$ (**Figure A2-2**). We next measured expression of the *CYP7A1* (cytochrome P450, family 7, subfamily A, polypeptide 1) gene, a target gene of FXR that encodes the rate-limiting enzyme of the neutral (classic) bile acid synthesis pathway, cholesterol 7 α-hydroxylase [17]. We found a significant difference in *CYP7A1* gene expression between groups ($P = .03$), with the PN/GLP-2 group having a 2-fold increase over both PN/Saline ($P = .049$) and

Sow-reared groups (P = .015). We also measured expression of the *CYP27A1* (cytochrome P450, family 27, subfamily A, polypeptide 1) gene, the product of which (sterol 27-hydroxylase) is the main enzyme of the acidic (alternative) bile acid synthesis pathway [17]. There was no difference in *CYP27A1* gene expression between groups; P = .37 (Figure A2-2). *CYP8B1* (cytochrome P450, family 8, subfamily B, polypeptide 1 gene) controls 12α-hydroxylation in bile acid synthesis, and

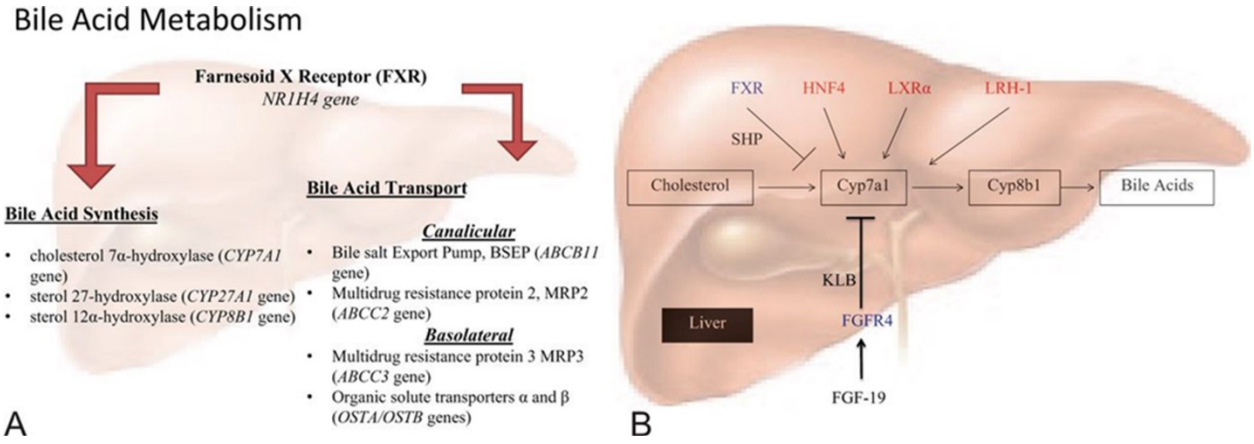

Figure A2-1. (A) Schematic representation of the genes involved in bile acid homeostasis that were analyzed. (B) CYP7A1 expression is controlled by a complex regulatory mechanism.

thus hydrophobicity of bile acid pool, and, like *CYP7A1*, is also negatively regulated by bile acids [17]. However, we found no difference in *CYP8B1* gene expression between groups; P = .13 (Figure A2-2).

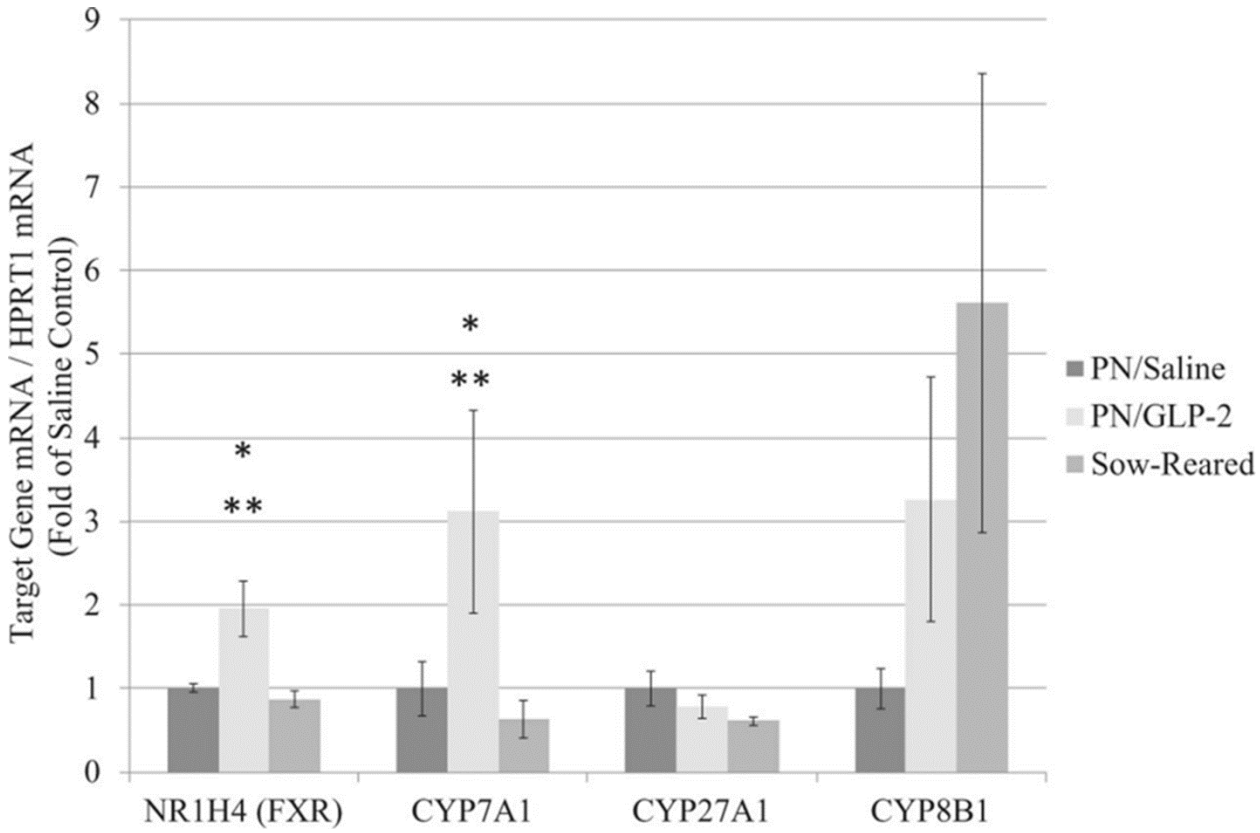

Figure A2-2. Relative expression of genes involved in bile acid synthesis and regulation.

A2.3.2. Bile acid transport

We next measured the expression of several genes whose products are involved in bile acid export from the liver, many of which are regulated by FXR (**Figure A2-1A**). Under physiological conditions, bile acids are preferentially excreted into bile via the bile salt export pump (BSEP) and the multidrug resistance protein 2 (MRP2). BSEP, encoded by the *ABCB11* (ATP-binding cassette, subfamily B member 11) gene, is transcriptionally induced by FXR [17]. We found a significant difference in *ABCB11* expression between groups (P = .03), with the Sow-reared group having decreased expression compared with both PN/Saline (P = .01) and PN/GLP-2 (P = .049) groups (**Figure A2-3**). In addition, there was a trend toward increased *BSEP* expression in the PN/GLP-2

group over the PN/Saline group ($P = .071$). MRP2, encoded by the *ABCC2* (ATP-binding cassette subfamily C member 2) gene, is a multi-specific ABC transporter that also is inducible by FXR and excretes sulfated and glucoronidated bile acids into bile [17]. We found a significant difference in *ABCC2* expression ($P < .01$), with the PN/GLP-2 group having a 0.5-fold increase over the PN/Saline group ($P = .002$) and a 1-fold increase over the Sow-reared group ($P < .001$) (**Figure A2-3**). Under cholestatic conditions, when bile acids accumulate in the liver at toxic levels, the expression of basolateral bile acid transporters, including organic solute transporters α and β (*OSTA* and *OSTB* genes, respectively) and multidrug resistance protein 3 (MRP3, encoded by the *ABCC3* [ATP-binding cassette subfamily C member 3] gene), is increased, allowing for the secretion of bile acids into the systemic circulation [18]. We found a significant difference in *ABCC3* gene expression between groups ($P < .001$), with all pairwise comparisons being significant and the PN/GLP-2 group having the highest expression and the Sow-reared group having the lowest ($P = .037$ between groups 1 and 2; $P < .01$ between groups 1 and 3; $P < .002$ between groups 2 and 3; **Figure A2-3**). *OSTA* expression was significantly increased in both PN-fed groups compared with the Sow-reared group ($P < .002$), with no difference between the PN/Saline and PN/GLP-2 groups ($P = .56$). Similarly, *OSTB* expression was significantly increased in both PN-fed groups compared with the Sow-reared group ($P < .01$), with a trend toward increased *OSTB* expression in the PN/GLP-2 group over the PN/Saline group ($P = .08$) (**Figure A2-3**).

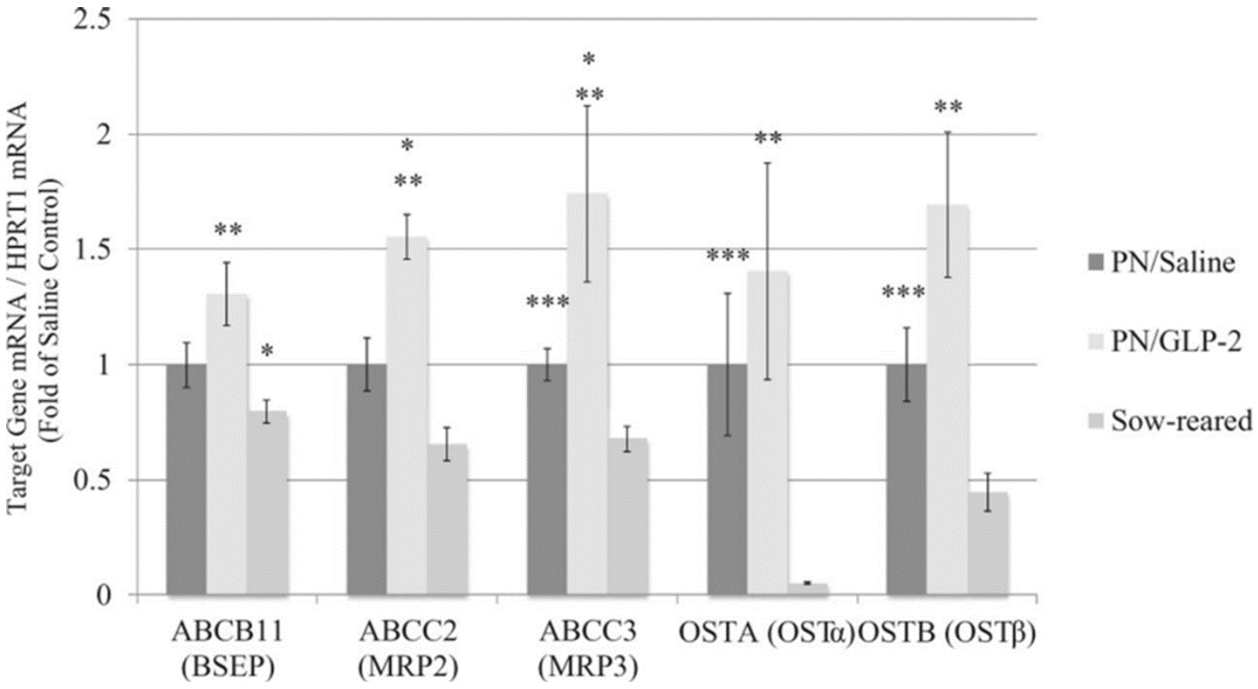

Figure A2-3. Relative expression of genes involved in hepatic bile acid export.

A2.3.3. Regulators of bile acid synthesis

The increased expression of *CYP7A1* in the PN/GLP-2 group over both PN/Saline and Sow-reared groups was unexpected, given that *FXR* expression was also increased in tandem and FXR is a known repressor of *CYP7A1* expression [17]. Given this, we measured the expression of genes whose products are known to transactivate CYP7A1 and compete with FXR repression (**Figure A2-1B**). We first measured the expression of the *NR0B2* (nuclear receptor subfamily 0, group B, member 2) gene, whose protein product is the atypical nuclear receptor small (or short) heterodimer partner (SHP). SHP is pertinent because FXR itself cannot repress *CYP7A1* transcription. Instead, FXR induces SHP expression, which, in turn, represses *CYP7A1* expression [17]. There was a significant difference in *NR0B2* expression between groups ($P = .01$), with the PN/Saline group having almost a 0.5-fold increased expression over the Sow-reared group ($P = .01$)

and the PN/GLP-2 group (P = .09, trend only). SHP represses *CYP7A1* expression by interacting with 2 nuclear receptors that transactivate *CYP7A1* at the bile acid response element (BARE) region: hepatocyte nuclear factor 4-α (HNF4α, encoded by the *NR2A1* [nuclear receptor subfamily 2, group A, member 1] gene) and liver receptor homolog-1 (LRH-1, encoded by the *NR5A2* [nuclear receptor subfamily 5, group A, member 2] gene). There was an overall significant difference in *NR2A1* (*HNF4α*) expression between groups (P = .04); however, on post hoc analysis, there was only a trend toward increased expression by 0.5-fold in the PN/GLP-2 group over the PN/Saline (P = .088) and Sow-reared (P = .07) groups (**Figure A2-4**). *NR5A2* (LRH-1) expression, in contrast, was significantly different between groups (P = .003), with the PN/GLP-2 group clearly demonstrating a 1.25-fold increased expression over the PN/Saline group (P = .02) and a 1.5-fold increased expression over the Sowreared group (P < .002) (**Figure A2-4**). Liver X receptor α (LXRα, encoded by the *NR1H3* [nuclear receptor subfamily 1, group H, member 3] gene) is another known regulator of CYP7A1 expression, but its regulating activity (activating vs repressing) is species-specific [19]. We found a significant difference in *NR1H3* (LXRα) gene expression between groups (P < .001), with the PN/GLP-2 group having a 1-fold increase over the PN/Saline group (P < .01) and the Sow-reared group (P < .01) (**Figure A2-4**). Lastly, the FGF-19/FGFR4 axis is a known regulating pathway of hepatic *CYP7A1* expression and is suggested to be implicated in the pathogenesis of PNALD [14, 17]. For this reason, we measured the hepatic expression of the *FGFR4* gene and found a significant difference between groups (P < .001). All pairwise comparisons were significant, with the PN/GLP-2 group having the greatest fold increase in *FGFR4* expression and the Sowreared group the least (P = .006 between groups 1 and 2; P = .03 between groups 1 and 3; P = .001 between groups 2 and 3) (**Figure A2-4**). Furthermore, the actions of FGFR4 signaling require the presence of the co-receptor, β-klotho. We found a trend toward

increased expression of its gene, *KLB*, in the PN/GLP-2 group over both the PN/Saline and Sow-reared groups ($P = .05$) (**Figure A2-4**).

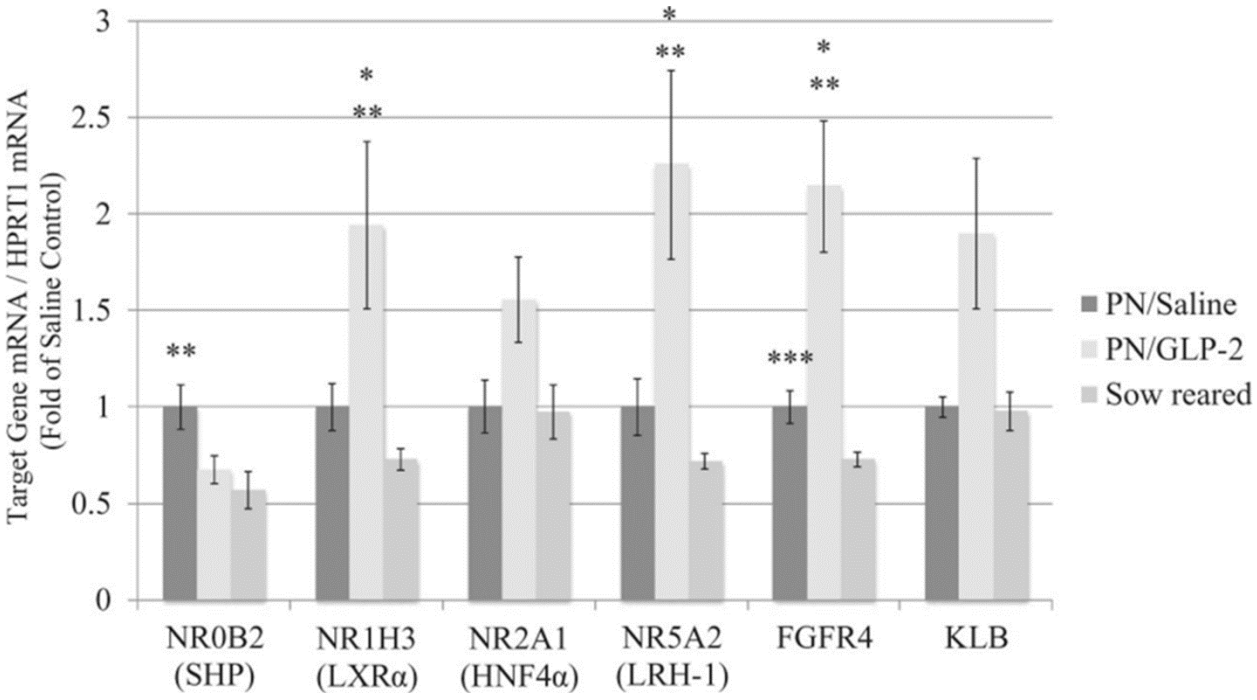

Figure A2-4. Relative expression of genes involved in the regulation of CYP7A1.

A2.3.4. TGR5 messenger RNA (mRNA) expression

The G-protein coupled bile salt receptor, TGR5, encoded by the *GPBAR1* (G protein-coupled bile acid receptor 1) gene, is expressed in many cell types of the liver with reported effects including anti-inflammatory actions and hepatoprotective effects [20, 21], mediation of bile acid-induced cell death [22], and improvement in hepatic microcirculation via the induction of nitric oxide synthase [23]. We felt it was pertinent to measure *GPBAR1* expression in the liver, given that bile acid accumulation in the liver in the setting of PNALD cholestasis could implicate TGR5-mediated effects. However, we did not find a difference in *GPBAR1* expression between groups ($P = .2$) (**Figure A2-5**).

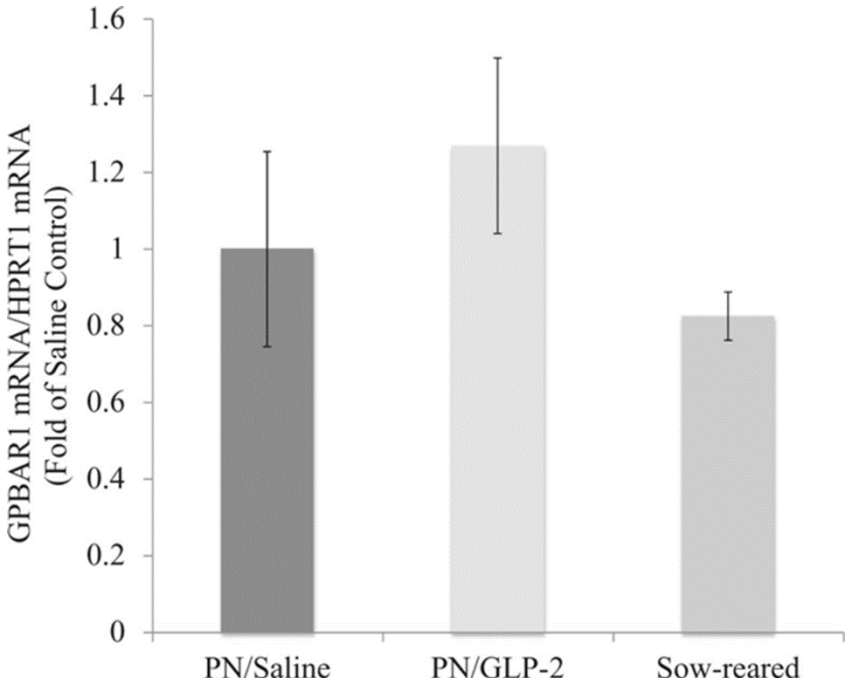

Figure A2-5. Relative expression of GPBAR1 mRNA.

A2.3.5. Bile acid composition in bile

There was a significantly greater total amount of bile acids (including taurine- and glycine-conjugated bile acids) in the Sow-reared group (3379 mcg mL^{-1}) compared with both PN-fed groups ($P < .001$) but no difference between PN/Saline (817 mcg mL^{-1}) and PN/GLP-2 (428 mcg mL^{-1}; $P = .6$) (**Table A2-1**). This parallels our measurements of total serum bile acids in our previous report [9]. Since the units of serum total bile acids in that previous report were micromolar, we have converted those serum values to micrograms per milliliter to illustrate the marked differences in bile acid concentrations between bile and plasma (**Table A2-1**). The majority of bile acids in all groups were taurine-conjugated bile acids: 81% in the PN/Saline group, 60% in the PN/GLP-2 group, and 72% in Sow-reared group. A smaller proportion of bile acids were glycine-conjugated: 19% in PN/Saline, 40% in PN/GLP-2, and 28% in Sow-reared (**Figure A2-6**). There

were significantly fewer taurine-conjugated bile acids in the PN/GLP-2 group (258 mcg mL^{-1}) compared with the PN/Saline group (660 mcg mL^{-1}; $P = .049$) but no difference in the amount of glycine-conjugated bile acids (Table A2-1). There were very few unconjugated bile acids in all groups (virtually none compared with conjugated bile acids), but the Sowreared group did have relatively more unconjugated bile acids than both total PN groups ($P < .01$) (Table A2-1).

Table A2-1. Bile acid identification and quantification in pig bile.

Identification/Quantification	PN/Saline[a]	PN/GLP-2[b]	Sow-Reared[c]	P Value
Bile acid quantification				
Total bile acids (in bile)	817.12 (625.13)	427.49 (267.33)	3378.75 (708.74)	<.0001[ac,bc]
Serum total bile acids	25.74 (6.96)	22.79 (13.01)	5.99 (2.51)	.0071[ac,bc]
Total taurine-conjugated bile acids	660.08 (582.52)	257.70 (179.58)	2421.15 (489.52)	.0003[ab,ac,bc]
Total glycine-conjugated bile acids	156.45 (114.22)	169.38 (159.56)	948.22 (422.02)	.0008[ac,bc]
Total unconjugated bile acids	0.59 (0.48)	0.41 (0.26)	9.39 (3.33)	.0005[ac,bc]
Bile acid identification				
Hyocholic acid (HCA)	0.41 (0.50)	0.24 (0.22)	9.10 (3.29)	.0005[ac,bc]
Tauro-hyocholic acid (t-HCA)	485.94 (406.11)	157.61 (118.75)	1353.18 (394.46)	.0004[ab,ac,bc]
Chenodeoxycholic acid (CDCA)	nd	nd	0.11 (0.04)	<.0001[ac,bc]
Tauro-chenodeoxycholic acid (t-CDCA)	98.61 (102.57)	64.03 (49.79)	476.24 (116.49)	<.0001[ac,bc]
Glyco-chenodeoxycholic acid (g-CDCA)	57.95 (12.45)	104.64 (51.88)	449.05 (59.57)	.0011[ac,bc]
Hyodeoxycholic acid (HDCA)	0.074 (0.021)	0.081 (0.027)	0.093 (0.020)	.27
Glyco-hyodeoxycholic acid (g-HDCA)	98.24 (79.40)	64.59 (56.07)	498.35 (264.80)	.0008[ac,bc]
Tauro-hyodeoxycholic acid (t-HDCA) or tauro-ursodeoxycholic acid (t-UDCA)	31.14 (28.87)	11.97 (9.84)	543.29 (204.23)	.0003[ac,bc]
Taurocholic acid (t-CA)	43.95 (50.98)	23.97 (29.22)	46.82 (12.26)	.049[bc]
Lithocholic acid (LCA)	0.11 (0.037)	0.089 (0.032)	0.093 (0.015)	.42
Tauro-lithocholic acid (t-LCA)	0.44 (0.52)	0.14 (0.02)	1.62 (0.83)	.0004[ab,ac,bc]
Glyco-lithocholic acid (g-LCA)	0.26 (0.10)	0.15 (0.02)	0.82 (0.27)	.0001[ab,ac,bc]

GLP-2, glucagon-like peptide-2; nd, not detectable; PN, parenteral nutrition. Values represent means (mcg mL^{-1}) and standard deviation (in parentheses). Superscripts refer to statistically significant differences.

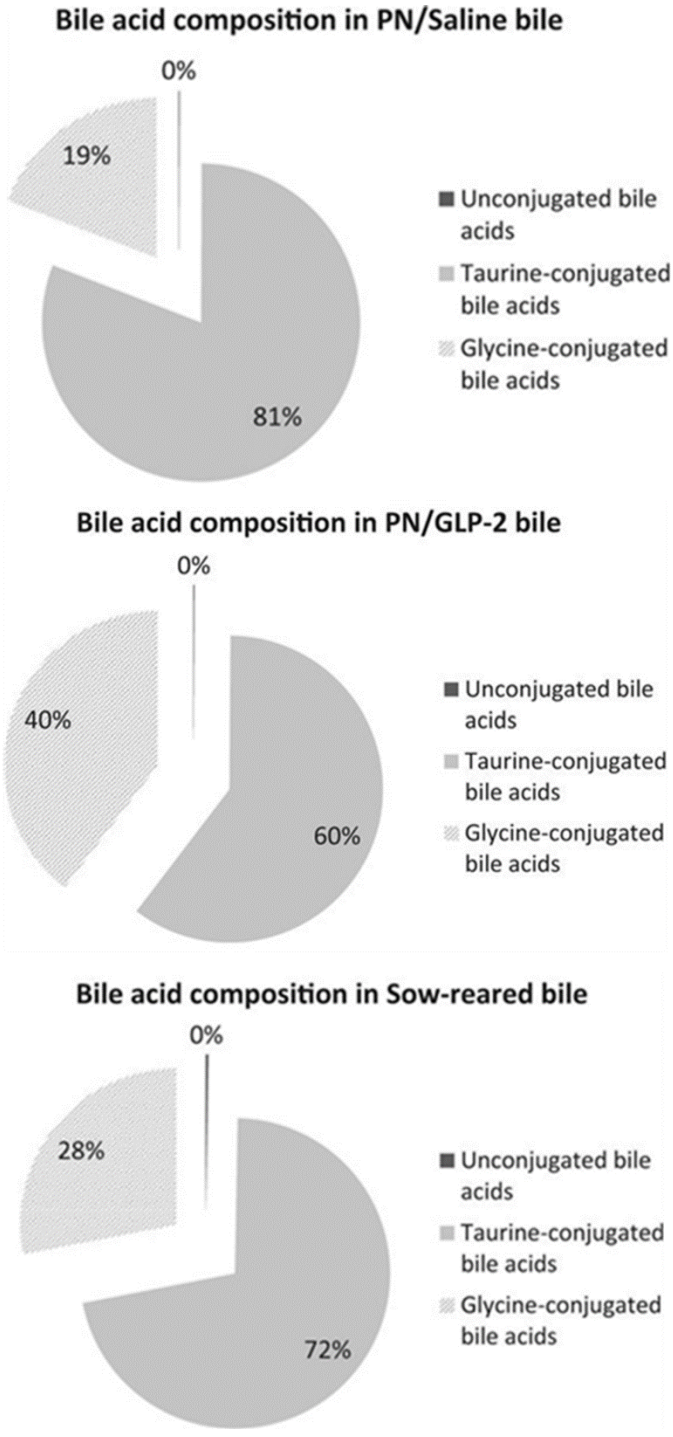

Figure A2-6. Bile acid composition in bile.

A2.3.6. Individual bile acid species in bile

Porcine bile is composed of 7 conjugated bile acids, of which the 3 main ones are hyodeoxycholic acid (HDCA), hyocholic acid (HCA, unique to pig bile), and chenodeoxycholic acid (CDCA) [24]. Using commercially available standards, we were able to measure these 3 bile acids and their taurine and glycine conjugates (designated t- and g-, respectively). The amount of unconjugated HCA, CDCA, and HDCA in our bile samples was virtually negligible in comparison to the amount of their corresponding taurine and glycine conjugates (**Table A2-1**). Consistent with a decreased bile acid pool in the PN-fed setting, the Sowreared group had significantly greater HCA ($P < .002$), t-HCA ($P< .005$), CDCA ($P < .0001$), t-CDCA ($P < .001$), g-CDCA ($P <.004$), g-HDCA ($P < .002$), and t-HDCA (or t-UDCA, tauroursodeoxycholic acid) ($P < .002$) than both PN-fed groups. Among the PN-fed groups, t-HCA was the most abundant bile acid, ranging from 100 to 500 mcg mL^{-1} of bile. There was, however, significantly less t-HCA in the PN/GLP-2 group compared with the PN/Saline group (157.6 vs 485.9 mcg mL^{-1} [**Table A2-1**]; $P =.02$). The taurine and glycine conjugates of CDCA and HDCA were less abundant in the bile of PN-fed pigs, ranging from 10 to 100 mcg mL^{-1}, and there was no difference in their amounts between the PN/Saline and the PN/GLP-2 groups (**Table A2-1**).

We also measured the amount of cholic acid (CA; a major component of bile in most other animals but found in small amounts or absent in pig) [24], lithocholic acid (LCA), and their conjugates. Unconjugated CA and g-CA were not detectable in our porcine bile samples. There was a relatively small amount of t-CA detected in our samples, ranging from 20 to 50 mcg mL^{-1}, with the Sow-reared group having relatively greater amounts of t-CA than the PN/GLP-2 group (46.8 *vs* 24.0 mcg mL^{-1} [**Table A2-1**], $P = .04$). Very small amounts of LCA (range, 0.08-0.12

mcg mL^{-1}), t-LCA (range, 0.12-2 mcg mL^{-1}), and g-LCA (range, 0.12-1 mcg mL^{-1}) were detected (Table A2-1). Despite these small amounts, the Sow-reared group had greater amounts of t-LCA ($P < .005$) and g-LCA ($P < .002$) compared with both total PN-fed groups. Furthermore, the PN/GLP-2 group had significantly less t-LCA ($P < .01$) and g-LCA ($P < .004$) than the PN/Saline group (Table A2-1). We did not detect any unconjugated or conjugated forms of deoxycholic acid (DCA), ursodeoxycholic acid (UDCA), and α-, β- and ω-muricholic acid (MCA) in pig bile, for which commercially available standards were purchased.

A2.3.7. Rates of biliary output of bile acid species

Using our previously reported bile flows [9], we were able to estimate the biliary output for our recovered bile acid species. As in the previous paper, the calculation of bile acid flow has been scaled for liver size. Compared with both PN-fed groups, the Sow-reared group had significantly greater rates of biliary excretion for all bile acid species (Table A2-2). The PN/GLP-2 group had increased biliary output of glycine-conjugated bile acids ($P = .028$) and the following bile acid species compared with the PN/Saline group: g-CDCA ($P = .015$), HDCA ($P = .01$), and a trend toward increased LCA excretion ($P = .08$).

Table A2-2. Estimated rates of biliary output for bile acid species.

Excretion Type	PN/Saline[a]	PN/GLP-2[b]	Sow-Reared[c]	P Value
Bile acid excretion				
Total bile acids	571.17 (384.87)	899.70 (384.02)	30962.52 (10079.77)	.0004[ac,bc]
Total taurine-conjugated bile acids	453.95 (330.52)	604.82 (373.56)	21877.08 (6049.97)	.0005[ac,bc]
Total glycine-conjugated bile acids	116.69 (97.28)	293.92 (164.85)	8996.52 (5119.17)	.0002[ab,ac,bc]
Total unconjugated bile acids	1.56 (1.39)	5.06 (5.34)	240.76 (114.28)	.0004[ac,bc]
Individual excretion				
Hyocholic acid (HCA)	0.37 (0.52)	0.51 (0.30)	86.22 (46.35)	.0003[ac,bc]

Tauro-hyocholic acid (t-HCA)	337.37 (241.36)	391.84 (284.58)	12074.57 (3865.14)	.0006[ac,bc]
Chenodeoxycholic acid (CDCA)	0 (0)	0 (0)	1.01 (0.56)	<.0001[ac,bc]
Tauro-chenodeoxycholic acid (t-CDCA)	67.11 (56.69)	130.01 (64.11)	4327.74 (1417.90)	.0003[ac,bc]
Glyco-chenodeoxycholic acid (g-CDCA)	45.07 (36.94)	172.79 (157.99)	4221.08 (2093.25)	.0002[ab,ac,bc]
Hyodeoxycholic acid (HDCA)	0.058 (0.038)	0.21 (0.13)	0.84 (0.27)	.0001[ab,ac,bc]
Glyco-hyodeoxycholic acid (g-HDCA)	71.41 (61.29)	120.75 (62.32)	4768.01 (3102.66)	.0003[ac,bc]
Tauro-hyodeoxycholic acid (t-HDCA) or tauro-ursodeoxycholic acid (t-UDCA)	20.90 (16.32)	28.79 (21.94)	5035.42 (2376.58)	.0005[ac,bc]
Taurocholic acid (t-CA)	28.27 (26.38)	53.83 (44.77)	424.91 (131.60)	.0005[ac,bc]
Lithocholic acid (LCA)	0.10 (0.087)	0.24 (0.19)	0.84 (0.25)	.0003[ac,bc]
Tauro-lithocholic acid (t-LCA)	0.30 (0.27)	0.35 (0.28)	14.44 (7.23)	.0005[ac,bc]
Glyco-lithocholic acid (g-LCA)	0.21 (0.14)	0.38 (0.25)	7.43 (2.79)	.0003[ac,bc]

GLP-2, glucagon-like peptide-2; PN, parenteral nutrition. The calculation of bile acid flow is made using our previously reported bile flows [9]. The calculation of bile acid flow has also been scaled for liver size, as in the previous paper. Values represent means (nanogram per gram of liver) and standard deviation (in parentheses). Superscripts refer to statistically significant differences.

A2.3.8. Liver bile acid concentration and content

There was a significant difference in liver bile acid concentration (P = .018), with the Sow-reared group (38.2 nmol g^{-1} protein) having a greater liver bile acid concentration than both PN-fed groups but no difference between the PN/Saline (29.6 nmol g^{-1} protein) and PN/GLP-2 (30.4 nmol g^{-1} protein) groups (**Figure A2-7A**). In contrast, the PN/GLP-2 group had a significantly greater liver total bile acid content (1623 nmol kg^{-1} body weight) compared with both the PN/Saline and Sow-reared groups (P < .001) (**Figure A2-7B**). There was no difference in the liver total bile acid content between the PN/Saline (1197 nmol kg^{-1} body weight) and Sow-reared (987 nmol kg^{-1} body weight) groups.

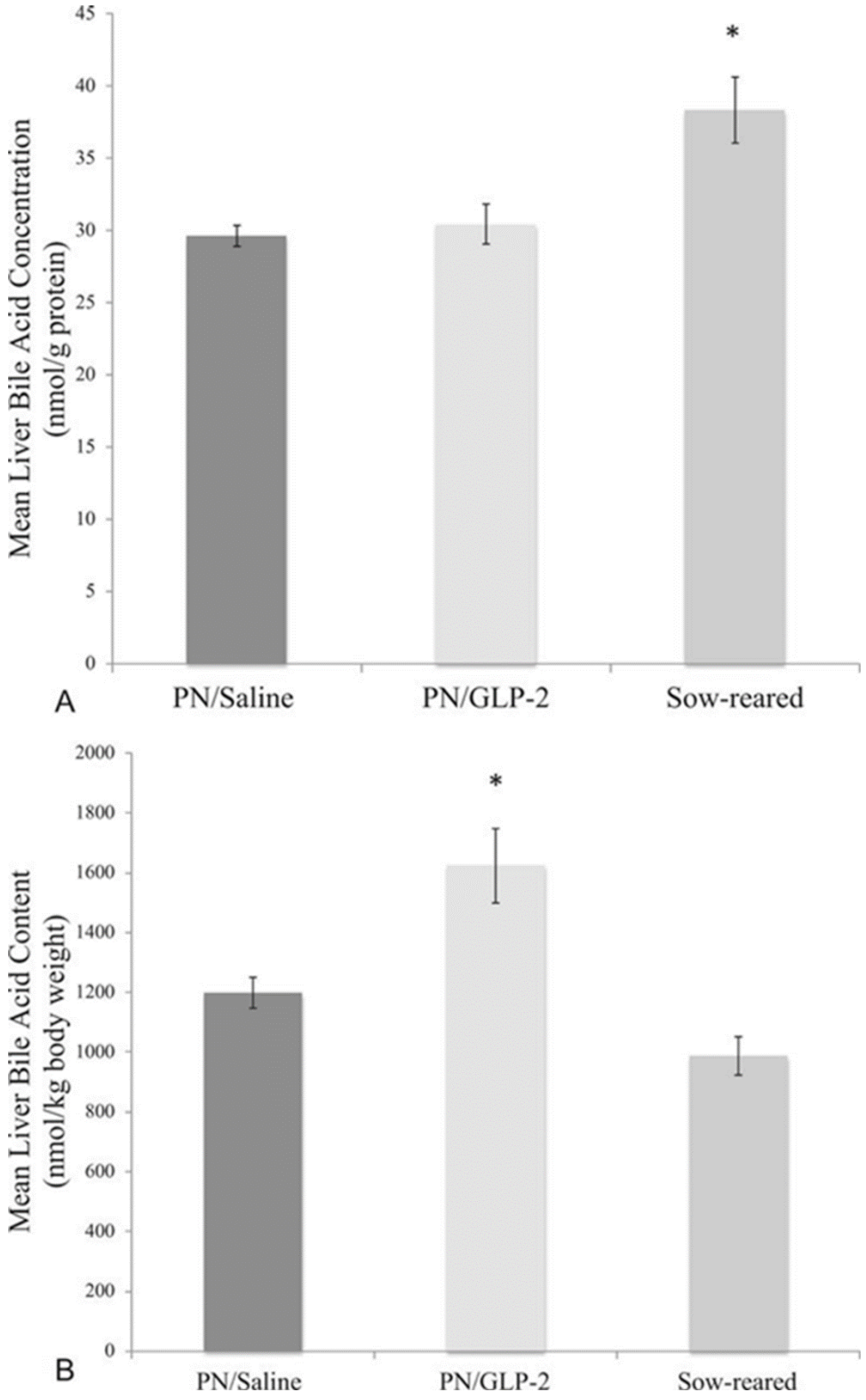

Figure A2-7. (A) Mean liver total bile acid concentration; (B) Mean liver total bile acid content.

A2.4. Discussion

PNALD remains a significant complication for infants needing long-term PN therapy [2]. The exact cause of PNALD remains undefined, but recurrent infection and sepsis and lipid emulsions that are plant-based have been long known to be significant risk factors [5]. The transition to lipid emulsions that are fish oil based and high in ω-3 polyunsaturated fats is an emerging, promising therapeutic strategy [25]. Despite this, the cellular and molecular mechanisms underlying PNALD remain ill-defined and, perhaps consequently, there have been limited effective therapeutic options. Our group recently reported the novel finding that intravenous GLP-2 therapy in our preclinical neonatal model of PNALD improved bile flow, reduced serum markers of cholestasis (total bilirubin and alkaline phosphatase levels), and decreased evidence of cholestatic pigmentation on liver histologic analysis [9]. We had posited potential mechanisms for our observations, the subject of which is the focus of the present study. The fact that neonatal PNALD begins largely as a cholestatic disease, with eventual steatosis, has led to the hypothesis that, similar to other cholestatic diseases such as nonalcoholic fatty liver disease, perturbations in bile acid homeostasis may underlie the pathogenesis of PNALD and represent potential therapeutic targets [1]. If this was the case, then perhaps our observations of an improved clinical phenotype with GLP-2 therapy may mechanistically involve alterations in bile acid synthesis and transport within the liver.

Our first evidence in support of this hypothesis relates to the increased expression of FXR, the major bile acid homeostatic regulator, with GLP-2 therapy over saline control (**Figure A2-2**). FXR, in turn, directly regulates the expression of genes involved in both bile acid synthesis and transport. Regarding transport, we observed a significant increase in MRP2 expression and a trend toward increased BSEP expression with GLP-2 therapy over saline control, both of which are directly

stimulated by FXR (**Figure A2-3**). More important, we observed an up-regulation in the expression of basolateral bile acid transporters, which help expel toxic bile acids into the systemic circulation in the setting of cholestasis. Indeed, there was a significant increase in MRP3, OSTA, and OSTB expression in both PN-fed groups compared with Sow-reared piglets (**Figure A2-3**). However, GLP-2 therapy further augmented MRP3 expression over saline control, with a trend also toward increased OSTB expression. Together, these results suggest mechanisms at the transcriptional level that may mediate increased bile acid export with GLP-2 therapy, into both bile and the systemic circulation. The setting of cholestasis is known to down-regulate the expression of MRP2 [26], and so an increase in its expression with GLP-2 therapy may mediate the maintenance or improvement of bile flow. This may be beneficial since there was no difference in *ABCB11* (BSEP) expression between the PN/Saline and PN/GLP-2 groups (only a trend) and if BSEP has hypothetically reached its maximal velocity (Vmax) in enzymatic activity. Increased bile acid export into the systemic circulation may also explain why both PN-fed groups had similar concentrations of serum bile acids in our previous report (**Table A2-1**) [9]. We initially expected the PN/Saline group to have a higher serum bile acid level than the PN/GLP-2 group, given the improvement in cholestasis with GLP-2 therapy. We can now surmise that one possible reason that the PN/GLP-2 group had a similar serum bile acid level as the PN/Saline group was due to an increase of bile acid efflux into the systemic circulation, as suggested by our transcriptomic data.

Regarding bile acid synthesis, we first found an increase in the expression of CYP7A1 with GLP-2 therapy over saline control (**Figure A2-2**). This would suggest increased bile acid synthesis, an unexpected finding given that the increased expression of FXR in the PN/GLP-2 group should have down-regulated the expression of CYP7A1. However, the regulation of CYP7A1 is complex and implicates both activators (HNF4α, LRH-1) and repressors (FXR, FGF-19 via FGFR4,

pregnane X receptor [PXR], and peroxisome proliferator-activated receptor α [PPARα]) (**Figure A2-1B**) [27]. Given the paradoxical increase in CYP7A1 expression despite increased FXR expression with GLP-2 therapy, we hypothesized that activating factors were potentially outcompeting FXR repression. We found some evidence of this, in that LRH-1 expression was significantly increased with GLP-2 therapy over saline control, and a trend toward increased HNF4α expression in the PN/GLP-2 group over the PN/Saline group (**Figure A2-4**). Furthermore, the repressive effects of FXR on CYP7A1 expression are indirect, mediated by SHP, and we found a trend toward increased SHP expression in the PN/Saline group compared with the PN/GLP-2 group and not vice versa. It has also been suggested in the literature that hepatic FXR does not regulate hepatic CYP7A1 but, rather, it is intestinal FXR that regulates hepatic CYP7A1 via induction of the FGF-19/FGFR4 pathway, which adds further complexity.28 LXRα is another known regulator of CYP7A1 expression that is species-specific. In rodents, which have the LXRα response element in the *CYP7A1* promoter, LXRα has a significant activating effect [27]. In higher animals, this element is either missing (rabbits and humans, and presumably pigs) or present and nonfunctional (hamsters); in humans in particular, LXRα has been shown to have a repressive effect on *CYP7A1* expression [27, 29]. We found a significant increase in LXRα expression with GLP-2 therapy (**Figure A2-4**), which in pigs, similar to humans, would have either a non-stimulatory or a repressive effect. Together, these results highlight the complexity under which *CYP7A1* expression is regulated and reveal some insight into why CYP7A1 expression was up-regulated with GLP-2 therapy, despite increased FXR expression. Regarding other key bile acid synthetic enzymes, we found no difference in CYP27A1 expression, which suggests that the alternative bile acid synthesis pathway is not implicated in the GLP-2-mediated improvement in cholestasis. There was also no difference in CYP8B1 expression, although the C(t) values for the

CYP8B1 quantitative PCR assay were relatively high (around 32) and needed greater amounts of complementary DNA, indicating a relatively low abundance of the *CYPB1* mRNA transcript.

The profiling of bile acid species in bile provides further insight into the improvement of PNALD with GLP-2 treatment. First, it is well known that PN decreases the bile acid pool, and this is observed in the total amount of bile acids in our PN-fed groups compared with healthy, sow-reared piglets, in both bile and plasma (**Table A2-1**). Most bile acids present in bile are conjugated with either taurine or glycine to reduce their hepatotoxicity, and this is reflected in our data, as the quantity of unconjugated bile acids in all groups was virtually negligible (**Table A2-1**). Taurine conjugates comprise the majority of conjugated bile acids in pigs [24], which was also observed in our data; however, while there was no difference in glycine conjugates between groups, GLP-2 therapy was associated with a decrease in the concentration of taurine-conjugated bile acids compared with saline control (**Table A2-1**). This may reflect either decreased synthesis (which would contradict our finding of increased CYP7A1 expression) or decreased taurine conjugation or a decreased proportion of taurine-conjugated bile acids being excreted into bile, perhaps owing to a larger proportion being secreted into the systemic circulation (which would parallel our findings of increased *MRP3* and *OSTB* [trend only] expression). Upon further inspection, it becomes clear that most of this decrease in taurine conjugates in the PN/GLP-2 group involves t-HCA, the most abundant bile acid in our pig bile (**Table A2-1**). While relatively less abundant than t-HCA, conjugated CDCA or HDCA was not different between groups. LCA is the least abundant bile acid, which is not surprising because it is the most hydrophobic and thus most hepatotoxic.30 Most of the LCA was present as a taurine conjugate, followed by its glycine conjugate and finally a very small quantity of unconjugated LCA (**Table A2-1**).

Interestingly, we found that GLP-2 therapy was associated with a decreased concentration of both t-LCA and g-LCA compared with saline control. This suggests that the processes governing the generation of toxic LCA may be affected by GLP-2 therapy. LCA is formed from 7-dehydroxylation of bile acids by colonic bacteria, and the input of LCA from the large intestine can increase when there is either an increased amount of precursor bile acid or increased microbial 7-dehydroxylation activity.31 LCA is formed from CDCA or UDCA in animals with a cecum.32 Since there was no difference in CDCA concentrations between our PN-fed groups, and UDCA was not even detected in our pig bile samples, we are left to hypothesize that differences in LCA between groups were due to differences in microbial 7-dehydroxylation activity.

We hypothesize that microbial populations can be differentially affected with PN therapy and GLP-2 treatment. PN and the fasted state are associated with intestinal hypoplasia and weakening of the intestinal barrier, with predisposition for bacterial translocation, subsequent inflammation, and ensuing sepsis [33]. Infants with SBS, who are most likely to receive long-term PN therapy, are also at significant risk for small intestinal bacterial overgrowth [34]. GLP-2, in contrast, has known enteric anti-inflammatory activity and strengthens the intestinal barrier [10, 33, 35]. Both these scenarios (PN *vs.* GLP-2) may therefore favor the differential growth of bacteria and the abundance of t- and g-LCA in our groups given saline *vs* GLP-2 treatment may be a reflection of differential bacterial populations. Furthermore, we administered 2 rounds of antibiotics to the PN-fed piglets in order to prevent line sepsis, which piglets receiving long-term PN are prone to develop. The administration of antibiotics will also have an impact on the intestinal microbiome in our studies. The impact of PN therapy and exogenous manipulations such as GLP-2 therapy, administration of different lipid emulsions, and antibiotic therapy on the intestinal microbiome in our translational animal model will be the subject of a separate publication.

Using our previously reported bile flow measurements, we were able to estimate the rate of biliary output for each bile acid species (**Table A2-2**). Not surprisingly, the Sow-reared group had higher bile acid excretion rates than both PN-fed groups. Interestingly, although GLP-2 therapy increased bile flow, it did not systematically increase the excretion rate of all bile acids, namely glycine-conjugated bile acids (especially g-CDCA), and unconjugated HDCA. The liver bile acid concentration and liver total bile acid content are also important elements of the bile acid homeostasis equation. We found that the Sow-reared group had higher liver bile acid concentrations than both PN-fed groups but there was no difference between the PN/Saline and PN/GLP-2 groups (**Figure A2-7A**). However, the PN/GLP-2 group had a greater liver total bile acid content compared with both PN/Saline and Sow-reared groups (**Figure A2-7B**), driven by the greater liver weights in that group as previously published [9]. In our previous report, we expressed the liver weight in absolute terms, yet the Sowreared piglets had greater body weights than the PN groups. When liver weights are scaled for body weights, one can further appreciate the hepatomegaly effect of total PN itself and the additional trophic effect of GLP-2: 40.42±3.95 g kg^{-1} (PN/Saline) versus 53.07±5.66 g kg^{-1} (PN/GLP-2) versus 25.73±1.34 g kg^{-1} (Sow-reared). Interestingly, the PN/Saline group did not have a significantly greater liver total bile acid content compared with the Sow-reared group. Given the increase in liver size with GLP-2 treatment, and in light of the increase in CYP7A1 gene expression, one hypothesis may be that GLP-2 triggers bile acid synthesis and this signals hepatic growth via protein synthesis.36 Furthermore, our previous report did not observe an increase in Ki67 labeling as evidence for cell proliferation. It is important to note that normally, the bile acid content in liver constitutes only 5% of the bile acid pool [36]. While PN may decrease the overall bile acid pool, GLP-2 treatment may stimulate the synthesis of more hepatoprotective bile acids in the liver, which may be the signal for increased

hepatic growth rather than cellular proliferation [36]. In pig, the more hepatoprotective bile acids, and thus more hydrophilic bile acids, are DCA and HDCA. Our hypothesis remains a speculation as we did not perform profiling of bile acids in liver tissue, nor did we see evidence of increased DCA and HDCA in our pig bile with GLP-2 therapy.

The transcriptomic data and bile acid profiles have provided insight regarding how bile acid metabolism is altered with GLP-2 therapy, favoring an improved clinical phenotype in PNALD. Future work will be aimed at identifying the signal to the liver that links GLP-2 therapy and alterations in bile acid transport and synthesis pathways. The link is hypothesized to exist because the GLP-2 receptor is not expressed on hepatocytes or nonparenchymal cells of the liver but is expressed along the intestine, confined to enteric neurons, enteroendocrine cells, and pericryptal subepithelial myofibroblasts [37, 38]. Many believe that the FGF-19/FGFR4 axis may represent the pertinent signal to the liver [13, 14]. Via the enterohepatic circulation, bile acids activate intestinal FXR, which induces ileal FGF-19 expression; FGF-19 in turns activates the FGFR4 receptor on hepatocytes, which represses CYP7A1 via c-Jun-N-terminal kinase [14, 28]. We attempted to measure plasma FGF-19 levels using commercially available porcine-specific FGF-19 ELISA assays from both Cusabio Biotech Co Ltd (Wuhan, Hubei, China) and MyBioSource (San Diego, CA, USA), but FGF-19 could not be detected in many samples. We consequently elected to measure the expression of *FGFR4*, and its cofactor, *KLB*, in liver and saw that both PN-fed groups had significantly increased FGFR4 expression over healthy, sow-reared piglets (**Figure A2-4**). In addition, GLP-2 therapy further augmented *FGFR4* expression and tended to increase *KLB* expression, over saline control, which adds evidence to the possible role of the FGF-19/FGFR4 pathway in PNALD and may be the link between GLP-2 therapy and the liver.

The data we have presented add to the emerging evidence of altered hepatic bile acid synthetic and transport pathways, but many interacting pathways and regulators have yet to be explored in PNALD. While bile acids are known to activate FXR, they also interact with other signal transduction pathways, such as the c-Jun N-terminal kinase (JNK) pathway, also known to mediate the downstream signaling of FGFR4 activation. Bile acids also activate other members of the nuclear receptor family, such as the pregnane X receptor (PXR) and the constitutive androstane receptor (CAR), both of which directly regulate *MRP3* expression. We also did not explore the bile acid conjugating enzymes, BACS (bile acid-CoA synthetase) and BAT (bile acid-CoA: amino acid N-acetyltransferase), or look at transporters that import bile acids into the liver from the portal circulation (NTCP, sodium-taurocholate cotransporting polypeptide). The exact magnitude and directions of alterations in bile acid synthetic and transport pathways under different conditions of PNALD also remain to be defined. For example, Pereira-Fantini *et al.* [13] recently reported perturbations in FXR signaling in a juvenile piglet model of intestinal failure–associated liver disease (without PN). Vlaardingerbroek and colleagues [12] recently investigated similar alterations in bile acid homeostasis in a similar preterm piglet model of PNALD. Interestingly, the investigators found decreased *FXR* expression in all PN-fed pigs compared with pigs fed enterally, whereas we found no difference between our PN/Saline group and healthy, sow-reared pigs (**Figure A2-2**). Vlaardingerbroek *et al.* also found decreased *CYP7A1* expression but increased *CYP7A1* protein abundance in pigs fed PN with Intralipid (the equivalent of our PN/Saline group) compared with pigs fed enterally, whereas we found no difference in *CYP7A1* expression between the PN/Saline and the Sow-reared groups. These differences between studies may be specific to the animal model, preterm versus term piglet, and/or may reflect differences in experimental conditions. There are also clear differences between studies with regard to the reporting of bile

acid composition in bile. We were not able to detect UDCA or DCA and its conjugates or CA and g-CA in our pig bile, whereas both Pereira-Fantini *et al.* and Vlaardingerbroek *et al.* did; the reasons for these differences between studies may relate to methodological differences between study groups.

There are several limitations to our study method. First, our results are focused on a transcriptional analysis, and we acknowledge that protein abundance may not be reflected by transcriptomic results. With regard to our bile acid analysis, we did perform the quantification of g-HCA. The analyte of g-HCA was identified in this study based on the specific MRM (multiple reaction monitoring) transition data (464.3/74.0) and the comparison of retention time with GCA-d_4 (glycocholic acid-2,2,4,4; a deuterated internal standard), but due to the lack of an available corresponding standard, quantitative information could not be obtained. In addition, we could not differentiate accurately between t-HDCA and t-UDCA for the peak detected under their mass transition due to the lack of commercially available reference standards for these compounds, which is why we have labeled this bile acid as "t-HDCA or t-UDCA." However, given that we were able to detect both unconjugated HDCA and g-HDCA and failed to detect any UDCA or g-UDCA in our samples (for which we had standards), we believe this bile acid is most likely t-HDCA. Regarding our gene expression data, we acknowledge that increased *MRP3* expression may represent a canalicular MRP3 (which exports phospholipids into bile) and/or the basolateral MRP3, which exports bile acids into the systemic circulation. In the setting of PNALD, we expect the increased *MRP3* expression associated with GLP-2 therapy to be likely basolateral MRP3; however, we did not confirm this with immune-histochemical analysis.

A2.5. Conclusions

We report the novel finding that exogenous GLP-2 administration in a neonatal piglet model of PNALD alters bile acid synthesis and transport pathways, which may mediate the GLP-2-associated improvement in cholestasis. The transcriptomic results do reveal some mechanisms at the transcriptional level acting to decrease bile acid synthesis (increased FXR, FGFR4 expression); however, we found that GLP-2 increases CYP7A1 expression and thus bile acid synthesis. Regarding transport, GLP-2 increases bile acid export from the liver via the increased expression of MRP2 and MRP3 and a trend toward increased BSEP and OSTB. The bile acid profiles in the bile reveal a decrease in taurine-conjugated bile acids, possibly secondary to increased excretion into the systemic circulation, and a decrease in the abundance of toxic lithocholic acid with GLP-2 therapy. GLP-2 treatment is associated with increased liver weight and a greater bile acid content in the liver. Altogether, our data suggests that GLP-2 may improve PNALD by the following, which lays foundation for future work: (1) improving bile flow, (2) increasing the excretion of toxic bile acids (either in bile or into the systemic circulation), and (3) perhaps stimulating the synthesis of more hepatoprotective bile acids in liver, which in turn stimulates liver growth. By providing evidence that GLP-2 therapy alters bile acid homeostatic pathways in ways that benefit PNALD, GLP-2 may potentially have a role in the armamentarium against PNALD. This would be especially pertinent for infants with SBS, who make up a large proportion of patients dependent on long-term PN therapy, where GLP-2 may therefore have dual benefit.

Supplementary Material

Supplementary material for this article is available on the Journal of Parenteral and Enteral Nutrition website at http://jpen.sagepub.com/supplemental.

A2.6. References

[1] D.G. Burrin, K. Ng, B. Stoll, M. Saenz de Pipaon, Impact of new-generation lipid emulsions on cellular mechanisms of parenteral nutrition-associated liver disease, Adv Nutr. 5 (2014) 82-91.

[2] S.J. Rangel, C.M. Calkins, RA. Cowles, D.C. Barnhart, E.Y. Huang, F. Abdullah, M.J. Arca, D.H. Teitelbaum, Parenteral nutrition-associated cholestasis: an American Pediatric Surgical Association Outcomes and Clinical Trials Committee systematic review, J Pediatr Surg. 47 (2012) 225-240.

[3] R.H. Squires, C. Duggan, D.H. Teitelbaum, P.W. Wales, J. Balint, R. Venick, S. Rhee, D. Sudan, D. Mercer, J.A. Martinez, B.A. Carter, Natural history of pediatric intestinal failure: initial report from the Pediatric Intestinal Failure Consortium. J Pediatr. 161 (2012) 723-728.

[4] I.R. Diamond, A. Sterescu, P.B. Pencharz, J.H. Kim, P.W. Wales, Changing the paradigm: omegaven for the treatment of liver failure in pediatric short bowel syndrome, J Pediatr Gastroenterol Nutr. 48 (2009) 209-215.

[5] E.M. Tillman, Review and clinical update on parenteral nutrition-associated liver disease, Nutr Clin Pract. 28 (2013) 30-39.

[6] B.A. Carter, R.J. Shulman, Mechanisms of disease: update on the molecular etiology and fundamentals of parenteral nutrition associated cholestasis, Nat Clin Pract Gastroenterol Hepatol. 4 (2007) 277-287.

[7] Z.W. Xu, Y.S. Li, Pathogenesis and treatment of parenteral nutrition-associated liver disease, Hepatobiliary Pancreat Dis Int. 11 (2012) 586-593.

[8] P.W. Wales, N. Allen, P. Worthington, D. George, C. Compher, D. Teitelbaum, A. Malone, T. Jaksic, P. Ayers, A. Baroccas, P.S. Goday, ASPEN clinical guidelines: support of pediatric patients with intestinal failure at risk of parenteral nutrition-associated liver disease, JPEN J Parenter Enteral Nutr. 38(2014) 538-557.

[9] D.W. Lim, P.W. Wales, J.K. Josephson, P.N. Nation, P.R. Wizzard, C.M. Sergi, C.J. Field, D.L. Sigalet, J.M. Turner, Glucagon-like peptide 2 improves cholestasis in parenteral nutrition-associated liver disease, JPEN J Parenter Enteral Nutr. 40 (2016) 14-21.

[10] E. de Heuvel, L. Wallace, K.A. Sharkey, D.L. Sigalet, Glucagon-like peptide 2 induces vasoactive intestinal polypeptide expression in enteric neurons via phosphatidylinositol 3-kinase-γ signaling, Am J Physiol Endocrinol Metabol. 303 (2012) E994-E1005.

[11] G.W. Moran, C. O'Neill, J.T. McLaughlin, GLP-2 enhances barrier formation and attenuates TNFα-induced changes in a Caco-2 cell model of the intestinal barrier, Regul Pept. 178 (2012) 95-101.

[12] H. Vlaardingerbroek, K. Ng, B. Stoll, N. Benight, S. Chacko, L.A. Kluijtmans, W. Kulik, E.J. Squires, O. Olutoye, D. Schady, M.L. Finegold, New generation lipid emulsions prevent PNALD in chronic parenterally fed preterm pigs, J Lipid Res. 55(2014) 466-477.

[13] P.M. Pereira-Fantini, S. Lapthorne, S.A. Joyce, N.L. Dellios, G. Wilson, F. Fouhy, S.L. Thomas, M. Scurr, C. Hill, C.G. Gahan, P.D. Cotter, Altered FXR signaling is associated with bile acid dysmetabolism in short bowel syndrome-associated liver disease, J Hepatol. 61 (2014) 1115-1125.

[14] A.K. Jain, B. Stoll, D.G. Burrin, J.J. Holst, D.D. Moore, Enteral bile acid treatment improves parenteral nutrition-related liver disease and intestinal mucosal atrophy in neonatal pigs, Am J Physiol Gastrointest Liver Physiol. 302 (2012) G218-G224.

[15] L.J. Wykes, R.O. Ball, P.B. Pencharz, Development and validation of a total parenteral nutrition model in the neonatal piglet, J Nutr. 123 (1993) 1248-1259.

[16] M. Suri, J.M. Turner, D.L. Sigalet, P.R. Wizzard, P.N. Nation, R.O. Ball, P.B. Pencharz, P.L. Brubaker, P.W. Wales, Exogenous glucagon-like peptide-2 improves outcomes of intestinal adaptation in a distal-intestinal resection neonatal piglet model of short bowel syndrome, Pediatr Res. 76(2014) 370-377.

[17] T. Claudel, B. Staels, F. Kuipers, The farnesoid X receptor: a molecular link between bile acid and lipid and glucose metabolism, Arterioscler Thromb Vasc Biol. 25 (2005) 2020-2030.

[18] S. Modica, R.M. Gadaleta, A. Moschetta, Deciphering the nuclear bile acid receptor FXR paradigm. Nucl Recept Signal. 8 (2010) e005.

[19] B. Goodwin, M.A. Watson, H. Kim, J. Miao, J.K. Kemper, S.A. Kliewer, Differential regulation of rat and human CYP7A1 by the nuclear oxysterol receptor liver X receptor-alpha,

Mol Endocrinol. 17 (2003) 386-394.

[20] N. Pean, I. Doignon, I. Garcin, A. Besnard, B. Julien, B. Liu, S. Branchereau, A. Spraul, C. Guettier, L. Humbert, K. Schoonjans, The receptor TGR5 protects the liver from bile acid overload during liver regeneration in mice, Hepatology. 58 (2013) 1451-1460.

[21] H. Duboc, Y. Tache, A. Hofmann, The bile acid TGR5 membrane receptor: from basic research to clinical application, Dig Liv Dis. 46 (2014) 302-312.

[22] J.I. Yang, J.H. Yoon, S.J. Myung, G.Y. Gwak, W. Kim, G.E. Chung, S.H. Lee, S.M. Lee, C.Y. Kim, H.S. Lee, Bile acid-induced TGR5-dependent c-Jun-N terminal kinase activation leads to enhanced caspase 8 activation in hepatocytes, Biochem Biophys Res Commun. 361 (2007) 156-161.

[23] V. Keitel, R. Reinehr, P. Gatsios, C. Rupprecht, B. Görg, O. Selbach, D. Häussinger, R. Kubitz, The G-protein coupled bile salt receptor TGR5 is expressed in liver sinusoidal endothelial cells, Hepatol. 45 (2007) 695-704.

[24] J.T. Yen, (2001). Anatomy of the digestive system and nutritional physiology. *Swine Nutrition,* pp. 40-42. Boca Raton: Taylor & Francis.

[25] I.R. Diamond, A. Sterescu, P.B. Pencharz, J.H. Kim, P.W. Wales, Changing the paradigm: omegaven for the treatment of liver failure in pediatric short bowel syndrome, J Pediatr Gastroenterol Nutr. 48 (2009) 209-215.

[26] M.G. Donner, D. Keppler, Up-regulation of basolateral multidrug resistance protein 3 (Mrp3) in cholestatic rat liver, Hepatology. 34 (2001) 351-359.

[27] R.A. Davis, J.H. Miyake, T.Y. Hui, N.J. Spann, Regulation of cholesterol-7α-hydroxylase: BAREly missing a SHP. J Lipid Res. 43 (2002) 553-543.

[28] T. Ingaki, M. Choi, A. Moschetta, L. Peng, C.L. Cummins, J.G. McDonald, G. Luo, S.A. Jones, B. Goodwin, J.A. Richardson, R.D. Gerard, Fibroblast growth factor 15 functions as an enterohepatic signal to regulate bile acid homeostasis, Cell Metab. 2 (2005) 217-225.

[29] D.W. Russell, The enzymes, regulation, and genetics of bile acid synthesis, Ann Rev Biochem. 72 (2003) 137-174.

[30] C. Thomas, R. Pellicciari, M. Pruzanski, J. Auwerx, K. Schoonjans, Targeting bile-acid signaling for metabolic diseases, Nat Rev Drug Dis. 7 (2008) 678-693.

[31] A.F. Hofmann, L.R. Hagey, (1998). Bile acids and intestinal bacteria. *Gut and the Liver,* pp. 85-102. Lancaster: Kluwer Academic.

[32. A.F. Hofmann, Detoxification of lithocholic acid, a toxic bile acid: relevance to drug hepatotoxicity, Drug Met Revs. 36 (2004) 703-722.

[33] W.T. Chance, T. Foley-Nelson, I. Thomas, A. Balasubramaniam, Prevention of parenteral nutrition–induced gut hypoplasia by coinfusion of glucagonlike peptide-2, Am J Physiol. 273 (1997) G559-G563.

[34] J.K. DiBaise, R.J. Young, J.A. Vanderhoof, Enteric microbial flora, bacterial overgrowth, and short-bowel syndrome, Clin Gastroenterol Hepatol. 4 (2006) 11-20.

[35] G.J. Kouris, Q. Liu, H. Rossi, G. Djuricin, P. Gattuso, C. Nathan, R.A. Weinstein, R.A. Prinz, The effect of glucagon-like peptide 2 on intestinal permeability and bacterial translocation in acute necrotizing pancreatitis, Am J Surg. 181 (2001) 571-575.

[36] W.D. Chen, Y.D. Wang, Z. Meng, L. Zhang, W. Huang, Nuclear bile acid receptor FXR in the hepatic regeneration, Biochim Biophys Acta. 1812 (2011) 888-892.

[37] D.J. Drucker, B. Yusta, Physiology and pharmacology of the enteroendocrine hormone glucagon-like peptide 2, Annu Rev Physiol. 76 (2014) 561-563.

[38] D.L. Sigalet, Nonruminant nutrition symposium: the role of glucagon-like peptide-2 in controlling intestinal function in human infants: regulator or bystander? J Anim Sci. 90 (2012) 1224-1232.

Appendix 3*

Lysosomotropic Agents Selectively Target Chronic Lymphocytic Leukemia Cells due to Altered Sphingolipid Metabolism

A3.1. Introduction

One of the major problems in cancer therapy is drug toxicity. Despite therapies designed to target cancer cells, many of the standard therapies are also toxic to normal cells. This is also the case in Chronic Lymphocytic Leukemia (CLL). CLL is a common leukemia and is characterized by the accumulation of abnormal monoclonal B cells. Typically the disease is divided into those with mutated IgV_H and those with un-mutated IgV_H. When treatment is required, the standard initial therapy is chemoimmunotherapy typically using a combination of fludarabine, cyclophosphamide, and rituximab (FCR) [1, 2]. In addition, the targeted kinase inhibitors ibrutinib and idelalisib have shown effectiveness; however, dose reductions, toxicities, and drug resistance remain problems [3, 4]. The type II monoclonal anti-CD20 antibody obinutuzumab has also shown effectiveness in treating CLL, and in combination with chlorambucil has become a standard regimen for patients unable to receive FCR [5, 6]. The increased efficacy of obinutuzumab (formerly GA101) compared to rituximab could be attributed to its unique ability to enter and lyse lysosomes in CLL cells [7, 8]. Thus, lysosomes could be a target for CLL therapy.

A novel therapeutic approach demonstrated in other cancer is the induction of lysosome membrane permeabilization (LMP). This has been investigated in breast cancer [9, 10], colon

* This appendix has been published as R.F. Dielschneider, H. Eisenstat, S. Mi, J.M. Curtis, W. Xiao, J.B. Johnston, S.B. Gibson, "Lysosomotropic Agents Selectively Target Chronic Lymphocytic Leukemia Cells Due to Altered Sphingolipid Metabolism", *Leukemia*, 30 (2016) 1290-1300. I performed the HPLC analysis of sphingolipids, collected and analyzed the data, interpretation of the sphingolipid composition in the cell samples, and revised the manuscript.

cancer [9, 11, 12], and acute myeloid leukemia (AML) [13]. Lysosomes are acidic membrane-bound organelles within the cytoplasm of all cells and are responsible for the degradation and recycling of many cellular components. Despite the ubiquitous nature of lysosomes in all mammalian cell types, these structures seem to be altered during the cancerous transformation of cells. Thus, disruption of lysosomes may preferentially induce cell death in cancer cells, as compared to normal cells. The literature has proposed numerous reasons for this cancer cell selectivity such as down-regulation of lysosome-associated membrane proteins 1 and 2 (LAMP-1 and 2) [9] altered localization of heat shock protein 70 (HSP-70) [12, 14], and down-regulation of acidic sphingomyelinase (ASM) [15, 16]. The latter study showed altered sphingolipid metabolism in cancer cells, and how the exploitation of this alteration is a viable therapeutic approach.

There are several reports that suggest alterations in sphingolipid metabolism in CLL. First, CLL cells have increased rigidity [17] that might be caused by high levels of sphingolipids [18, 19]. Secondly, many CLL cells have increased fragility, as demonstrated by the increased number of smudge cells observed in peripheral blood morphology [20]. Increased membrane fragility can be caused by high levels of sphingolipids [18]. Lastly, CLL cells exhibit constitutive signaling in many pathways requiring lipid rafts [21]. Since sphingolipids are prominent and vital membrane components in lipids rafts [22], altered sphingolipid metabolism could alter signaling in CLL.

Although numerous reports have suggested that sphingolipid metabolism is altered in CLL cells, there still lacks concrete evidence for altered sphingolipid metabolism and altered sphingolipid levels in this disease. Furthermore, little is known about lysosomes in CLL cells and whether these cells are selectively susceptible to lysosome disruption. Thus, in the present study we have investigated lysosome-targeting drugs, herein referred to as lysosomotropic agents, which are under clinical investigation or clinically used for other functions as a potential therapeutic

strategy in CLL cells, and examined the role of sphingolipid metabolism in this process.

A3.2. Materials and Methods

A3.2.1. Cell culture

Peripheral blood samples were collected from patients following informed consent in accordance with the Research Ethics Board at the University of Manitoba. Samples were mixed with RosetteSep (Stemcell Technologies) if the lymphocyte count was less than $40\times109\ L^{-1}$ and then purified on a Ficoll-Paque gradient (GE Healthcare). Red blood cells (RBCs) were lysed with RBC lysis buffer (eBioscience). All blood samples were processed within 24 hours after collection and used fresh. For experiments, the leukemia cells were grown in Hybridoma serumfree medium with glutamine (SFM, Life Technologies). Data for all patient samples used in this study can be seen in Supplemental Table A3-1. Patient samples were only excluded from the study based on low cell yield after processing or low viability. Samples were randomly used for different experiments; no selection occurred. Lab personnel were blinded to patient characteristics until after all experiments had been performed.

The human bone marrow-derived stromal cell line HS-5 (obtained as a kind gift from Dr. Peng Huang, MD Anderson Cancer Centre) were cultured in DMEM with high glucose (Hyclone, GE Healthcare) and 10% fetal bovine serum (Hyclone, GE Healthcare) and 1X penicillin and streptomycin (Gibco, Life Technologies). Stromal cells were seeded at 5×104 cells per well of a 48-well plate 24 hours prior to addition of 5×106 CLL cells. This represents a 1:100 HS-5: CLL co-culture ratio. Co-cultures were maintained in a humid 37 ºC incubator for 24 hours prior to the addition of 5 μM siramesine. After 1 hour, CLL cells were collected and cell viability analysis was performed.

A3.2.2. Drugs and stimuli

Siramesine (kindly provided by Lundbeck) was dissolved in DMSO and kept at room temperature. Nortriptyline (Sigma) was dissolved in ethanol and stored at 4 ºC. Desipramine (Sigma) was dissolved in water and stored at 4 ºC. Fludarabine (Sigma) was dissolved in DMSO and frozen stocks were stored at -80 °C. Ciprofloxacin (Sigma) was dissolved in 1 mM acetic acid and stored at 4 °C. D-Sphingosine (Sigma) was dissolved in DMSO and stored in single-use aliquots at -20 ºC.

Various inhibitors were added 1 hour prior to drug treatment: α-tocopherol (Sigma) was dissolved in ethanol and prepared fresh for each experiment; lycopene (Sigma) was dissolved in ethanol; N-acetyl cysteine (NAC, Sigma) was dissolved in 1X phosphate-buffered saline (PBS) at pH 7.4 and made fresh for each experiment; Glutathione (Sigma) was dissolved in 1X PBS and made fresh for each experiment; Ca-074-Me (Enzo Life Sciences) was dissolved in DMSO; Chymostatin (Sigma) was dissolved in DMSO; E64 (Sigma) was dissolved in water; zVAD-fmk (Caspase Inhibitor VI, Millipore) was dissolved in DMSO; and SKI II (Sigma) was dissolved in DMSO. Unless preparations were made fresh, drug stocks were frozen at -20 °C. See Supplemental Tables A3-2, A3-3, and A3-4 for details on drugs and concentrations used.

A3.2.3. Western blotting

Cell lysates were collected at the indicated times in 1% NP-40 lysis buffer with complete protease inhibitor tablet (Roche), 1mM phenylmethanesulfonylfluoride (PMSF), and 2 mM sodium orthovanadate (New England BioLabs). Protein levels were quantified in triplicate with Pierce BCA kit (Thermo Scientific) according to manufacturer's instructions. Samples were run on 10% polyacrylamide gels and transferred onto nitrocellulose membranes (BioRad) blocked in

5% BSA (Sigma) in tris-buffered saline with 0.1% tween-20 (TBS-T, Sigma). Primary antibodies included anti-rabbit SPP1 (#108435, Abcam), anti-TFEB (#4240, Cell Signaling), anti-Sp1 (#07-645, Millipore), anti-hexanoyl lysine (HEL, #93056, Abcam), anti-GADPH (#G8795, Sigma), and anti-actin (#A2066 or A3853, Sigma). Secondary antibodies were goat anti-rabbit-HRP or goat anti-mouse-HRP (BioRad). Detection of protein was with Pierce ECL or Pierce Supersignal Pico (Thermo Scientific) reagents.

A3.2.4. Flow cytometry

For cell viability analysis, cells were stained with Annexin V-FITC (BD) and 7AAD (BD) for 15 minutes at room temperature. For lysosome staining, cells were stained with 50 Nm Lysotracker Red DND-99 (Invitrogen) for 30 minutes at 37 °C. For mitochondrial membrane potential and soluble reactive oxygen species analysis, cells were stained with 25 nM DIOC6 (Sigma) and 3.2 μM DHE (Sigma) together for 30 minutes at 37 °C. For lipid peroxidation analysis, cells were stained with 1 μM BODIPY 581/591 (Invitrogen) for 30 minutes at 37 °C. Prior to analysis, all stained cells were diluted in 1X PBS or 1X Annexin V Binding Buffer (Invitrogen). Flow cytometry experiments were done alongside unstained and single stained controls using a BD FACSCalibur machine and CellQuestPro software.

A3.2.5. Confocal microscopy

CLL cells were isolated from patient peripheral blood and cultured in Nunc Lab-Tek II chambered coverglass (Thermo Scientific) overnight. The following morning, after adhering to the coverglass, cells were stained with 50 nM Lysotracker for 30 minutes in a humid incubator at 37 ºC. Staining solution was removed and Live Cell Imaging Solution (Life Technologies) was added prior to viewing under the Olympus IX82 confocal microscope and viewed using FLUOVIEW 4.3

software.

A3.2.6. Lipid analysis

Cell pellets were re-suspended in LC/MS-grade water, vortexed for 15 seconds and sonicated for 20 minutes. Then 50 µL of a 1 µM solution containing each of the internal standards (IS) C17:1-Sphingosine, C17:0-Sphinganine, C17:1-Sphingosine-1-phosphate, C17:0-Sphinganine-1-phosphate, C17:0-Ceramide, C17:0-Glucosylceramide was added to 80 µL of the cell solution. To this solution was added 300 µL of extraction solvent (chloroform/methanol, 1:2). The mixture was vortexed, centrifuged at 2500 rpm for 15 minutes and the resultant supernatant was transferred into a separate glass vial. The extraction procedure was repeated and the two supernatants were combined. The final extract was dried under a nitrogen stream, redissolved into 500 µL of methanol and then filtered through a 0.22 µm membrane for subsequent LC/MS/MS analysis.

The analysis of sphingolipids was performed on an Agilent 1200 series HPLC (Agilent Technologies, Palo Alto, CA, USA) coupled to a 3200 QTRAP mass spectrometer (AB SCIEX, Concord, ON, Canada) with Analyst 1.4.2 software. The identification of individual sphingolipid molecules in the cell extracts was achieved by comparison of their retention times to the known standards, accurate mass measurements and fragmentation patterns. Their quantification was achieved via calibration curves of analyte to IS peak area ratio vs. the concentration for each sphingolipid molecule.

Sphingosine-1-phosphate (S1P) was measured by ELISA (Echelon Biosciences). Experiment was done exactly according to kit manual. Cell were lysed in lysis buffer at pH 7.0 containing 1% Triton X-100 (Sigma), 20 mM PIPES (Sigma), 150 mM NaCl (Sigma), 1Mm EGTA (Sigma), 1.5 mM MgCl2 (Sigma), 0.1% SDS (Sigma), and 1mM sodium orthovanadate. Lysates were

quantified using the Pierce BCA kit (Thermo Scientific) according to manufacturer's instructions and 30 µg was used for the S1P ELISA.

A3.2.7. Statistical analysis

Graphs were created and statistics were performed using GraphPad Prism4 software for windows (GraphPad Software, La Jolla California USA). Unless otherwise noted, a paired or unpaired two-tailed *t* test was performed according to the nature of data. When results from multiple different patient samples are shown on one graph, the median and the standard errors are shown. When multiple human samples are compared, the variances within groups (ex: unmutated *vs* mutated, or CLL *vs* healthy) are similar and not significantly different except for **Figure A3-6e** and Supplemental Figure A3-4c. The standard F test was used to compare variances. Statistical significance noted in figures as * ($p<0.05$), ** ($p<0.01$), or *** ($p<0.001$). Densitometry of western blot results was calculated using ImageJ [23].

A3.3. Results

A3.3.1. CLL cells are sensitive to lysosome disruption

Lysosome membrane permeabilization (LMP) has been recognized as a novel therapeutic strategy in cancer [24], but little is known regarding its efficacy in CLL cells. In the present study we treated primary CLL cells with a variety of known lysosomotropic agents: siramesine [10, 25], ciprofloxacin [11, 26], nortriptyline [16], and desipramine [16]. All agents except ciprofloxacin induced cell death at doses reported in the literature as measured by the Annexin V apoptotic assay (**Figure A3-1a-d**). The doses of drugs required to kill 50% of CLL cells were 5 mM siramesine, 100 µM desipramine, 100 µM nortriptyline (**Figure A3-1a, b, c**), or greater than 300 µg mL^{-1} ciprofloxacin (data not shown). Siramesine induced cell death was an early event as measured after

1 hour and remained the same after 24 hours (Supplemental Figure A3-1). Since siramesine had the greatest activity at the lowest doses, MTT assays were done on 4 different CLL samples to confirm loss of cell viability. The IC50 values for siramesine within these four samples was 2.4, 2.8, 5.4, and 6.0 μM. Thus, the dose of 5 μM siramesine was effective at killing CLL cells and was used in subsequent experiments. We also tested total cell death with trypan blue staining method but this was not as sensitive as Annexin V assay (Supplemental Figure A3-2). This could be due Annexin V detecting earlier loss of cell viability than trypan blue. Thus, Annexin V and 7AAD staining was used in all subsequent experiments.

To confirm that these agents were acting through LMP, primary CLL cells were stained with lysotracker and the staining intensity was measured using flow cytometry both before and after drug treatment in 5 minute time intervals. All drugs which caused cell death induced permeabilization of lysosomes (**Figure A3-1e-h**). LMP was further confirmed using confocal microscopy (**Figure A3-2a**), flow cytometry (Supplemental Figure A3-3), and western blot for the nuclear translocation of transcription factor EB (TFEB), a master regulator of lysosome biogenesis [27]. Approximately 50% of the cytosolic TFEB moved into the nucleus at 15 minutes (data not shown) and 30 minutes post-drug treatment (**Figure A3-2b, c**). This confirms that these lysosomotropic agents rapidly induce LMP in CLL cells which is followed by cell death.

A total of 123 CLL patient samples were tested in various experiments (Supplemental Table A3-1). Of these, 71 CLL patient samples were analyzed for cell death when treated with 5 mM siramesine. When comparing the cell death response with siramesine to various clinical parameters such as patient age, Rai stage, ZAP-70, and IgV_H mutational status (Supplemental Figure A3-4), no significant correlations were found. Thus, siramesine kills CLL cells regardless of poor

prognostic factors such as unmutated IgV_H and ZAP-70 expression.

To investigate the role of the microenvironment on siramesine-induced cell death, CLL cells were co-cultured with the human bone marrow-derived stromal cell line HS-5 for 24 hours and then treated with siramesine for 1 hour (Supplemental Figure A3-5). Co-culture conditions decreased siramesine-induced cell death, but was not statistically-significant.

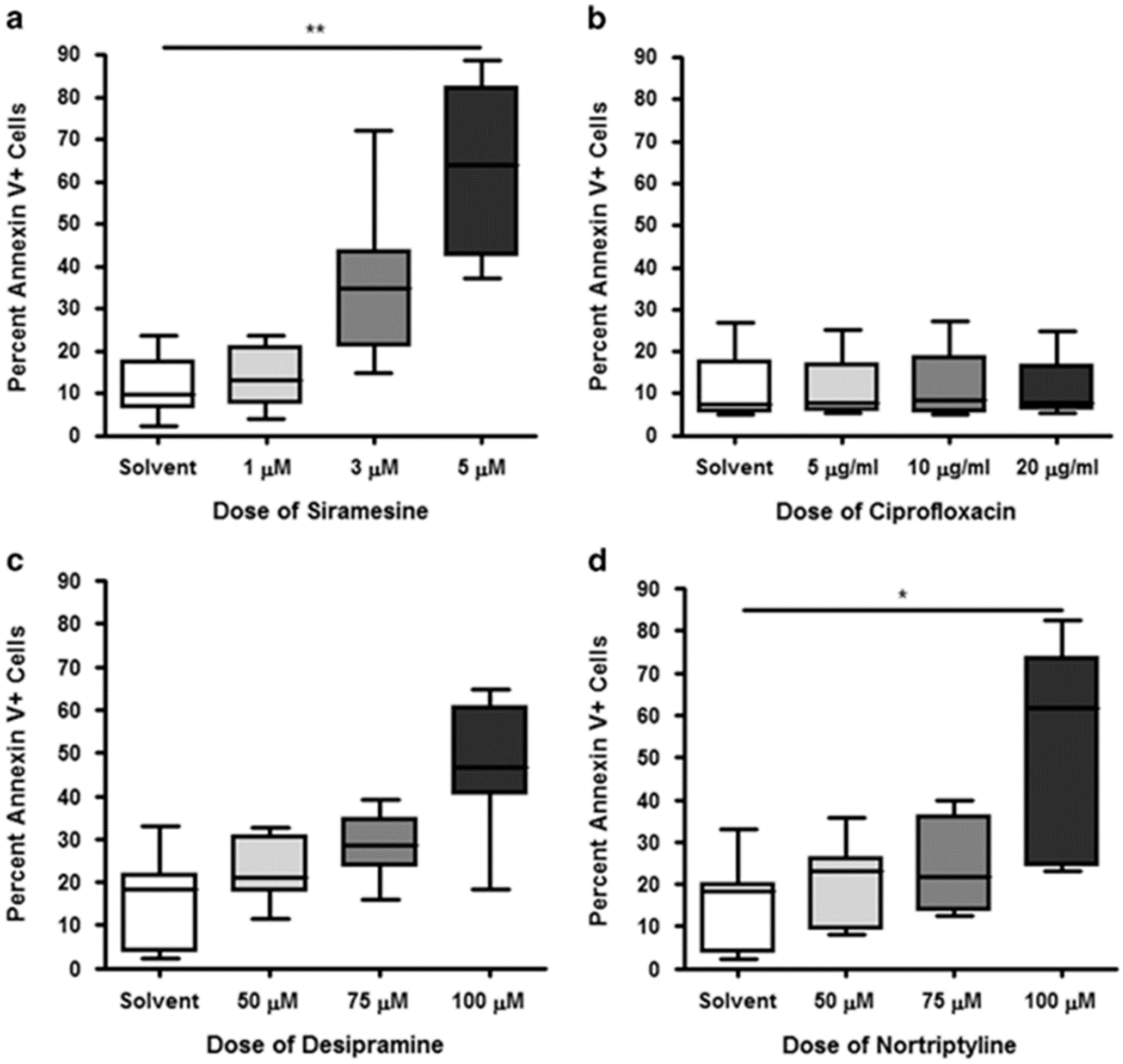

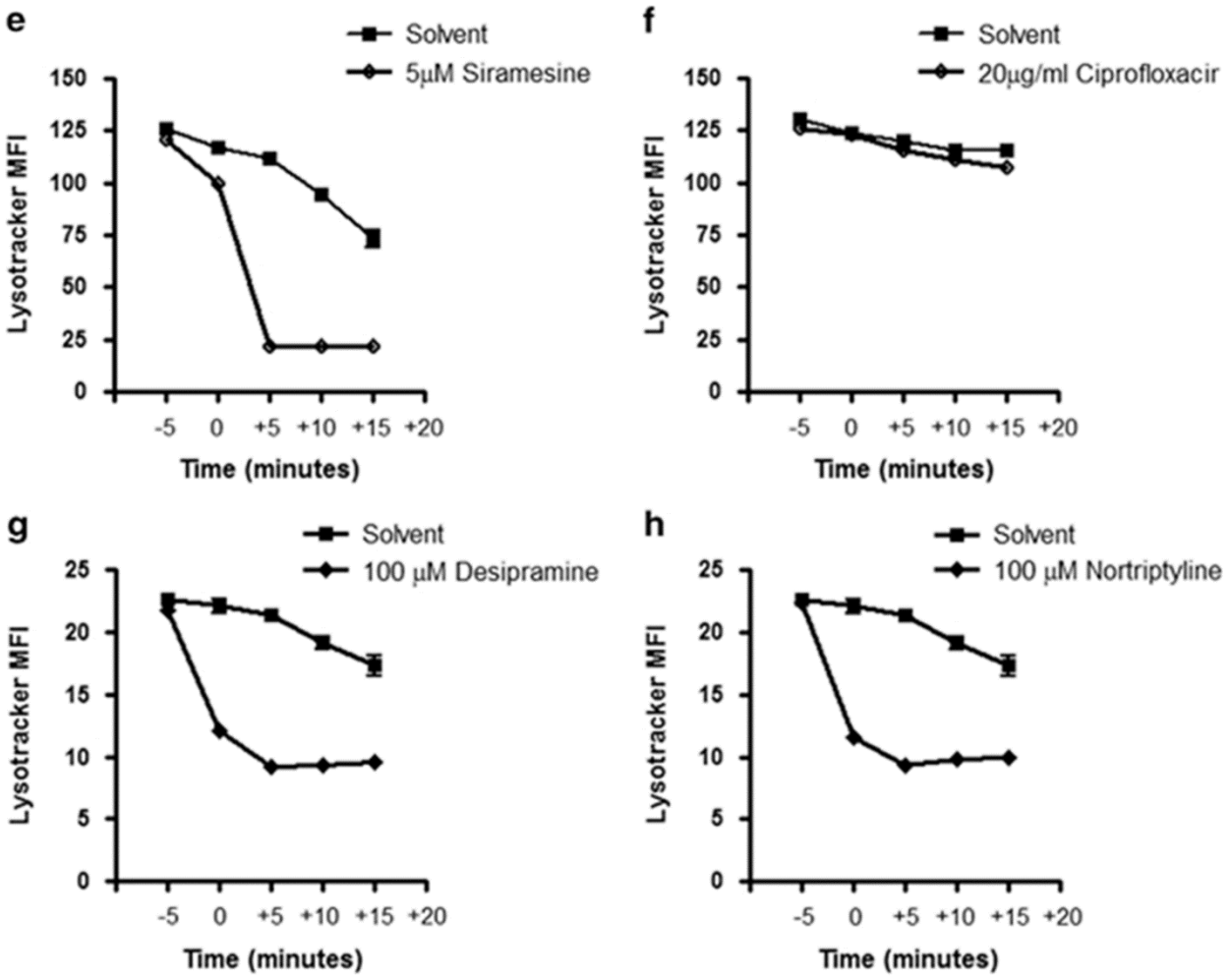

Figure A3-1. CLL cells are sensitive to lysosome disruptors.

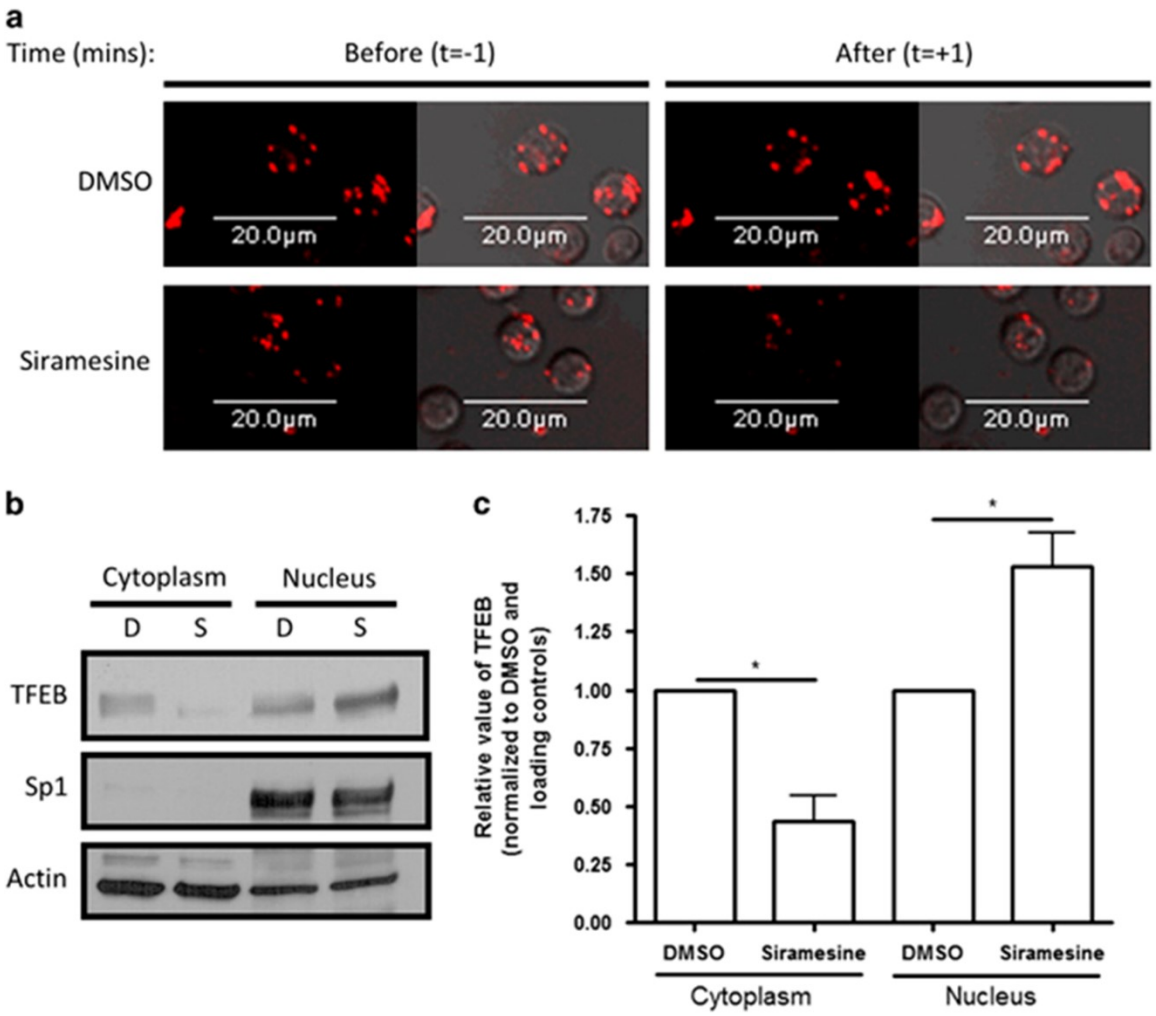

Figure A3-2. Lysosome permeabilization is accompanied by TFEB translocation.

A3.3.2. Siramesine-induced LMP causes mitochondrial dysfunction and subsequent cell death

As the mechanism of cell death with lysosome disruption appears to depend on the type of cell studied [11, 26, 28, 29], we evaluated the biological changes leading to cell death following siramesine treatment of CLL cells. Primary CLL cells were stained with lysotracker, BODIPY 581/591, DiOC6, or DHE which identify intact lysosomes, lipid peroxidation, mitochondrial membrane potential, and soluble reactive oxygen species (ROS), respectively. Staining intensity was measured by flow cytometry in 5 minute intervals before and after drug treatment. Within 5 minutes of drug treatment, lysotracker and BODIPY red fluorescence decreased while BODIPY green fluorescence increased (**Figure A3-3a, b, c**), indicating lysosome permeability and lipid peroxidation. At the same time, the lipid peroxidation product, hexanoyl lysine (HEL) adduct on proteins, was slightly increased by western blot (**Figure A3-3d, e**). This slight increase in HEL adduct formation observed after 5 minutes of siramesine treatment did not increase over time (Supplemental Figure A3-6). Over a 40 minute time course, there was a gradual decrease in DiOC6 and increase in DHE fluorescence, indicating a loss of mitochondrial membrane potential and increased levels of soluble ROS, respectively (**Figure A3-3f, g**). These results indicate that LMP with siramesine in CLL cells occurs prior to mitochondrial dysfunction.

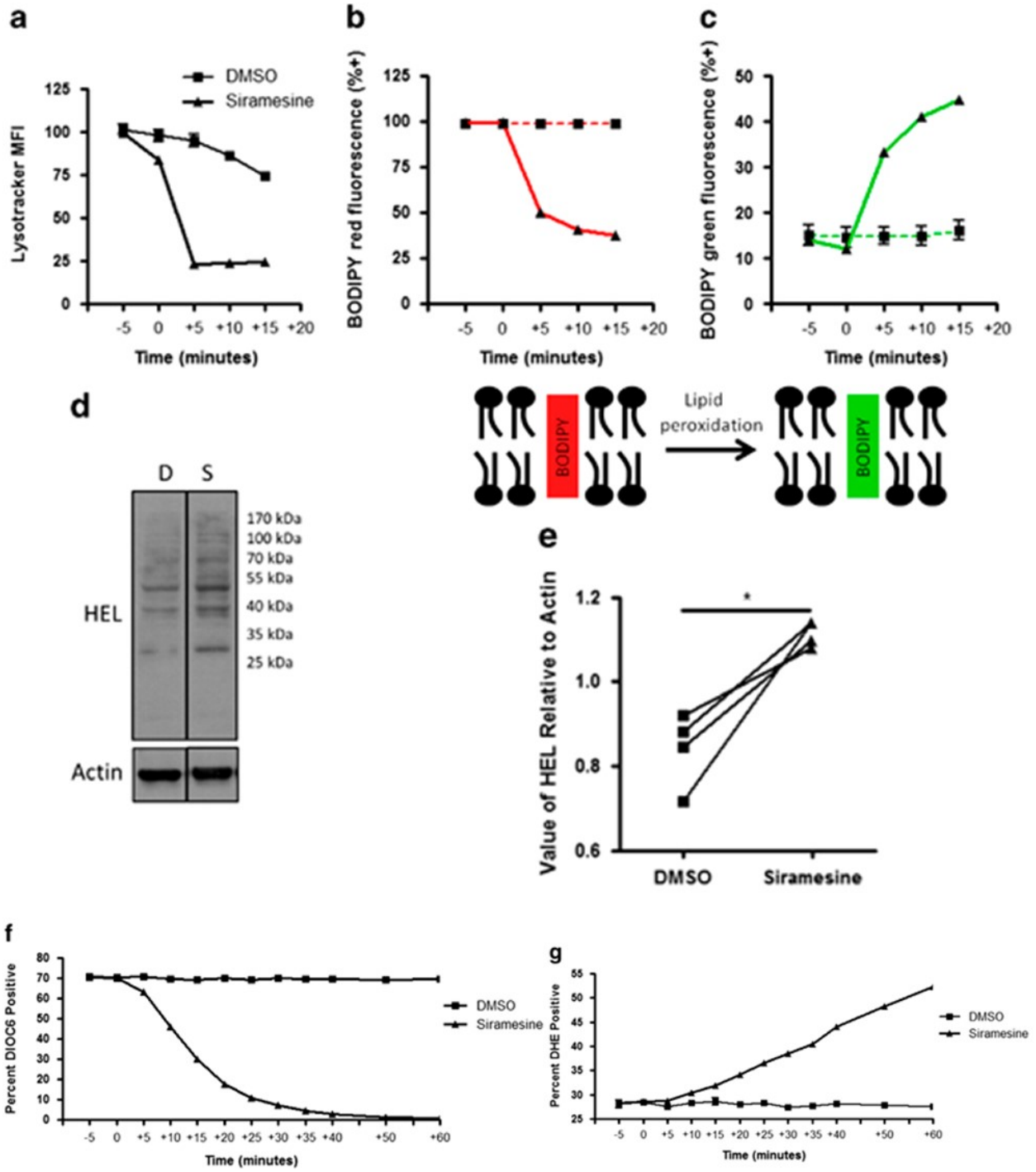

Figure A3-3. Siramesine-induced cell death involves lipid peroxidation and loss of mitochondrial membrane potential.

A3.3.3. Siramesine-induced cell death requires lipid peroxidation

It has previously been shown that siramesine-induced cell death is mediated by proteases and ROS [10, 28]. Furthermore, the protease cathepsin B is required by valproic acid and fludarabine to kill CLL cells [30]. To investigate the role of proteases and ROS in siramesineinduced CLL cell death, CLL cells were pretreated with various inhibitors and scavengers for 1 hour. Protease inhibitors CA-074-Me, Chymostatin, E64, and z-VAD-fmk did not prevent siramesine-induced cell death (Supplemental Figure A3-7). In contrast, scavengers of lipid ROS, such as α-tocopherol and to a lesser extent lycopene, blocked siramesine-induced cell death (**Figure A3-4a, b**), whereas soluble ROS scavengers *N*-acetyl cysteine (NAC) and Glutathione failed to prevent cell death (**Figure A3-4c, d**). To determine if lipid peroxidation involved oxidases, inhibitors of xanthine oxidase and NADPH oxidase were tested. These failed to prevent siramesine-induced cell death (Supplemental Figure A3-7).

To further investigate the role of lipid ROS in the process of siramesine-induced cell death, we evaluated the effect of α-tocopherol on LMP and mitochondrial membrane potential in CLL cells treated with siramesine. α-Tocopherol failed to prevent LMP (**Figure A3-5a, b**) but blocked lipid peroxidation, changes in mitochondrial membrane potential, and the increase in soluble ROS (**Figure A3-5c-h**). These results indicate that lipid ROS are not required for LMP but are a consequence of LMP, leading to mitochondria dysfunction and cell death.

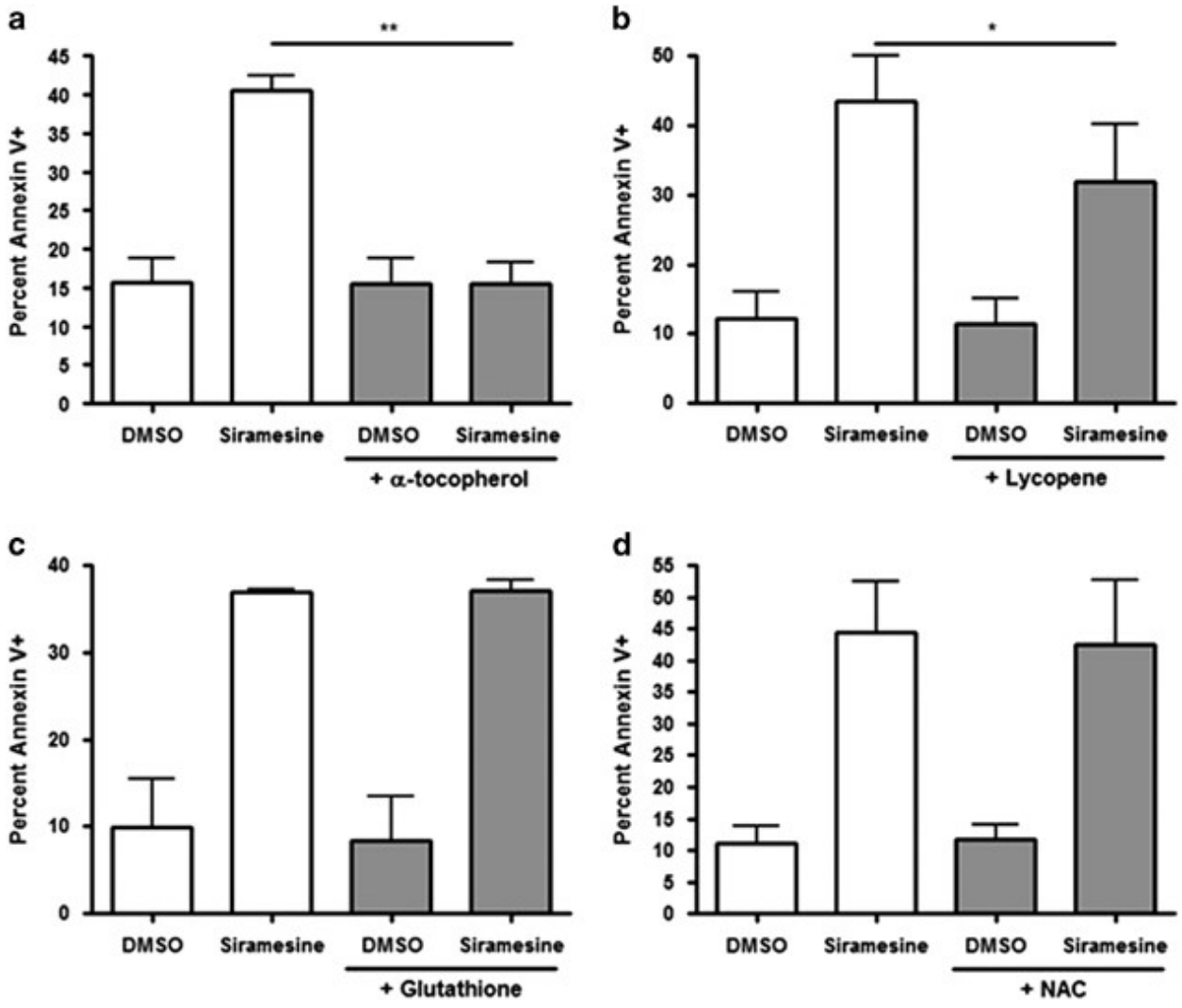

Figure A3-4. Siramesine-induced cell death requires lipid ROS, but not soluble ROS.

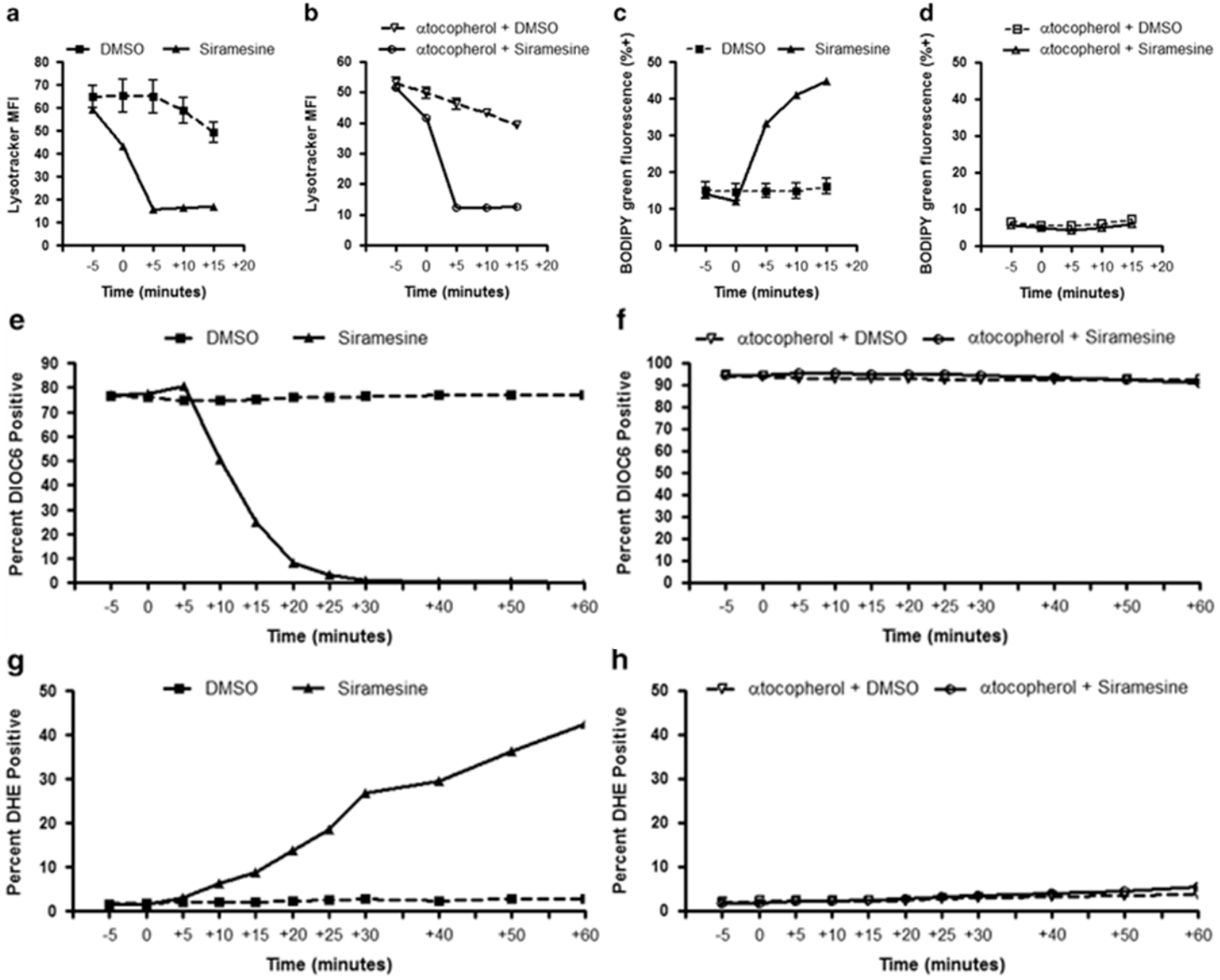

Figure A3-5. Early lipid peroxidation is required to affect mitochondria.

A3.3.4. Altered sphingolipid metabolism in CLL cells primes the lysosomes for disruption

To determine whether CLL cells are more sensitive than normal B cells to siramesine treatment, peripheral blood mononuclear cells (PBMCs) from CLL patients and age-matched normal donors were isolated and treated with 1, 3, or 5 μM siramesine. Using flow cytometry, samples were gated on CD3+ T cells or CD19+ B cells and cell death was analyzed. Results showed that CLL cells were more sensitive to siramesine treatment than normal T cells (data not shown), CLL T cells, and normal B cells (**Figure A3-6a**). A median of 15% of normal B cells or 40% of CLL cells were killed by 5 μM siramesine. Even CLL cells with deletion 17p, which typically lack p53, were sensitive to siramesine (**Figure A3-6a** and Supplemental Figure A3-8). Thus, CLL cells are more sensitive than normal B cells to lysosome-mediated cell death mediated by siramesine.

To investigate the possible mechanisms for this differential sensitivity, we first determined the number of lysosomes in CLL cells. Lysosomes from 100 CLL cells or normal B cells were counted from images acquired using confocal microscopy. Lysosomes were counted from a single focal plane. CLL cells were found to have a slight, but statistically-significant, higher average number of lysosomes per cell than normal B cells, with means of 6 lysosomes/cell and 4 lysosomes/cell, respectively (Supplemental Figure A3-9).

Sphingolipid metabolism was compared in CLL and normal B cells as the lysosome is a major storage site for lipids in the cell and alterations in lipid metabolism have profound effects on lysosome function [31, 32, 33]. To determine differences between normal B and CLL cells, the GEO and ONCOMINE databases were mined for differences in lysosome or lipid metabolism proteins. One alteration that we found consistently was an over-expression of sphingosine 1-phosphate phosphatase 1 (SPP1) in CLL cells compared to normal B cells (**Figure A3-6c**) [34].

Western blot analysis confirmed this over-expression at the protein level (**Figure A3-6d** and Supplemental Figure A3-10a). There was no difference in SPP1 mRNA or protein expression among CLL samples of mutated IgV_H or un-mutated IgV_H (Supplemental Figure A3-10b, c). In addition, the product of this enzyme, C18:1 sphingosine, was also increased in CLL cells, as compared to normal B cells (**Figure A3-6e**). Levels of other sphingolipids such as sphingosine-1-phosphate, C18:0 ceramide, C16:0 glucosylceramide, and C20:0 glucosylceramide did not differ between CLL and normal B cells (Supplemental Figure A3-11).

To confirm the role of sphingosine in sensitizing lysosomes to disruption, we treated CLL cells directly with sphingosine. The addition of sphingosine significantly increased siramesine-induced cell death (**Figure A3-7a**). Likewise, increasing sphingosine levels by inhibiting sphingosine kinase (SK) with sphingosine kinase inhibitor (SKI) II also increased siramesine-induced cell death (**Figure A3-7b**). A lower dose of 3 μM siramesine was used for these experiments. Similar to siramesine, sphingosine was found to disrupt lysosomes and cause permeabilization within minutes (**Figure A3-7c, d**) which led to a later effect on mitochondria (**Figure A3-7e, f**). In addition, 5 and 10 μM sphingosine caused significant cell death in CLL cells within 1 hour (**Figure A3-7g**) but was not toxic to normal B cells (**Figure A3-7h**). This effect was presumably because CLL cells already have high levels of sphingosine. These results show that sphingolipid metabolism, particularly sphingosine metabolism, is altered in CLL cells and the high levels of sphingosine increase lysosomal disruption from agents such as siramesine.

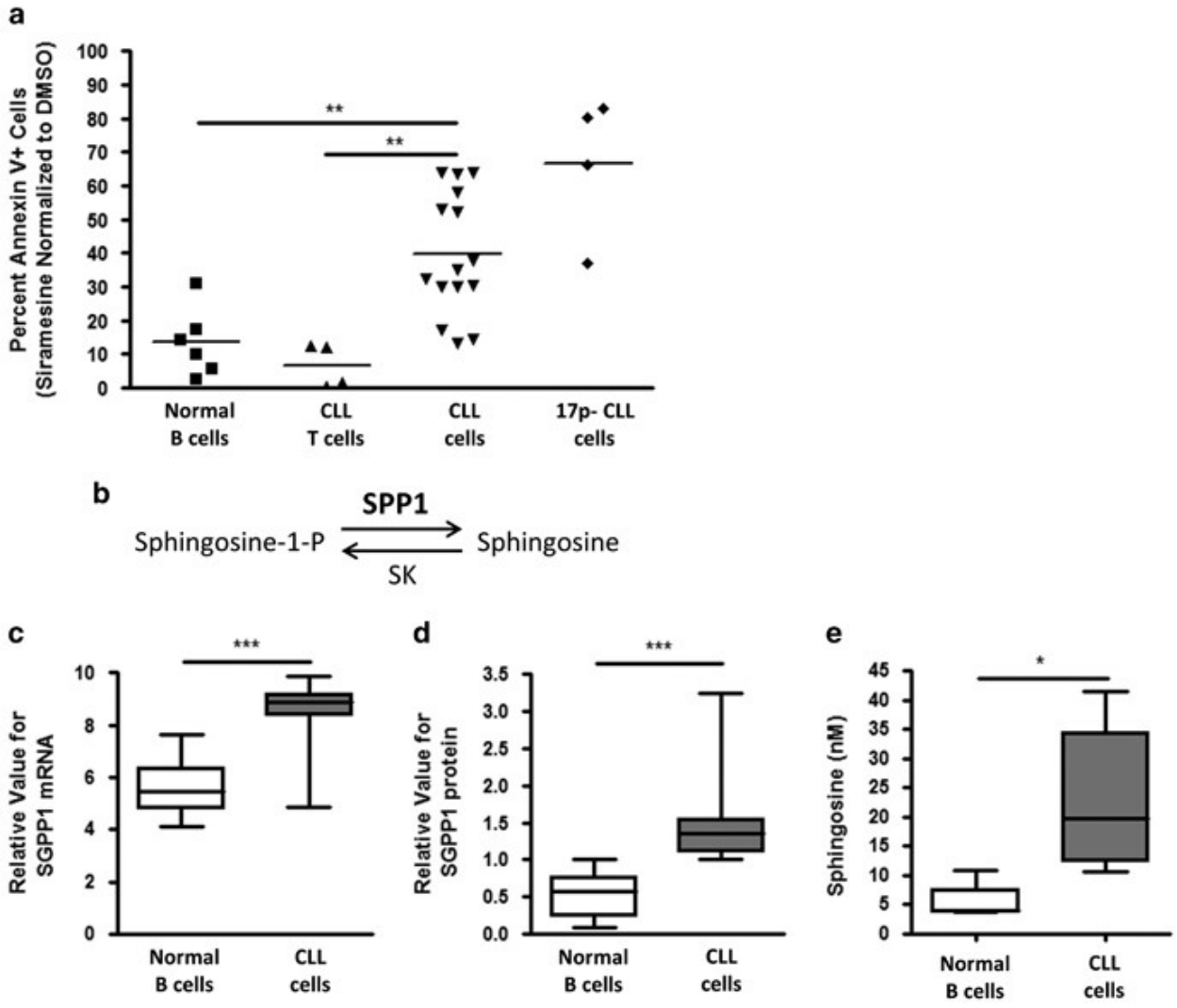

Figure A3-6. CLL cells are more sensitive to siramesine and have more lysosomes, SPP1, and sphingosine than normal B cells.

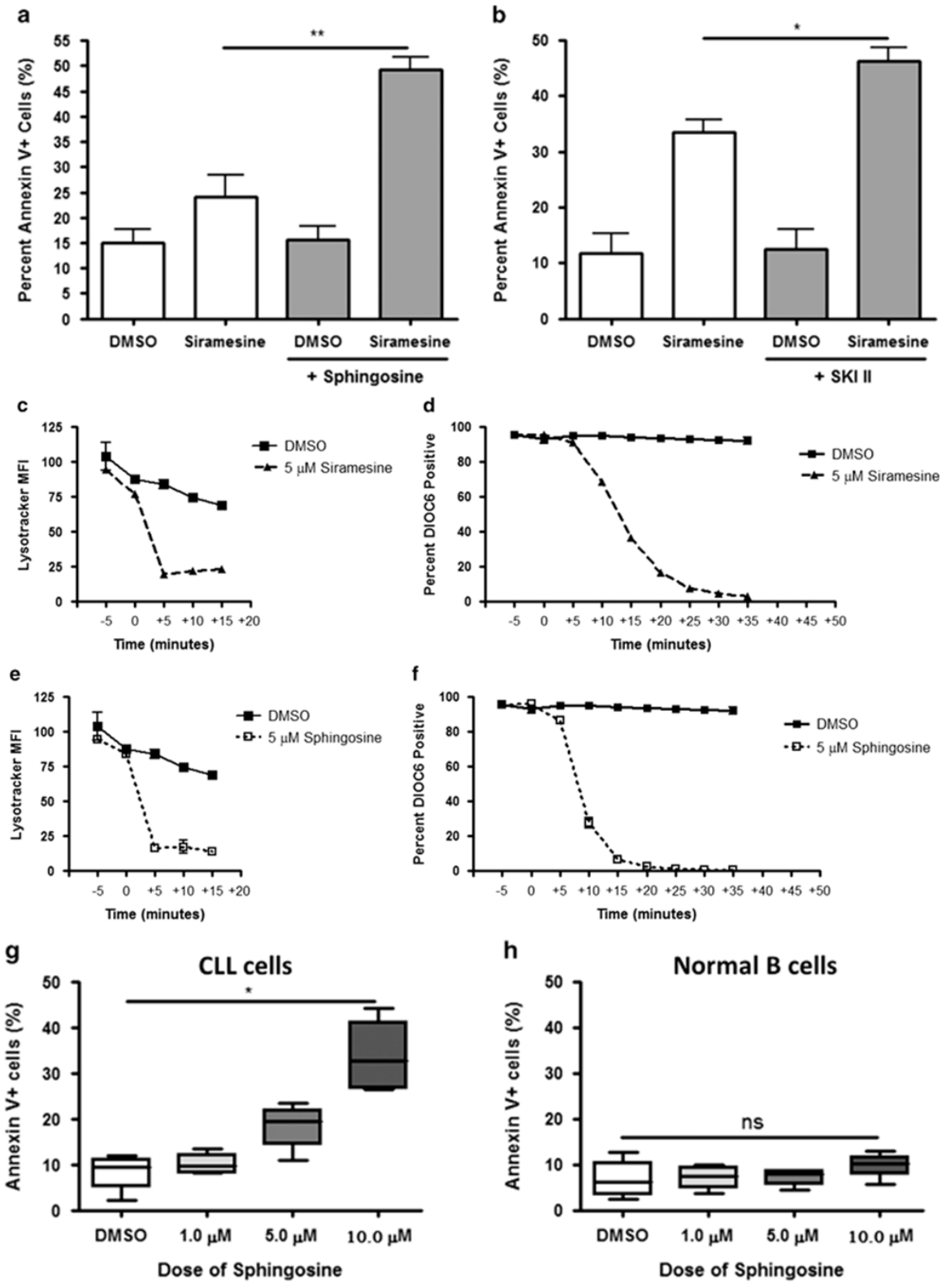

Figure A3-7. Excess sphingosine causes lysosome disruption.

A3.4. Discussion

Since their discovery as the suicide bags of the cell, lysosomes have been explored as therapeutic targets in cancer. However, little is known about lysosomes and lysosome-mediated cell death in CLL. The results of the present study demonstrate that CLL cells are susceptible to lysosome-mediated cell death, particularly to siramesine treatment. In addition, we demonstrated that following siramesine induced LMP, lipid peroxidation occurs which leads to mitochondrial permeabilization and cell death. Moreover, siramesine had little effect on normal B cells and the selective killing of CLL cells appeared related to the increased number of lysosomes in these cells and increased lysosome fragility due to altered sphingolipid metabolism (Supplemental Figure 12).

Clinically-tested agents were chosen for evaluation in CLL cells. Siramesine was originally developed as a sigma receptor antagonist for the treatment of depression [35]. Nortriptyline and desipramine are FDA-approved anti-depressants [36]. Ciprofloxacin is a FDA approved antibiotic [37]. All these agents have been shown to induce LMP in cancer cells. Among the lysosome disruptors investigated, siramesine was the most potent, as it was effective at the lowest doses that correspond to its cytotoxicity in other cancer cells. It was effective in cells regardless of patient age, IgV_H mutational status, ZAP-70 expression, and cytogenetics; siramesine was even effective in CLL cells with deletion 17p, which are typically resistant to standard chemotherapy. We also found that bone marrow stromal cells did not confer significant protection from siramesine-induced cell death. This suggests that clinically relevant lysosomotropic agents are effective at inducing cell death in CLL cells.

Lysosomotropic agents induce cell death through increased ROS and activation of cathepsins. We found that siramesine caused lipid peroxidation leading to cell death. The pivotal role of lipid

peroxidation in siramesine-induced cell death has been demonstrated in other models such as those with breast cancer cells [9, 10, 28] and AML cells [13]. CLL cells may be particularly sensitive to lipid peroxidation, as one report found that they lack endogenous inhibitors of lipid peroxidation: tocopherols [38]. Furthermore, B cells have previously been shown to be more sensitive to oxidative stress than other cells, including T cells [39].

Lysosomotropic agents, such as siramesine, activate cathepsins leading to degradation of anti-apoptotic proteins in a variety of different cancer cells. In CLL cells, we previously demonstrated that VPA and fludarabine in combination increases cathepsin B expression and cathepsin B-mediated cell death in CLL cells [30]. Despite the role of cathepsins in siramesine treatment in other cancer cells [16, 35, 40], we found that cathepsins are not required for siramesine-induced cell death in CLL cells. This suggests the main mechanism of action for siramesine in CLL cells is through lipid peroxidation and not cathepsins.

The direct mechanism by which lysosome permeabilization leads to loss of mitochondrial membrane potential is unknown in CLL cells. We speculate that lipid peroxidation generated at the lysosomal membrane could directly oxidize and open the mitochondrial permeability transition pore, as this has been shown in other models [41, 42, 43]. The exact mechanism of lysosome-mitochondria crosstalk is unknown and is the focus of future investigations.

Aside from characterizing the efficacy and the mechanism of action of siramesine, we investigated alterations in lysosomes that could explain the differential sensitivity of CLL cells to normal B cells. To this end, we showed that CLL cells tend to have more lysosomes compared with normal B cells. An increase in lysosome size or biogenesis has been noted in other cancers such as AML [13] contributing to their sensitization to lysosomotropic agent treatment. The role

of CLL lysosome numbers in response to siramesine is unknown, and would require future investigation.

Similar to the slight increase in lysosome number, a slight increase in mitochondria has been noted in CLL cells compared to normal B cells [44]. Mitochondrial functions are also altered in cancer cells including CLL cells contributing to increased ROS levels [44, 45], but their role in siramesine-induced cell death is controversial. Indeed, one study has suggested that siramesine functions through mitochondria rather than through lysosomes to induce cell death [28]. In CLL cells, siramesine permeabilized lysosome membranes before changes in mitochondrial function occur, and blocking caspases or mitochondrial soluble ROS production did not prevent siramesine-induced cell death. This suggested that although mitochondria are involved in cell death, it is the initial LMP and lipid peroxidation that is required.

Aside from alterations in lysosome numbers, lysosome function could be effected by altered sphingolipid metabolism. Altered sphingolipid metabolism has been described in cancer cells [15, 16, 46], however this is the first study that has found an increased expression of sphingosine 1-phosphate phosphatase (SPP1). Studies have found alterations in sphingosine kinase (SK) [47, 48, 49, 50] and acidic sphingomyelinase (ASM) [15, 16] in cancer cells; however, according to cancer expression databases these proteins are not altered in CLL cells. Although siramesine inhibits ASM, it is unlikely that this plays a role in the enhanced sensitivity of CLL cells to lysosome disruption compared to normal B cells. Instead, the elevated sphingosine content appears to make CLL cells more sensitive to sphingosine or siramesine, as compared to normal B cells. This agrees with published studies that have shown that addition of sphingosine causes cell death [51, 52, 53].

Sphingolipid metabolism is a complex process which centers on the reversible metabolism of

sphingosine-1-phosphate into sphingosine, then into ceramide, and onto more complex glucosylceramides. Many of these components, particularly sphingosine-1-phosphate and ceramide, act as second messengers to promote signaling and affect the balance between cell survival and cell death. We found that sphingosine was the only sphingolipid in excess in CLL cells; there was no difference in the levels of sphingosine-1-phosphate, ceramide, and glucosylceramides between CLL cells and normal B cells. Excess sphingosine could affect all membranes within the cell, but the lysosome membrane can be specifically permeabilized with a pH-activated drug like siramesine. It is unclear at this point if excess sphingosine confers any benefit to the CLL cells, and this will be the focus of future investigation.

Taken together, our findings provide evidence that lysosomotropic agents such as siramesine selectively induce cell death in primary CLL cells compared to normal B cells. This selectivity is at least partially due to alterations in sphingolipid metabolism and provides rationale to develop lysosomotropic agents for treatment of CLL. Using lysosomotropic agents in combination with chemotherapeutic agents is the focus of future investigation.

Supplementary information is available at Leukemia's website.

A3.5. References

[1] M. Hallek, K. Fischer, G. Fingerle-Rowson, A.M. Fink, R. Busch, J. Mayer, M. Hensel, G. Hopfinger, G. Hess, U. Von Grünhagen, M. Bergmann, Addition of rituximab to fludarabine and cyclophosphamide in patients with chronic lymphocytic leukaemia: a randomised, open-label, phase 3 trial, Lancet. 376 (2010) 1164-1174.

[2] M.J. Keating, S. O'Brien, M. Albitar, S. Lerner, W. Plunkett, F. Giles, M. Andreeff, J. Cortes, S. Faderl, D. Thomas, C. Koller, Early results of a chemoimmunotherapy regimen of fludarabine, cyclophosphamide, and rituximab as initial therapy for chronic lymphocytic leukemia, J Clin Oncol. 23 (2005) 4079-4088.

[3] P. Jain, M. Keating, W. Wierda, Z. Estrov, A. Ferrajoli, N. Jain, B. George, D. James, H. Kantarjian, J. Burger, S. O'Brien, Outcomes of patients with chronic lymphocytic leukemia (CLL) after discontinuing ibrutinib, Blood. 2015 Jan 8 [cited 2015 Jan 16].

[4] F. Morabito, M. Gentile, J.F. Seymour, A. Polliack, Ibrutinib, idelalisib and obinutuzumab for the treatment of patients with chronic lymphocytic leukemia: three new arrows aiming at the target, Leuk Lymphoma. 56 (2015) 1-20.

[5] V. Goede, K. Fischer, R. Busch, A. Engelke, B. Eichhorst, C.M. Wendtner, T. Chagorova, J. de la Serna, M.S. Dilhuydy, T. Illmer, S. Opat, Obinutuzumab plus chlorambucil in patients with CLL and coexisting conditions, N Engl J Med. 370 (2014) 1101-1110.

[6] G. Cartron, S. de Guibert, M-S. Dilhuydy, F. Morschhauser, V. Leblond, J. Dupuis, B. Mahe, R. Bouabdallah, G. Lei, M. Wenger, E. Wassner-Fritsch, Obinutuzumab (GA101) in relapsed/refractory chronic lymphocytic leukemia: final data from the phase 1/2 GAUGUIN study, Blood. 124 (2014) 2196-2202.

[7] M. Jak, G.G.W. van Bochove, E.A. Reits, W.W. Kallemeijn, J.M. Tromp, P. Umana, C. Klein, R.A. van Lier, M.H. van Oers, E. Eldering, CD40 stimulation sensitizes CLL cells to lysosomal cell death induction by type II anti-CD20 mAb GA101, Blood. 118 (2011) 5178-5188.

[8] W. Alduaij, A. Ivanov, J. Honeychurch, E.J. Cheadle, S. Potluri, S.H. Lim, K. Shimada, C.H. Chan, A. Tutt, S.A. Beers, M.J. Glennie, Novel type II anti-CD20 monoclonal antibody (GA101) evokes homotypic adhesion and actindependent, lysosome-mediated cell death in B-cell malignancies, Blood. 117 (2011) 4519-4529.

[9] N. Fehrenbacher, L. Bastholm, T. Kirkegaard-Sørensen, B. Rafn, T. Bøttzauw, C. Nielsen, E. Weber, S. Shirasawa, T. Kallunki, M. Jäättelä, Sensitization to the lysosomal cell death pathway by oncogene-induced downregulation of lysosome-associated membrane proteins 1 and 2, Cancer Res. 68 (2008) 6623-6633.

[10] M.S. Ostenfeld, N. Fehrenbacher, M. Høyer-Hansen, C. Thomsen, T. Farkas, M. Jäättelä, Effective tumor cell death by sigma-2 receptor ligand siramesine involves lysosomal leakage and oxidative stress, Cancer Res. 65 (2005) 8975-8983.

[11] H. Erdal, M. Berndtsson, J. Castro, U. Brunk, M.C. Shoshan, S. Linder, Induction of

lysosomal membrane permeabilization by compounds that activate p53-independent apoptosis, Proc Natl Acad Sci U S A. 102 (2005) 192-197.

[12] S. Mena, M.L. Rodríguez, X. Ponsoda, J.M. Estrela, M. Jäättela, A.L. Ortega, Pterostilbene-induced tumor cytotoxicity: a lysosomal membrane permeabilization-dependent mechanism, PLoS One. Public Library of Science. 7 (2012) e44524.

[13] M.A. Sukhai, S. Prabha, R. Hurren, A.C. Rutledge, A.Y. Lee, S. Sriskanthadevan, H. Sun, X. Wang, M. Skrtic, A. Seneviratne, M. Cusimano, Lysosomal disruption preferentially targets acute myeloid leukemia cells and progenitors, J Clin Invest. 123 (2013) 315-328.

[14] T. Mijatovic, V. Mathieu, J.F. Gaussin, N. De Nève, F. Ribaucour, E. Van Quaquebeke, P. Dumont, F. Darro, R. Kiss, Cardenolide-induced lysosomal membrane permeabilization demonstrates therapeutic benefits in experimental human non-small cell lung cancers, Neoplasia. 8 (2006) 402-412.

[15] A.S. Don, X.Y. Lim, T.A. Couttas, Re-configuration of sphingolipid metabolism by oncogenic transformation, Biomolecules. 4 (2014) 315-353.

[16] N.H.T. Petersen, O.D. Olsen, L. Groth-Pedersen, A.M. Ellegaard, M. Bilgin, S. Redmer, M.S. Ostenfeld, D. Ulanet, T.H. Dovmark, A. Lønborg, S.D. Vindeløv, Transformation-associated changes in sphingolipid metabolism sensitize cells to lysosomal cell death induced by inhibitors of acid sphingomyelinase, Cancer Cell. 24 (2013) 379-393.

[17] Y. Zheng, J. Wen, J. Nguyen, M.A. Cachia, C. Wang, Y. Sun, Decreased deformability of lymphocytes in chronic lymphocytic leukemia, Sci Rep. 5 (2015).

[18] F.M. Goñi, A. Alonso, Effects of ceramide and other simple sphingolipids on membrane lateral structure, Biochim Biophys Acta. 1788 (2009) 169-177.

[19] D.K. Breslow, J.S. Weissman, Membranes in balance: mechanisms of sphingolipid homeostasis. Mol Cell. 40 (2010) 267-279.

[20] G.S. Nowakowski, J.D. Hoyer, T.D. Shanafelt, C.S. Zent, T.G. Call, N.D. Bone, B. LaPlant, G.W. Dewald, R.C. Tschumper, D.F. Jelinek, T.E. Witzig, Percentage of smudge cells on routine blood smear predicts survival in chronic lymphocytic leukemia, J Clin Oncol. 27 (2009) 1844-1849.

[21] J.A. Woyach, A.J. Johnson, J.C. Byrd, The B-cell receptor signaling pathway as a therapeutic target in CLL, Blood. 120 (2012) 1175-1184.

[22] D.A. Brown, E. London, Structure and function of sphingolipid- and cholesterol-rich membrane rafts, J Biol Chem. 275 (2000) 17221-17224.

[23] M. Abramoff, P. Magalhaes, S. Ram, Image Processing with ImageJ, Biophotonics Int. 11 (2004) 36-42.

[24] N. Fehrenbacher, M. Jäättelä, Lysosomes as targets for cancer therapy, Cancer Res. 65 (2005) 2993-2995.

[25] M.S. Ostenfeld, M. Høyer-Hansen, L. Bastholm, N. Fehrenbacher, O.D. Olsen, L. Groth-Pedersen, P. Puustinen, T. Kirkegaard-Sørensen, J. Nylandsted, T. Farkas, M. Jäättelä, Anti-cancer agent siramesine is a lysosomotropic detergent that induces cytoprotective autophagosome accumulation, Autophagy. 4 (2008) 487-499.

[26] P. Boya, K. Andreau, D. Poncet, N. Zamzami, J.L. Perfettini, D. Metivier, D.M. Ojcius, M. Jäättelä, G. Kroemer, Lysosomal membrane permeabilization induces cell death in a mitochondrion-dependent fashion, J Exp Med. 197 (2003) 1323-1334.

[27] M. Sardiello, M. Palmieri, A. di Ronza, D.L. Medina, M. Valenza, V.A. Gennarino, C. Di Malta, F. Donaudy, V. Embrione, R.S. Polishchuk, S. Banfi, A gene network regulating lysosomal biogenesis and function, Science. 325 (2009) 473-477.

[28] M.H. Česen, U. Repnik, V. Turk, B. Turk, Siramesine triggers cell death through destabilisation of mitochondria, but not lysosomes, Cell Death Dis. 4 (2013) e818.

[29] S. Aits, M. Jäättelä, Lysosomal cell death at a glance, J Cell Sci. 126 (2013) 1905-1912.

[30] J.Y. Yoon, D. Szwajcer, G. Ishdorj, P. Benjaminson, W. Xiao, R. Kumar, J.B. Johnston, S.B. Gibson, Synergistic apoptotic response between valproic acid and fludarabine in chronic lymphocytic leukaemia (CLL) cells involves the lysosomal protease cathepsin B, Blood Cancer J. 3 (2013) e153.

[31] C. Settembre, A. Ballabio, Lysosome: regulator of lipid degradation pathways, Trends Cell Biol. 24 (2014) 743-750.

[32] I. Hamer, G. Van Beersel, T. Arnould, M. Jadot, Lipids and lysosomes, Curr Drug Metab. 13 (2012) 1371-1387.

[33] R. Pralhada Rao, N. Vaidyanathan, M. Rengasamy, A. Mammen Oommen, N. Somaiya, M.R. Jagannath, Sphingolipid metabolic pathway: an overview of major roles played in human diseases, J Lipids. 2013 (2013).

[34] A. Gutierrez, R.C. Tschumper, X. Wu, T.D. Shanafelt, J. Eckel-Passow, P.M. Huddleston, S.L. Slager, N.E. Kay, D.F. Jelinek, LEF-1 is a prosurvival factor in chronic lymphocytic leukemia and is expressed in the preleukemic state of monoclonal B-cell lymphocytosis, Blood. 116 (2010) 2975-2983.

[35] C. Heading, Siramesine H Lundbeck, Curr Opin Investig Drugs. 2 (2001) 266-270.

[36] L.E. Hollister, Plasma concentrations of tricyclic antidepressants in clinical practice, J Clin Psychiatry. 43 (1982) 66-69.

[37] A. Meyerhoff, R. Albrecht, J.M. Meyer, P. Dionne, K. Higgins, D. Murphy, US Food and Drug Administration approval of ciprofloxacin hydrochloride for management of postexposure inhalational anthrax, Clin Infect Dis. 39 (2004) 303-308.

[38] H.J. Kayden, L. Hatam, M.G. Traber, M. Conklyn, L.F. Liebes, R. Silber, Reduced tocopherol content of B cells from patients with chronic lymphocytic leukemia, Blood. 63 (1984) 213-215.

[39] C.M. Farber, L.F. Liebes, D.N. Kanganis, R. Silber, Human B lymphocytes show greater susceptibility to H_2O_2 toxicity than T lymphocytes, J Immunol. 132 (1984) 2543-2546.

[40] P. Boya, K. Andreau, D. Poncet, N. Zamzami, J.L. Perfettini, D. Metivier, D.M. Ojcius, M. Jäättelä, G. Kroemer, Lysosomal membrane permeabilization induces cell death in a mitochondrion-dependent fashion, J Exp Med. 197 (2003) 1323-1334.

[41] A. Vianello, V. Casolo, E. Petrussa, C. Peresson, S. Patui, A. Bertolini, S. Passamonti, E. Braidot, M. Zancani, The mitochondrial permeability transition pore (PTP)-an example of multiple molecular exaptation? Biochim Biophys Acta. 1817 (2012) 2072-86.

[42] C. Brenner, M. Moulin, Physiological roles of the permeability transition pore, Circ Res. 111 (2012) 1237-1247.

[43] M. Zoratti, I. Szab, Electrophysiology of the inner mitochondrial membrane， J Bioenerg Biomembr. 26 (1994) 543-553.

[44] R. Jitschin, A.D. Hofmann, H. Bruns, A. Giessl, J. Bricks, J. Berger, D. Saul, M.J. Eckart, A. Mackensen, D. Mougiakakos, Mitochondrial metabolism contributes to oxidative stress and reveals therapeutic targets in chronic lymphocytic leukemia, Blood. 123 (2014) 2663-2672.

[45] J.S. Carew, S.T. Nawrocki, R.H. Xu, K. Dunner, D.J. McConkey, W.G. Wierda, M.J. Keating, P. Huang, Increased mitochondrial biogenesis in primary leukemia cells: the role of endogenous nitric oxide and impact on sensitivity to fludarabine, Leukemia. 18 (2004) 1934-1940.

[46] L.K. Ryland, T.E. Fox, X. Liu, T.P. Loughran, M. Kester, Dysregulation of sphingolipid metabolism in cancer, Cancer Biol Ther. 11 (2011) 138-149.

[47] M.B. Chen, L. Yang, P.H. Lu, X.L. Fu, Y. Zhang, Y.Q. Zhu, Y. Tian, MicroRNA-101 downregulates sphingosine kinase 1 in colorectal cancer cells, Biochem Biophys Res Commun. 463 (2015) 954-960.

[48] T. Kawamori, W. Osta, K.R. Johnson, B.J. Pettus, J. Bielawski, T. Tanaka, M.J. Wargovich, B.S. Reddy, Y.A. Hannun, L.M. Obeid, D. Zhou, Sphingosine kinase 1 is up-regulated in colon carcinogenesis, FASEB J. 20 (2006) 386-388.

[49] E. Le Scolan, D. Pchejetski, Y. Banno, N. Denis, P. Mayeux, W. Vainchenker, T. Levade, F. Moreau-Gachelin, Overexpression of sphingosine kinase 1 is an oncogenic event in erythroleukemic progression, Blood. 106 (2005) 1808-1816.

[50] V.E. Nava, J.P. Hobson, S. Murthy, S. Milstien, S. Spiegel, Sphingosine kinase type 1 promotes estrogen-dependent tumorigenesis of breast cancer MCF-7 cells, Exp Cell Res. 281 (2002) 115-127.

[51] V.E. Nava, O. Cuvillier, L.C. Edsall, K. Kimura, S. Milstien, E.P. Gelmann, S. Spiegel, Sphingosine enhances apoptosis of radiation-resistant prostate cancer cells, Cancer Res. 60 (2000) 4468-4474.

[52] C. Ullio, J. Casas, U.T. Brunk, G. Sala, G. Fabriàs, R. Ghidoni, G. Bonelli, F.M. Baccino, R. Autelli, Sphingosine mediates TNFα-induced lysosomal membrane permeabilization and ensuing programmed cell death in hepatoma cells, J Lipid Res. 53 (2012) 1134-1143.

[53] K. Kågedal, M. Zhao, I. Svensson, U.T. Brunk, Sphingosine-induced apoptosis is dependent on lysosomal proteases, Biochem J. 359 (2001) 335-343.

COPYRIGHT PERMISSIONS

Title: Determination of Bile Acids in Piglet Bile by Solid Phase Extraction and Liquid Chromatography-Electrospray Tandem Mass Spectrometry

Authors: Si Mi, David W. Lim, Justine M. Turner, Paul W. Wales, and Jonathan M. Curtis

Publication: Lipids

Publisher: Springer

Date: Jun 01, 2016

License Number: 3880460821356

Limited License

COPYRIGHT PERMISSIONS

Permission is valid upon payment of the fee as indicated in the licensing process. If permission is granted free of charge on this occasion that does not prejudice any rights we might have to charge for reproduction of our copyrighted material in the future.

-If your request is for reuse in a Thesis, permission is granted free of charge under the following conditions:

This license is valid for one-time use only for the purpose of defending your thesis and with a maximum of 100 extra copies in paper. If the thesis is going to be published, permission needs to be reobtained.

- includes use in an electronic form, provided it is an author-created version of the thesis on his/her own website and his/her university's repository, including UMI (according to the definition on the Sherpa website: http://www.sherpa.ac.uk/romeo/);

- is subject to courtesy information to the co-author or corresponding author.

Geographic Rights: Scope

Licenses may be exercised anywhere in the world.

Altering/Modifying Material: Not Permitted

Figures, tables, and illustrations may be altered minimally to serve your work. You may not alter or modify text in any manner. Abbreviations, additions, deletions and/or any other alterations shall be made only with prior written authorization of the author(s).

Reservation of Rights

Springer reserves all rights not specifically granted in the combination of (i) the license details provided by you and accepted in the course of this licensing transaction and (ii) these terms and conditions and (iii) CCC's Billing and Payment terms and conditions.

License Contingent on Payment

While you may exercise the rights licensed immediately upon issuance of the license at the end of the licensing process for the transaction, provided that you have disclosed complete and accurate details of your proposed use, no license is finally effective unless and until full payment is received from you (either by Springer or by CCC) as provided in CCC's Billing and Payment terms and conditions. If full payment is not received by the date due, then any license preliminarily granted shall be deemed automatically revoked and shall be void as if never granted. Further, in the event that you breach any of these terms and conditions or any of CCC's Billing and Payment terms and conditions, the license is automatically revoked and shall be void as if never granted. Use of materials as described in a revoked license, as well as any use of the materials beyond the scope of an unrevoked license, may constitute copyright infringement and Springer reserves the right to take any and all action to protect its copyright in the materials.

Copyright Notice: Disclaimer

You must include the following copyright and permission notice in connection with any reproduction of the licensed material:

"Springer book/journal title, chapter/article title, volume, year of publication, page, name(s) of author(s), (original copyright notice as given in the publication in which the material was originally published) "With permission of Springer"

In case of use of a graph or illustration, the caption of the graph or illustration must be included, as it is indicated in the original publication.

Warranties: None

Springer makes no representations or warranties with respect to the licensed material and adopts on its own behalf the limitations and disclaimers established by CCC on its behalf in its Billing and Payment terms and conditions for this licensing transaction.

Indemnity

You hereby indemnify and agree to hold harmless Springer and CCC, and their respective officers, directors, employees and agents, from and against any and all claims arising out of your use of the licensed material other than as specifically authorized pursuant to this license.

No Transfer of License

This license is personal to you and may not be sublicensed, assigned, or transferred by you without Springer's written permission.

No Amendment Except in Writing

This license may not be amended except in a writing signed by both parties (or, in the case of Springer, by CCC on Springer's behalf).

Objection to Contrary Terms

Springer hereby objects to any terms contained in any purchase order, acknowledgment, check endorsement or other writing prepared by you, which terms are inconsistent with these terms and conditions or CCC's Billing and Payment terms and conditions. These terms and conditions, together with CCC's Billing and Payment terms and conditions (which are incorporated herein), comprise the entire agreement between you and Springer (and CCC) concerning this licensing transaction. In the event of any conflict between your obligations established by these terms and conditions and those established by CCC's Billing and Payment terms and conditions, these terms and conditions shall control.

Jurisdiction

All disputes that may arise in connection with this present License, or the breach thereof, shall be settled exclusively by arbitration, to be held in the Federal Republic of Germany, in accordance with German law.

COPYRIGHT PERMISSIONS

Title: An LC/MS/MS method for the simultaneous determination of individual sphingolipid species in B cells

Authors: Si Mi, Yuan-Yuan Zhao, Rebecca F. Dielschneider, Spencer B. Gibson, Jonathan M. Curtis

Publication: Journal of Chromatography B

Publisher: Elsevier

Date: Available online 16 July 2016

Terms and Conditions

GENERAL TERMS

2. Elsevier hereby grants you permission to reproduce the aforementioned material subject to the terms and conditions indicated.

3. Acknowledgement: If any part of the material to be used (for example, figures) has appeared in our publication with credit or acknowledgement to another source, permission must also be sought from that source. If such permission is not obtained then that material may not be included in your publication/copies. Suitable acknowledgement to the source must be made, either as a footnote or in a reference list at the end of your publication, as follows:

"Reprinted from Publication title, Vol /edition number, Author(s), Title of article / title of chapter, Pages No., Copyright (Year), with permission from Elsevier [OR APPLICABLE SOCIETY COPYRIGHT OWNER]." Also Lancet special credit - "Reprinted from The Lancet, Vol. number, Author(s), Title of article, Pages No., Copyright (Year), with permission from Elsevier."

4. Reproduction of this material is confined to the purpose and/or media for which permission is hereby given.

5. Altering/Modifying Material: Not Permitted. However figures and illustrations may be altered/adapted minimally to serve your work. Any other abbreviations, additions, deletions and/or any other alterations shall be made only with prior written authorization of Elsevier Ltd. (Please contact Elsevier at permissions@elsevier.com)

6. If the permission fee for the requested use of our material is waived in this instance, please be advised that your future requests for Elsevier materials may attract a fee.

7. Reservation of Rights: Publisher reserves all rights not specifically granted in the combination of (i) the license details provided by you and accepted in the course of this licensing transaction, (ii) these terms and conditions and (iii) CCC's Billing and Payment terms and conditions.

8. License Contingent Upon Payment: While you may exercise the rights licensed immediately upon issuance of the license at the end of the licensing process for the transaction, provided that you have disclosed complete and accurate details of your proposed use, no license is finally effective unless and until full payment is received from you (either by publisher or by CCC) as provided in CCC's Billing and Payment terms and conditions. If full payment is not received on a timely basis, then any license preliminarily granted shall be deemed automatically revoked and shall be void as if never granted. Further, in the event that you breach any of these terms and conditions or any of CCC's Billing and Payment terms and conditions, the license is automatically revoked and shall be void as if never granted. Use of materials as described in a revoked license, as well as any use of the materials beyond the scope of an unrevoked license, may constitute copyright infringement and publisher reserves the right to take any and all action to protect its copyright in the materials.

9. Warranties: Publisher makes no representations or warranties with respect to the licensed material.

10. Indemnity: You hereby indemnify and agree to hold harmless publisher and CCC, and their respective officers, directors, employees and agents, from and against any and all claims arising out of your use of the licensed material other than as specifically authorized pursuant to this license.

11. No Transfer of License: This license is personal to you and may not be sublicensed, assigned, or transferred by you to any other person without publisher's written permission.

12. No Amendment Except in Writing: This license may not be amended except in a writing signed by both parties (or, in the case of publisher, by CCC on publisher's behalf).

13. Objection to Contrary Terms: Publisher hereby objects to any terms contained in any purchase order, acknowledgment, check endorsement or other writing prepared by you, which terms are inconsistent with these terms and conditions or CCC's Billing and Payment terms and conditions. These terms and conditions, together with CCC's Billing and Payment terms and conditions (which are incorporated herein), comprise the entire agreement between you and publisher (and CCC) concerning this licensing transaction. In the event of any conflict between your obligations established by these terms and conditions and those established by CCC's Billing and Payment terms and conditions, these terms and conditions shall control.

14. Revocation: Elsevier or Copyright Clearance Center may deny the permissions described in this License at their sole discretion, for any reason or no reason, with a full refund payable to you. Notice of such denial will be made using the contact information provided by you. Failure to receive such notice will not alter or invalidate the denial. In no event will Elsevier or Copyright Clearance Center be responsible or liable for any costs, expenses or damage incurred by you as a result of a denial of your permission request, other than a refund of the amount(s) paid by you to Elsevier and/or Copyright Clearance Center for denied permissions.

LIMITED LICENSE

The following terms and conditions apply only to specific license types:

15. **Translation:** This permission is granted for non-exclusive world English rights only unless your license was granted for translation rights. If you licensed translation rights you may only translate this content into the languages you requested. A professional translator must perform all translations and reproduce the content word for word preserving the integrity of the article.

16. **Posting licensed content on any Website:** The following terms and conditions apply as follows: Licensing material from an Elsevier journal: All content posted to the web site must maintain the copyright information line on the bottom of each image; A hyper-text must be included to the Homepage of the journal from which you are licensing at http://www.sciencedirect.com/science/journal/xxxxx or the Elsevier homepage for books at http://www.elsevier.com; Central Storage: This license does not include permission for a scanned version of the material to be stored in a central repository such as that provided by Heron/XanEdu.

Licensing material from an Elsevier book: A hyper-text link must be included to the Elsevier homepage at http://www.elsevier.com. All content posted to the web site must maintain the copyright information line on the bottom of each image.

Posting licensed content on Electronic reserve: In addition to the above the following clauses are applicable: The web site must be password-protected and made available only to bona fide students registered on a relevant course. This permission is granted for 1 year only. You may obtain a new license for future website posting.

17. **For journal authors:** the following clauses are applicable in addition to the above:

Preprints:

A preprint is an author's own write-up of research results and analysis, it has not been peer-reviewed, nor has it had any other value added to it by a publisher (such as formatting, copyright, technical enhancement etc.).

COPYRIGHT PERMISSIONS

Authors can share their preprints anywhere at any time. Preprints should not be added to or enhanced in any way in order to appear more like, or to substitute for, the final versions of articles however authors can update their preprints on arXiv or RePEc with their Accepted Author Manuscript (see below).

If accepted for publication, we encourage authors to link from the preprint to their formal publication via its DOI. Millions of researchers have access to the formal publications on ScienceDirect, and so links will help users to find, access, cite and use the best available version. Please note that Cell Press, The Lancet and some society-owned have different preprint policies. Information on these policies is available on the journal homepage.

Accepted Author Manuscripts: An accepted author manuscript is the manuscript of an article that has been accepted for publication and which typically includes author-incorporated changes suggested during submission, peer review and editor-author communications.

Authors can share their accepted author manuscript:

-immediately

- via their non-commercial person homepage or blog
- by updating a preprint in arXiv or RePEc with the accepted manuscript
- via their research institute or institutional repository for internal institutional uses or as part of an invitation-only research collaboration work-group
- directly by providing copies to their students or to research collaborators for their personal use
- for private scholarly sharing as part of an invitation-only work group on commercial sites with which Elsevier has an agreement

-after the embargo period

- via non-commercial hosting platforms such as their institutional repository
- via commercial sites with which Elsevier has an agreement

In all cases accepted manuscripts should:

-link to the formal publication via its DOI

- bear a CC-BY-NC-ND license - this is easy to do

- if aggregated with other manuscripts, for example in a repository or other site, be shared in alignment with our hosting policy not be added to or enhanced in any way to appear more like, or to substitute for, the published journal article.

Published journal article (JPA): A published journal article (PJA) is the definitive final record of published research that appears or will appear in the journal and embodies all value-adding publishing activities including peer review co-ordination, copy-editing, formatting, (if relevant) pagination and online enrichment.

Policies for sharing publishing journal articles differ for subscription and gold open access articles:

Subscription Articles: If you are an author, please share a link to your article rather than the full-text. Millions of researchers have access to the formal publications on ScienceDirect, and so links will help your users to find, access, cite, and use the best available version.

Theses and dissertations which contain embedded PJAs as part of the formal submission can be posted publicly by the awarding institution with DOI links back to the formal publications on ScienceDirect.

If you are affiliated with a library that subscribes to ScienceDirect you have additional private sharing rights for others' research accessed under that agreement. This includes use for classroom teaching and internal training at the institution (including use in course packs and courseware programs), and inclusion of the article for grant funding purposes.

Gold Open Access Articles: May be shared according to the author-selected end-user license and should contain a CrossMark logo, the end user license, and a DOI link to the formal publication on ScienceDirect.

Please refer to Elsevier's posting policy for further information.

18. **For book authors** the following clauses are applicable in addition to the above: Authors are permitted to place a brief summary of their work online only. You are not allowed to download and post the published electronic version of your chapter, nor may you scan the printed edition to create an electronic version. Posting to a repository: Authors are permitted to post a summary of their chapter only in their institution's repository.

19. **Thesis/Dissertation:** If your license is for use in a thesis/dissertation your thesis may be submitted to your institution in either print or electronic form. Should your thesis be published commercially, please reapply for permission. These requirements include permission for the Library and Archives of Canada to supply single copies, on demand, of the complete thesis and include permission for Proquest/UMI to supply single copies, on demand, of the complete thesis. Should your thesis be published commercially, please reapply for permission. Theses and dissertations which contain embedded PJAs as part of the formal submission can be posted publicly by the awarding institution with DOI links back to the formal publications on ScienceDirect.

COPYRIGHT PERMISSIONS

Title: Hydrophilic Interaction Liquid Chromatography for Determination of Betaine

Authors: Jonathan M. Curtis and Si Mi

Publication: Betaine: Chemistry, Analysis, Function and Effects

Publisher: The Royal Society of Chemistry

Date: 28 May 2015

COPYRIGHT PERMISSIONS

Title: Glucagon-Like Peptide-2 Alters Bile Acid Metabolism in Parenteral Nutrition-Associated Liver Disease

Authors: David W. Lim, Paul W. Wales, Si Mi, Jason Y. K. Yap, Jonathan M. Curtis, Diana R. Mager, Vera C. Mazurak, Pamela R. Wizzard, David L. Sigalet, Justine M. Turner

Publication: Journal of Parenteral and Enteral Nutrition

Publisher: SAGE Publications

Date: 01/01/2016

Gratis Reuse

- Without further permission, as the Author of the journal article you may:
    - post the accepted version (version 2) on your personal website, department's website or your institution's repository. You may NOT post the published version (version 3) on a website or in a repository without permission from SAGE.
    - post the accepted version (version 2) of the article in any repository other than those listed above 12 months after official publication of the article.
    - use the published version (version 3) for your own teaching needs or to supply on an individual basis to research colleagues, provided that such supply is not for commercial purposes.
    - use the accepted or published version (version 2 or 3) in a book written or edited by you. To republish the article in a book NOT written or edited by you, permissions must be cleared on the previous page under the option 'Republish in a Book/Journal' by the publisher, editor or author who is compiling the new work.
- When posting or re-using the article electronically, please link to the original article and cite the DOI.
- All other re-use of the published article should be referred to SAGE. Contact information can be found on the bottom of our 'Journal Permissions' page.

COPYRIGHT PERMISSIONS

Title: Lysosomotropic agents selectively target chronic lymphocytic leukemia cells due to altered sphingolipid metabolism

Author: R F Dielschneider, H Eisenstat, S Mi, J M Curtis, W Xiao, J B Johnston, S B Gibson

Publication: Leukemia

Publisher: Nature Publishing Group

Date: Feb 23, 2015

Terms and Conditions for Permissions
Nature Publishing Group hereby grants you a non-exclusive license to reproduce this material for this purpose, and for no other use, subject to the conditions below:

1. NPG warrants that it has, to the best of its knowledge, the rights to license reuse of this material. However, you should ensure that the material you are requesting is original to Nature Publishing Group and does not carry the copyright of another entity (as credited in the published version). If the credit line on any part of the material you have requested indicates that it was reprinted or adapted by NPG with permission from another source, then you should also seek permission from that source to reuse the material.

2. Permission granted free of charge for material in print is also usually granted for any electronic version of that work, provided that the material is incidental to the work as a whole and that the electronic version is essentially equivalent to, or substitutes for, the print version. Where print permission has been granted for a fee, separate permission must be obtained for any additional, electronic re-use (unless, as in the case of a full paper, this has already been accounted for during your initial request in the calculation of a print run).NB: In all cases, web-based use of full-text articles must be authorized separately through the 'Use on a Web Site' option when requesting permission.

3. Permission granted for a first edition does not apply to second and subsequent editions and for editions in other languages (except for signatories to the STM Permissions Guidelines, or where the first edition permission was granted for free).

4. Nature Publishing Group's permission must be acknowledged next to the figure, table or abstract in print. In electronic form, this acknowledgement must be visible at the same time as the figure/table/abstract, and must be hyperlinked to the journal's homepage.

5. The credit line should read:
   Reprinted by permission from Macmillan Publishers Ltd: [JOURNAL NAME] (reference citation), copyright (year of publication)
   For AOP papers, the credit line should read:
   Reprinted by permission from Macmillan Publishers Ltd: [JOURNAL NAME], advance online publication, day month year (doi: 10.1038/sj.[JOURNAL ACRONYM].XXXXX)

6. Adaptations of single figures do not require NPG approval. However, the adaptation should be credited as follows:
   Adapted by permission from Macmillan Publishers Ltd: [JOURNAL NAME] (reference citation), copyright (year of publication)

7. Translations of 401 words up to a whole article require NPG approval. Please visit http://www.macmillanmedicalcommunications.com for more information. Translations of up to a 400 words do not require NPG approval. The translation should be credited as follows:

   Translated by permission from Macmillan Publishers Ltd: [JOURNAL NAME] (reference citation), copyright (year of publication).